UC Riverside

UC Riverside Electronic Theses and Dissertations

Title

Computational Modeling and Mechanistic Elucidation of the Complement System Under Homeostasis, Disease, and Therapeutic Interventions

Permalink

https://escholarship.org/uc/item/5gw6w7g9

Author

Zewde, Nehemiah Tefera

Publication Date

2019

Supplemental Material

https://escholarship.org/uc/item/5gw6w7g9#supplemental

Copyright Information

This work is made available under the terms of a Creative Commons Attribution License, availalbe at https://creativecommons.org/licenses/by/4.0/

Peer reviewed|Thesis/dissertation

eScholarship.org Powered by the California Digital Library
University of California

UNIVERSITY OF CALIFORNIA
RIVERSIDE

Computational Modeling and Mechanistic Elucidation of the Complement System under Homeostasis, Disease, and Therapeutic Interventions

A Dissertation submitted in partial satisfaction
of the requirements for the degree of

Doctor of Philosophy

in

Bioengineering

by

Nehemiah Tefera Zewde

September 2019

Dissertation Committee:
Dr. Mark Alber, Chairperson
Dr. Kaustabh Ghosh
Dr. Giulia Palermo
Late Dr. Dimitrios Morikis

Copyright by
Nehemiah Tefera Zewde
2019

The Dissertation of Nehemiah Tefera Zewde is approved:

_____

_____

_____

Committee Chairperson

University of California, Riverside

ACKNOWLEDGEMENTS

This dissertation would not have been possible without the amazing support I received from a number of wonderful individuals. First, I would like to express my sincere gratitude to my advisor Professor Dimitrios Morikis for the continuous support, patience, and guidance. Your contributions have helped me mature into the scientist and person that I am today. Thank you to my committee members Dr. Mark Alber, Dr. Kaustabh Ghosh, and Dr. Giulia Palermo for the invaluable discussions and for always being available to me whenever I needed guidance. Thanks also to my collaborators that have made my research endeavors possible and allowing me to expand my modeling frontiers.

I am exceedingly grateful to the past members of Biomolecular Modeling & Design Lab (BioMoDeL). Many thanks to Dr. Ron Gorham, Dr. Chris A Kieslich, Dr. Aliana López de Victoria, Dr. Zied Gaieb, Dr. Rohith Mohan, and Dr. Reed Harrison for the continuous support and aspiring guidance throughout this entire process. Thank you to the current member Dr. Yogesh Narkhede for the insightful discussion on computational chemistry and modeling. I would also like to extend my deepest gratitude to Rohaine Hsu for helping through my final years. Thank you for being so meticulous on making sure my code was error free.

I would like to extend my sincere thanks to the graduate students and staff of the Bioengineering Department at UCR. Special thanks to Dr. Andrea Cabrera, Sanychen Muk, Belinda Le, and Dr. Dieanira Erudaitius for the wonderful discussions on daily routes, life,

and diet. I thoroughly enjoyed our moments and thank you for giving me the necessary distraction from research.

Finally, the completion of my dissertation would not have been possible without the unyielding love and support of my family. I especially thank my parents (Zewde Tefera and Azeb Weyessa), sisters (Betesida, Yordanos, and Bathsheba), uncle (Worku), aunties (Yeshihareg and Gennet), grandparents (Tiruwork and Lakche), and to the families of Dr. Yayehirad (Cynthia, Jasmine, and Leo) and Hagos (Aster and Eyassu). Without you, I would have not made it this far. I would also like to extend my deepest gratitude to my closest friend Eunice Kim for the fun times and continuous encouragement. Thank you all.

The text of this dissertation, in part, is a reprint of the material as it appears in:

1. Zewde N, Jr RDG, Dorado A, Morikis D. Quantitative Modeling of the Alternative Pathway of the Complement System. PLOS ONE. 2016;11: e0152337. doi:10.1371/journal.pone.0152337.
2. Zewde N, Morikis D. A computational model for the evaluation of complement system regulation under homeostasis, disease, and drug intervention. PLOS ONE. 2018;13: e0198644. doi:10.1371/journal.pone.0198644.
3. Zewde N, Mohan RR, Morikis D. Immunophysical Evaluation of the Initiating Step in the Formation of the Membrane Attack Complex. Front Phys. 2018;6. doi:10.3389/fphy.2018.00130.

The co-author Dimitrios Morikis directed and supervised the research which forms the basis for this dissertation. Other co-authors provided technical expertise.

DEDICATION

I dedicate this dissertation to
my loving family.

ABSTRACT OF THE DISSERTATION

Computational Modeling and Mechanistic Elucidation of the Complement System under Homeostasis, Disease, and Therapeutic Interventions

by

Nehemiah Tefera Zewde

Doctor of Philosophy, Graduate Program in Bioengineering
University of California, Riverside, September 2019
Dr. Mark Alber, Chairperson

The complement system is a major part of the innate immune system that targets invading pathogens and assists in maintaining host homeostasis. Complement is composed of three pathways known as alternative (AP), classical (CP), and lectin (LP) that work in concert to mediate an immune response. Although activation of the complement system is tightly controlled by endogenous regulators, dysregulation leads to a cascade of events that brings about misdirected attacks on host cells. Here, to gain a systems-level understanding of the complement system, we developed comprehensive quantitative models to describe the biochemical reactions of the alternative, classical, and lectin pathways. We also present the first factor H (FH) mediated disease model (mimicking dysfunction of the alternative pathway) and complement intervention model by using known inhibitors, a compstatin variant (C3 inhibitor) and eculizumab (C5 inhibitor). Furthermore, our complement system model is coupled with other segments of humoral immunity that contains immunoglobulins G and M (IgG and IgM), complement factor H-related proteins (CFHRs) 1-5, and pentraxins (C-reactive protein, CRP; serum-amyloid P component, SAP; long pentraxin 3,

PTX3). Our model also contains three pathogen types: (type 1) cannot evade complement system, (type 2) evades immune system by recruiting complement regulators, and (type 3) pathogen specific model of *Neisseria meningitidis (N. meningitidis)* located in either nasopharynx or bloodstream. In addition to mathematical models, we also utilize molecular dynamics simulations and electrostatics calculations to elucidate the molecular mechanisms of C5b and C6 interactions that lead to the complement terminal product, membrane attack complex. Altogether, our final mathematical model contains 670 ordinary differential equations (ODEs) with 328 kinetic parameters to describe complex interplay of the immune system. Our comprehensive models can also serve as a framework to simulate disease-specific scenarios which can be used in diagnosis and patient-specific treatments. Insights obtained from our models may also serve as a foundation for developing diagnostic tools for pathological situations that involve complement deficiencies or mutations. Furthermore, our model can aid in drug discovery by incorporating points of intervention to identify novel inhibitory sites.

TABLE OF CONTENTS

APPENDICES

LIST OF FIGURES

LIST OF TABLES

CHAPTER 1

Introduction

1.1 History of the complement system

In the latter half of the 19th century, scientific research aimed at uncovering resistance against microbial infections gave birth to modern immunology [1]. The discovery of phagocytes and phagocytosis by Elie Metchnikoff in 1883 laid the foundation for cellular immunity, whereas work done by Josef von Fodor (1887), George Nuttall (1888), and Hans Buchner (1889) demonstrated acellular immunity of serum [2–4]. Furthermore, Nuttall (1888) highlighted bactericidal activity of blood disappeared when heated to 52°C. Although this work set the basic discovery for complement, it was Buchner's studies that set the theoretical basis for humoral immunity. Moreover, Buchner coined the bactericidal action of blood as 'alexin' (in Greek means 'to ward off'). In 1895, this heat-labile phenomena of blood (alexin) gained further support as Jules Bordet demonstrated bactericidal action of heat-inactivated serum could be restored by the addition of freshly drawn blood [5]. Bordet also showed heat-inactivated serum still agglutinated cholera but required the subsequent addition of fresh serum to restore bacteriolysis. These observations indicated the presence of two factors for bacterial killing: a heat-labile component which Bordet attributed to alexin, and a heat-stable component which he called sensitiser (now known as antibody) [5]. Subsequently, the German bacteriologist Paul Ehrlich proposed the side-chain theory of antibody (**Figure 1.1**) formation and mechanism on how antibodies induce bacterial lysis with the help of alexin.

This heat-liable factor, alexin, was renamed to ‘complement’ by Ehrlich to signify that it complemented the actions of antibodies [2].

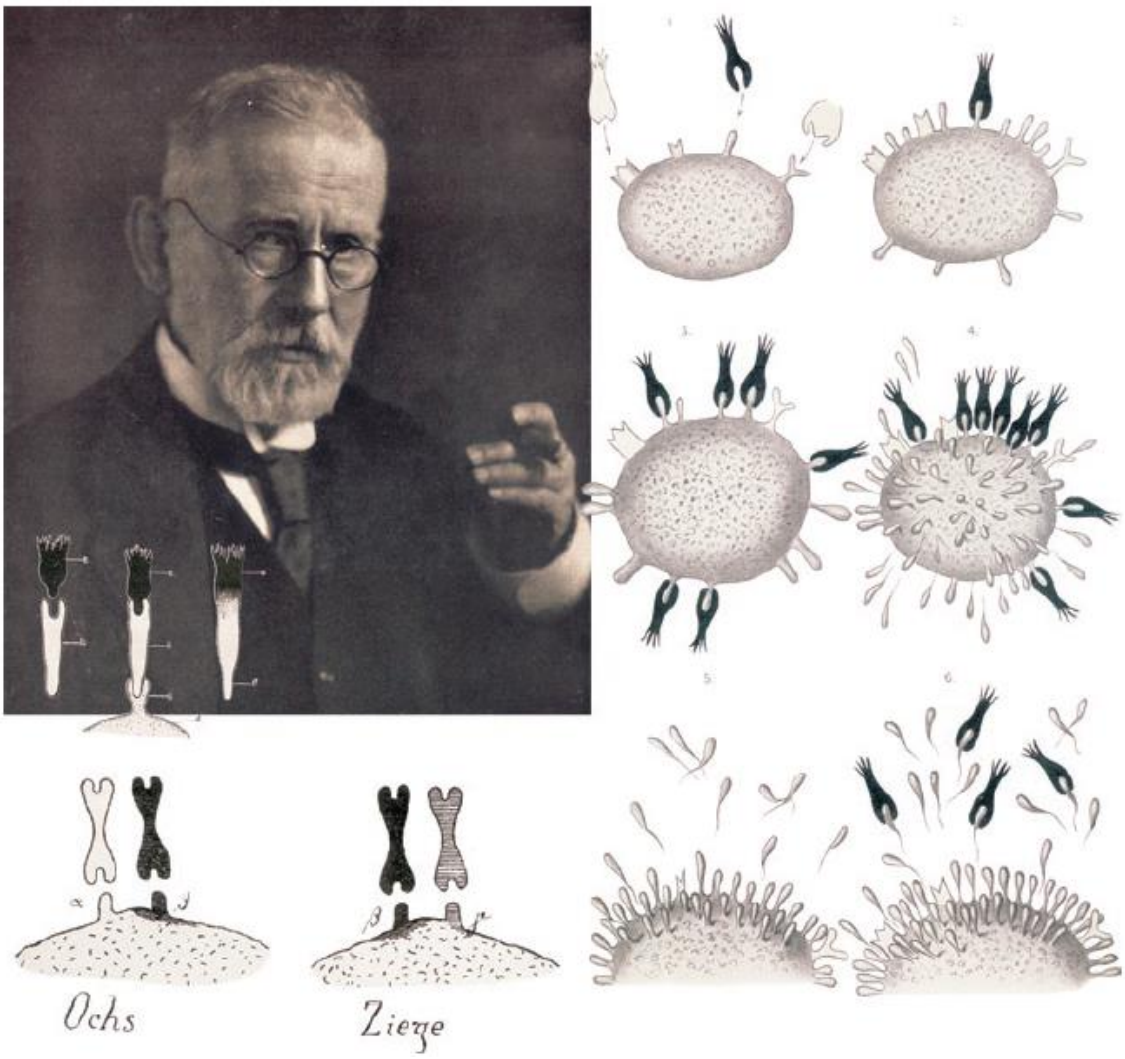

Figure 1.1. Paul Ehrlich (1854-1915) and the side-chain theory. Image from [2].

In the ensuing years, it became evident that complement was not a single factor of blood but rather a multifactorial entity that contained numerous components. By 1907, Ferrata and Brand demonstrated complement can be separated into fractions of ‘midpiece’

and ‘endpiece’, now known as C1 and C2, respectively [6]. Subsequently, studies utilizing yeast cells identified complement C3, while complement C4 was soon isolated using ammonia [6]. With the discovery of a fourth component in 1926, complement was now known to contain at least four components. Although the identified complement components were assigned names in the order of their discovery: C1, C2, C3, and C4, it later became clear that the reaction sequence did not match the order of their discovery [7]. However, the 1950s and 1960s brought about novel experimental techniques that led to the discovery of additional complement proteins and reaction sequences [8]. By the mid-1960s, a number of notable scientists such as Hans Müller-Eberhard, Ulf Nilsson, Robert Nelson, Jr., and Paul Klein led to the characterization of complement proteins such as C5, C6, C7, C8, and C9 [8]. Furthermore, Lepow and colleagues demonstrated that C1 was comprised of three separate proteins (C1q, C1r, and C1s) and thus bringing the number of identified complement proteins to 11. With this, in 1968 the complement nomenclature was updated to match order of activation: C1, C4, C2, C3, C5, C6, C7, C8 and C9 [6].

1.2 Pathways of the Complement System

It is now known the complement system is a part of the innate immune system that plays a major role in host homeostasis and defense. Complement is composed of proteins present in plasma and cell surfaces that interact sequentially to mediate immune surveillance. Three pathways known as alternative, classical, and lectin makeup the complement system.

1.2.1 Alternative pathway

The alternative pathway activates by the spontaneous hydrolysis of the complement protein C3. This auto-activation will generate a molecule known as C3(H_2O) and then associates with factor B (FB) to form a proconvertase known as C3(H_2O)B [9,10]. This complex is then activated by protease factor D (FD) to form the initial C3 convertase of the alternative pathway, C3(H_2O)Bb [9,11]. This fluid phase convertase cleaves C3 into a C3a and C3b. While C3a plays a major role in mediating inflammation, nascent fluid-phase C3b (nfC3b) is capable of indiscriminately binding to different surfaces via covalent bond [12–14]. Once bond to the surface of a pathogen, C3b will associate with FB and subsequently with FD to form the convertase C3bBb [11,15]. However, C3bBb is unstable and has a short half-life. Properdin will associate with C3bBb to from C3bBbP and subsequently extend its half-life by 10-fold. Similar to C3(H_2O)Bb, C3bBb will cleave C3 to form C3a and nascent fluid C3b. In addition, C3bBb can cleave C5 into C5a and C5b. The first product, C5a, is a potent mediator of inflammation, whereas C5b initiates the terminal step by interacting sequentially with C6, C7, C8, and C9 to form the membrane attack complex [16–18].

1.2.2 Classical pathway

Similar to the alternative pathway, the classical pathway auto-activates in the fluid phase through the intramolecular activation of complement C1 [19–21]. Activated C1 (C1*) will cleave complement protein C4 into C4a and nascent fluid C4b (nC4b) [22]. Rapid hydrolysis will convert nC4b into fluid C4b, which subsequently interacts with C2

to form C4bC2. Activated C1 will then activate C4bC2 into the C3/C5 convertase C4bC2a. Through the presence of the classical pathway convertase C4bC2a, the alternative pathway is activated through the cleavage of C3 into C3a and nC3b. Furthermore, with the continuous cleavage of C4, through C1*, and C3 through convertases of either the alternative or classical pathway convertases, generated nC4b and nC3b can associate together to form hybrid complexes such as C4bC3b or homodimers such as C3bC3b/C4bC4b. The dimers can associate with complement protein C2 or factor B to form a heterocomplex convertase C4bC3bBb/C4bC3bC2a and C3bC3bBb/C4bC4bC2a [23–25]. Moreover, the classical pathway can activate on pathogens through the formation of antigen-antibody complexes [26]. C1 will associate to fragment crystallizable portion region of IgG and IgM [26–30] and C1 subsequently activates and cleaves both C4 and C4bC2, to form surface bound convertases (C4bC2a).

1.2.3 Lectin pathway

One of the last pathways to be discovered pathways in the complement system, the lectin pathway activates by directly binding to pathogens without the presence of antigen-antibody complexes. Unlike the classical pathway that has a single pattern recognition molecule (C1q), the lectin pathway contains more than seven. These include mannose-binding lectin (MBL), ficolin-1 (M-ficolin), ficolin-2 (L-ficolin), and ficolin-3 (H-ficolin), collectin liver 1 (CL-L1), collectin kidney 1 (CL-K1), heteromeric CL-L1/K1 [31,32]. Furthermore, the lectin pathway's pattern recognition molecules are associated with three types of serine proteases known as MBL-associated serine proteases (MASPs)-1, MASP-

2, and MASP-3. These MASPs can either autoactivate or cross-activate on the surface of pathogens [33–35]. Subsequently, activated MASPs will cleave complement C4 and C4bC2 to form the C3/C5 convertase C4bC2a [36,37]. However, the pattern recognition molecules of the lectin pathway can also interact with MBL-associated proteins known as MAp19 and MAp44 that do not contain a serine protease domain [38,39]. The molecules do not activate complement but rather may inhibit the lectin pathway.

1.3 Regulation

Complement activation has to be properly regulated to ensure healthy host cells are not attacked. Due to the dangers of complement activation, numerous checkpoints are present in fluid phase and bound to membranes of host cells to deactivate active complement fragments. The alternative pathway contains complement FH and its spice variant factor H-like protein 1 (FHL-1) as one of the main regulators that target C3b and C3/C5 convertase C3bBb. In the first case of C3b, FH and FHL-1 will associate with C3b and act as cofactors for factor I (FI) to deactivate C3b into iC3b (inactive C3b) [40–42]. On the latter case, FH and FHL-1 will associate with C3/C5 convertases and rapidly accelerate the rate of decay into C3b and Bb [40–42]. Similarly, the classical and lectin pathways also deploy complement regulators C1 inhibitor (C1-INH) and C4b-binding protein (C4BP) that act in the early stages of activation (activated C1/MASPs and C4b) or at the propagation step (C4bC2a). For instance, C4BP will bind to C4b and act as a cofactor for FI mediated deactivation [43]. Furthermore, C1-INH can inhibit activated C1 or MASPs by targeting their respective protease domains [44,45].

In addition to fluid phase regulation, membrane bound complement regulators also deactivate complement fragments. Complement receptor 1 (CR1), decay-accelerating factor (DAF), and membrane cofactor protein (MCP) play integral roles in inhibit the propagation of complement on host cells [42,46–49]. For instance, CR1 and MCP act as cofactors for FI mediated deactivation of C3b/C4b. DAF and CR1 target C3/C5 convertases such as C3bBb or C4bC2a and accelerate the decay into their respective components. Moreover, the terminal step is also regulated through a mix of fluid vitronectin (Vn) or clusterin (Cn) and membrane bound CD59 (protectin) regulators that inhibit MAC pore formation [42,50].

1.4 Diseases associated with deficiencies of the complement system

Over-activation or under-regulation of the complement system has been associated with numerous diseases that affect host cells or tissues. Diseases such as age-related macular degeneration (AMD), atypical hemolytic uremic syndrome (aHUS), and C3 glomerulopathy (C3G) are associated with complement dysregulation [42,51,52]. For instance, mutations affecting complement regulators FH, FHL-1, FI, and MCP are linked with renal diseases mentioned above (aHUS and C3G) [42,51,52]. Loss-of-function variants on FH/FHL-1 will reduce binding efficiency to C3b, whereas FI mutations reduces the catalytic efficiency in deactivating C3b. Moreover, function-blocking autoantibodies targeting complement regulators also lead to complement abnormalities in aHUS and C3G patients. These mutations targeting complement regulators or presence of antibodies to regulators account for 60% of aHUS patients and 50% of C3G patients [51,52].

In addition to chronic kidney diseases associated with loss-of-function FH mutations, a single polymorphism on FH Y402H is highly associated with developing AMD [53–56]. Homozygotes individuals with Y402H polymorphism have a five- to six-fold increase in developing AMD whereas heterozygous individuals have a two- to three-fold higher risk [51]. Altogether, the dynamic interplay between complement activation and regulation is essential to maintaining homeostasis. However, imbalances caused by genetic variation and complement deficiencies will instigate a vicious cycle of over-activation/under-regulation that may lead to the progression of various diseases.

1.5 Infections and immune evasion associated with complement deficiencies

The complement system has developed a range of mechanism that surveils and kills invading microbes. Consequently, pathogenic organisms have elaborate mechanism to the escape the deadly effects of complement [57–61]. These include recruitment of complement regulators, secretion of proteases that deactivate effector proteins, and surface proteins that mimic host regulators. Complement regulators C4BP, FH, and FHL-1 are recruited to bacterial surface and subsequently inhibit complement activation from taking root. Furthermore, complement regulators Cn and Vn are also recruited to pathogen surface to inhibit the terminal step that forms MAC. In addition to recruitment, pathogens can also secrete proteases pseudomonas elastase (PaE) and pseudomonas alkaline protease (PaAP) to cleave complement proteins C1q and C3. This subsequently prevents complement activation and promotes survival against complement-mediated attacks.

The importance of the complement system against invading microbes is reflected in studies that show how genetic deficiencies in complement components lead to recurrent infections [62]. For instance, deficiencies in the classical pathway are associated with *Streptococcus pneumoniae* bacteremia, *Haemophilus influenzae* meningitis, and recurrent respiratory infections [62,63]. Furthermore, hereditary deficiency of complement protein C2 led to severe infections of mainly septicemia or meningitis caused by *Streptococcus pneumoniae* [64]. In addition to the classical pathway, deficiencies in the lectin pathway are associated with an increased risk in meningococcal and pneumococcal infections [62,63]. Moreover, an individual with LP deficiency suffered from multiple lower respiratory tract infections, cerebral abscess, and several episodes of bacterial pneumonia [65]. Lastly, deficiencies in the alternative pathway are also associated with invasive diseases. Individuals with inherited as well as acquired deficiency in C3 develop recurrent and sever infections such as meningitis, bacteremia, pneumonia, and otitis media [62,63,66,67]. In light of C3 deficiency, bacterial species responsible for causing these infections include *Streptococcus pneumoniae, Neisseria meningitidis, Haemophilus influenzae, Escherichia coli, Staphylococcus aureus,* and *Streptococcus pyogenes.*

1.6 References

1. Cruse JM, Lewis RE. Atlas of Immunology [Internet]. Berlin Heidelberg: Springer-Verlag; 1999. Available: https://www.springer.com/gp/book/9783662111987

2. Kaufmann SHE. Immunology's foundation: the 100-year anniversary of the Nobel Prize to Paul Ehrlich and Elie Metchnikoff. Nat Immunol. 2008;9: 705–712. doi:10.1038/ni0708-705

3. Tauber AI, Chernyak L. The birth of immunology. II. Metchnikoff and his critics. Cell Immunol. 1989;121: 447–473.

4. Lachmann P. Complement before molecular biology. Mol Immunol. 2006;43: 496–508. doi:10.1016/j.molimm.2005.04.005

5. Oakley CL. Jules Jean Baptiste Vincent Bordet. 1870-1961. Biogr Mem Fellows R Soc. 1962;8: 19–25.

6. Nesargikar PN, Spiller B, Chavez R. The complement system: history, pathways, cascade and inhibitors. Eur J Microbiol Immunol. 2012;2: 103–111. doi:10.1556/EuJMI.2.2012.2.2

7. Chaplin H. Review: the burgeoning history of the complement system 1888-2005. Immunohematology. 2005;21: 85–93.

8. Cooper NR. Complement: a nostalgic journey The Hans J. Müller-Eberhard Memorial Lecture, Honolulu, June 14, 2004. Mol Immunol. 2006;43: 487–495. doi:10.1016/j.molimm.2005.04.018

9. Pangburn MK, Schreiber RD, Müller-Eberhard HJ. Formation of the initial C3 convertase of the alternative complement pathway. Acquisition of C3b-like activities by spontaneous hydrolysis of the putative thioester in native C3. J Exp Med. 1981;154: 856–867.

10. Laich A, Sim RB. Complement C4bC2 complex formation: an investigation by surface plasmon resonance. Biochim Biophys Acta. 2001;1544: 96–112.

11. Pangburn MK, Müller-Eberhard HJ. The C3 convertase of the alternative pathway of human complement. Enzymic properties of the bimolecular proteinase. Biochem J. 1986;235: 723–730.

12. Law SK, Lichtenberg NA, Levine RP. Evidence for an ester linkage between the labile binding site of C3b and receptive surfaces. J Immunol Baltim Md 1950. 1979;123: 1388–1394.

13. Tack BF, Harrison RA, Janatova J, Thomas ML, Prahl JW. Evidence for presence of an internal thiolester bond in third component of human complement. Proc Natl Acad Sci U S A. 1980;77: 5764–5768.

14. Law SK, Levine RP. Interaction between the third complement protein and cell surface macromolecules. Proc Natl Acad Sci U S A. 1977;74: 2701–2705.

15. Rawal N, Pangburn MK. C5 convertase of the alternative pathway of complement. Kinetic analysis of the free and surface-bound forms of the enzyme. J Biol Chem. 1998;273: 16828–16835.

16. Bayly-Jones C, Bubeck D, Dunstone MA. The mystery behind membrane insertion: a review of the complement membrane attack complex. Philos Trans R Soc Lond B Biol Sci. 2017;372. doi:10.1098/rstb.2016.0221

17. Sharp TH, Koster AJ, Gros P. Heterogeneous MAC Initiator and Pore Structures in a Lipid Bilayer by Phase-Plate Cryo-electron Tomography. Cell Rep. 2016;15: 1–8. doi:10.1016/j.celrep.2016.03.002

18. Zalman LS, Müller-Eberhard HJ. Comparison of channels formed by poly C9, C5b-8 and the membrane attack complex of complement. Mol Immunol. 1990;27: 533–537.

19. Tseng Y, Poon PH, Zavodszky P, Schumaker VN. Spontaneous activation of serum C1 in vitro. Role of C1 inhibitor. J Immunol. 1991;147: 1884–1890.

20. Bianchino AC, Poon PH, Schumaker VN. A mechanism for the spontaneous activation of the first component of complement, C1, and its regulation by C1-inhibitor. J Immunol. 1988;141: 3930–3936.

21. Ziccardi RJ. Spontaneous activation of the first component of human complement (C1) by an intramolecular autocatalytic mechanism. J Immunol Baltim Md 1950. 1982;128: 2500–2504.

22. Sepp A, Dodds AW, Anderson MJ, Campbell RD, Willis AC, Law SK. Covalent binding properties of the human complement protein C4 and hydrolysis rate of the internal thioester upon activation. Protein Sci Publ Protein Soc. 1993;2: 706–716. doi:10.1002/pro.5560020502

23. Meri S, Pangburn MK. A mechanism of activation of the alternative complement pathway by the classical pathway: protection of C3b from inactivation by covalent attachment to C4b. Eur J Immunol. 1990;20: 2555–2561. doi:10.1002/eji.1830201205

24. Rawal N, Pangburn M. Formation of high-affinity C5 convertases of the alternative pathway of complement. J Immunol Baltim Md 1950. 2001;166: 2635–2642.

25. Rawal N, Pangburn MK. Formation of High Affinity C5 Convertase of the Classical Pathway of Complement. J Biol Chem. 2003;278: 38476–38483. doi:10.1074/jbc.M307017200

26. Kishore U, Ghai R, Greenhough TJ, Shrive AK, Bonifati DM, Gadjeva MG, et al. Structural and functional anatomy of the globular domain of complement protein C1q. Immunol Lett. 2004;95: 113–128. doi:10.1016/j.imlet.2004.06.015

27. Diebolder CA, Beurskens FJ, de Jong RN, Koning RI, Strumane K, Lindorfer MA, et al. Complement is activated by IgG hexamers assembled at the cell surface. Science. 2014;343: 1260–1263. doi:10.1126/science.1248943

28. Bally I, Inforzato A, Dalonneau F, Stravalaci M, Bottazzi B, Gaboriaud C, et al. Interaction of C1q With Pentraxin 3 and IgM Revisited: Mutational Studies With Recombinant C1q Variants. Front Immunol. 2019;10: 461. doi:10.3389/fimmu.2019.00461

29. Wang G, de Jong RN, van den Bremer ETJ, Beurskens FJ, Labrijn AF, Ugurlar D, et al. Molecular Basis of Assembly and Activation of Complement Component C1 in Complex with Immunoglobulin G1 and Antigen. Mol Cell. 2016;63: 135–145. doi:10.1016/j.molcel.2016.05.016

30. Ugurlar D, Howes SC, de Kreuk B-J, Koning RI, de Jong RN, Beurskens FJ, et al. Structures of C1-IgG1 provide insights into how danger pattern recognition activates complement. Science. 2018;359: 794–797. doi:10.1126/science.aao4988

31. Garred P, Genster N, Pilely K, Bayarri-Olmos R, Rosbjerg A, Ma YJ, et al. A journey through the lectin pathway of complement-MBL and beyond. Immunol Rev. 2016;274: 74–97. doi:10.1111/imr.12468

32. Degn SE, Thiel S. Humoral pattern recognition and the complement system. Scand J Immunol. 2013;78: 181–193. doi:10.1111/sji.12070

33. Megyeri M, Harmat V, Major B, Végh Á, Balczer J, Héja D, et al. Quantitative characterization of the activation steps of mannan-binding lectin (MBL)-associated serine proteases (MASPs) points to the central role of MASP-1 in the initiation of the complement lectin pathway. J Biol Chem. 2013;288: 8922–8934. doi:10.1074/jbc.M112.446500

34. Degn SE, Kjaer TR, Kidmose RT, Jensen L, Hansen AG, Tekin M, et al. Complement activation by ligand-driven juxtaposition of discrete pattern recognition complexes. Proc Natl Acad Sci U S A. 2014;111: 13445–13450. doi:10.1073/pnas.1406849111

35. Héja D, Kocsis A, Dobó J, Szilágyi K, Szász R, Závodszky P, et al. Revised mechanism of complement lectin-pathway activation revealing the role of serine protease MASP-1 as the exclusive activator of MASP-2. Proc Natl Acad Sci U S A. 2012;109: 10498–10503. doi:10.1073/pnas.1202588109

36. Ambrus G, Gál P, Kojima M, Szilágyi K, Balczer J, Antal J, et al. Natural Substrates and Inhibitors of Mannan-Binding Lectin-Associated Serine Protease-1 and -2: A Study on Recombinant Catalytic Fragments. J Immunol. 2003;170: 1374–1382. doi:10.4049/jimmunol.170.3.1374

37. Rossi V, Teillet F, Thielens NM, Bally I, Arlaud GJ. Functional Characterization of Complement Proteases C1s/Mannan-binding Lectin-associated Serine Protease-2 (MASP-2) Chimeras Reveals the Higher C4 Recognition Efficacy of the MASP-2 Complement Control Protein Modules. J Biol Chem. 2005;280: 41811–41818. doi:10.1074/jbc.M503813200

38. Degn SE, Thiel S, Nielsen O, Hansen AG, Steffensen R, Jensenius JC. MAp19, the alternative splice product of the MASP2 gene. J Immunol Methods. 2011;373: 89–101. doi:10.1016/j.jim.2011.08.006

39. Degn SE, Hansen AG, Steffensen R, Jacobsen C, Jensenius JC, Thiel S. MAp44, a human protein associated with pattern recognition molecules of the complement system and regulating the lectin pathway of complement activation. J Immunol Baltim Md 1950. 2009;183: 7371–7378. doi:10.4049/jimmunol.0902388

40. Dopler A, Guntau L, Harder MJ, Palmer A, Höchsmann B, Schrezenmeier H, et al. Self versus Nonself Discrimination by the Soluble Complement Regulators Factor H and FHL-1. J Immunol Baltim Md 1950. 2019;202: 2082–2094. doi:10.4049/jimmunol.1801545

41. Zipfel PF, Skerka C. FHL-1/reconectin: a human complement and immune regulator with cell-adhesive function. Immunol Today. 1999;20: 135–140.

42. Schmidt CQ, Lambris JD, Ricklin D. Protection of host cells by complement regulators. Immunol Rev. 2016;274: 152–171. doi:10.1111/imr.12475

43. Ermert D, Blom AM. C4b-binding protein: The good, the bad and the deadly. Novel functions of an old friend. Immunol Lett. 2016;169: 82–92. doi:10.1016/j.imlet.2015.11.014

44. Rossi V, Bally I, Ancelet S, Xu Y, Frémeaux-Bacchi V, Vivès RR, et al. Functional characterization of the recombinant human C1 inhibitor serpin domain: insights into heparin binding. J Immunol Baltim Md 1950. 2010;184: 4982–4989. doi:10.4049/jimmunol.0902016

45. Kerr FK, Thomas AR, Wijeyewickrema LC, Whisstock JC, Boyd SE, Kaiserman D, et al. Elucidation of the substrate specificity of the MASP-2 protease of the lectin complement pathway and identification of the enzyme as a major physiological target of the serpin, C1-inhibitor. Mol Immunol. 2008;45: 670–677. doi:10.1016/j.molimm.2007.07.008

46. Krych-Goldberg M, Atkinson JP. Structure-function relationships of complement receptor type 1. Immunol Rev. 2001;180: 112–122.

47. Krych-Goldberg M, Hauhart RE, Subramanian VB, Yurcisin BM, Crimmins DL, Hourcade DE, et al. Decay accelerating activity of complement receptor type 1 (CD35). Two active sites are required for dissociating C5 convertases. J Biol Chem. 1999;274: 31160–31168.

48. Harris CL, Abbott RJM, Smith RA, Morgan BP, Lea SM. Molecular Dissection of Interactions between Components of the Alternative Pathway of Complement and Decay Accelerating Factor (CD55). J Biol Chem. 2005;280: 2569–2578. doi:10.1074/jbc.M410179200

49. Claire L Harris DMP. Decay-accelerating factor must bind both components of the complement alternative pathway C3 convertase to mediate efficient decay. J Immunol Baltim Md 1950. 2007;178: 352–9. doi:10.4049/jimmunol.178.1.352

50. Morgan BP, Boyd C, Bubeck D. Molecular cell biology of complement membrane attack. Semin Cell Dev Biol. 2017; doi:10.1016/j.semcdb.2017.06.009

51. Liszewski MK, Java A, Schramm EC, Atkinson JP. Complement Dysregulation and Disease: Insights from Contemporary Genetics. Annu Rev Pathol. 2017;12: 25–52. doi:10.1146/annurev-pathol-012615-044145

52. Merle NS, Noe R, Halbwachs-Mecarelli L, Fremeaux-Bacchi V, Roumenina LT. Complement System Part II: Role in Immunity. Front Immunol. 2015;6. doi:10.3389/fimmu.2015.00257

53. Hageman GS, Anderson DH, Johnson LV, Hancox LS, Taiber AJ, Hardisty LI, et al. A common haplotype in the complement regulatory gene factor H (HF1/CFH) predisposes individuals to age-related macular degeneration. Proc Natl Acad Sci U S A. 2005;102: 7227–7232. doi:10.1073/pnas.0501536102

54. Edwards AO, Ritter R, Abel KJ, Manning A, Panhuysen C, Farrer LA. Complement factor H polymorphism and age-related macular degeneration. Science. 2005;308: 421–424. doi:10.1126/science.1110189

55. Haines JL, Hauser MA, Schmidt S, Scott WK, Olson LM, Gallins P, et al. Complement factor H variant increases the risk of age-related macular degeneration. Science. 2005;308: 419–421. doi:10.1126/science.1110359

56. Klein RJ, Zeiss C, Chew EY, Tsai J-Y, Sackler RS, Haynes C, et al. Complement factor H polymorphism in age-related macular degeneration. Science. 2005;308: 385–389. doi:10.1126/science.1109557

57. Hovingh ES, van den Broek B, Jongerius I. Hijacking Complement Regulatory Proteins for Bacterial Immune Evasion. Front Microbiol. 2016;7. doi:10.3389/fmicb.2016.02004

58. Bennett KM, Rooijakkers SHM, Gorham RD. Let's Tie the Knot: Marriage of Complement and Adaptive Immunity in Pathogen Evasion, for Better or Worse. Front Microbiol. 2017;8: 89. doi:10.3389/fmicb.2017.00089

59. Zipfel PF, Hallström T, Riesbeck K. Human complement control and complement evasion by pathogenic microbes--tipping the balance. Mol Immunol. 2013;56: 152–160. doi:10.1016/j.molimm.2013.05.222

60. Lambris JD, Ricklin D, Geisbrecht BV. Complement evasion by human pathogens. Nat Rev Microbiol. 2008;6: 132–142. doi:10.1038/nrmicro1824

61. Garcia BL, Zwarthoff SA, Rooijakkers SHM, Geisbrecht BV. Novel Evasion Mechanisms of the Classical Complement Pathway. J Immunol Baltim Md 1950. 2016;197: 2051–2060. doi:10.4049/jimmunol.1600863

62. Skattum L, van Deuren M, van der Poll T, Truedsson L. Complement deficiency states and associated infections. Mol Immunol. 2011;48: 1643–1655. doi:10.1016/j.molimm.2011.05.001

63. Ram S, Lewis LA, Rice PA. Infections of People with Complement Deficiencies and Patients Who Have Undergone Splenectomy. Clin Microbiol Rev. 2010;23: 740–780. doi:10.1128/CMR.00048-09

64. Jönsson G, Truedsson L, Sturfelt G, Oxelius V-A, Braconier JH, Sjöholm AG. Hereditary C2 deficiency in Sweden: frequent occurrence of invasive infection, atherosclerosis, and rheumatic disease. Medicine (Baltimore). 2005;84: 23–34.

65. Munthe-Fog L, Hummelshøj T, Honoré C, Madsen HO, Permin H, Garred P. Immunodeficiency associated with FCN3 mutation and ficolin-3 deficiency. N Engl J Med. 2009;360: 2637–2644. doi:10.1056/NEJMoa0900381

66. Wright V, Hibberd M, Levin M. Genetic polymorphisms in host response to meningococcal infection: the role of susceptibility and severity genes. Vaccine. 2009;27 Suppl 2: B90-102. doi:10.1016/j.vaccine.2009.05.002

67. S Reis E, Falcão DA, Isaac L. Clinical aspects and molecular basis of primary deficiencies of complement component C3 and its regulatory proteins factor I and factor H. Scand J Immunol. 2006;63: 155–168. doi:10.1111/j.1365-3083.2006.01729.x

CHAPTER 2

Quantitative Modeling of the Alternative Pathway of the Complement System

2.1 Introduction

The complement system is one of our primary defense mechanisms that plays a vital role in coordinating immune responses. Complement function and regulation are induced by more than 30 distinct proteins present in plasma and on cell surfaces. The soluble proteins normally circulate as inactive precursors but once stimulated initiate cascades of biochemical reactions that propagate the activation of the complement system through three distinct pathways, the classical, lectin, and alternative pathways. The activation of these pathways leads to recognition and elimination of invading pathogens, recruitment of adaptive immunity, and facilitation of the removal of apoptotic cells [1–4]. Despite having similar roles, all three pathways have different sources for activation. The classical pathway is triggered by C1q binding to antigen-bound antibody complexes and also by direct attachment of C1q to pathogen surfaces. This leads to the production of C4b and C2a, which together form the C3 cleaving enzyme of the classical pathway, C4bC2a, called C3 convertase. Upon enzymatic cleavage, C3 is converted to the anaphylactic peptide C3a and opsonin C3b, which covalently attaches to cell surfaces via a thioester bond. The lectin pathway is activated by binding of mannose-binding lectin (MBL) with carbohydrate structures on bacterial and viral surfaces. This pathway is homologous to the classical pathway since the lectin pathway initiates complement cascade using MBL, a protein that is similar to C1q. The lectin pathway also forms the C3 convertase C4bC2a.

Finally, the alternative pathway activation starts in the fluid phase by the spontaneous hydrolysis of the internal thioester bond of C3 to form a molecule known as hydrolyzed C3, C3(H_2O). This molecule follows a cascade of reactions that involves complement proteins factor B and factor D to form the initial C3 convertase of the alternative pathway, C3(H_2O)Bb. This protease complex like its counterparts in the classical and lectin pathway also generates C3a and C3b fragments by cleaving C3. Once C3b attaches to the surface of the pathogen it plays a crucial role in initiating a robust AP activation that results in an amplification loop. The cleavage of C3 is the convergence point of all three activation pathways and the initiation point of the common pathway towards the formation of the membrane attack complex that produces a pore on the surface of pathogens to cause lysis. **Figure 2.1** shows the set of biochemical reactions involved in the alternative pathway through its initiation in the fluid phase, continued propagation on pathogen surface, and regulation on host cell.

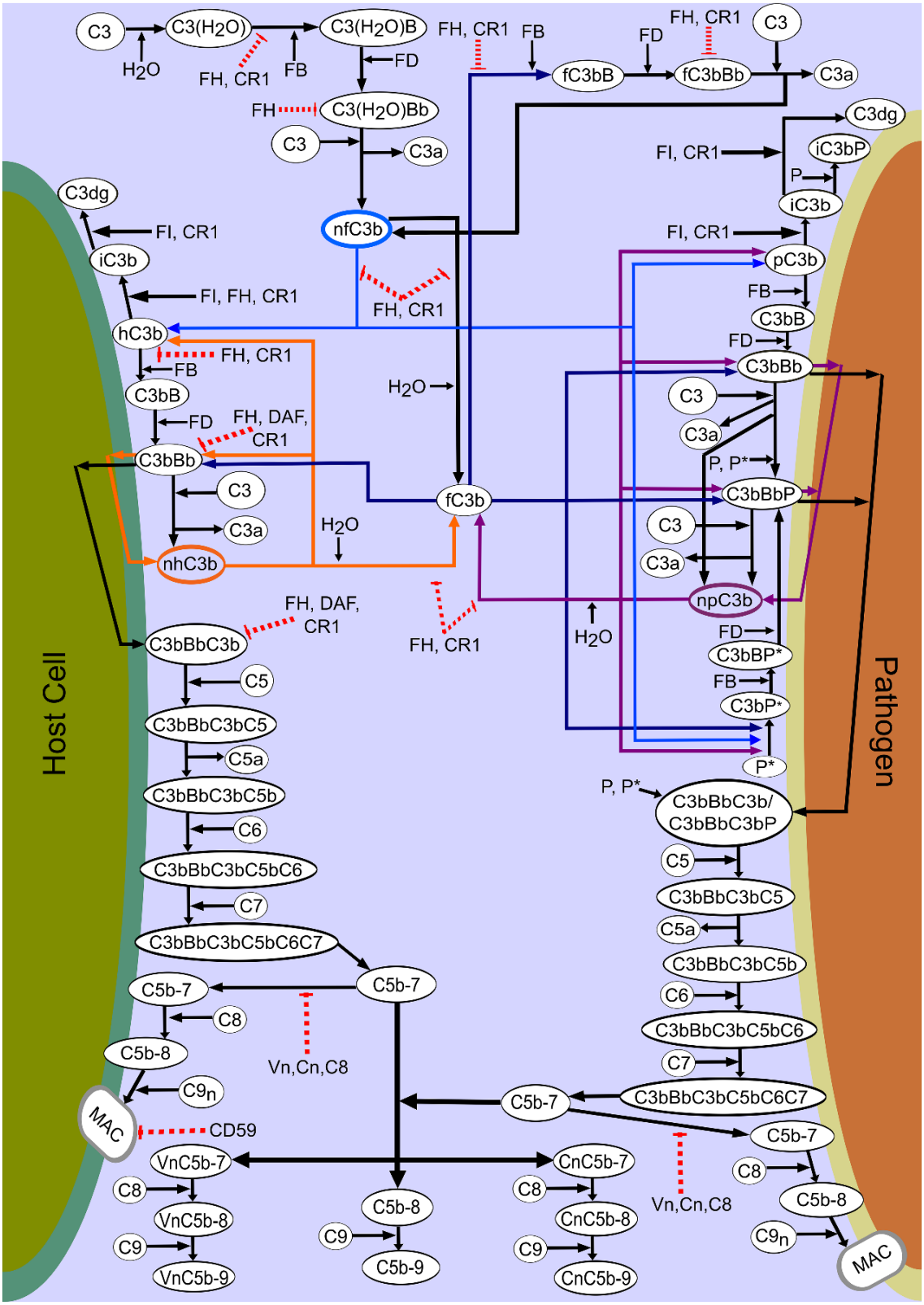
Host Cell
Pathogen
C3
C3(H2O)
C3(H2O)B
C3(H2O)Bb
H2O
FH, CR1
FB
FD
FH
C3a
fC3bB
fC3bBb
C3dg
FI, CR1
iC3bP
P
iC3b
nfC3b
pC3b
FI, FH, CR1
hC3b
C3bB
C3bBb
fC3b
C3bBbP
nhC3b
FH, DAF, CR1
npC3b
C3bBP*
C3bP*
P*
P, P*
C3bBbC3b
C3bBbC3b/ C3bBbC3bP
C5
C3bBbC3bC5
C5a
C3bBbC3bC5b
C6
C3bBbC3bC5bC6
C7
C3bBbC3bC5bC6C7
C5b-7
C8
C5b-8
C9n
MAC
CD59
Vn,Cn,C8
VnC5b-7
CnC5b-7
VnC5b-8
CnC5b-8
C9
C5b-9
VnC5b-9
CnC5b-9

Figure 2.1. The biochemical reactions of the alternative pathway. Fluid state activation of the alternative pathway leads to C3b that can indiscriminately bind to host or pathogen surface. On the right (pathogen), complement activity propagates without the disruption of regulatory proteins. On the left (host), plasma proteins in conjunction with surface-bound regulators actively inhibit complement propagation by disrupting complement interaction at different points of the alternative pathway. Abbreviations: C3, complement component 3; C3(H_2O), thioester-hydrolyzed form of C3; C3(H_2O)Bb, initial C3 convertase of AP; C3a, anaphylatoxin fragment from C3; C3b, activated fragment from C3; iC3b, inactivated C3b; nfC3b, nascent fluid phase C3b; nhC3b, nascent host C3b; npC3b, nascent pathogen C3b; fC3b, fluid phase C3b; fC3bBb, fluid phase C3 convertase, C3bBb, C3 convertase; C3bBbP, C3 convertase with properdin; C3bBbP*, C3 convertase with properdin* released from neutrophils; C5, complement component 5; C5a anaphylatoxin fragment from C5; C5b, activated fragment from C5; C3bBbC3b, C5 convertase; FB, factor B; FD, factor D; FI, factor I; CR1, complement receptor 1; DAF, decay-accelerating factor; Vn, vitronectin; Cn, clusterin; CD59, protectin. Lines and colors: solid lines with an arrow tip denote activation and dashed lines with a straight tip denote inhibition. Red line color denotes inhibition. The rest of line colors denote clusters of reactions involving different C3b molecules, i.e. nhC3b (orange), nfC3b (light blue), npC3b (purple), fC3b (dark blue).

Due to the detrimental effects of the complement system, a delicate balance must be kept between activation and inhibition to prevent host cell damage. The complement system is regulated through the actions of complement control proteins (CCPs), which are present in blood plasma and on the surfaces of host cells. In cases of impaired complement regulation, inadequate activation (or hyper-regulation) may cause susceptibility to infection, whereas excessive complement activation (or hypo-regulation) can harm host cells and tissues, resulting in autoimmune and inflammatory diseases. For instance, systemic lupus erythematosus (SLE) [2,5,6], atypical hemolytic uremic syndrome [5,7,8], paroxysmal nocturnal hemoglobinuria (PNH) [2,5], and age related macular degeneration [9,10] are all related to the malfunction of the complement regulation.

The complexity of the interplay between complement function and regulation makes mathematical modeling of the complement pathways an indispensable tool in understanding the dynamics of the biochemical reactions during activation and inhibition. Differential equations can be used to model the effects of complement proteins under pathological situations, such as protein deficiencies, sequence deletions, or amino acid mutations, and compare their effects on the global dynamics of the system. The goal of the present work is to mathematically model and interpret the dynamics of the biochemical reactions in the alternative pathway of the complement system during infections (pathogens) and homeostasis (host cells).

Earlier studies of mathematical modeling of the complement system began with the classical pathway in which the dynamics of the system were assumed to be linear [11]. A subsequent model was proposed in which the dynamics were assumed to be non-linear and

also included the alternative pathway [12]. A later work [13] was then performed on the classical and lectin pathways that also added an experimental study. Our study is the first to incorporate a comprehensive mathematical model that highlights the four time-dependent dynamic steps of the alternative pathway: (i) initiation (fluid phase), (ii) amplification (surfaces), (iii) termination (pathogen), and (iv) regulation (host cell and fluid state). We also have incorporated representative bacteria (*E. coli*) and representative host cells (human erythrocytes) to account for complement activation and regulation on different surfaces. In addition, our proposed model incorporates all the known complement regulatory proteins that act in the fluid phase, host cell membranes, and also exogenously on bacteria. Finally, we included neutrophil-secreted properdin in our dynamic system because neutrophils, once stimulated, they have the ability to release properdin (P*), the only known positive complement regulator that has been shown to bind to surfaces and initiate complement activation.

2.2 Results

2.2.1 Activation and propagation

Our model incorporates a set of rate equations that describes the biochemical reactions shown in **Figure 2.1**. The alternative pathway is activated by the tick-over reaction of C3 and leads to a C3b molecule that indiscriminately binds to host cells/pathogens and initiates a set of cascade reactions. **Figure 2.2** shows the percentage of host and pathogenic cell surfaces occupied by complement components, including C3/C5 convertases, C3b, iC3b, iC3bP, C3dg, P*, MAC, and all intermediate species like C3bB,

C3bBP, C5b6-7, C5b6-8, and others. A sigmoidal response is generated on the surface of pathogens that plateaus in 54 minutes. Preceding the robust activation, there was a lag phase of 11 minutes. Complement components occupy half of the available space on the pathogen surface in 24 minutes during the exponential phase of the sigmoidal response. However, due to the presence of complement regulators on host cells, significantly less than 1 percent of their surface is covered by complement components, as shown in **Figure 2.2**. Extended time profiles to 180 minutes are shown in **Figure A.1**. One of the main catalysts for the amplification loop in the alternative pathway is the production of C3 convertases that rapidly cleave C3 into C3a and C3b. **Figure 2.3** shows the response generated for the initial (fluid phase) convertase, $C3(H_2O)Bb$, and fluid phase convertase, fC3bBb. In 35 minutes, fC3bBb reaches a peak concentration of 4.6×10^{-13} M and starts declining to reach a concentration of 2.7×10^{-13} M in 60 minutes while $C3(H_2O)Bb$ reaches a concentration of 2.9×10^{-11} M in 35 minutes and continues to reach a concentration of 3.8×10^{-11} M in 60 minutes. Thus, $C3(H_2O)Bb$ seems to be the primary fluid phase convertase responsible for C3 cleavage, with significantly higher concentration than fC3bBb, despite possibly minor differences in their enzymatic activity against C3. Extended time frames to 180 minutes (**Figure A.2**), show that the concentration profile of both $C3(H_2O)Bb$ and fC3bBb flattens in 105 and 75 minutes, respectively, owed to the dissociation of Bb subunit and the regulatory action of FH that degrades formed convertases.

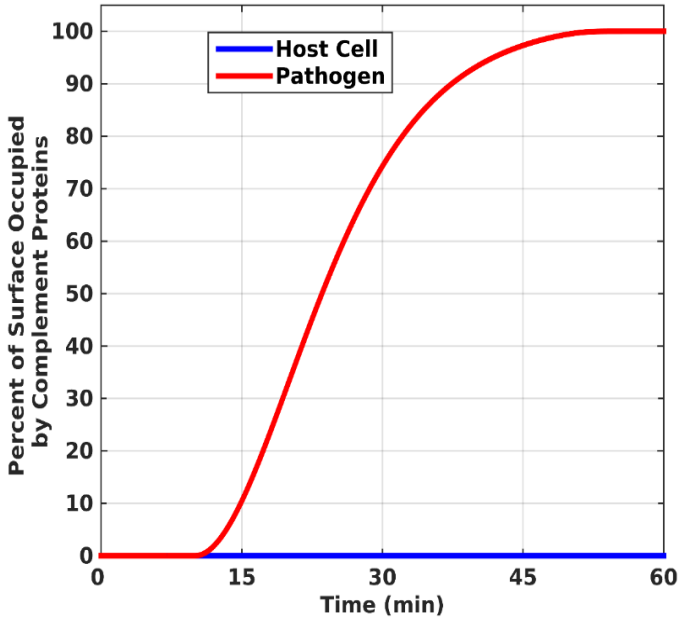

Figure 2.2. Complement deposition on pathogen and host surfaces. Saturation of pathogen surface is reached in 54 minutes with complement proteins such as C3b, iC3b, iC3bP (pathogen), C3dg, C3/C5 convertases, properdin (P*), MAC, and intermediates such as C3bB, C3bBP, C5b6-7, C5b6-8, and others. Propagation of the alternative pathway is inhibited on host cells resulting in complement proteins occupying significantly less than 1 percent**.**

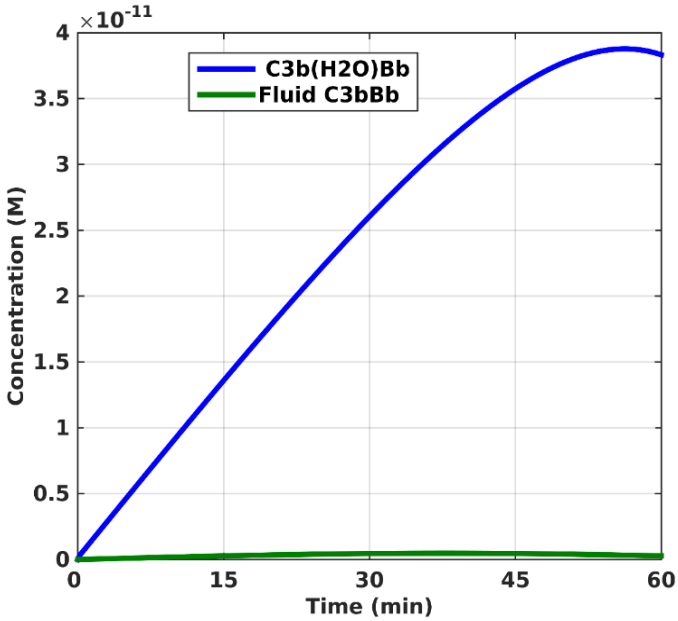

Figure 2.3. Concentration of assembled fluid phase convertases, C3(H_2O)Bb and C3bBb, of the alternative pathway. The time profiles show that the concentration of C3(H_2O)Bb increases significantly within 60 minutes compared to the concentration of C3bBb.

The cascade of reactions initiated by C3b also form convertases on the surface of pathogens and host cells as shown in **Figure 2.4.** Despite the presences of three types of convertases on the surface of pathogens (C3bBb, C3bBbP, and C3bBbP*), the properdin-initiated activation of the alternative pathway convertase, C3bBbP*, is the dominant C3 cleaving enzyme present. The asterisk means that properdin is secreted from neutrophils and binds to the surface first to act as an initiator of *de novo* formation of convertase, whereas lack of asterisk means that C3b binds first to the surface and initiates convertase formation. In 51 minutes, C3bBbP* occupies 2.7 percent of the pathogen surface while C3bBb and C3bBbP occupy significantly less than 1 percent. On the surface of host cells, C3bBb also occupies significantly less than 1 percent. The characteristic response of C3bBbP* production shows a lag phase of approximately 11 minutes followed by an accelerated production (surface occupational) phase. This phase starts slowing down after 53 minutes to eventually reach the decelerated occupational phase of the convertase. A similar characteristic response was also observed for pathogen-bound C3bBb but at significantly less than 1 percent occupation, if one zooms in **Figure 2.4** (zoom-in data not shown). Even in extended time frames of 180 minutes, all three convertases, (C3bBb-Pathogen, C3bBbP-Pathogen, and C3bBb-Host Cell), occupy significantly less than 1 percent (**Figure A.3**). However, the extended half-life of C3bBbP* highlights the intricate role P* plays for the amplification loop of the alternative pathway.

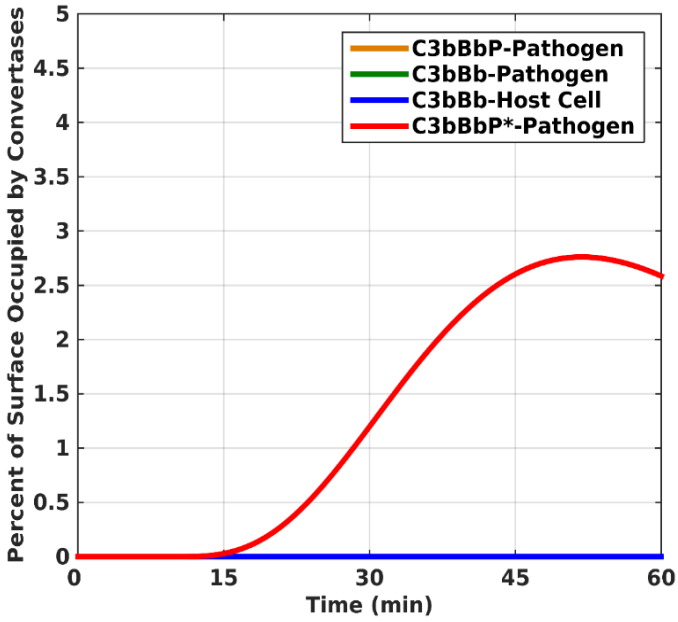

Figure 2.4. Formation of C3 cleaving enzymes on the surface of host cells and pathogens. C3bBbP* occupies 2.7 percent of the pathogen surface in 51 minutes. The asterisk denotes properdin released from neutrophils. The time profile of C3bBbP* shows a curve with a lag phase followed by an accelerated production (surface occupational) phase. The production of C3bBb and C3bBbP occupies significantly less than 1 percent on pathogens and even less on host cells. The orange and green lines are obscured by the blue line in the figure.

As concentrations of the surface bound convertases decreases over time due to the Bb subunit dissociating and C3 convertase enzymes becoming C5 convertases (C3bBbC3b), the formation of C3bBbC3b initiates the cleavage process of C5a from C5. The total amount of anaphylatoxins C3a and C5a produced from C3 and C5 convertases are shown in **Figure 2.5**. Within 60 minutes, C3a reaches a concentration of 7.6×10^{-8} M while C5a reaches 8.4×10^{-16} M (**Figure 2.5**). We can see from the response generated that the amount of C3a produced in 1 hour is 10^{8}times greater than C5a. However, C3a does plateau in 105 minutes with a concentration of 11.5×10^{-8} M while that of C5a reaches a concentration of 2.4×10^{-16} M within the same time frame (**Figure A.4**).

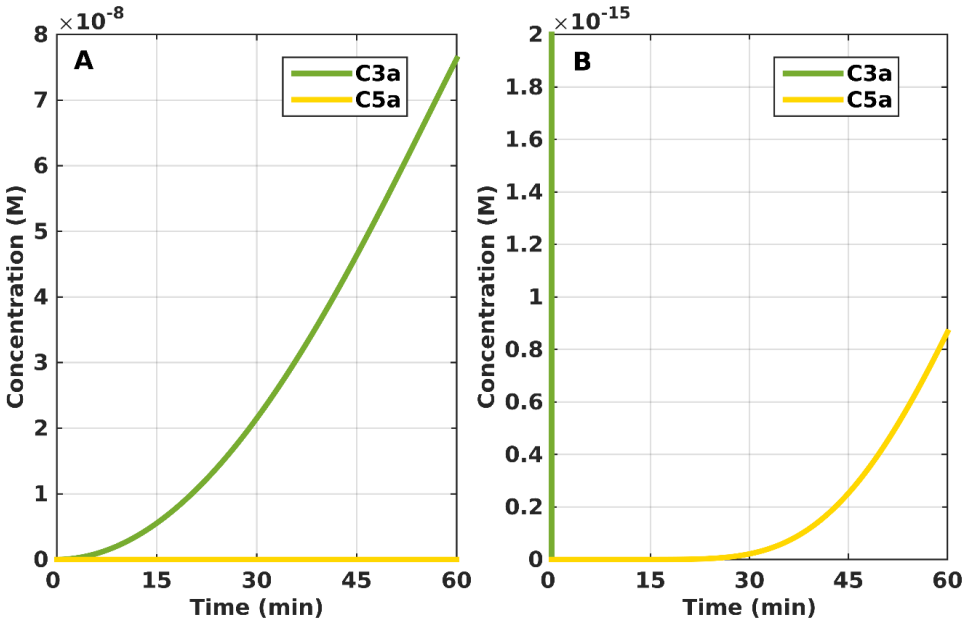

Figure 2.5. Time profile for the production of C3a and C5a. (A) The response generated for C3a shows a lag phase that is followed by an accelerated production phase. In 60 minutes, the amount of C3a produced is 10^8 times greater than that of C5a. (B) Zoom-in of panel (A) to show the time profile of C5a.

Surface-bound (host cell) and fluid phase regulators bind and act as cofactors for FI, which then cleaves C3b to its inactive derivative, iC3b. Factor I also further degrades iC3b into C3dg, through the intermediate C3c. The formation of iC3b and C3dg on pathogen surface is also possible due to the CR1 acting exogenously from the surface it is expressed. The final outputs of iC3b and C3dg are shown in **Figure 2.6**. Our data for surface-bound iC3b (**Figure 2.6A**) and C3dg (**Figure 2.6B**) shows that they account for significantly less than 1 percent of the pathogen and host cell surface.

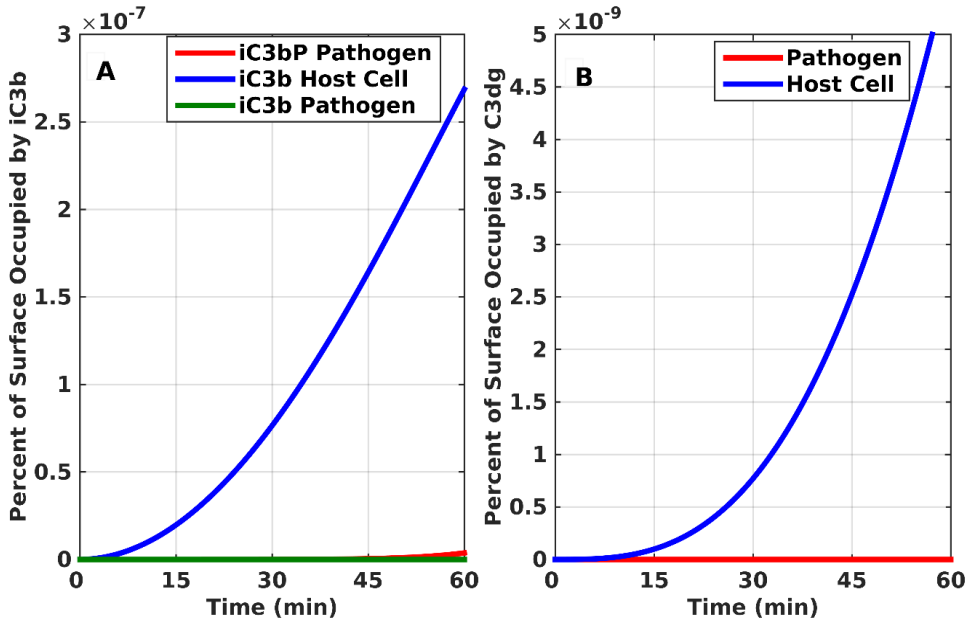

Figure 2.6. Time profile production for cleavage products of C3b. (A) iC3b. (B) C3dg. Both proteins take significantly less than 1 percent of pathogen and host cell surfaces.

After the formation of the C5 convertase, a cascade of reactions is initiated that forms MAC. This complex produces pores that render the pathogen/host cell amenable to lysis. In **Figure 2.7**, the amount of formed MAC pores occupies 3.3 percent of total pathogen surface, while taking significantly less than 1 percent on the surface of a host cell. The MAC pore production on pathogens is characterized by three phases: lag phase, production phase, and a steady state phase. The lag phase is 22 minutes long and is followed by a pronounced production of MAC pores that plateaus in 54 minutes. It is worth noting the time frame for MAC pore production to plateau is the same as the time frame for covering the entire pathogen surface (**Figure 2.7**) by complement components (**Figure 2.2**). Furthermore, this process highlights the rapidity of complement cascade that leaves no more than 3.3 percent of the pathogen surface for MAC pores to take root, also shown at extended time frames of 180 minutes in **Figure A.5**.

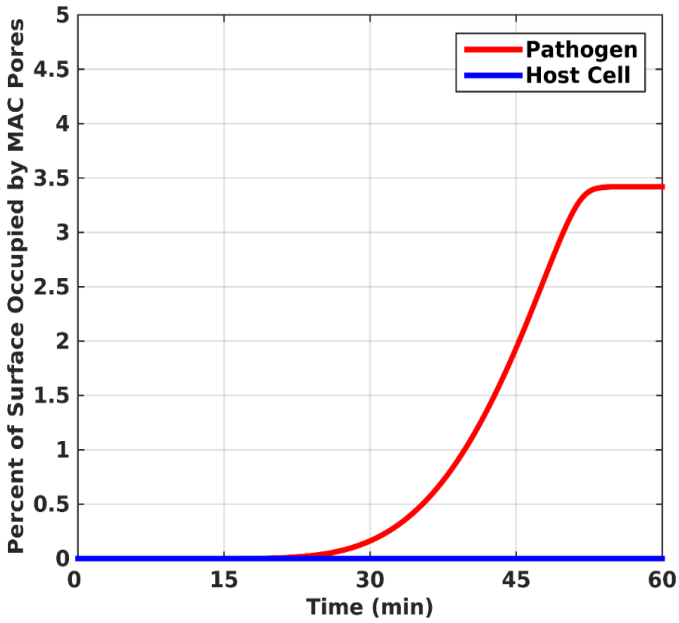

Figure 2.7. Formation of MAC pores are characterized by three phases: lag phase, production phase, and a steady state phase. The first 22 minutes present a lag phase that is followed by a rapid production of MAC pores, which plateaus in 54 minutes and occupies 3.3 percent of the pathogen surface. However, on host cells the MAC pores take significantly less than 1 percent.

The only positive regulatory protein of the complement system, properdin, has emerged more than a stabilizer of the C3 and C5 convertases. It has been shown as a molecule that distinguishably binds to specific cell surfaces and initiates complement activation [14–22]. To gain a deeper understanding on the role of neutrophil-secreted properdin (P*) during complement activation, we inhibited the ability of properdin (P*) to bind to surfaces and recruit C3b, but the stabilizing role of properdin (P/P*) on convertases was not inhibited. The results are shown in shown in **Figure 2.8**. Compared to **Figure 2.2** where the pathogen was fully saturated by complement components in 54 minutes, we see in **Figure 2.8A** that complement components account for significantly less than 1 percent of the pathogen surface. The key enzyme responsible for the robust activation of the alternative pathway is the assembly of the C3 convertase. We can see from **Figure**

2.8B that the convertase in its various forms also accounts for significantly less than 1 percent of the pathogen surface. In contrast, in **Figure 2.4**, the convertase assembled from properdin (P*) accounted for 2.7 percent of pathogen surface. Besides affecting the amplification loop of the alternative pathway, properdin (P*) also affects the end product of the terminal cascade, MAC pores. Compared to **Figure 2.7**, where MAC pores accounted for 3.3 percent of pathogen surface, **Figure 2.8C** shows that MAC pores take significantly less than 1 percent of the pathogen surface. Extension of the time frame beyond 60 min leaves the plotted surface areas in **Figure 2.8A–2.8C** at significantly less than 1 percent (data not shown).

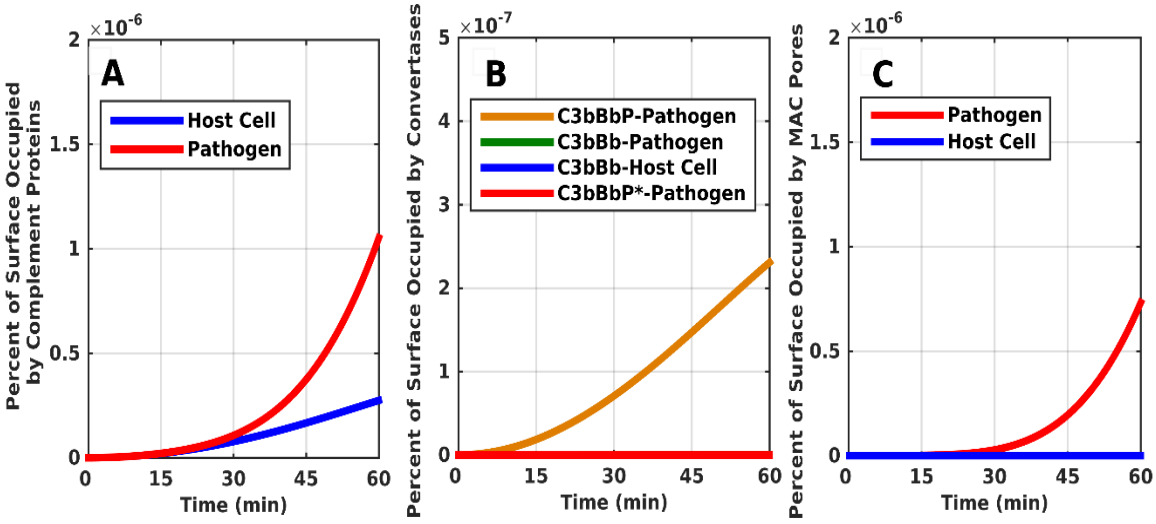

Figure 2.8. Time course for properdin (P*) as a stabilizer and not an initiator of the alternative pathway. (A) More than 99 percent of pathogen surface remains unoccupied by complement components. (B, C) The C3 convertases and MAC pores occupy significantly less than 1 percent on pathogens and even less on host cells.

2.2.2 Regulation (host cell and fluid phase)

Due to the destructive effects of the complement system on pathogens, the body has implemented several mechanisms to prevent its uncontrolled activation on host cells by using complement control proteins that are present in plasma and bound on host cell membranes. **Figure 2.9** presents the results generated for fluid phase (FH, Vn, Cn) and surface-bound (CR1, DAF, CD59) complement regulators. The time profile of the concentration of FH rapidly decreases (**Figure 2.9A**), while that of CR1 also decreases, but the decrease is not as rapid as FH. (**Figure 2.9B**). This is expected because despite the fact that both FH and CR1 regulate the initial complement protein of the alternative pathway, C3(H_2O), FH has a higher binding affinity. In addition to regulating the hydrolyzed C3 (C3H_2O), FH can also bind to C3bBb and C3(H_2O)Bb to promote their rapid decay. Regulatory proteins on host cell membranes, such as CR1 and DAF also inhibit the formation and/or promote rapid dissociation of convertases [23–25]. While the concentration of CR1 decreases (**Figure 2.9B**), that of DAF does not change (**Figure 2.9C**). This highlights how rapidly CR1 and FH inactivate C3b to inhibit the formation of the C3 convertases on host cells and also their continued complement regulation in the fluid state. The time profiles of FH, CR1, and DAF at extended timeframes are shown in **Figures A.6A–A.6C**. If the formation of the C3 convertase is tightly controlled, one can conclude that the terminal cascade will be effectively shut down because the formation of the C5 convertase will also be inhibited.

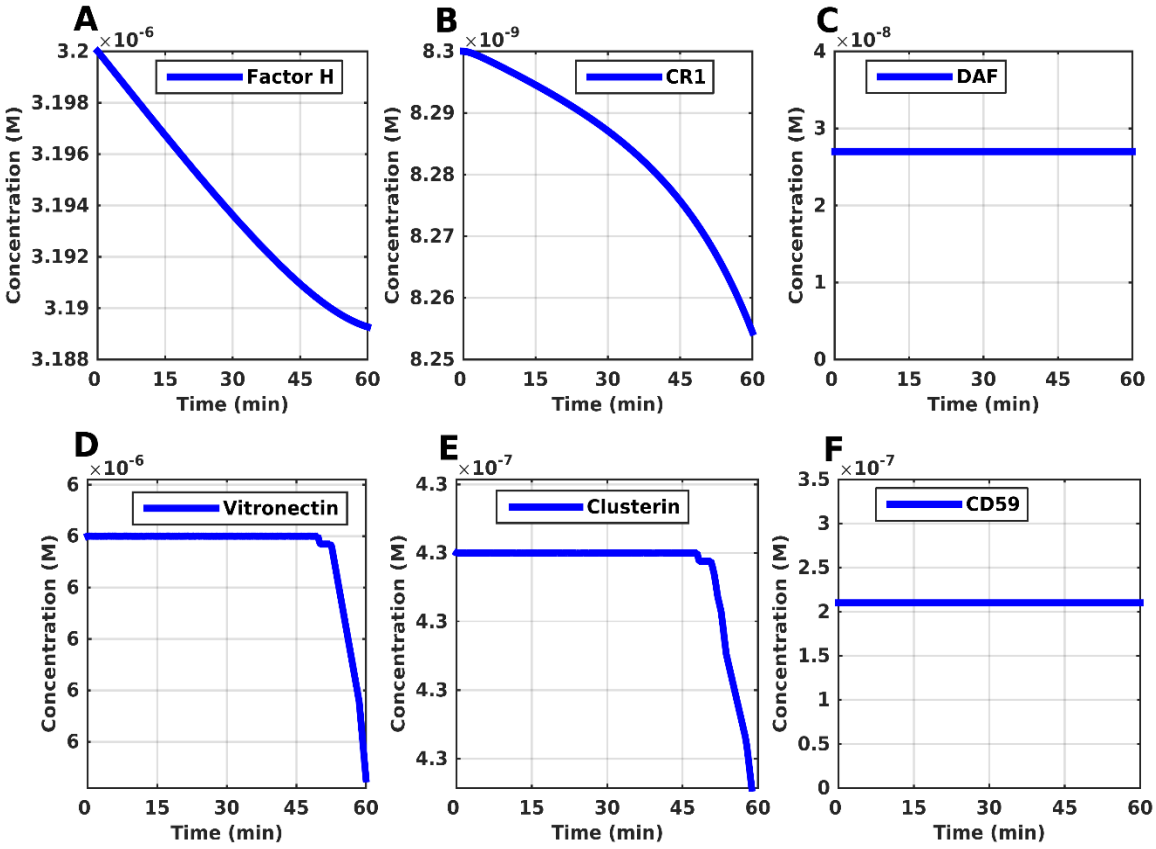

Figure 2.9. Time profiles for complement regulators FH, CR1, DAF, vitronectin, clusterin, and CD59. (A, B) The concentrations of FH and CR1 decrease, with FH showing initially a linear like response. The initial response of FH signifies the regulation taking root at the start of the AP by inhibiting C3(H_2O) and C3(H_2O)Bb. (C) The concentration of DAF remains constant and does not change, which highlights the rapid deactivation of any C3b by FH and CR1. (D,E) Vitronectin and clusterin experience a long delay of 52 and 51 minutes respectively before their concentration starts decreasing. Their regulatory component takes root at the formation of fluid C5b-7, which comes at a later stage of complement activation. (F) The response generated for CD59 is the same as that of DAF (no change in concentration). This is expected since DAF remains the same (inhibition of C3 convertase formation), the terminal cascade for MAC pore formation will not take root because formation C5 convertases will also be inhibited.

MAC production is inhibited on host cells by a combination of complement regulatory proteins that reside on host cells and in fluid phase. Vitronectin and clusterin are fluid phase regulators that inhibit MAC formation by binding to C5b-7, while CD59 inhibits C9 polymerization to prevent pore formation on the lipid bilayer of host cells [23–27]. **Figure 2.9D–2.9F** shows the time profiles generated for Vn, Cn, and CD59, respectively. Both Vn and Cn experience a long delay of about 52 and 51 minutes, respectively, before their concentration is reduced (**Figure 2.9D and 2.9E**). The lag response is expected because Vn/Cn inhibit C5b-7 from attaching to host cells and the production of C5b-7 comes at a later stage of complement activation. However, the concentrations of Vn and Cn do reach a steady state in 105 minutes and 124 minutes, respectively (**Figures A.6D and A.6E**). Lastly, the time profile generated for CD59 (**Figure 2.9F and Figure A.6F**) shows that its concentration does not change. This type of response is also seen for DAF. Since CR1 and FH inhibit the formation of C3/C5 convertases, the propagation of the terminal cascade is tightly controlled, thus effectively leaving no MAC pores to be regulated by CD59, under physiological conditions.

2.2.3 Sensitivity analysis

Multi-parametric sensitivity analysis (MPSA) was used to identify initial complement concentrations and kinetic parameters that are critical for the four dynamic steps of the alternative pathway. **Table A.1** shows the results of the relative sensitivity of the initial concentrations on the surface of pathogens and host cells. C3, the central protein of the alternative pathway, strongly influences the response of the system, in contrast to initial concentrations of all other complement components that have low sensitivities. This is likely due to the fact that C3 cleavage is required for both activation and amplification of the alternative pathway, and thus most rates and kinetic parameters are dependent on the amount of C3 in the system. Next, sensitivity analysis was performed in order to identify the critical kinetic parameters for the output of the model. The results are shown in **Figure 2.10** and indicate that while responses on both host cells and pathogens are mildly influenced by most of the kinetic parameters, the association rate constant of properdin (P*) to the surface of pathogens and the rate at which neutrophils release properdin (P*), are greatly important for the activation and amplification of the alternative pathway on pathogen surfaces. In addition, complement response on host cells was more sensitive to parameters involving fluid-phase reactions compared to surface-bound reactions. These rates include association rate constant of Factor H to fluid C3(H_2O), formation of fC3b from nfC3b (half-life of the thioester bond), and the Michaelis-Menten constants that govern the cleavage rate of C3 by the fluid phase convertase, C3(H_2O)Bb. Thus, the response of the system is sensitive to the parameters $k^{+}_{\mathrm{P*surface}}$, $k^{+}_{\mathrm{p*released}}$, $k^{+}_{\mathrm{C3(H_2O)}}$, k^{+}_{fC3b}, and k_{cat}, and K_{m} of C3(H_2O)Bb.

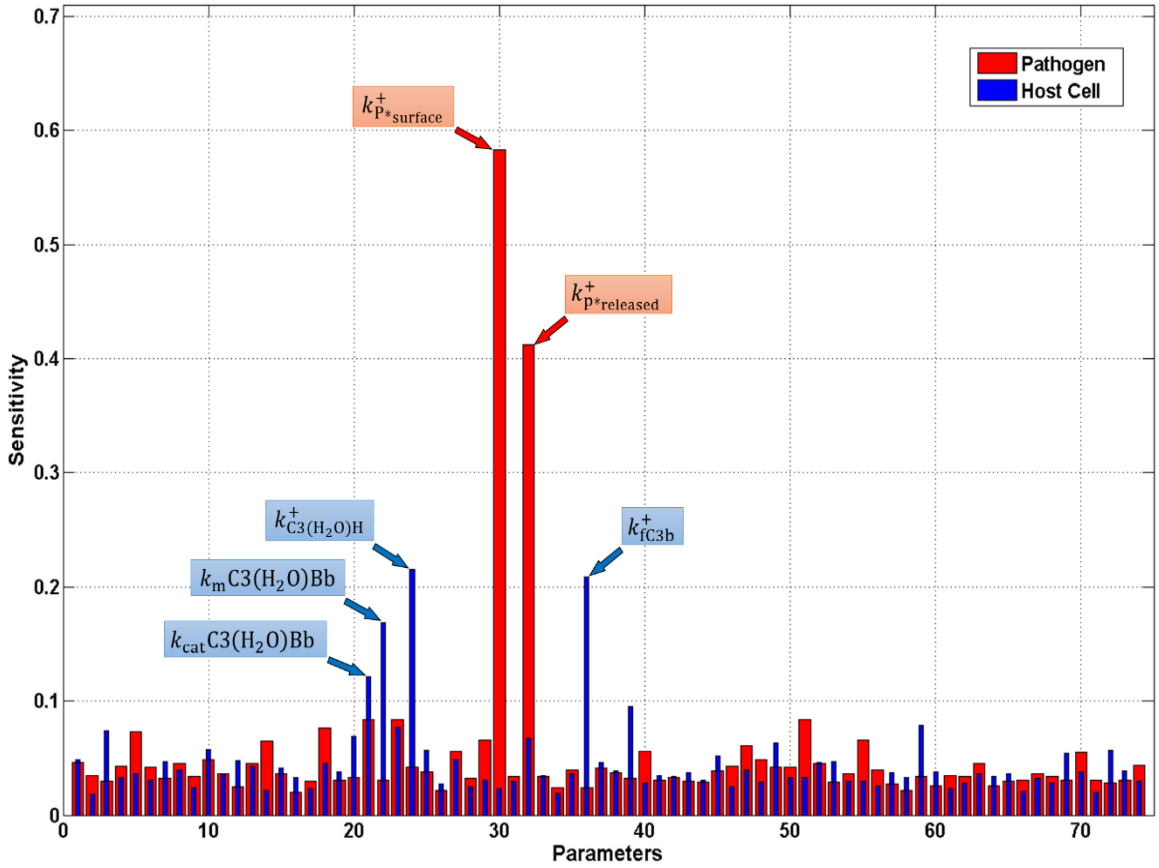

Figure 2.10. Results of global multi-parametric sensitivity analysis to kinetic parameter values. The most sensitive rates on the surface of pathogens (red) are $k^+_{P^*surface}$, and $k^+_{p^*released}$, which represent the rate at which properdin associates to the surface and the rate at which it is released from neutrophils, respectively. While most kinetic parameter are mildly sensitive on host cells (blue), $k^+_{C3(H_2O)}$ and k^+_{fC3b} ,which represent association of factor H to hydrolyzed C3 and conversion rate of nfC3b to fC3b, respectively, are more sensitive to parameter variations. The Michaelis–Menten kinetic parameters, k_{cat} and K_m of the fluid phase convertase $C3(H_2O)Bb$ are also sensitive.

2.3 Discussion

We have developed a mathematical model that describes the dynamics of the alternative pathway of the complement system, initiating in fluid phase with activation of C3, surface-bound amplification of C3b and C3b-contaning convertase formation, and terminating at surface-bound MAC (**Figure 2.1**). We modeled two surfaces, a host cell and a bacterial cell surface, using an erythrocyte and an *E coli* cell as examples for

quantification. Cells were used as a basis for extracting dimensions, without accounting for cell surface markers and chemical compositions. We have also incorporated in the model complement regulation in fluid phase and on host cells. The mathematical model consists of a system of 107 ordinary differential equations, describing the time course of the concentrations of 107 proteins, protein fragments, or protein complexes, and we have generated graphs of their concentration time profiles. We have asked questions of the type: (i) What are the quantitative contributions of different modules of the alternative pathway propagation, such as fluid phase activation, the amplification loop, and terminal cascade beyond C3 and C5, in generating opsonins, inflammatory proteins C3a/C5a, and MAC? (ii) What is the difference in complement deposition on pathogen and host cells? (iii) What are the subtleties of negative and positive complement regulation in inhibiting or promoting complement deposition on host and pathogen cells, respectively.

We present key differences in complement function on pathogen and host surfaces, demonstrating the significance of negative complement regulation on host surfaces. We also present the tremendous influence of properdin (P*) in positive complement regulation on pathogen surfaces, and discriminate the contribution of different types of properdin (P, P*) molecules in eventually promoting MAC formation.

We have shown the efficiency of the alternative pathway in saturating the surface of pathogen with complement proteins, such as C3/C5 convertases, C3b, iC3b, iC3bP (pathogen), C3dg, properdin P*, and MAC, while regulation on host cells limits complement component deposition to less than 1 percent (**Figure 2.2**). The response generated on host cells is expected due to the function of surface-bound or circulating

regulatory proteins to ensure inhibition on host cells, while not hindering activation on pathogens. Convertases play a critical role in the propagation and amplification of the alternative pathway. The initial alternative pathway convertase, C3(H_2O)Bb, is a fluid phase convertase that cleaves C3 into C3a and C3b [28]. This nascent C3b, nC3b, is a very reactive complement protein due to its exposed internal thioester bond that is capable of indiscriminately binding to pathogens and host cells via covalent bond [29–31]. However, the short half-life of the thioester (60 μsec) ensures most of the nC3b produced will interact with water and form the fluid phase C3b, fC3b, that never attaches to a surface [32]. This fC3b can also form a convertase that is capable of cleaving C3 in the fluid phase. Due to the dangers these fluid phase convertases present if left unregulated, complement regulatory proteins promote their rapid decay, both in fluid phase and on host cell surfaces. In **Figure 2.3**, we see the concentration of fC3bBb is smaller than that of C3(H_2O)Bb. This is because only one complement protein, FH, regulates C3(H_2O)Bb, while fC3bBb is regulated by FH and CR1 [28,33–39]. However, the possibility for C3(H_2O)Bb regulation by CR1 cannot be excluded because it has been shown that CR1 can bind to C3(H_2O) [40]. In addition, we must exercise caution in interpreting the results for C3(H_2O)Bb activity, as sensitivity analysis showed that complement activation on host cells is influenced by the Michaelis-Menten kinetic parameters of this enzyme. In any case, CR1 and FH regulate AP by (i) competitively binding to C3b, (ii) inhibiting FB binding, and (iii) by accelerating the decay rate of convertases.

If the nascent C3b reacts and forms a covalent bond on either the pathogen or host surface, it will associate with FB, which becomes cleaved by FD to yield the membrane-

bound C3 convertase, C3bBb [41–44]. **Figure 2.4** shows difference in the amount of area these convertases occupy on the host cells and pathogens. The destructive effects of complement activation on host cells are tightly regulated through surface-bound regulators such as CR1, DAF, and plasma proteins such as, FH in conjunction with FI [33,36,37,39,45–47]. However, these regulators leave complement activation unchecked on the surface of pathogens. Furthermore, it is also evident from **Figure 2.4** that C3bBbP* is the more dominant convertase than C3bBb and C3bBbP. (Note that the asterisk denotes properdin released from neutrophils which binds to the surface first and acts as an initiator of *de novo* formation of convertase, whereas lack of asterisk means that C3b binds first to the surface and initiates convertase formation, subsequently stabilized by properdin.) While C3bBb is relatively unstable with a half-life of about 90 seconds, the positive regulatory protein, properdin, associates with C3bBb [41,48], which stabilizes and increases the half-life of the convertase by about 10 fold. However, it has been shown that properdin bound to a surface can initiate *in situ* complement activation by forming C3bBbP* [14–22]. And unlike the standard AP activation through nC3b attaching to a surface and initiate complement, properdin (P*) can attach to a surface and recruit nC3b or fC3b to form C3 convertase.

The cleavage of C3 and C5 by their respective convertases also produces complement fragments C3a and C5a. They belong to a family of anaphylatoxins that are released into the fluid phase during complement activation [49,50] (**Figure 2.5**). But there are differences in amount released, with C3a being more abundant than C5a (**Figure 2.5A**). This stems from having more C3 convertases on the surface of the pathogen/host cell than

C5 convertases that are responsible for generating C5a. In addition, the large number of C3 cleaving enzymes can be attributed to properdin (P/P*) stabilizing preformed C3bBb, and also by neutrophil-secreted properdin (P*) that can accelerate the association of C3b and FB to subsequently form a stabilized convertase, C3bBbP*. However, C5 can also be cleaved by the monomeric C3 convertase (C3bBb) but has been shown to have a weak affinity for C5 (K_m = 24 μM) [51]. In the absence of control factors, the monomeric C3 convertase will cleave 9000 C3 molecules for every C5 molecule cleaved [52,53]. While both fragments play an important role in mediating inflammatory response, C5a is a more potent mediator than C3a. Furthermore, C5a is also a potent chemoattractant for neutrophils, T cells, and tonsillar B cells [54–56]. It is likely that because of the strong C5a effect in inducing a more pronounced inflammatory response compared to C3a, less of C5a is released during complement activation to achieve the desired response (**Figure 2.5B**).

In **Figure 2.6A**, we present the response of the inactive derivative of C3b known as iC3b on the surface of pathogens and host cells. Surface-bound regulator CR1 binds to C3b and acts as a cofactor for FI cleavage of C3b into iC3b [37–39]. In addition, CR1 is the main cofactor for FI mediated enzymatic breakdown of membrane-bound iC3b into C3dg (**Figure 2.6B**). However, CR1 is unique in its ability to also function extrinsically (on surrounding cells), from the cell in which it is expressed [25,57,58]. This explains that even though pathogens lack membrane-bound complement inhibitor CR1, the inactive derivative iC3b and subsequently C3dg are present on pathogen surface. Although iC3b and C3dg are inactive in forming convertases and contributing to the propagation of

complement activation, their deposition on pathogen cell surfaces is critical for efficient phagocytic clearance and enhancement of adaptive immune response.

Continued activation of the alternative pathway leads to the terminal cascade that is responsible for the production of MAC. This terminal multi-component C5b-9_{18} complex forms pores on the surface of a pathogen/host cell, which causes lysis due to disruption of the osmotic balance inside/outside the cell. The MAC pores occupy significantly less than 1 percent on the surface of host cell because of regulators that are present in fluid phase and also bound to the surface (**Figure 2.7**). For instance, Vn and Cn are fluid phase regulators that bind to C5b-7 and inhibit its insertion into the lipid bilayer [59,60]. Surface-bound regulators such as CD59 inhibit polymerization of C9, while DAF and CR1 accelerate the decay of C5 convertase by altering the interaction between C3bBb [27,45–47,61]. However, the absence of these regulatory proteins on pathogens leads to unchecked terminal cascade activation that results in 3.3 percent occupation of the pathogen surface by MAC pores (**Figure 2.7**).

An important aspect of our study is the re-emergence of the role of properdin in complement function. Properdin is more than a stabilizer of the C3/C5 convertase by its role in initiating *in situ* complement activation on different surfaces. The role of properdin as an instigator of the alternative pathway was first described by Louis Pillemer and his associates over 50 years ago [62]. This idea of properdin-directed activation was challenged by Robert Nelson, who suggested the role of antibodies in explaining the observed complement activation [63]. By eliminating the surface binding ability of neutrophil-secreted properdin (which also inhibits C3b recruitment) and keeping its

convertase stabilizing role, we observe that complement activation products occupy significantly less than 1 percent of pathogen surfaces, as shown in **Figure 2.8A–2.8C**. Our results show that eliminating properdin's (P*) surface binding and C3b recruitment abilities effectively reduced propagation of the alternative pathway. In addition, results from the sensitivity analysis showed that the response of the system is sensitive to the surface binding ability of properdin (**Figure 2.10**). Binding to surfaces is soon followed by the recruitment of C3b, to form convertases. This sets in motion the amplification loop, which is very important for the propagation of alternative pathway. The key substrate that makes this step possible is C3, and is also indicated by the results of the sensitivity analysis as the most important complement component (**Table A.1**). Thus, the widely-accepted role of properdin as just a stabilizer of convertases is not sufficient to support robust propagation of the alternative pathway. To highlight this point, a study by Gupta-Bansal et al [64] showed that anti-properdin MoAbs that blocked binding of properdin to C3b caused a dose-dependent inhibition of AP in vitro.

It is interesting to note that studies performed in serum-derived properdin, in which long term storage, freezing, and thawing were involved, formed highly activated properdin aggregates that not only stabilized convertases but also activated complement in solution [21,65]. However, a recent finding showed serum-derived properdin (without aggregates) was able to attach to activated platelets and recruit both C3b and C3(H_2O) to generate C3 convertases (C3bBb and C3(H_2O)Bb), thus initiating complement activation on the surface [20]. In addition, properdin bound to activated platelets was 3- and 2-fold more capable of recruiting C3b and C3(H_2O), respectively, compared with activated platelets alone. The

same study also showed platelets that first received C3(H_2O) or C3b, only formed convertases after properdin was recruited. Although these studies used serum properdin, our results are consistent with their data because robust propagation of AP (by forming convertases) was achieved only after properdin that had the ability to bind to surfaces and recruit C3b was added. This event was considered in our system for neutrophil-derived properdin (P*), while serum-properdin (P) only stabilized convertases. Our multi-parametric sensitivity analysis indicates that kinetic parameters associated with C3(H_2O) and C3b are sensitive to variations (**Figure 2.10**), thus making the fluid phase a pivotal battlefront for protecting/shielding host cells.

Gupta-Bansal et al [64] also used the anti-properdin antibody to inhibit activation of AP and reduce neutrophil and platelet activation in their cardiopulmonary bypass model. We believe the reduction of neutrophil activation is an important step because after neutrophils are stimulated they have the ability to not only release properdin (P*) but also release C3, FB, C6, and C7 [22,66–68]. In the presence of FD, properdin (P*) and the released C3, FB, C6, and C7 constitute all the components needed for the activation of the alternative pathway and terminal cascade with the generation of C3 and C5 convertases. This was shown on activated platelets after the release of properdin (P*) from neutrophils [20]. Conceivably, this observation may explain why Gupta-Bansal et al [64] saw reduced neutrophil activation and near complete inhibition of the C3a/C5b-9 formation with the anti-properdin antibody.

It is worth noting that in a standard AP hemolytic assay, T cell-derived properdin was shown to be 100 times more functionally active than serum-derived properdin [69].

Just as nC3b is an active form of C3 that must be constantly regulated to prevent unnecessary complement activation, the more active properdin (P/P*) must also be regulated. In light of the aforementioned recent findings, we speculate that the body constantly regulates properdin (P*) by only releasing it at sites of infection (inflammatory response) or by protease cleavage of functional sites that are involved in surface binding/C3b recruitment. Even serum properdin (P), was only able to bind to activated platelets (present during inflammation) and not resting platelets. However, to the best of our knowledge, there are no studies that describe how the body regulates properdin (P/P*).

The notion of properdin as a positive regulator of AP by stabilizing convertases must be re-examined. We speculate, in conjunction with experimental data cited above, that for the occurrence of robust activation and propagation of the alternative pathway, properdin either derived from serum or neutrophils must satisfy three criteria: (i) ability to bind to surfaces, (ii) ability to recognize selective patterns (activated *versus* nonactivated platelets), (iii) recruitment C3b/C3(H2O) and FB by properdin-bound surface to initiate complement activity. We believe all three criteria must be met and the sole role of stabilizing convertases is not enough to warrant properdin as a positive regulator of the alternative pathway. This is predicted by our model and is highlighted in the literature cited above. This notion also is consistent with what Pillemer and his colleagues observed over 50 years ago.

2.4 Conclusions

We have presented a comprehensive mathematical model that describes the dynamics of the alternative pathway of the complement system, including activation, amplification, termination, and regulation. Our study quantitatively explains many known features of the complement system, but also reveals some less obvious or unexpected features. We have shown the profound differences of complement deposition on pathogen surfaces and MAC pore formation, compared to host surfaces. This result demonstrates the fine balance between activation and negative regulation during homeostasis, and the significant role of positive regulation in augmenting activation on pathogen surfaces. Complement deposition refers to C3b, iC3b, iC3bP (pathogen), C3dg, C3/C5 convertases, P*, MAC, and intermediates such as C3bB, C3bBP, C5b6-7, C5b6-8, and others. We have also shown many other features, described below. The initial C3 convertase of the alternative pathway, $C3(H_2O)Bb$, has higher influence in the propagation of the alternative pathway, compared to the fluid phase C3 convertase, fC3bBb, suggesting the importance of the tick-over reaction in not only initiating, but also dominating the fluid state. Significantly higher concentrations of C3a are produced during the alternative pathway than C5a. The amounts of various forms of fluid phase or surface-bound C3b (nfC3b, nhC3b, npC3b, fC3b), and surface (pathogen or host) bound iC3b and C3dg are miniscule compared to those of fluid phase iC3b and fluid phase C3dg. Finally, neutrophil-secreted properdin (P*) re-emerges as an intriguing factor of complement activation, in addition to existing serum properdin (P) that is a C3/C5 convertase stabilizer. Properdin P* is a function enhancer by recruiting C3b ligand and FB to form a stabilized convertase,

C3bBbP*, and also stabilize preformed C3/C5 convertases. The function of C3b as an opsonin is well-recognized, but our model highlights an alternative opsonin comprised of properdin (P*) and C3b (C3bP*), that may also serve as a pathogen tag. Our study suggests that the role of properdin (P*) in complement activation and positive regulation requires more experimental attention.

In conclusion, expanding on a characterization of C3 by a *Nature* Editorial [70], we consider the complement system as a sophisticated and well regulated "bloodstream patrol" that aims at attacking and possibly eliminating foreign bodies, while being controlled from harming self-tissues. A quantitative understanding of the intricacies and sophistication of the dynamics of complement activation, function, and regulation, as well as the mechanisms of inhibition by pathogens, will be an indispensable aid in the development of therapeutics targeting pathogenic infections, autoimmune and inflammatory diseases, and incompatibilities with biomaterial surfaces in the case of prosthetics and devices.

2.5 Methods

2.5.1 Numerical methods

Reactions in the alternative pathway of the complement system were formulated based on known interactions and kinetic parameters from the literature (**Figure 2.1** and **Table A.2**). Based on these reactions, we generated a system of 107 ordinary differential equations and 74 kinetic parameters that describes the alternative pathway of the complement system (**Supplemental Equation A.1**). We have organized the biochemical reactions, equations, and subsequent discussion into four parts, which describe

the following four modules of complement system activation and propagation: (i) initiation (fluid phase), Eqs 1–8 in **Supplemental Equation A.1**; (ii) amplification (pathogen), Eqs 1–18 in **Supplemental Equation A.1**; (iii) termination (pathogen), Eqs 1–19 in **Supplemental Equation A.1**; and (iv) regulation (host cell and fluid phase), Eqs 1–42 in **Supplemental Equation A.1**. In addition, we have grouped all the complement proteins present in fluid phase and bound on host cells into a fifth module, Eqs 1–20 in **Supplemental Equation A.1**. Law of mass action was used to assemble the equations. Enzymatic reactions were based on the Michaelis–Menten kinetics, and substrate competitions for enzymes such as C3 convertases was also taken into consideration. Known kinetic parameters were acquired from literature, while unknown parameters were attained via several different approaches. First, we implemented parameters estimated from Korotaevskiy et al [12], which used optimization procedure (combines solving of direct and inverse optimization problems) to estimate rate constants. Some parameters were implemented based on interactions of structurally or functionally homologous proteins, for which parameters are already known. For example, the rate constants of the interaction between C3b and FB are known, while those of C3(H_2O) and FB are not. However, we assumed the same rate constants for the second case because C3(H_2O) is known to be a C3b-like molecule that also has C3b-like functions. Remaining unknown parameters were estimated based on association and dissociation constants. For instance, since $K_D = k^- / k^+$, if the K_D was known, we implemented a combination of k^- and k^+ that would generate the given K_D based on physically relevant ranges of parameters (k^+: 10^3 to 10^9 $M^{-1}s^{-1}$, k^-: 10^{-1} to 10^{-5} s^{-1}) [71–73]. These parameter combinations were tested and determined their

effects on the dynamics of the system to be negligible in all cases **(Figure 2.10**). The remaining (9) parameters were completely unknown, and values were estimated based on functional data for other complexes and constrained according to physiological ranges of association and dissociation rate constants. Two of these parameters have a profound effect on the response of the system and are discussed in the Results and Discussion sections. Initial concentrations of soluble complement components were obtained from literature, based on known homeostatic concentrations of these factors in human plasma (**Table A.3**). Furthermore, properdin released from neutrophils has been shown to be more active by initiating the alternative pathway through recruitment of C3b and FB, while the plasma properdin does not. Therefore, we have included neutrophil-secreted properdin in our model, referred with an asterisk (properdin P*). In addition, neutrophil-derived properdin (P*) concentration was estimated based on [22,74]. Cell-bound complement protein concentrations were estimated based on [75]. Lastly, a delay of 10 minutes was incorporated into our model (for neutrophil-secreted properdin) to account for neutrophil transmigration from the vasculature to the site of infection [76].

Production of complement components was neglected in our model (with the exception of properdin P*), since we examined only the short time frame following pathogen recognition. All equations were solved using the ode15s solver in Matlab (Mathworks, Natick, MA). Since complement activation is localized on cell surfaces, we included representative pathogen and host cell species in our model. We used human erythrocytes as a model host cell, due to the availability of information regarding cell dimensions [77] and densities of complement receptors [75]. *Escherichia coli* was used as

the representative pathogen cell. Cell number densities were selected based on the homeostatic number of erythrocytes per milliliter of blood (5×10^9 per ml) and the typical number of bacteria found in blood during sepsis (10^2–10^5 per ml) [78,79]. In order to model complement deposition on cell surfaces, we first calculated a theoretical maximum number of binding sites for complement proteins and complexes, based on the dimensions of cells and the various complement species. For instance, we acquired the area that C3b would occupy on the surface from literature and used this area as basis to estimate the area occupied by C5b-7 (due to the lack of literature data) [80]. The number of binding sites was translated into a concentration, by multiplying the cell number density. Reaction rate constants for complement species with available cell binding sites were derived based on rates of diffusion in blood and species inactivation (i.e. C3b thioester hydrolysis and C5b-7 spontaneous micelle formation) (**Supplemental Equation A.2**). Furthermore, in order to account for complement amplification and deposition on pathogen surfaces, an apparent concentration of nascent C3b and cell binding sites was calculated, based on the hemispheric region in which C3b molecules can diffuse before thioester hydrolysis (the radius and corresponding volume of this region was calculated based on thioester half-life). In this hemispheric region, scaling factors were calculated so that in this way a nascent C3b molecule from a surface-bound convertase is much more likely to attach to the cell surface compared to a nascent C3b molecule from a fluid phase convertase. Nascent C5b-7 was treated in the same way, according to the half-life of the C5b-7 hydrophilic-amphipathic transition. All the parameter data can be found in **Table A.2**. Reaction rate constants that were acquired from literature are cited in **Table A.2**, including those determined through

optimization procedure. Parameters attained through structural/functional homologous interactions and association/dissociation constants are marked in **Table A.2** as estimation, while parameters that are completely unknown are marked as assumptions. Lastly, reaction rate constants calculated through the diffusion/species inactivation are also marked as such.

2.5.2 Initiation (fluid phase)

Activation of the alternative pathway initiates in plasma by the spontaneous hydrolysis and activation of the complement component C3. Turnover of C3 is the critical step in the activation of the alternative pathway. The tick-over of C3 generates C3(H_2O), a C3b-like molecule that has a hydrolyzed internal thioester bond (**Figure 2.1**). This molecule then associates with Factor B to produce C3(H_2O)B. This initial convertase complex is prone to enzymatic cleavage by Factor D, resulting in the production of C3(H_2O)Bb. This protease is a short-lived fluid phase convertase that cleaves C3 into a smaller fragment C3a and larger fragment C3b (**Figure 2.1**). C3a plays an important role in mediating inflammatory responses including vasodilation, histamine release from mast cells, smooth muscle contraction, and also antimicrobial activity during complement activation [81,82], and is one of the terminal complement activation products in our model. The larger product of C3 cleavage, nascent fluid-phase C3b (nfC3b), is a very reactive protein due to its exposed internal thioester bond that is capable of indiscriminately binding to different surfaces via covalent bond [29–31]. However, the short half-life of the thioester (60 μsec) ensures most of the C3b produced interacts with water and form the fluid phase C3b (fC3b), which loses its ability to covalently attach to cell surfaces [32].

2.5.3 Amplification (pathogen surface)

If the nascent C3b reacts and forms a covalent bond on the pathogen surface (pC3b), it also follows the same reaction scheme of the fluid phase C3(H_2O) by associating with FB and leading to the cleavage by FD to yield the surface-bound C3 convertase, C3bBb. This complement enzyme sets in motion the amplification loop of the alternative pathway by cleaving native C3 and releasing C3a and nascent C3b fragments. Since surface-bound convertases produce C3b near the cell surface, these nascent C3b molecules (npC3b) have a high propensity for binding back to the same cell surface. The newly produced C3b recruits FB and FD, further building C3bBb convertases on the surface of pathogens (**Figure 2.1**). However, the C3bBb complex is rather unstable and has a half-life of about 90 seconds [41]. A positive regulatory protein known as properdin (P), associates with C3bBb, thus stabilizing and increasing the half-life of the convertase 10-fold [83]. Properdin has however recently reemerged as more than a stabilizing factor for the C3 convertase by the multiple roles it plays during complement activity. It has been demonstrated that properdin not only binds to formed alternative pathway C3 convertase but also once bound to a surface could accelerate the association of C3b and FB, subsequently forming the properdin stabilized convertase C3bBbP [18]. The latter study has also shown a model in which properdin, a dimer, trimer, or tetramer, bound to C3b through one site, can use its other vacant binding sites to recruit C3b, C3bB, and C3bBb, thus directing complement activation. Furthermore, properdin has been shown to be a pattern-recognition molecule that distinguishably binds to specific cell surfaces and serves as a platform for de novo convertase assembly to initiate the alternative pathway C3bBbP

[14–22]. However, for our studies we focused on neutrophil-secreted properdin that has been shown to bind on the surface of the neutrophil [22,66]. Although these findings demonstrate properdin as a molecule that distinguishably binds to specific cell surfaces, purified physiological forms of properdin do not bind to certain surfaces [17,84]. To compensate for the differences, our model has included two kinds of properdin, in which the neutrophil-secreted properdin (P*) has the ability of attaching to surfaces and recruit C3b, while plasma properdin (P) does not. In addition, our model incorporates a delay of 10 minutes for P* release, to account for neutrophil transmigration from the vasculature to the site of infection [76].

2.5.4 Termination (pathogen)

The accumulation of C3b molecules on the surface of a pathogen leads to opsonization, thus rendering the pathogen subject to phagocytosis. However, C3b also binds with the C3 convertase to form a C5 convertase ($C3b_2Bb$) of the alternative pathway. This protein complex cleaves C5, resulting to C5a and C5b on which the latter product remains loosely bound to the convertase while C5a is released in the fluid phase. Like C3a, belonging to a group of complement anaphylatoxins, C5a is a potent mediator of inflammatory responses [85–87], and is considered a terminal complement activation product in our model. C5b initiates a cascade of biochemical reactions that lead to the formation of the membrane attack complex (MAC). Following C5 cleavage, C5b undergoes a conformational transition, during which C6 binds. The half-life of C5b was shown to be 2.3 minutes before it irreversibly loses binding capabilities to C6 [88]. C5

convertase-bound C5b-6 may then bind C7, at which point the C5b-7 complex dissociates and undergoes a hydrophilic-amphiphilic transition, generating a membrane binding site. The formed metastable C5b-7 is released into the fluid phase and has the ability to insert itself into the lipid bilayer but can also form inactive protein micelles in the absence of membranes [85,86,89]. Once C5b-7 attaches to a membrane, it establishes a binding site for C8 [90–92]. Complement protein C8 will then inserts itself into the lipid bilayer of the pathogen and also induce the oligomerization of C9 to form a MAC complex, which is responsible for cell lysis [85,93].

2.5.5 Regulation (host cell and fluid phase)

The complement system is tightly regulated to prevent damage to host cells. Several soluble and cell-bound regulator proteins bind to complement proteins and complexes, inhibiting activation at several points in the activation cascade. Complement amplification is regulated through inhibition of convertase formation (mediated by FH and CR1), dissociation of existing convertases (mediated by FH, CR1, and DAF), cleavage of C3b into iC3b (mediated by FI using CR1 or FH as a cofactor), and subsequent cleavage of iC3b to C3dg (mediated by FI using CR1 as a cofactor). In addition, the terminal pathway is regulated by soluble Vn and Cn, and cell-bound (CD59) complement regulators. MCP, another cell-bound C3b inactivator, is not considered in our model, since it is not expressed on erythrocyte surfaces.

2.5.6 Sensitivity analysis

Sensitivity analysis was implemented using the multi-parametric sensitivity analysis (MPSA) method [94]. The procedure of MPSA is described in the following steps. First, we selected all parameters to be tested. This includes 17 initial concentrations and 74 kinetic parameters. Second, the range of each selected parameter was set large enough to cover all feasible variations (increasing and decreasing by a factor of 10 for the rate constants and by factor 5 for the concentrations). The parameter ranges used for the sensitivity can be found in **Tables A.4** and **A.5**. Third, for each selected parameter, a series of independent random numbers were generated with a uniform distribution within the defined range. The Latin hypercube sampling method was used to sample 2000 random parameter vectors due to the large number of rate constants. This ensures maximal sampling through each parameter dimension while also computationally managing large number of rate constants [94,95]. The Matlab function 'lhsdesign' was used to produce the 2000 parameter vectors. Next, the model was simulated for each chosen set of parameter values to calculate the objective function values. The objective function is defined as the sum of squared errors between the observed and perturbed system output values

$$f_{obj}(k) = \sum_{i}^{n} \left(x_{obj}(i) - x_{cal}(i,k) \right)^2$$

where $x_{obj}(i)$ and $x_{cal}(i,k)$ denote the observed values calculated from the reference parameter values at the *i*th sampling time and perturbed system output values at the *i*th sampling time for the parameter variation set *k*, respectively. The output values denote the surface occupation (pathogen/host cell) by complement proteins and *n* is the sampling time point, which is set to be each time point through the simulations. Then it was determined

whether the parameter set is acceptable or unacceptable by comparing the objective function value to a given threshold. If the objective function value is greater than or less than the threshold, the parameter set of values is classified as unacceptable or acceptable, respectively. Since MPSA results are not affected by the choice of subjective threshold [94,96], here we used a 50% divisions of 2000 sorted objective functions. Lastly, we statistically evaluated the parameter sensitivity by quantitatively comparing the distributions of acceptable and unacceptable values. The cumulative frequency is computed for each selected parameter with both acceptable and unacceptable cases. Sensitivity was evaluated by the measure of separation between the two cumulative frequency distributions of acceptable and unacceptable cases using Kolmogorov-Smirnov (K-S) statistic

$$K\text{–}S = \max_{x} |C_a(x) - C_u(x)|$$

where C_a and C_u correspond to the cumulative frequency functions that are acceptable and unacceptable cases, and x is the given parameter. Large values of K-S test indicate the model output is sensitive to the given parameter variations.

2.6 References

1. Walport MJ. Complement. Second of two parts. N Engl J Med. 2001;344: 1140–1144. doi:10.1056/NEJM200104123441506

2. Walport MJ. Complement. First of two parts. N Engl J Med. 2001;344: 1058–1066. doi:10.1056/NEJM200104053441406

3. Fishelson Z, Attali G, Mevorach D. Complement and apoptosis. Mol Immunol. 2001;38: 207–219.

4. Charles A Janeway J, Travers P, Walport M, Shlomchik MJ. The complement system and innate immunity. Immunobiol Immune Syst Health Dis 5th Ed. 2001

5. Holers VM. The spectrum of complement alternative pathway-mediated diseases. Immunol Rev. 2008;223: 300–316. doi:10.1111/j.1600-065X.2008.00641.x

6. Manderson AP, Botto M, Walport MJ. The role of complement in the development of systemic lupus erythematosus. Annu Rev Immunol. 2004;22: 431–456. doi:10.1146/annurev.immunol.22.012703.104549

7. Noris M, Remuzzi G. Hemolytic Uremic Syndrome. J Am Soc Nephrol. 2005;16: 1035–1050. doi:10.1681/ASN.2004100861

8. Kavanagh D, Goodship TH, Richards A. Atypical Hemolytic Uremic Syndrome. Semin Nephrol. 2013;33: 508–530. doi:10.1016/j.semnephrol.2013.08.003

9. De Jong PTVM. Age-Related Macular Degeneration. N Engl J Med. 2006;355: 1474–1485. doi:10.1056/NEJMra062326

10. Anderson DH, Radeke MJ, Gallo NB, Chapin EA, Johnson PT, Curletti CR, et al. The Pivotal Role of the Complement System in Aging and Age-related Macular Degeneration: Hypothesis Re-visited. Prog Retin Eye Res. 2010;29: 95–112. doi:10.1016/j.preteyeres.2009.11.003

11. Hirayama H, Yoshii K, Ojima H, Kawai N, Gotoh S, Fukuyama Y. Linear systems analysis of activating processes of complement system as a defense mechanism. Biosystems. 1996;39: 173–185. doi:10.1016/0303-2647(96)01617-6

12. Korotaevskiy AA, Hanin LG, Khanin MA. Non-linear dynamics of the complement system activation. Math Biosci. 2009;222: 127–143. doi:10.1016/j.mbs.2009.10.003

13. Liu B, Zhang J, Tan PY, Hsu D, Blom AM, Leong B, et al. A Computational and Experimental Study of the Regulatory Mechanisms of the Complement System. PLoS Comput Biol. 2011;7: e1001059. doi:10.1371/journal.pcbi.1001059

14. Spitzer D, Mitchell LM, Atkinson JP, Hourcade DE. Properdin can initiate complement activation by binding specific target surfaces and providing a platform for de novo convertase assembly. J Immunol Baltim Md 1950. 2007;179: 2600–2608.

15. Kemper C, Mitchell LM, Zhang L, Hourcade DE. The complement protein properdin binds apoptotic T cells and promotes complement activation and phagocytosis. Proc Natl Acad Sci U S A. 2008;105: 9023–9028. doi:10.1073/pnas.0801015105

16. Xu W, Berger SP, Trouw LA, Boer HC de, Schlagwein N, Mutsaers C, et al. Properdin Binds to Late Apoptotic and Necrotic Cells Independently of C3b and Regulates Alternative Pathway Complement Activation. J Immunol. 2008;180: 7613–7621. doi:10.4049/jimmunol.180.11.7613

17. Ferreira VP, Cortes C, Pangburn MK. Native polymeric forms of properdin selectively bind to targets and promote activation of the alternative pathway of complement. Immunobiology. 2010;215: 932–940. doi:10.1016/j.imbio.2010.02.002

18. Hourcade DE. The role of properdin in the assembly of the alternative pathway C3 convertases of complement. J Biol Chem. 2006;281: 2128–2132. doi:10.1074/jbc.M508928200

19. Cortes C, Ferreira VP, Pangburn MK. Native Properdin Binds to Chlamydia pneumoniae and Promotes Complement Activation. Infect Immun. 2011;79: 724–731. doi:10.1128/IAI.00980-10

20. Saggu G, Cortes C, Emch HN, Ramirez G, Worth RG, Ferreira VP. Identification of a novel mode of complement activation on stimulated platelets mediated by properdin and C3(H2O). J Immunol Baltim Md 1950. 2013;190: 6457–6467. doi:10.4049/jimmunol.1300610

21. Cortes C, Ohtola JA, Saggu G, Ferreira VP. Local release of properdin in the cellular microenvironment: role in pattern recognition and amplification of the alternative pathway of complement. Front Immunol. 2013;3. doi:10.3389/fimmu.2012.00412

22. Camous L, Roumenina L, Bigot S, Brachemi S, Frémeaux-Bacchi V, Lesavre P, et al. Complement alternative pathway acts as a positive feedback amplification of neutrophil activation. Blood. 2011;117: 1340–1349. doi:10.1182/blood-2010-05-283564

23. Hourcade D, Holers VM, Atkinson JP. The regulators of complement activation (RCA) gene cluster. Adv Immunol. 1989;45: 381–416.

24. Fodor WL, Rollins SA, Guilmette ER, Setter E, Squinto SP. A novel bifunctional chimeric complement inhibitor that regulates C3 convertase and formation of the membrane attack complex. J Immunol Baltim Md 1950. 1995;155: 4135–4138.

25. Zipfel PF, Skerka C. Complement regulators and inhibitory proteins. Nat Rev Immunol. 2009;9: 729–740. doi:10.1038/nri2620

26. Chauhan AK, Moore TL. Presence of plasma complement regulatory proteins clusterin (Apo J) and vitronectin (S40) on circulating immune complexes (CIC). Clin Exp Immunol. 2006;145: 398–406. doi:10.1111/j.1365-2249.2006.03135.x

27. Rollins SA, Sims PJ. The complement-inhibitory activity of CD59 resides in its capacity to block incorporation of C9 into membrane C5b-9. J Immunol Baltim Md 1950. 1990;144: 3478–3483.

28. Pangburn MK, Schreiber RD, Müller-Eberhard HJ. Formation of the initial C3 convertase of the alternative complement pathway. Acquisition of C3b-like activities by spontaneous hydrolysis of the putative thioester in native C3. J Exp Med. 1981;154: 856–867.

29. Law SK, Lichtenberg NA, Levine RP. Evidence for an ester linkage between the labile binding site of C3b and receptive surfaces. J Immunol Baltim Md 1950. 1979;123: 1388–1394.

30. Tack BF, Harrison RA, Janatova J, Thomas ML, Prahl JW. Evidence for presence of an internal thiolester bond in third component of human complement. Proc Natl Acad Sci U S A. 1980;77: 5764–5768.

31. Law SK, Levine RP. Interaction between the third complement protein and cell surface macromolecules. Proc Natl Acad Sci U S A. 1977;74: 2701–2705.

32. Sim RB, Twose TM, Paterson DS, Sim E. The covalent-binding reaction of complement component C3. Biochem J. 1981;193: 115–127.

33. Weiler JM, Daha MR, Austen KF, Fearon DT. Control of the amplification convertase of complement by the plasma protein beta1H. Proc Natl Acad Sci U S A. 1976;73: 3268–3272.

34. Whaley K, Ruddy S. Modulation of the alternative complement pathways by beta 1 H globulin. J Exp Med. 1976;144: 1147–1163. doi:10.1084/jem.144.5.1147

35. Pangburn MK, Müller-Eberhard HJ. Kinetic and thermodynamic analysis of the control of C3b by the complement regulatory proteins factors H and I. Biochemistry (Mosc). 1983;22: 178–185.

36. Pangburn MK, Schreiber RD, Müller-Eberhard HJ. Human complement C3b inactivator: isolation, characterization, and demonstration of an absolute requirement for the serum protein beta1H for cleavage of C3b and C4b in solution. J Exp Med. 1977;146: 257–270. doi:10.1084/jem.146.1.257

37. Ahearn JM, Fearon DT. Structure and Function of the Complement Receptors, CR1 (CD35) and CR2 (CD21). In: Dixon FJ, editor. Advances in Immunology. Academic Press; 1989. pp. 183–219. Available: http://www.sciencedirect.com/science/article/pii/S0065277608606549

38. Porteu F, Halbwachs-Mecarelli L. Interaction of human monomeric C3b with its receptor (complement receptor type 1, CR1) on neutrophils. Evidence for negative cooperativity. J Biol Chem. 1988;263: 5091–5097.

39. Ross D, Newman SL, Lambris JD, Devery-pocius JE, Cain JA, Peter, et al. Generation of three different fragments of bound C3 with purified factor I or serum. I. Requirements for factor H vs. CR cofactor activity.J. 1982.

40. Józsi M, Prechl J, Bajtay Z, Erdei A. Complement receptor type 1 (CD35) mediates inhibitory signals in human B lymphocytes. J Immunol Baltim Md 1950. 2002;168: 2782–2788.

41. Pangburn MK, Müller-Eberhard HJ. The C3 convertase of the alternative pathway of human complement. Enzymic properties of the bimolecular proteinase. Biochem J. 1986;235: 723–730.

42. Müller-Eberhard HJ, Götze O. C3 proactivator convertase and its mode of action. J Exp Med. 1972;135: 1003–1008. doi:10.1084/jem.135.4.1003

43. Hunsicker LG, Ruddy S, Austen KF. Alternate complement pathway: factors involved in cobra venom factor (CoVF) activation of the third component of complement (C3). J Immunol Baltim Md 1950. 1973;110: 128–138.

44. Chen H, Ricklin D, Hammel M, Garcia BL, McWhorter WJ, Sfyroera G, et al. Allosteric inhibition of complement function by a staphylococcal immune evasion protein. Proc Natl Acad Sci U S A. 2010;107: 17621–17626. doi:10.1073/pnas.1003750107

45. Brodbeck WG, Mold C, Atkinson JP, Medof ME. Cooperation between decay-accelerating factor and membrane cofactor protein in protecting cells from autologous complement attack. J Immunol Baltim Md 1950. 2000;165: 3999–4006.

46. Morgan BP, Meri S. Membrane proteins that protect against complement lysis. Springer Semin Immunopathol. 1994;15: 369–396. doi:10.1007/BF01837366

47. Claire L Harris DMP. Decay-accelerating factor must bind both components of the complement alternative pathway C3 convertase to mediate efficient decay. J Immunol Baltim Md 1950. 2007;178: 352–9. doi:10.4049/jimmunol.178.1.352

48. Medicus RG, Götze O, Müller-Eberhard HJ. Alternative pathway of complement: recruitment of precursor properdin by the labile C3/C5 convertase and the potentiation of the pathway. J Exp Med. 1976;144: 1076–1093.

49. Cochrane CG, Müller-Eberhard HJ. The derivation of two distinct anaphylatoxin activities from the third and fifth components of human complement. J Exp Med. 1968;127: 371–386.

50. da Silva WD, Eisele JW, Lepow IH. Complement as a mediator of inflammation. 3. Purification of the activity with anaphylatoxin properties generated by interaction of

the first four components of complement and its identification as a cleavage product of C'3. J Exp Med. 1967;126: 1027–1048. doi:10.1084/jem.126.6.1027

51. Rawal N, Pangburn M. Formation of high-affinity C5 convertases of the alternative pathway of complement. J Immunol Baltim Md 1950. 2001;166: 2635–2642.

52. Rawal N, Pangburn MK. C5 convertase of the alternative pathway of complement. Kinetic analysis of the free and surface-bound forms of the enzyme. J Biol Chem. 1998;273: 16828–16835.

53. Rawal N, Pangburn MK. Functional Role of the Noncatalytic Subunit of Complement C5 Convertase. J Immunol. 2000;164: 1379–1385. doi:10.4049/jimmunol.164.3.1379

54. Wetsel RA. Structure, function and cellular expression of complement anaphylatoxin receptors. Curr Opin Immunol. 1995;7: 48–53.

55. Nataf S, Davoust N, Ames RS, Barnum SR. Human T cells express the C5a receptor and are chemoattracted to C5a. J Immunol Baltim Md 1950. 1999;162: 4018–4023.

56. Ottonello L, Corcione A, Tortolina G, Airoldi I, Albesiano E, Favre A, et al. rC5a directs the in vitro migration of human memory and naive tonsillar B lymphocytes: implications for B cell trafficking in secondary lymphoid tissues. J Immunol Baltim Md 1950. 1999;162: 6510–6517.

57. Makrides SC, Scesney SM, Ford PJ, Evans KS, Carson GR, Marsh HC. Cell surface expression of the C3b/C4b receptor (CR1) protects Chinese hamster ovary cells from lysis by human complement. J Biol Chem. 1992;267: 24754–24761.

58. Medof ME, Iida K, Mold C, Nussenzweig V. Unique role of the complement receptor CR1 in the degradation of C3b associated with immune complexes. J Exp Med. 1982;156: 1739–1754. doi:10.1084/jem.156.6.1739

59. Tschopp J, Chonn A, Hertig S, French LE. Clusterin, the human apolipoprotein and complement inhibitor, binds to complement C7, C8 beta, and the b domain of C9. J Immunol Baltim Md 1950. 1993;151: 2159–2165.

60. Müller-Eberhard HJ. The membrane attack complex of complement. Annu Rev Immunol. 1986;4: 503–528. doi:10.1146/annurev.iy.04.040186.002443

61. Krych-Goldberg M, Hauhart RE, Subramanian VB, Yurcisin BM, Crimmins DL, Hourcade DE, et al. Decay accelerating activity of complement receptor type 1 (CD35). Two active sites are required for dissociating C5 convertases. J Biol Chem. 1999;274: 31160–31168.

62. Pillemer L, Blum L, Lepow IH, Ross OA, Todd EW, Wardlaw AC. The properdin system and immunity. I. Demonstration and isolation of a new serum protein, properdin, and its role in immune phenomena. Science. 1954;120: 279–285.

63. Nelson RA. An alternative mechanism for the properdin system. J Exp Med. 1958;108: 515–535. doi:10.1084/jem.108.4.515

64. Gupta-Bansal R, Parent JB, Brunden KR. Inhibition of complement alternative pathway function with anti-properdin monoclonal antibodies. Mol Immunol. 2000;37: 191–201.

65. Pangburn MK. Analysis of the natural polymeric forms of human properdin and their functions in complement activation. J Immunol. 1989;142: 202–207.

66. Wirthmueller U, Dewald B, Thelen M, Schäfer MK, Stover C, Whaley K, et al. Properdin, a positive regulator of complement activation, is released from secondary granules of stimulated peripheral blood neutrophils. J Immunol Baltim Md 1950. 1997;158: 4444–4451.

67. Botto M, Lissandrini D, Sorio C, Walport MJ. Biosynthesis and secretion of complement component (C3) by activated human polymorphonuclear leukocytes. J Immunol Baltim Md 1950. 1992;149: 1348–1355.

68. Høgåsen AK, Würzner R, Abrahamsen TG, Dierich MP. Human polymorphonuclear leukocytes store large amounts of terminal complement components C7 and C6, which may be released on stimulation. J Immunol Baltim Md 1950. 1995;154: 4734–4740.

69. Schwaeble W, Dippold WG, Schäfer MK, Pohla H, Jonas D, Luttig B, et al. Properdin, a positive regulator of complement activation, is expressed in human T cell lines and peripheral blood T cells. J Immunol. 1993;151: 2521–2528.

70. Liddington R, Bankston L. Structural biology: origins of chemical biodefence. Nature. 2005;437: 484–485. doi:10.1038/437484a

71. Gizeli E, Lowe CR. Biomolecular Sensors. CRC Press; 2003.

72. Schlosshauer M, Baker D. Realistic protein-protein association rates from a simple diffusional model neglecting long-range interactions, free energy barriers, and landscape ruggedness. Protein Sci Publ Protein Soc. 2004;13: 1660–1669. doi:10.1110/ps.03517304

73. Gabdoulline RR, Wade RC. Simulation of the diffusional association of barnase and barstar. Biophys J. 1997;72: 1917–1929. doi:10.1016/S0006-3495(97)78838-6

74. Li Y, Karlin A, Loike JD, Silverstein SC. A critical concentration of neutrophils is required for effective bacterial killing in suspension. Proc Natl Acad Sci U S A. 2002;99: 8289–8294. doi:10.1073/pnas.122244799

75. Seya T. Human Regulator of Complement Activation (RCA) Gene Family Proteins and Their Relationship to Microbial Infection. Microbiol Immunol. 1995;39: 295–305. doi:10.1111/j.1348-0421.1995.tb02205.x

76. Ley K, Laudanna C, Cybulsky MI, Nourshargh S. Getting to the site of inflammation: the leukocyte adhesion cascade updated. Nat Rev Immunol. 2007;7: 678–689. doi:10.1038/nri2156

77. Greer JP. Wintrobe's Clinical Hematology. Lippincott Williams & Wilkins; 2009.

78. Kellogg JA, Manzella JP, McConville JH. Clinical laboratory comparison of the 10-ml isolator blood culture system with BACTEC radiometric blood culture media. J Clin Microbiol. 1984;20: 618–623.

79. Schrier RW. Manual of Nephrology. Lippincott Williams & Wilkins; 2008.

80. Pangburn MK, Schreiber RD, Müller-Eberhard HJ. C3b deposition during activation of the alternative complement pathway and the effect of deposition on the activating surface. J Immunol Baltim Md 1950. 1983;131: 1930–1935.

81. Hugli TE. Structure and function of C3a anaphylatoxin. Curr Top Microbiol Immunol. 1990;153: 181–208.

82. Nordahl EA, Rydengård V, Nyberg P, Nitsche DP, Mörgelin M, Malmsten M, et al. Activation of the complement system generates antibacterial peptides. Proc Natl Acad Sci U S A. 2004;101: 16879–16884. doi:10.1073/pnas.0406678101

83. Fearon DT, Austen KF. Properdin: binding to C3b and stabilization of the C3b-dependent C3 convertase. J Exp Med. 1975;142: 856–863. doi:10.1084/jem.142.4.856

84. Agarwal S, Ferreira VP, Cortes C, Pangburn MK, Rice PA, Ram S. An evaluation of the role of properdin in alternative pathway activation on Neisseria meningitidis and Neisseria gonorrhoeae. J Immunol Baltim Md 1950. 2010;185: 507–516. doi:10.4049/jimmunol.0903598

85. Muller-Eberhard HJ. Molecular Organization and Function of the Complement System. Annu Rev Biochem. 1988;57: 321–347. doi:10.1146/annurev.bi.57.070188.001541

86. Ember JA, Hugli TE. Complement factors and their receptors. Immunopharmacology. 1997;38: 3–15.

87. Cooper NR, Müller-Eberhard HJ. The reaction mechanism of human C5 in immune hemolysis. J Exp Med. 1970;132: 775–793. doi:10.1084/jem.132.4.775

88. Preissner KT, Podack ER, Müller-Eberhard HJ. The membrane attack complex of complement: relation of C7 to the metastable membrane binding site of the intermediate complex C5b-7. J Immunol Baltim Md 1950. 1985;135: 445–451.

89. Monahan JB, Sodetz JM. Role of the beta subunit in interaction of the eighth component of human complement with the membrane-bound cytolytic complex. J Biol Chem. 1981;256: 3258–3262.

90. Brannen CL, Sodetz JM. Incorporation of human complement C8 into the membrane attack complex is mediated by a binding site located within the C8beta MACPF domain. Mol Immunol. 2007;44: 960–965. doi:10.1016/j.molimm.2006.03.012

91. Stewart JL, Kolb WP, Sodetz JM. Evidence that C5b recognizes and mediates C8 incorporation into the cytolytic complex of complement. J Immunol Baltim Md 1950. 1987;139: 1960–1964.

92. Podack E, Tschoop J, Muller-Eberhard H. Molecular organization of C9 within the membrane attack complex of complement. Induction of circular C9 polymerization by the C5b-8 assembly. J Exp Med. 1982;156: 268–282.

93. Zi Z, Cho K-H, Sung M-H, Xia X, Zheng J, Sun Z. In silico identification of the key components and steps in IFN-γ induced JAK-STAT signaling pathway. FEBS Lett. 2005;579: 1101–1108. doi:10.1016/j.febslet.2005.01.009

94. McKay MD, Beckman RJ, Conover WJ. Comparison of Three Methods for Selecting Values of Input Variables in the Analysis of Output from a Computer Code. Technometrics. 1979;21: 239–245. doi:10.1080/00401706.1979.10489755

95. Choi J, Hulseapple SM, Conklin MH, Harvey JW. Modeling CO2 degassing and pH in a stream–aquifer system. J Hydrol. 1998;209: 297–310. doi:10.1016/S0022-1694(98)00093-6

CHAPTER 3

A Computational Model for the Evaluation of Complement System Regulation under Homeostasis, Disease, and Drug Intervention

3.1 Introduction

A pivotal arm of innate immunity, the complement system is comprised of proteins present in both plasma and cell membranes that work in concert to mediate immune responses against invading pathogens and altered host cells, while at the same time shielding healthy host cells from destruction [1,2]. The coordination of the complement system is induced through three pathways known as alternative, classical, and lectin. The alternative pathway is constitutively activated in plasma through the so-called tick-over mechanism of complement protein C3, while the latter two pathways, classical and lectin, are initiated on microbes or apoptotic/necrotic cells by their respective pattern recognition molecules [3]. Similar to alternative pathway, the classical pathway can also be induced in the fluid phase through the spontaneous intramolecular activation of complement complex C1 [4]. Central points of convergence for all three pathways of complement activation and propagation are complement proteins C3 and C5, whose cleavage fragments C3a/C3b and C5a/C5b, respectively, results in inflammatory responses, opsonophagocytosis, and formation of the membrane attack complex (MAC/C5b-9_n) [5,6]. The fragments C3a and C5a are anaphylatoxins that mediate activation of immune cells, such as macrophages and T cells, while C3b is an opsonin that tags foreign or altered cells for recognition and elimination by phagocytes [5,6]. Lastly, the MAC complex penetrates lipid bilayers and

induces lysis through osmotic effects [7]. Propagation of complement activation occurs through cleavage of C3 or C5 by convertases, which are complexes of cleavage products of C3, C4, and proteases FB and C2 [8–11].

The complexity of the complement system comes from the number of proteins and their networks of interactions involved in all three pathways. However, recent mathematical models targeting complement pathways have been developed to aid our understanding in the dynamics involved in mediating immune response through activation and regulation of complement species [12–16]. To further these efforts, we previously developed a comprehensive model of the alternative pathway divided into four modules: (i) initiation (fluid phase); (ii) amplification (surfaces); (iii) termination (pathogen); and (iv) regulation (host cell and fluid phase) [17]. Based on these four modules we generated a system of 107 ordinary differential equations (ODEs) and 74 kinetic parameters. Here we present an updated and refined alternative pathway model of the complement system that takes into account dimerization states of complement fragments C3b and C4b, additional C3 and C5 convertases, IgG interactions with the C3b, and regulation of anaphylatoxins C3a and C5a. Relative to our first model [17], this new model also contains fluid phase activation and propagation of the classical pathway, owed to the spontaneous autoactivation of C1. With these additions, our updated and refined model is now composed of 290 ordinary differential equations and 142 kinetic parameters.

The cascade of reactions “innate” to the complement system is equally supplemented with interactions that protect healthy host cells from destruction, under homeostasis. Recent studies highlight a number of diseases that are associated with under-

regulation/over-activation of the alternative pathway due to mutations that target regulators (e.g. FH) or propagators (convertases) of the alternative pathway [18–23]. Diseases such as such as aHUS, AMD, C3 glomerulonephritis (C3GN), and dense-deposit disease (DDD) are associated with overly active alternative pathway [19–22,24–28]. To better understand the dynamics of these disorders at the complement level, we have developed a generic disease state by targeting the most potent complement regulator FH. This regulator is chosen because alternative pathway-mediated disorders, mentioned above, implicate FH dysfunctionality, owed to altered effective concentrations or mutations that impair regulatory capabilities. In addition to modeling the disease state, we have also added to two therapy states by incorporating complement inhibitors, compstatin, targeting C3 [29–33], and eculizumab, targeting C5 [34–36], and compared their relative effects on regulating an over-activated complement system under FH regulatory impairment. Furthermore, we implemented different doses of compstatin and eculizumab to investigate their relative roles on mediating early- and late-stage complement biomarkers. In summary, we have generated four states of alternative and classical pathways with time profiles describing concentration levels of biomarkers C3, C3a-desArg, C5, C5a-desArg, FB and its fragments Ba and Bb, and fC5b-9 (a general term for fluid phase MAC/C5b-9) that are associated with alternative pathway dysregulation.

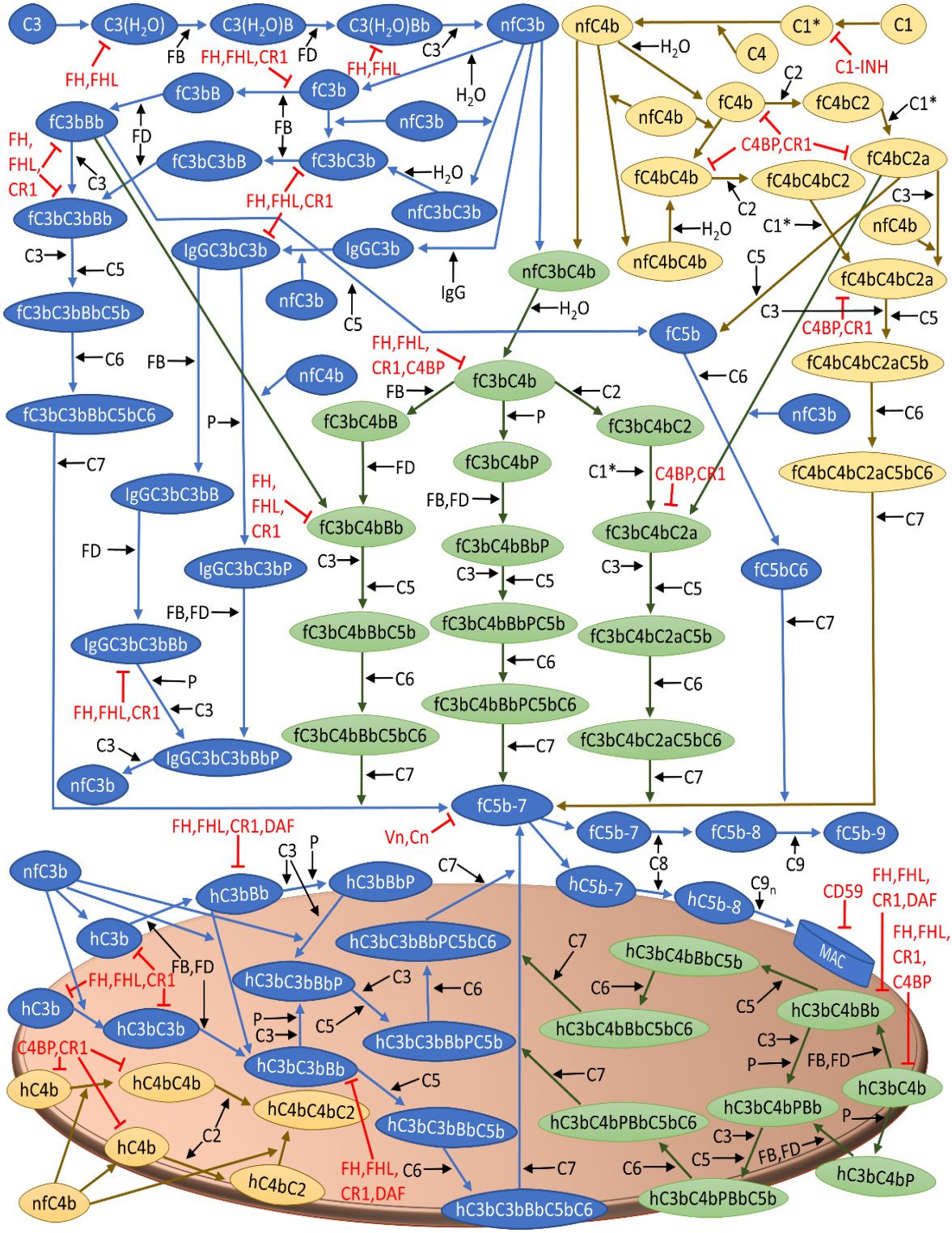
C3
C3(H2O)
C3(H2O)B
C3(H2O)Bb
nfC3b
FH,FHL
FB
FH,FHL,CR1
FD
FH,FHL
C3
H2O
fC3bB
fC3b
fC3bBb
FH,
FHL,
CR1
FD
FB
nfC3b
fC3bC3bB
fC3bC3b
H2O
C3
FH,FHL,CR1
nfC3bC3b
fC3bC3bBb
C3
C5
IgGC3bC3b
IgGC3b
IgG
nfC3b
C5
fC3bC3bBbC5b
C6
FB
nfC3bC4b
H2O
fC5b
FH,FHL,
CR1,C4BP
fC3bC4b
FB
C2
nfC4b
fC3bC3bBbC5bC6
P
fC3bC4bB
fC3bC4bC2
C6
P
C7
FD
fC3bC4bP
C1*
C4BP,CR1
IgGC3bC3bB
FH,
FHL,
CR1
fC3bC4bBb
FB,FD
fC3bC4bC2a
FD
C3
C5
IgGC3bC3bP
fC3bC4bBbP
fC5bC6
FB,FD
fC3bC4bBbC5b
fC3bC4bBbPC5b
fC3bC4bC2aC5b
C6
C7
IgGC3bC3bBb
P
FH,FHL,CR1
C3
fC3bC4bBbPC5bC6
C3
IgGC3bC3bBbP
fC3bC4bBbC5bC6
fC3bC4bC2aC5bC6
nfC3b
C7
fC5b-7
FH,FHL,CR1,DAF
Vn,Cn
fC5b-7
fC5b-8
fC5b-9
C8
C9
C3
P
C7
nfC3b
hC3bBb
hC3bBbP
hC5b-7
hC5b-8
C9n
CD59
FH,FHL,
CR1,DAF
hC3b
FB,FD
hC3bC3bBbPC5bC6
C7
hC3bC4bBbC5b
MAC
FH,FHL,CR1
hC3bC3bBbP
C3
C6
C6
C5
hC3b
hC3bC4bBb
hC3bC3b
P
C3
C5
hC3bC3bBbPC5b
hC3bC4bBbC5bC6
C3
P
FB,FD
C4BP,CR1
hC3bC3bBbP
C5
C7
hC3bC4b
hC4b
hC4bC4b
hC4bC4bC2
hC3bC3bBbC5b
hC3bC4bPBb
hC3bC4bPBbC5bC6
P
C2
C3
C5
FB,FD
hC4b
FH,FHL, C6
CR1,DAF
C7
C6
hC3bC4bP
hC4bC2
hC3bC4bPBbC5b
nfC4b
hC3bC3bBbC5bC6
nfC4b
H2O
C4
C1*
C1
C1-INH
C2
fC4b
fC4bC2
C1*
nfC4b
C4BP,CR1
fC4bC2a
fC4bC4b
fC4bC4bC2
C2
C3
H2O
C1*
nfC4b
nfC4bC4b
C5
fC4bC4bC2a
C3
C4BP,CR1
C5
fC4bC4bC2aC5b
C6
nfC3b
C6
fC4bC4bC2aC5bC6
C7

Figure 3.1. Biochemical reactions originating from fluid phase activation of the alternative and classical pathways. A complete explanation of the various steps, grouped in modules of initiation (fluid phase), amplification, termination, and regulation can be found below in Methods (Biochemical Model, Section 5.2). Initiation of the alternative pathway (blue) is induced through the tick-over reaction of C3, while classical pathway (yellow) is activated through the spontaneous intramolecular activation of complement complex C1. The tick-over of C3 in the alternative pathway forms the C3 convertase, $C3(H_2O)Bb$, that cleaves C3 to generate nascent fluid phase C3b (nfC3b) and C3a, whereas activation of C1 cleaves C4 into nascent fluid phase C4b (nfC4b) and C4a. Subsequently, nfC3b and nfC4b can bind to host cells, form dimers such as C3bC4b (green), C3bC3b, and C4bC4b, or generate fluid phase C3b and C4b (fC3b and fC4b). Formation of fC3b and fC4b initiates a cascade of reactions that forms C3 and C5 convertases (fC3bBb and fC4bC2a). These enzymes (fC3bBb and fC4bC2a) further cleave plasma C3 to produce more nfC3b and C3a. Furthermore, fC3bBb and fC4bC2a can also cleave C5 to generate C5a and C5b. Continued propagation of complement through C5b leads to C5b-7 that can also attach to host cells and initiate a cascade of reactions to form MAC ($C5b\text{-}9_n$). However, healthy host cells are shielded from complement attack due to fluid phase and surface bound complement regulators shown in red. Regulators FH, FHL-1, C4BP, C1-INH, CR1, and DAF provide early-phase checkpoints for complement activation and propagation, while late-step regulation of the terminal cascade is provided by fluid regulators Vn/Cn and surface bound regulator CD59. The nomenclature of complement system for selected proteins, fragments, and complexes is listed in **Table B.1**.

3.2 Results

3.2.1 Dynamics of complement activation, propagation, regulation, and inhibition

Our study presents the time profiles of the concentrations of complement components for biochemical reactions involved in the alternative and classical pathway of the complement system shown in **Figure 3.1**, under four conditions: (i) normal state, corresponding to homeostasis in a healthy person, (ii) FH disorder state, corresponding to alternative pathway dysregulation owed to FH impairment, (iii) FH disorder state with compstatin treatment, and (iv) FH disorder state with eculizumab treatment.

3.2.2 C3 and its cleavage fragment, C3a-desArg, as biomarkers for FH disorder state

We first generated time profiles for the complement system's key substrate, C3, and its deactivated anaphylatoxin, C3a-desArg, as shown in **Figure 3.2A** and **3.2B**. C3 under normal condition has a slow rate of consumption in which C3 levels reach a concentration of 6.6×10^{-6}M within the first 25 minutes from a starting concentration of 7.1×10^{-6}M (**Figure 3.2A**). This change corresponds to a 7% decrease in blood plasma C3 within 25 minutes. The trend of C3 reduction continues but the rate of consumption is significantly reduced after 25 minutes. C3 levels however in FH disorder state and FH disorder state with eculizumab treatment reach a concentration of 1.7×10^{-6}M and 1.6×10^{-6}M, respectively, within the first 25 minutes as shown in **Figure 3.2A**. (Eculizumab acts on C5 in a downstream step, and therefore has a small effect on C3 concentration.) This change corresponds to a 76% and 77% decrease, respectively, relative to normal condition. In contrast, FH disorder with compstatin treatment left small amounts blood plasma C3

(1.2×10^{-8}M), because C3 forms a new complex with compstatin, CompC3 (291-293 **Supplemental Equations B.2**). In other words, this is not owed to C3 being consumed in a biochemical reaction, such as a cleavage process where C3 is converted into nC3b and C3a through the actions of C3/C5 convertases. Rather, through compstatin binding to free C3, a new compstatin:C3 complex is formed. However, for the remaining C3 concentration, not in complex with compstatin, cleavage will follow to form nC3b and C3a. The latter product (C3a) is then rapidly deactivated by carboxypeptidase to form C3a-desArg. Because of this rapid deactivation, C3a-desArg is a better biomarker than C3a. Levels of C3a-desArg are indicators of the degree of complement activation and propagation, and in FH disorder state and FH disorder state with eculizumab treatment, C3a-desArg shows the highest production levels reaching concentrations of 5.4×10^{-6}M and 5.5×10^{-6}M within 25 minutes, respectively (**Figure 3.2B**). In contrast, C3a-desArg levels are about an order of magnitude lower (4.6×10^{-7}M) in the normal state, and about three orders of magnitude lower (3.5×10^{-9}M) FH disorder state with compstatin treatment, relative to the FH disorder state and FH disorder state with eculizumab treatment.

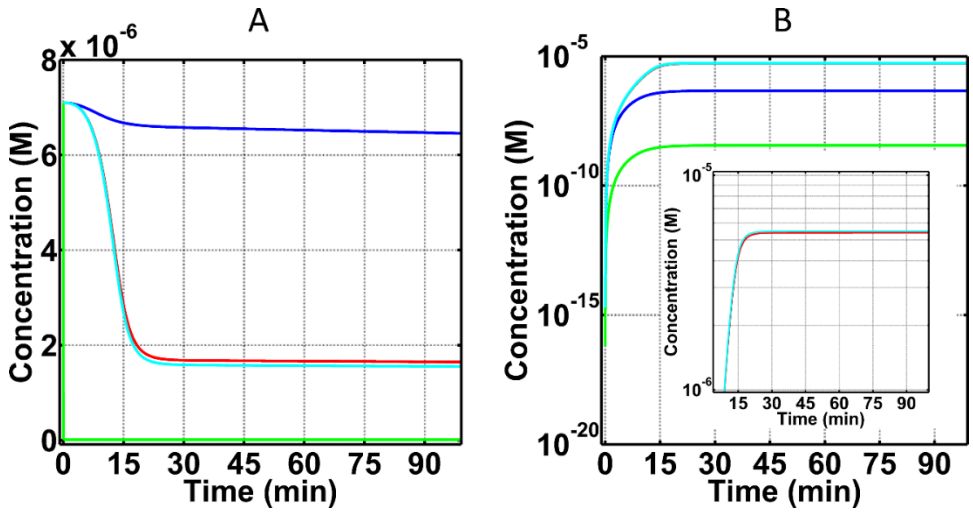

Figure 3.2. Concentration-time profiles for C3 and C3a-desArg concentrations under four conditions: (i) normal state (blue), (ii) FH disorder state (red), (iii) FH disorder state with compstatin treatment (green), and (iv) FH disorder state with eculizumab treatment (cyan). (A) Consumption of C3 under the four conditions. Plasma C3 is mostly consumed in the FH disorder state, while treatment with eculizumab had small effects on the consumption of C3. Treatment with compstatin leads to the formation of compstatin:C3 complexes, thus leaving small amounts of unbound C3 remain in plasma. (B) Production of C3a-desArg after cleavage of C3. Compstatin shows an over-restoration effect in the FH disorder state. Eculizumab has minor effects on C3 and C3a-desArg in the FH disorder state, with the effect on C3a-desArg being shown with more clarity in the zoomed-in inset of (B).

3.2.3 C5 and its cleavage fragment, C5a-desArg, as biomarkers for FH disorder state

Terminal component C5, shown in **Figure 3.3A**, exhibits minor changes in blood plasma concentrations with the exception being under treatment with eculizumab. All three conditions of normal state, FH disorder state, and FH disorder state with compstatin treatment generate time profiles of C5 where the percent change is < 1% relative to the starting blood plasma concentration of C5 (3.7×10^{-7}M). Conversely, treatment with eculizumab significantly reduces blood plasma C5 (1.0×10^{-12}M) as shown **in Figure 3.3A**. This reduction of C5 is not caused by cleavage, but it is because of the formation of a new species, the eculizumab:C5 complex, EcuC5 in 294-296 **Supplemental Equations B.2**.

However, for the remaining C5 concentration that is not in complex with eculizumab, cleavage will follow to produce C5b and C5a in which C5a is rapidly deactivated by carboxypeptidase to form C5a-desArg. As is the case of C3a/C3a-desArg, this rapid cleavage makes C5a-desArg a better biomarker than C5a. **Figure 3.3B** presents the production levels of C5a-desArg in the four states (normal, FH disorder, FH disorder with compstatin treatment, and FH disorder with eculizumab treatment). The highest C5a-desArg levels are produced in FH disorder state, where the concentration of C5a-desArg reaches 5.4×10^{-10}M within the first 25 minutes. This upward trajectory continues but the rate of production is significantly reduced after 25 minutes. In contrast, FH disorder state with compstatin treatment produced lower levels of C5a-desArg with concentration 1.2×10^{-10}M. This concentration is higher than in the normal state, which produces 2.7×10^{-11}M of C5a-desArg within the same 25 minutes. Lastly, treatment with eculizumab produced the largest difference in C5a-desArg levels, where the concentration reached 3.5×10^{-15}M, about five orders of magnitude lower compared to that of FH disorder state C5a-desArg levels (5.4×10^{-10}M).

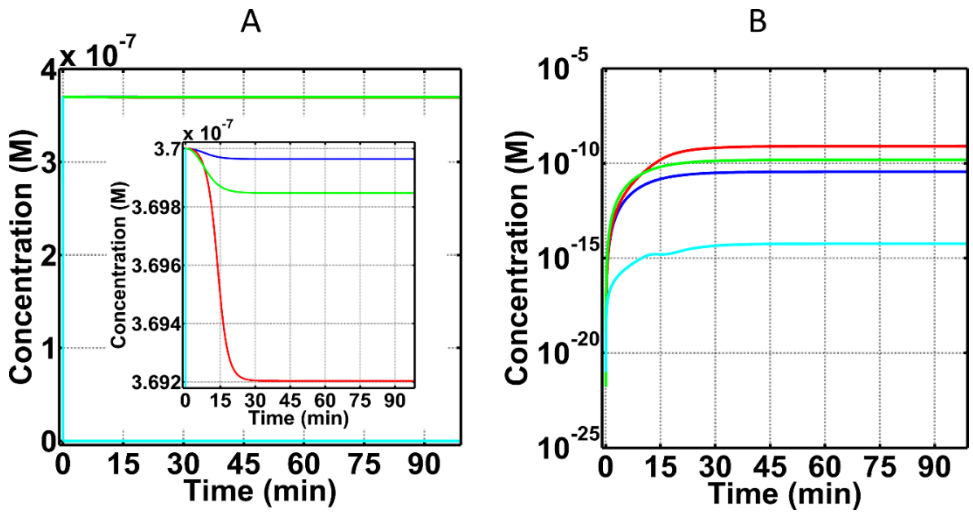

Figure 3.3. Concentration-time profiles for C5 and C5a-desArg under four conditions: (i) normal state (blue), (ii) FH disorder state (red), (iii) FH disorder state with compstatin treatment (green), and (iv) FH disorder state with eculizumab treatment (cyan). (A) Consumption of C5 under the four conditions. The inset is a zoom-in, showing that small amounts of C5 are consumed under the first three conditions (i–iii). Addition of eculizumab removed most of blood plasma C5 to form eculizumab:C5 complex (not shown). (B) Production of C5a-desArg after cleavage of C5. Treatment with eculizumab produced the lowest C5a-desArg levels, corresponding to about five orders of magnitude lower concentration compared with that of alternative pathway FH disorder.

3.2.4 FB and its cleavage fragments, Ba and Bb, as biomarkers for FH disorder state

Complement FB plays a pivotal role in the consumption of C3 and C5 by providing the cleaving unit of the C3/C5 convertases. Once FB is in complex with C3b (C3bB), FD cleaves FB to form Ba and C3bBb. C3/C5 convertase C3bBb, however is very unstable and dissociates into C3b and Bb. In addition, complement regulators such as FH, CR1, and DAF can also increase the rate at which C3bBb dissociates. **Figure 3.4** presents the time profiles of FB and its cleavage products Ba and Bb. In the normal state and FH disorder state with compstatin treatment, FB is reduced by < 2% relative to its blood plasma concentration (2.2×10^{-6}M). This minor reduction in FB highlights the regulatory role of FH when unimpaired but also the compensatory role of compstatin under compromised FH. However, in FH disorder state and FH disorder state with eculizumab treatment, the

difference of FB relative to its blood plasma concentration is 48% and 49%, respectively. These values correspond to concentrations of 1.14×10^{-6}M and 1.12×10^{-6}M, respectively. Similarly, **Figure 3.4B** and **3.4C** show time profiles for Ba and Bb where their levels are higher in FH disorder state and FH disorder state with eculizumab treatment. The concentrations of Ba and Bb reach values of ~1.05×10^{-6}M in FH disorder state, while Ba and Bb reach ~1.07×10^{-6}M in FH disorder state with eculizumab treatment. In contrast, levels of Ba and Bb are about one order of magnitude lower under the normal state, reaching a concentration of 2.5×10^{-8}M. Similarly, levels of Ba and Bb are reduced by about three orders of magnitude under FH impairment with compstatin treatment, reaching a concentration of 8.1×10^{-10}M.

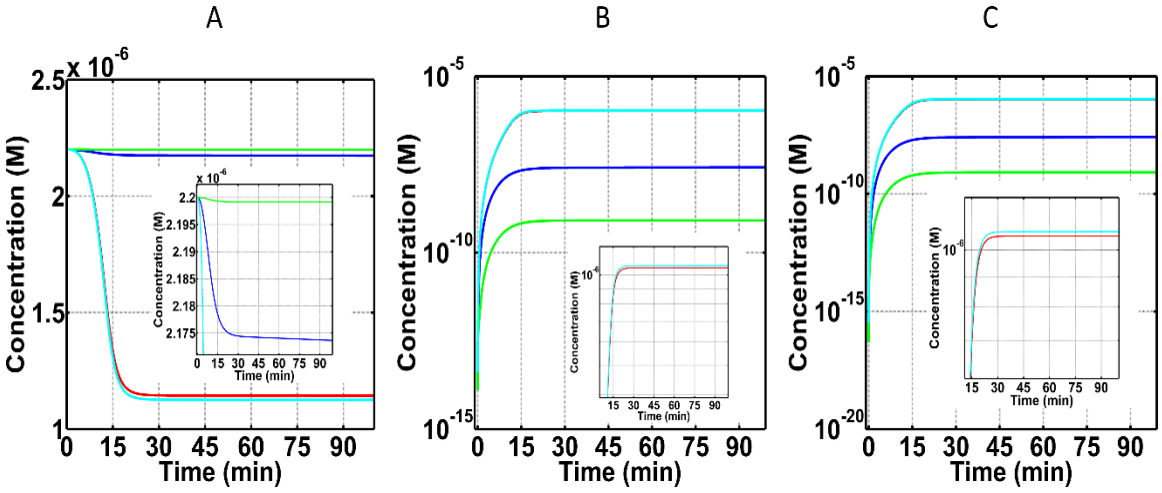

Figure 3.4. Concentration-time profiles for FB, Ba, and Bb under four conditions: (i) normal state (blue), (ii) FH disorder state (red), (iii) FH disorder state with compstatin treatment (green), and (iv) FH disorder state with eculizumab treatment (cyan). (A) FB shows the highest level of consumption in the FH disorder state and FH disorder state with eculizumab, demonstrating the minor effects of eculizumab on FB. On the contrary, compstatin nearly restores the concentration-time profile of FB to that of normal. (B and C) Similar, but opposite in magnitude effects for FB cleavage fragments Ba (Panel B) and Bb (Panel C). The FH disorder results to overproduction of Ba and Bb (view of the red graph is obscured by the cyan graph, see insets for distinction). Compstatin has a strong over-restorative effect (compare green with red and blue graphs), whereas eculizumab has a small effect (compare cyan with red and blue graphs). Insets are zoomed-in portions of the parent Panels, showing that FB levels are tightly controlled in normal state and FH disorder state with compstatin treatment (A), whereas Ba and Bb reach the highest production levels in the FH disorder state and FH disorder state with eculizumab treatment (B and C, respectively).

3.2.5 Fluid phase MAC (fC5b-9) as a biomarker for FH disorder state

After the cleavage of C5, a cascade of reactions ensues to form fluid phase C5b-9 (fC5b-9 or fMAC). As shown in **Figure 3.5**, the time profiles of fC5b-9 follow similar trends as C5a-desArg. The highest concentration of fC5b-9 (8.2×10^{-16}M) was in FH disorder state, while the FH disorder state with compstatin treatment generated a lower fC5b-9 concentration of 1.6×10^{-16}M. The normal state produced about one order of magnitude lower of fC5b-9, with concentration 3.7×10^{-17}M, relative to FH disorder state. However, in FH disorder state with eculizumab treatment, fC5b-9 levels are about four orders of magnitude lower (7.7×10^{-21}M) relative to those in FH disorder state with compstatin treatment.

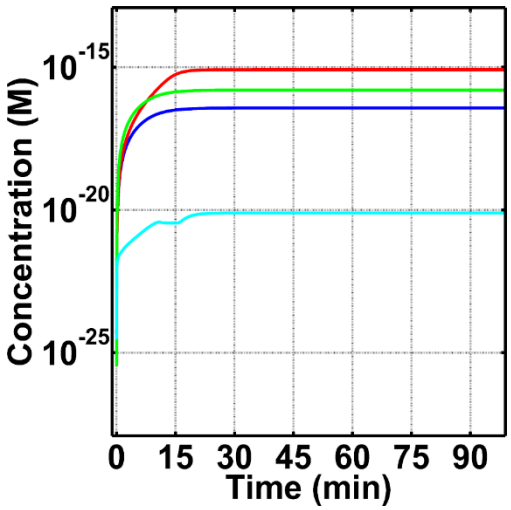

Figure 3.5. Concentration-time profiles for fC5b-9 under four conditions: (i) normal state (blue), (ii) FH disorder state (red), (iii) FH disorder state with compstatin treatment (green), and (iv) FH disorder state with eculizumab treatment (cyan). Highest concentration of fC5b-9 is produced in FH disorder state, with compstatin showing a restorative trend, but incomplete restoration, and eculizumab showing an over-restorative effect. Production of fC5b-9 under FH disorder is about one order of magnitude higher than normal. Compstatin treatment generates lower levels of fC5b-9 than FH disorder state, but fC5b-9 levels are still higher compared to normal state. Finally, eculizumab treatment shows production of fC5b-9 to be about three orders of magnitude lower than normal.

3.2.6 Sensitivity analysis

Global sensitivity analysis is performed using multi-parametric sensitivity analysis (MPSA) to identify critical parameters that affect the central complement substrate C3 and the terminal substrate C5 under normal condition. The results are shown in **Figure 3.6A** and **3.6B**. C3 levels are predominately affected by classical pathway activation and propagation in the fluid state. The most sensitive parameter is the one that governs the interaction between regulator C1-INH and activated fluid phase C1*, as shown in **Figure 3.6A**. This is followed by other classical pathway regulation steps between C4BP:fC4b, decay of C3 convertase (C4bC2a:C4BP), and enzymatic parameters (k_{cat} and K_m) of C1* targeting C4bC2. Similarly, the enhancement of the terminal cascade through the classical pathway is seen for the key interactions that affect levels of C5 (**Figure 3.6B**). This includes the activation step of C5 through the k_{cat} of C3bC4bC2a, dissociation rate constant of C3bC4bC2a, and the regulatory steps of C4BP with fC4b and C3/C5 convertase (C4bC2a). Lastly, key interactions of the alternative pathway that affect the levels of C3 and C5 involve the inactivation step of C3b in complex with FH (C3bH). This complex is targeted by FI to form iC3b. **Figure 3.6A** and **3.6B** show that inactivation of C3b in C3bH by the action of FI is an important step in mediating the levels of C3 and C5.

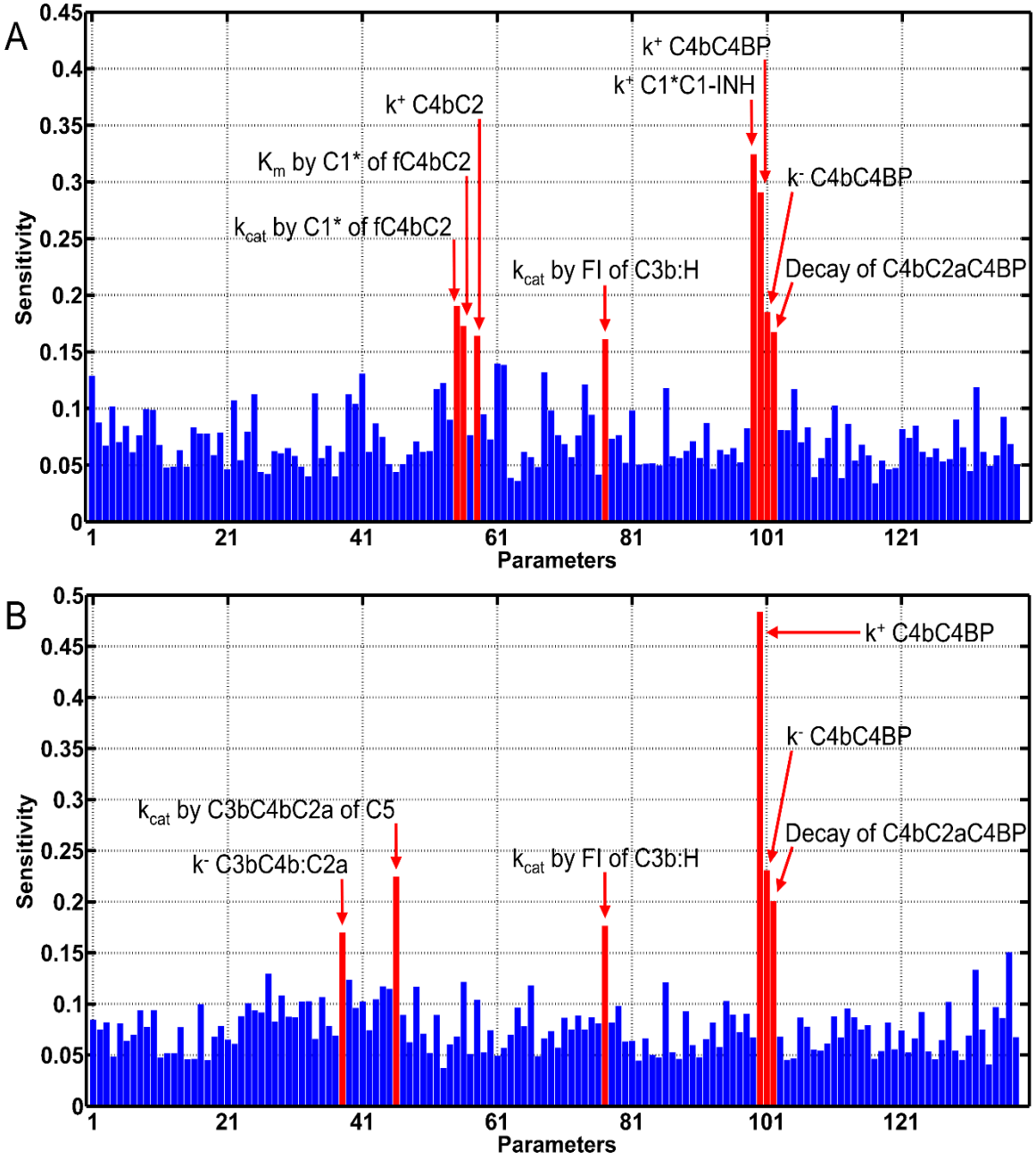

Figure 3.6. Global sensitivity analysis. Multi-parametric sensitivity analysis was performed to identify parameters that affect central substrates C3 and C5 under normal conditions. Both substrates are sensitive to the activation and propagation of the classical pathway. (A) Regulation of C1* through the action of C1-INH is the most sensitivity parameter that mediates C3 levels. (B) C5 levels are predominantly affected by regulation of C4b through C4BP. This step inhibits formation of C3/C5 convertases. In addition, both C3 and C5 are affected by the alternative pathway regulation step that inactivates C3b through the actions of FH in conjunction with FI (Panels A and B).

3.2.7 Dose dependence analysis for compstatin and eculizumab in modulating FH disorder state

Our results thus far have shown that using compstatin and eculizumab with a concentration of 20-fold higher than the concentration of their respective targets, C3 and C5, to be more than adequate in modulating complement biomarkers in the FH disorder state. Furthermore, these concentrations outperformed complement regulators under normal conditions by generating lower levels of complement biomarkers such as C3a-desArg, Ba, Bb, and fC5b-9 (**Figures 3.2B, 3.4** and **3.5**). Because of this, we consider the concentration of compstatin of 1.4×10^{-4}M (20-fold higher than C3), and the concentration of eculizumab of 7.4×10^{-6}M (20-fold higher than C5), to be upper bounds, and investigated the effect of inhibitor lower doses on complement biomarkers. We use C3a-desArg as early-stage biomarker and fC5b-9 as late-stage biomarker to assess the effects of the two inhibitors in complement modulation. **Figures B.1-B.6** show the concentration dependences of the remaining biomarkers, C3, C5, C5a-desArg, FB, Ba, and Bb.

Figure 3.7 shows concentration-time profiles for C3a-desArg in the FH disorder state with compstatin concentrations of 7.1×10^{-6}M (one-to-one to C3; **Figure 3.7A**), and 1.4×10^{-6}M (5-fold lower than C3; **Figure 3.7B**), for comparison to **Figure 3.2B** (compstatin concentrations of 1.4×10^{-4}M, 20-fold higher than C3). The same fold-change in concentration was used for eculizumab: 3.7×10^{-7}M (one-to-one to C5; **Figure 3.7A**), and 7.4×10^{-8}M (5-fold lower than C5; **Figure 3.7B**), for comparison to **Figure 3.2 B** (eculizumab concentration of 7.4×10^{-6}M, 20-fold higher than C5). The results show that the effect of one-to-one compstatin-C3 concentration nearly recovers the C3a-desArg

concentration-time profile to that of normal state (**Figure 3.7A**), whereas 5-fold lower compstatin concentration than C3 concentration is insufficient to regulate (**Figure 3.7B**). On the other hand, the effect of 20-fold higher compstatin concentration than C3 concentration is over-regulating (or over-restorative), keeping the C3a-desArg levels lower than those of the normal state (**Figure 3.2B**). Lastly, variations in eculizumab have minor effects on regulating early complement fragment C3a-desArg (**Figure 3.7A** and **3.7B**).

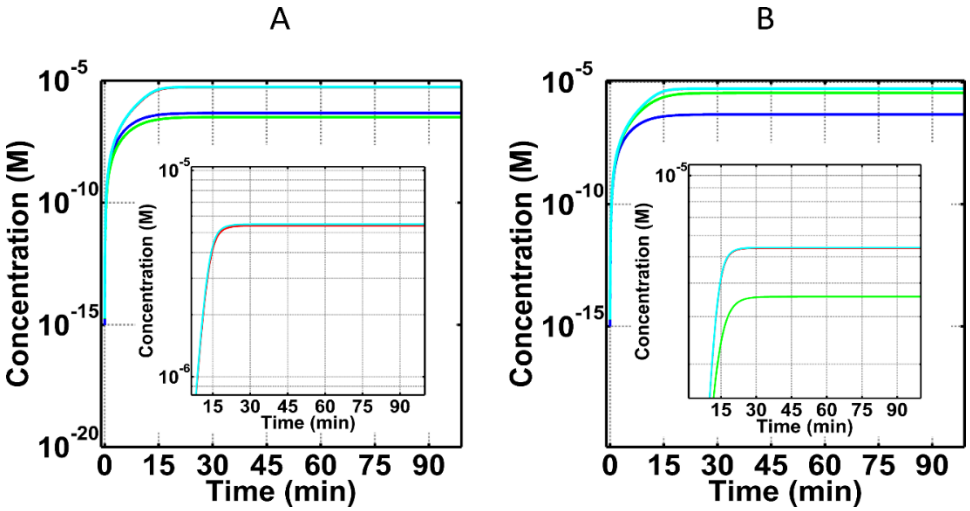

Figure 3.7. Concentration-time profiles for C3a-desArg under four conditions: (i) normal state (blue), (ii) FH disorder state (red), (iii) FH disorder state with compstatin treatment (green), and (iv) FH disorder state with eculizumab treatment (cyan). Concentrations of compstatin used: 7.1×10^{-6}M (one-to-one with C3; A), and 1.4×10^{-6}M (5-fold lower than that of C3; B). Concentrations of eculizumab used: 3.7×10^{-7}M (one-to-one with C5; A), and 7.4×10^{-8}M (5-fold lower concentration than that of C5; B). A dose-dependent response is observed for C3a-desArg under different concentrations of compstatin. Low levels of C3a-desArg are produced under the higher compstatin concentration of 7.1×10^{-6}M (A), whereas high levels of C3a-desArg are produced under the lowest compstatin concentration of 1.4×10^{-6}M (B). Restorative effects of compstatin are compromised at a dose of 5-fold lower concentration than the concentration of target protein C3. Conversely, varying concentrations of eculizumab had minor effects on the levels of C3a-desArg, as shown in the insets of Panels (A and B).

After examining the effects of varying the concentrations of compstatin and eculizumab on C3a-desArg, we next investigated the effects of these inhibitors on late stage biomarker fC5b-9 (**Figure 3.8**). We used the same variations in concentrations for compstatin and eculizumab as used for C3a-desArg, described above. Different doses of compstatin had small effect and never recovered the fC5b-9 concentration-time profile to that of the normal state (**Figures 3.5** and **3.8**). In contrast, one-to-one eculizumab-C5 concentration nearly recovers the fC5b-9 concentration-time profile to that of normal state (**Figure 3.8A**), whereas 5-fold lower eculizumab concentration than C5 concentration is insufficient to regulate (**Figure 3.8B**). As discussed above, the effect of 20-fold higher eculizumab concentration than C5 concentration is over-regulating (or over-restorative), keeping the fC5b-9 levels lower than those of the normal state (**Figure 3.5**).

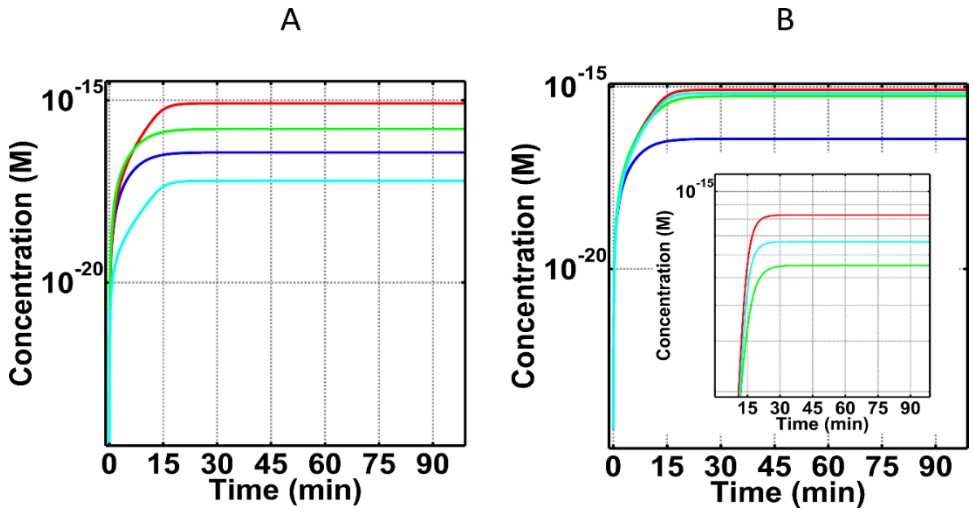

Figure 3.8. Concentration-time profiles for fC5b-9 under four conditions (i) normal state (blue), (ii) FH disorder state (red), (iii) FH disorder state with compstatin treatment (green), and (iv) FH disorder state with eculizumab treatment (cyan). Concentrations of compstatin used: 7.1×10^{-6}M (one-to-one with C3; A), and 1.4×10^{-6}M (5-fold lower than that of C3; B). Concentrations for eculizumab used: 3.7×10^{-7}M (one-to-one with C5; A), and 7.4×10^{-8}M (5-fold lower than C5; B). Treatment with different doses of compstatin showed small effects on fC5b-9 levels. In contrast, treatment with varying concentrations of eculizumab generated a dose-dependent response for fC5b-9. Lowest fC5b-9 levels are produced under the highest eculizumab dosage, and vice versa. Similar to the insufficient dose of compstatin in restoring C3a-desArg, eculizumab also loses restorative effects if the used dose is 5-fold lower than the concentration of the target protein C5.

3.2.8 Combined treatment with compstatin and eculizumab in modulating FH disorder state

Treatment with compstatin (20-fold higher concentration than C3) showed over-restoration in early-stage biomarkers, while treatment with eculizumab (20-fold higher concentration than C5) showed over-restoration of late-stage biomarkers. These results suggest that a combined dose of compstatin and eculizumab at 20-fold higher concentrations than the concentrations of their respective targets would lead to an over-regulation of complement activity in all stages. We next investigated the effects of using dual treatment with compstatin and eculizumab in FH disorder state. We assess early complement activity through the level of C3a-desArg, whereas we use fC5b-9 to assess late-stage complement activity, as shown in **Figure 3.9**. The results for the remaining biomarkers of C3, C5, FB, Ba, and Bb can be found in **Figures B.7-B.9**. For completion of the comparisons, we also provide data for the combined effects of compstatin and eculizumab on the normal state in **Figures B.13-B.10**.

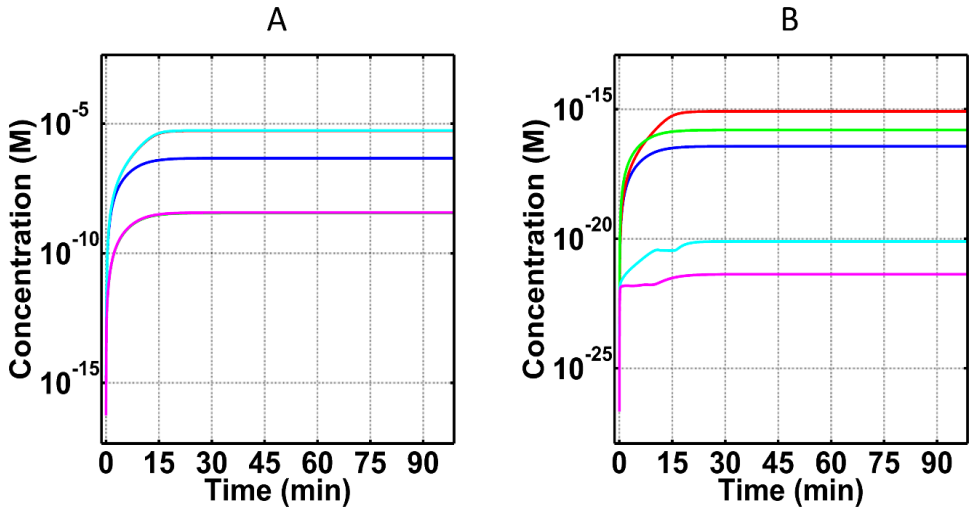

Figure 3.9. Concentration-time profiles for C3a-desArg and fC5b-9 concentrations under five conditions: (i) normal state (blue), (ii) FH disorder state (red), (iii) FH disorder state with compstatin treatment (green), (iv) FH disorder state with eculizumab treatment (cyan), and (v) FH disorder state with compstatin and eculizumab treatment (magenta). Compstatin and eculizumab are at concentrations 20-fold higher than the concentrations of their respective targets, C3 and C5. (A) Production of C3a-desArg. Dual treatment with compstatin and eculizumab and treatment with compstatin-alone over-restore the level of C3a-desArg to the same extent (overlapping concentration-time profiles), as opposed to treatment with eculizumab-alone that has little effect (overlapping time profile with that of the FH disorder state). (B) Production of fC5b-9. Dual treatment with eculizumab and compstatin and treatment with eculizumab-alone over-restore the level of fC5b-9, but treatment with eculizumab-alone over-restores to a lesser extent than dual treatment. On the other hand, treatment with compstatin-alone is not as effective, regulating towards normal state, but not restoring or over-restoring the level of fC5b-9.

Dual treatment with compstatin and eculizumab in the FH disorder state produced C3a-desArg at 3.7×10^{-9}M concentration within 25 minutes (**Figure 3.9A**), a result that is very similar to treatment with compstatin alone (3.5×10^{-9}M within 25 minutes). Given that the FH disorder state shows C3a-desArg production of 5.4×10^{-6}M and the normal state shows C3a-desArg production of 4.6×10^{-7}M concentration within 25 minutes, the dual inhibitor and compstatin-alone effects over-restore C3a-desArg concentration to a level below the normal state. Hence, our model shows that dual treatment has similar effect in the early-stages of complement activation as compstatin treatment alone.

Continued complement activation is marked by the concentration levels of terminal stage biomarker fC5b-9. Dual treatment with compstatin and eculizumab in the FH disorder state produced fC5b-9 at 4.2×10^{-22}M concentration within 25 minutes, compared to treatment with eculizumab-alone (7.7×10^{-21}M) and compstatin-alone (1.6×10^{-16}M) (**Figure 3.9B**). Given that the FH disorder state shows fC5b-9 production of 8.2×10^{-16}M and the normal state shows fC5b-9 production of 3.7×10^{-17}M within 25 minutes, the dual inhibitor and eculizumab-alone effects over-restore fC5b-9 concentration to a level below that of the normal state. However, treatment with compstatin-alone regulates fC5b-9 concentration towards the normal state, but does not fully restore the normal state. Hence, our model shows that both dual treatment and eculizumab-alone treatment have over-restorative effects at the late-stages of complement activation, with dual treatment displaying the most potent regulatory effect.

3.3 Discussion

3.3.1 Modeling of fluid phase alternative and classical pathway activation, and relation to FH-based diseases

In the present study, we used mathematical modeling of the complement system to understand the complex interplay between complement activation/propagation and regulation. First, differential equations were used to model the biochemical reactions involved in the alternative and classical pathways of the complement system under normal condition (physiological condition in homeostasis). Second, we modeled an alternative pathway disordered state by impairing FH to better understand the dynamics of

complement pathology in FH-mediated diseases, called herein FH disorder state. This negative regulator, FH, was chosen because alternative pathway-associated disorders, such as AMD, aHUS, C3GN, DDD, implicate FH impairment at the levels of lower effective concentration or altered binding kinetic parameters leading to improper regulation. Third, we added two complement therapeutic states by incorporating FH disorder state with compstatin treatment (targeting C3) and FH disorder state with eculizumab treatment (targeting C5). And lastly, using these four computational states, we generated concentration-time profiles for biomarkers associated with alternative pathway dysregulation, such as C3, C3a-desArg, C5, C5a-desArg, FB, Ba, Bb, and fC5b-9.

3.3.2 Biomarkers under normal state

Our results show only 7% consumption of C3 (**Figure 3.2A**) and <1% consumption of C5 (**Figure 3.3A**) relative to their respective starting blood plasma concentrations, under normal state. This low consumption reflects the potent regulatory effect of a physiological (unperturbed) FH has on the system. For instance, FH can induce regulation on early phases of the alternative pathway by targeting and inactivating (in conjunction with FI) complement components such as C3(H_2O) and C3b. In addition, FH can regulate enzymes C3(H_2O)Bb and C3bBb, by accelerating their decay rates and inhibiting propagation of complement in the fluid and surface phases. Moreover, another indicator of proper regulations is shown on the levels of FB consumption and generation of its cleavage product Ba and Bb. Binding of FB to either C3(H_2O) or C3b will form the proconvertases of alternative pathway that later become activated through FD to form C3(H_2O)Bb and

C3bBb. However, presence of FH modulates early complement species to ensure most of plasma FB will not be involved in either forming proconvertases or activated through cleavage. The results of **Figure 3.4A** reflect these regulatory events where small amounts of FB are consumed in the process of forming short-lived alternative pathway convertases and cleavage fragments of FB, Ba (after cleavage by FD; **Figure 3.4B**) and Bb (after convertase dissociation by FH, FHL, and CR1, or self-dissociation; **Figure 3.4C**), are also produced in small amounts. Subsequently, proper regulation of convertases also leads to proper modulation of the cleavage rates of C3 and C5. This results in lower amounts of C3 being converted to nC3b and C3a (further deactivated to C3a-desArg), and C5 into C5b and C5a (further deactivated to C5a-desArg). Our model shows these events where the production of biomarkers C3a-desArg (**Figure 3.2B**) and C5a-desArg (**Figure 3.3B**) are produced in low amounts under normal conditions. However, C3a-desArg is shown to be at a higher concentration than C5a-desArg. And lastly, a termination step of the complement system is instigated by C5b associating with C6, C7, C8, and C9 to form fluid phase MAC/fC5b-9. Since the conversion of C5 into C5b and C5a is properly modulated, small amounts of fC5b-9 are produced as a result in the normal state (**Figure 3.5**).

3.3.3 Comparison of normal and FH disorder states

Introduction of alternative pathway dysregulation, through FH impairment, referred herein as FH disorder state, significantly reduced C3 levels by 76% relative to C3 blood plasma concentration (**Figure 3.2A**). This means that suboptimal FH function results in increased levels and stability of alternative pathway C3/C5 convertases. These enzymes

rapidly consume blood plasma C3 to produce elevated levels of C3a-desArg (after C3a deactivation; **Figure 3.2B**) and nC3b compared with the normal state. Presence of elevated nC3b subsequently forms the basis for more production of convertases that later enhance the propagation step of alternative pathway by not only cleaving more C3, but also C5. **Figure 3.3A** and **3.3B** exemplify this event where more C5 is consumed, and C5a-desArg (after C5a deactivation) levels are elevated under the alternative pathway dysregulation of the FH disorder state than in the normal state. Additionally, levels of plasma C5b rise as more C5 is consumed. This initiates the terminal step by C5b starting a cascade of reactions to form fluid phase MAC/fC5b-9. In comparison to the normal state, elevated levels of fC5b-9 are generated under FH disordered state (**Figure 3.5**).

Altogether these data show that impairing FH has the effect of compromising the regulatory checkpoints to generate an overly active complement system with reduced levels of C3 and C5, coupled with elevated levels of inflammation markers C3a-desArg and C5a-desArg.

3.3.4 Effect of compstatin on FH disorder state

Compstatin inhibits cleavage of C3 to C3a and nC3b, and thus inhibits C3 consumption. The rapid reduction of C3 concentration shown in **Figure 3.2A** is not due to consumption, but rather it is owed to C3 being in complex with compstatin to form compstatin:C3 complexes (not shown in **Figure 3.2**). Compstatin has an over-restorative effect on C3a-desArg, meaning that it brings down the concentration of C3a-desArg in the FH disorder state by about three orders of magnitude, while C3a-desArg levels in the

normal state are about one order of magnitude lower than the FH disorder state. In contrast, compstatin has an under-restorative effect on C5a-desArg, meaning that although it brings down the concentration of C5a-desArg in the FH disorder state, it is still about one order of magnitude higher than the C5a-desArg concentration under the normal state (**Figure 3.3B**).

In summary, an overly active complement system under compstatin treatment better modulates levels of C3a-desArg than C5a-desArg. This outcome is due to regulation induced by compstatin in the early-phases of complement activation to generate lower amounts of C3a, later becoming deactivated to form C3a-desArg. Although there is a compensatory effect, it is not clear what is the net effect of compstatin inhibition on C3a-/C5a-induced inflammatory response, given that C5a is a more potent pro-inflammatory protein than C3a. It has been suggested that C3a has both proinflammatory and anti-inflammatory properties [37], whereas C5a is proinflammatory. Therefore, in certain pathologies, C3a and C5a may have opposite roles, and this should be taken into account when selecting treatment drugs.

Furthermore, treatment with compstatin generates a trend for fC5b-9 that is similar to C5a-desArg but smaller in concentration magnitude (**Figure 3.5**). This is because the formation of fC5b-9 is based on the other C5 cleavage product, C5b, which is equivalent in concentration to C5a immediately after cleavage; however C5b is further involved in biochemical reactions that include inactivation, propagation on host cells, and regulation in fluid and host cells (**Figure 3.1**).

In terms of FB and its cleavage fragments (Ba and Bb), compstatin has nearly complete restorative effect on FB, and over-restorative effects on Ba and Bb. These results highlight on the compensatory role that compstatin plays in cases of FH impairment. The potency of FH lies on its ability to target early fragments of the complement activation (C3b) and enzymes (C3/C5 convertases) which initiate and extend the propagation step of the alternative pathway. But in cases of FH impairment, compstatin can aid complement regulation by first targeting C3. This results in reduced levels of early complement fragment C3b. In addition, since initiation and extension of the propagation step depends on C3b and FB, the presence of compstatin reduces C3b levels and this reduces the rate of FB consumption and generation of its cleavage products (Ba and Bb) as shown in **Figure 3.4**.

3.3.5 Effect of eculizumab on FH disorder state

Eculizumab has a minor effect on C3 and its cleavage fragments, C3a and nC3b (**Figure 3.2**), and on FB and its cleavage fragments, Ba and Bb (**Figure 3.4**). This is because eculizumab acts on C5, and inhibits cleavage of C5 to C5a and C5b, thus inhibiting C5 consumption. The dramatic reduction of C5 concentration shown in **Figure 3.3A** is not due to consumption, but rather because treatment with eculizumab generates eculizumab:C5 complexes (not shown in **Figure 3.3**). Eculizumab over-restores the concentrations of C5a-desArg and fC5b-9 in the FH disorder state to about four and three, respectively, orders of magnitude lower than the C5a-desArg and fC5b-9 concentrations in the normal state.

These results suggest that eculizumab may be a better inhibitor than compstatin for diseases that are driven by excess MAC/C5b-9 formation. The potency of eculizumab as a terminal cascade inhibitor is shown on the levels C5a-desArg and fC5b-9 concentrations. However, even in the absence of compstatin and eculizumab, in the FH disorder state the change in C5 concentration is small compared with the change in C3 concentration, relative to their concentration changes in the normal state. Depending on the disease, a treatment with inhibition at the early-stages of the complement pathway (e.g. C3), or a treatment at the late stages of complement pathway (e.g. C5), or a dual treatment may be necessary. The model may be useful to select the point of inhibition, at C3, C5, or other (e.g. FB, FD, fC5b-9, etc), depending on the specific effect we aim to suppress, e.g. inflammation, opsonophagocytosis, MAC/C5b-9 formation.

3.3.6 Sensitivity analysis

Our sensitivity analysis showed the classical pathway fluid phase activation as a major cross activator of the alternative pathway (**Figure 3.6**) under normal conditions. The alternative pathway is initiated through tick-over process with a first order kinetic rate constant of 4.5×10^{-6} s^{-1} while the classical pathway is spontaneously activated much faster through C1 with a kinetic rate constant of 2.8×10^{-3} s^{-1} [4,38]. Activated C1 cleaves C4, followed by C4bC2 to form the classical pathway C3/C5 convertase C4bC2a. This enzyme can initiate the alternative pathway by cleaving C3 before the tick-over forms the initial convertase of the alternative pathway, $C3(H_2O)Bb$. Thus, having a faster activation rate makes C1 the critical step in forming enzymes that can activate and propagate the

alternative pathway in the fluid phase. **Figure 3.6A** displays this notion where the kinetic parameter that regulates C1* by the action of C1-INH is the most sensitive parameter that mediates levels of C3. Lastly, while the remaining critical parameters of the classical pathway are involved in interactions that affect steps that either form or inhibit C3/C5 convertases of the classical pathway, the alternative pathway has a single key regulation step mediated by FH in conjunction with FI that controls the levels of C3 and C5 (**Figure 3.6**). The potency of FH not only lies in accelerating the decay rate of convertases, but also working in concert with FI to cleave C3b into iC3b. This cleavage step reduces the rate of C3/C5 convertases formation since iC3b does not from convertases.

3.3.7 Effects of varying doses of compstatin and eculizumab on C3a-desArg and fC5b-9 in FH disorder state

Varying concentrations of compstatin affect levels of C3a-desArg in a dose-dependent manner, while different doses of eculizumab showed minor effects on C3a-desArg (**Figures 3.2B** and **3.7**). Unlike eculizumab, treatment with compstatin generate compstatin:C3 complexes that are shielded from cleavage by C3/C5 convertases. This step inhibits early cascade of reactions induced by nC3b and C3a that later form C3/C5 convertases and C3a-desArg, respectively. However, reducing the levels of compstatin further compromises regulation and increase the levels of C3a-desArg. For instance, restorative capabilities of compstatin are significantly impaired when the concentration of compstatin is 5-fold lower than that of C3. Under this concentration, compstatin has an

under-restorative effect by generating C3a-desArg levels that are closer to the FH disorder state than the normal state.

Although production of the early-stage complement biomarker C3a-desArg is highly dependent on compstatin and not eculizumab, late-stage complement fC5b-9 is more dependent on eculizumab than compstatin (**Figures 3.5** and **3.8**). Varying the doses of compstatin generated fC5b-9 levels that were closer to fC5b-9 levels under the FH disorder state. However, treatment with eculizumab generates a dose-dependent response of fC5b-9 levels because of the eculizumab:C5 complexes that are formed. This eculizumab:C5 complex is protected from cleavage by convertases to C5a/C5b fragments, and thus C5b-based initiation of the cascade of reactions that lead to fC5b-9 formation is inhibited. As the levels of eculizumab increase, less fC5b-9 complexes are formed. Comparison of the results of **Figures 3.5** and **3.8** show this relation where fC5b-9 levels are the lowest under the highest eculizumab concentration (20-fold higher than the concentration of C5). Conversely, highest levels of fC5b-9 are generated under the lowest eculizumab concentration (5-fold lower than the concentration of C5).

In summary, compstatin shows higher restorative efficacy for early-stage biomarker C3a-desArg, whereas eculizumab has higher restorative efficacy for late-stage biomarker fC5b-9. Also, one-to-one inhibitor-to-target protein concentrations are sufficient for complete restoration of the FH disorder state to the normal state in this model. However, we should point out that this concentration ratio may change when we incorporate in the model inhibitor metabolism and complement protein turnover steps.

3.3.8 Effects of dual complement inhibitors on FH disorder state

Dual treatments of compstatin and eculizumab show similar effect as compstatin treatment alone in regulating early-stage complement biomarker C3a-desArg (**Figure 3.9A**). Both forms of treatment include compstatin which acts early in the complement cascade by targeting complement C3. The cleavage of C3 is inhibited by compstatin through the formation of compstatin:C3 complexes. Our results show the addition of eculizumab, as a secondary treatment (in a dual treatment), may be unnecessary in cases of early-stage complement over-activation leading to opsonophagocytosis. In this case targeting of complement C3 only is sufficient to restore early biomarkers under FH dysfunction. This presents an additional avenue in developing complement therapeutics where targeting early-stage complement instigators, such as FB and FD, may be adequate in regulating the early stages of the complement system, and perhaps at low drug concentrations since FD and FB are found at lower concentrations than C3 in blood. It should be noted that our current model does not account for the half-lives and bioavailability of the complement inhibitors used (compstatin and eculizumab). Thus, the results presented here are indicative of effects by drugs with similar and optimal bioavailabilities in order to induce and sustain their effects under FH dysfunction.

Dual treatments on the other hand, show differences in regulating late-stage complement biomarker fC5b-9. Eculizumab treatment alone over-restores the level of fC5b-9, and compstatin alone regulates but does not over-restore (**Figure 3.9B**); however dual treatment is more potent in regulating fC5b-9 in FH disorder state. Dual treatments can reduce the available blood plasma C3 and C5, regulating terminal functions of

opsonophagocytosis and lysis, in diseases like PNH that demonstrate extra- and intra-vascular hemolysis.

3.3.9 Relation of the model to clinical disorders and therapeutics

Altogether our data highlight the importance of FH in regulating the levels of the central substrate of the complement system, C3. Furthermore, the presence of unimpaired FH is also essential for regulating the levels of blood plasma FB. Disorders related to the alternative pathway, such as C3GN, DDD, and aHUS are typically characterized with low levels of plasma C3 and FB, while FB cleavage products, Ba and Bb, are elevated [24–28]. Although these disorders are also associated with mutations/polymorphisms in other complement protein, such as C3, FI, FB, and FH related proteins, in addition to FH mutations/polymorphisms, our data shows that just impairing FH is sufficient to generate clinically observed trends for C3, FB, Ba, and Bb. In support of this notion, biomarker profiling of patients with C3GN and DDD shows that having type 1 mutation in FH (reduced levels of FH concentration) was sufficient to generate to low levels of plasma C3 and FB [28]. Furthermore, absence of plasma FH has also been observed to cause C3 glomerulopathies in humans [28]. Another disease related to alternative pathway dysregulation, aHUS, also frequently has FH concentration deficiencies [28]. Hence, our computational model predicts that mutations on FH alone may be sufficient factors in propagating diseases such as C3GN and aHUS, despite of a possible presence of multiple disease-related mutations on other complement proteins. Thus, FH plays a pivotal role in

ensuring proper regulation, and mutations that alter concentration or kinetics of FH will instigate the dysregulation of the alternative pathway.

In addition to generating biomarker trends associated with the alternative pathway dysregulation, our computational model also shows treatment with eculizumab effectively regulates terminal complement activity while having a minor effect on early complement activity induced by C3. This coupled effect was observed for PNH patients where treatment with eculizumab regulated terminal complement activation but some patients still suffered from extravascular opsonophagocytosis (also referred to as extravascular hemolysis) that is attributed to early-phase complement activation and propagation induced by C3 [39]. Subsequently, a recent study showed that complement intervention by compstatin protected PNH erythrocytes from complement mediated lysis and modulated early-phase complement deposition and propagation induced by C3 [40]. These findings are consistent with our computational model where eculizumab shows little effect on C3 level under FH impairment, whereas compstatin regulates potently early-stage complement activity and less potently late-stage complement activation. However, our model also shows eculizumab is much more potent regulator of late-stage complement activation and propagation than compstatin. Thus, efficient complement therapy may require disease-specific biomarker targeting, or dual point targeting.

Overall, this study serves as a proof-of-concept on the capabilities of the model in predicting the dynamics of the complement system under homeostasis and disease states, and in predicting the effects of drugs in restoring the complement system from a disease state to the normal state.

3.4 Conclusions

We have generated a comprehensive model of the alternative and classical pathway of the complement system that is divided into: (i) normal state, corresponding to homeostasis in a healthy person, (ii) alternative pathway dysregulation through FH impairment, called FH disorder state, (iii) FH disorder state with compstatin treatment, and (iv) FH disorder state with eculizumab treatment. We analyzed the state of the system by generating time profiles for biomarkers associated with alternative pathway FH disorders: C3, C3a-desArg, C5, C5a-desArg, FB, Ba, Bb, and fC5b-9. The computational model shows major changes on these biomarkers in the FH disorder state, compared with the normal state. The model shows restorative effects in the biomarker concentration levels, from the FH disorder state towards the normal state, upon treatment with compstatin and eculizumab. Compstatin is more effective in restoring biomarker concentrations at the early-stages of the complement cascade, compared with biomarkers of the late stages. Conversely, eculizumab is more effective in restoring concentrations at the late stages of the complement cascade, compared to the effects of compstatin on late stage biomarkers. Lastly, the model predicts effective doses of compstatin and eculizumab to be one-to-one against their respective targets, C3 and C5, to properly restore early- and late-stage biomarkers.

The model serves as the basis for developing disease-specific models, and even patient-specific models if sufficient genetic and clinical data is available, by perturbing other complement proteins (than or in addition to FH), or combinations of proteins. This can be achieved by obtaining blood plasma concentrations of impaired complement

proteins/regulators from patients with alternative pathway disorders to perform in vitro binding experiments. Such experiments will measure kinetic parameters for the binding of impaired regulators or propagators to their target proteins. Subsequently, patient-specific disease models can be generated using the experimentally determined kinetic parameters to perform comparative analyses to clinical observations. The results can further be used to identify which biomarkers are suitable in assessing the degree of complement dysregulation. The patient-specific disease model can also be used to identify the optimal point of inhibition within the complement cascade, and if a pool of drugs is available, the model can be used to select the right drug or combination of drugs for treatment. Currently, eculizumab is approved for use in the clinic, and variants of compstatin are undergoing clinical trials. There are other approved drugs targeting C1-INH, and there are several other drugs in the pre-clinical and clinical trial pipeline, targeting C1r, C1s, C3, C3a, C5, C5a, C6, FH, FD, FB, FP, etc [41], and soon we expect to have approval for clinical use a pool of several drugs against complement-mediated inflammatory and autoimmune diseases. Overall, our system sets the stage to generate disease-specific models that are suitable for patient-specific diagnosis.

3.5 Methods

3.5.1 Mathematical model

Our mathematical model is based on the biochemical reactions shown in **Figure 3.1**. The biochemical reactions are generated from critical reading of papers with experimental and clinical data, published in the scientific literature. Using the cascade of

biochemical reactions in the classical and alternative pathway, we generated a system of 290 ODEs with 142 kinetic parameters. Similar to our previous model [17], we organized the biochemical reactions and equations into modules that describe complement system: (i) initiation, 1–55 **Supplemental Equations B.1**; (ii) amplification, 56–77 **Supplemental Equations B.1**; (iii) termination, 78–110 **Supplemental Equations B.1**; (iv) regulation 111–256 **Supplemental Equations B.1**; and (v) complement proteins in fluid phase and derived from bound components on host cells, 257–290 **Supplemental Equations B.1**. It should be noted, initial concentrations of complement species are based on the normal ranges with individuals that are not influenced by disease states of the complement system. This limits our model.

In addition, we added two more modules that describe complement therapeutic states brought by the actions of known complement inhibitors compstatin, 291-293 **Supplemental Equations B.2**, and eculizumab, 294-296 **Supplemental Equations B.2**. As mentioned above, compstatin targets complement component C3 and eculizumab targets complement component C5. In this study, we use kinetic parameters for the compstatin analog with sequence Ac-I[CVWQDWGAHRC]T-NH_2 (brackets denote disulfide bridge cyclization) from Ref [33]. Perturbation that leads to regulatory disorder is modeled by reducing FH concentration and kinetics by an order of magnitude as shown in Tables B.2-B.8. The biochemical reactions are converted to a system of ODEs, describing the mass balance for each complement protein, protein fragment, or protein complex. Enzymatic reactions are based on Michaelis–Menten kinetics and substrate competitions for the same enzyme are considered for complement species such as C3 and

C5 convertases. Equations are solved using the ode23tb solver of Matlab (Mathworks, Natick, MA).

Methods for parameter estimations or calculations, when experimental values are not available (Tables B.2-B.9), and multi-parametric sensitivity analysis (MPSA) for global sensitivity are described in our previous paper [17]. Briefly, for MPSA we first selected kinetic parameters involved in our biochemical reactions of alternative and classical pathways. Then we generated ranges for each parameter to be large enough to cover all feasible variations. For each parameter set, we calculated the sum of squared errors between the observed and perturbed system output values. We used the results of this calculation to determine if the chosen set of parameters is acceptable or unacceptable. The cumulative frequency was calculated for both acceptable and unacceptable cases and was used to evaluate the sensitivity of each parameter using Kolmogorov-Smirnov statistic. Parameter ranges used in multi-parametric sensitivity analysis can be found in **Table B.9**.

For unknown parameters, we assumed the kinetic rate constants to be the same as in those of structurally or functionally homologous proteins with known experimental parameter values. For instance, the kinetic parameters for C3(H_2O) and FB interaction are not known, whereas those for C3b and FB interaction are known. Since C3(H_2O) is known to be a C3b-like molecule that functions similarly to C3b by forming alternative pathway proconvertases and C3 convertases, we assumed C3(H_2O) to have the same kinetic parameters as C3b. In addition, since the convertases C3(H_2O)Bb and C3bBb decay with similar rates, 9.0×10^{-3} s^{-1} and 7.7×10^{-3} s^{-1}, respectively [42], we assumed the rate of decay induced by FH on C3bBb and on C3(H_2O)Bb to be the same. This assumption is consistent

with similar biochemical interaction between FH and serine protease, Bb, that is present on both convertases (C3(H_2O)Bb, C3bBb). Lastly, due to the lack of kinetic data on the decay rates induced by complement regulators such as decay-accelerating factor, complement receptor 1, and C4b-binding protein we assumed they will also have the same decay accelerating rate as FH because these regulators function in a FH-like manner by either inhibiting or deactivating C3/C5 convertases.

3.5.2 Biochemical model

Below, we will describe the complement system pathways of **Figure 3.1**. These pathways entail activation, propagation, and regulation of the complement system. The pathways describe interactions of complement proteins, fragments, and complexes that operate entirely in the fluid phase, as well as those that bind to cell surfaces, undergoing further processing, and returning products to fluid phase. The characteristics of the surface of a red blood cell are used in the model [17].

3.5.3 Initiation (fluid phase)

The alternative pathway is spontaneously activated in plasma through a process known as the tick-over reaction, and involves the spontaneous hydrolysis of an internal thioester bond in C3. This is an irreversible step that produces a C3b-like molecule, C3(H_2O), with its internal thioester bond hydrolyzed. The complement protease FB associates with C3(H_2O) to form a proconvertase, C3(H_2O)B. Subsequently, enzymatic cleavage of C3(H_2O)-bound FB by Factor D follows to form the initial convertase of the

alternative pathway, C3(H_2O)Bb. This short-lived enzyme can cleave C3 to form C3a and nascent fluid phase C3b (nfC3b). While C3a is anaphaytoxin [5], nfC3b has an exposed highly-reactive internal thioester bond that is capable of indiscriminately binding to different surfaces via covalent attachment, or forming fluid phase C3b (fC3b) by interacting with water [43–45]. The fC3b fragment cannot covalently attach to cells but can still propagate the alternative pathway by associating with FB and following the same cascade of reactions as C3(H_2O), forming form the fluid C3/C5 convertase, C3bBb [42,46].

Similar to the alternative pathway, the classical pathway also initiates in the fluid phase through the spontaneous autoactivation of component complex C1 [4]. This leads to the formation of C1* that cleaves C4. This process leads to the formation of C4a and nascent fluid phase C4b (nfC4b). Similar to nfC3b, nascent fluid C4b can covalently attach to nearby surface or form fluid phase C4b (fC4b) by interacting with water [47]. Complement C2 then interacts with C4b to form the proconvertase of the classical pathway, C4bC2. Similar to C4, this complex is also activated by C1* to form the C3/C5 convertase, C4bC2a.

In addition to the covalent bonds formed between nfC3b/nfC4b to cell membranes, covalent linkage can occur between C3b and C4b fragments, forming C3bC4b, C3bC3b, or C4bC4b complexes. These complexes can associate with FB or C2 to form C3/C5 convertases, fC4bC3bBb, fC3bC3bBb, fC3bC4bC2a, and fC4bC4bC2a [9–11]. Furthermore, C3b dimers, C3bC3b, can also covalently attach with immunoglobulin G, IgG, to form IgGC3bC3b [8]. This complex functions as a C3 convertase that cleaves C3 into C3a and nfC3b.

3.5.4 Amplification

Once nfC3b attaches covalently to a host surface, a cascade of reactions ensues where FB is recruited first, followed by FD cleavage to yield the surface bound C3/C5 convertase, C3bBb. Since this enzyme is rather unstable, the only positive regulator of the alternative pathway, known as properdin, binds and extend the half-life of C3bBb by 10-fold [48,49]. Similar to the propagation step in the fluid phase, formation of dimers associated with C3b or C4b occurs on the surface of host cells. These dimers, C3bC3b/C3bC4b, can associate with either FB, followed by activation step with FD to form the C3/C5 convertases (C3bC3bBb/C4bC3bBb). However, unlike C3bC3b/C3bC4b dimers in the fluid phase that can also bind to C2, the surface activation mechanism for C1* is not added since it requires antigens to anchor to the surface first [50–52]. Here, host cells are under normal conditions while the impairment in our model only applies to FH in the fluid phase. Lastly, C3b dimers can also associate with properdin to form stabilized C3/C5 convertase that enhances complement activation within the vicinity of this convertase.

3.5.5 Termination

Cleavage of complement C5 by C3/C5 convertases such as fC3bBb or fC4bC2a, leads to the formation of C5a and C5b. Like C3a, C5a is a mediator of inflammation [5]. C5b binds to C6 and subsequently to C7 and forms C5b-7. This complex can insert itself into the lipid bilayer but also can form inactive micelles in the absence of cell membranes [53,54]. Furthermore, C5b-7 binds to C8, followed by C9 to form fluid phase MACs (fC5b-

9). However, if C5b-7 attaches to a cell, C8 binding occurs, followed by the attachments of multiple C9 molecules to from a MAC. Presence of MACs compromise the integrity of cell membranes and induce cell death. In addition to fC3bBb/fC4bC2a cleaving C5, dimerized forms such as fC4bC3bBb or fC3bC4bC2a can also cleave C5 but C5b remains loosely bound to the convertase while C5a is released in the fluid phase. When C5b is still bound to the convertase, it is capable of binding to C6. Complement C7 then binds and subsequently leads to C5b-7 complex dissociating from the C3/C5 convertase.

3.5.6 Regulation

Multiple check-points are in place to ensure proper regulation of the complement system. FH and FHL-1 proteins are primarily regulators of the alternative pathway that can act in both fluid and surface phases, while C1-INH and C4BP are the primary regulators for the classical pathway in both phases (fluid and surface). These regulators of complement act on the early-stages of the activation by targeting C1* (by C1-INH), or C3b and C4b (by C4BP) to suppress the propagation step. Inactivation of C3b is mediated through its cleavage to inactivated C3b (iC3b) by FI in conjunction with either FH, FHL-1, or CR1 as cofactors, while C4b is deactivated into C4d by FI with C4BP as its cofactor. Further cleavage of iC3b to C3dg is mediated by FI, using CR1 as a cofactor [1,2]. In addition, other membrane bound regulators such DAF can also act in concert with FH, FHL-1, and C4BP to accelerate the decay of C3/C5 convertases [1,2]. Furthermore, MCP is another cell-bound regulator that acts as a cofactor to deactivate C3b/C4b in conjunction with FI. Since MCP is not expressed on erythrocytes, it was not included in the model.

Finally, late stage complement propagation in the terminal cascade is tightly controlled through fluid phase regulators such as Vn or Cn that act on fC5b-7, while surface bound regulator CD59 inhibits C9 polymerization [7,55].

3.5.7 FH disorder with compstatin and eculizumab treatments

Disorders of the alternative pathway, such as C3GN, DDD, AMD, and aHUS all implicate FH impairment through either reduced concentration (type 1 mutation) or binding/regulatory functionality (type 2 mutation) [19–28]. To mimic clinical observations, we generated an FH disorder model by reducing its concentration and association rate constant by one order of magnitude (Tables B.2-B.8). After modeling FH disorder, we subsequently generated complement therapeutic states by incorporating into the FH disorder state known complement inhibitors, such as a compstatin family peptide and the monoclonal antibody eculizumab. Compstatin is small peptide that targets complement C3 and inhibits the cleavage of C3 by C3/C5 convertases [29–31]. Similar in functionality to compstatin, eculizumab targets complement C5 and inhibits the cleavage of C5 by C3/C5 convertases [34–36].

3.5.8 Dose dependence for compstatin and eculizumab

In the initial calculations, the concentrations of compstatin and eculizumab were taken to be 20-fold higher than the concentrations of their respective targets, C3 and C5 (**Figure B.1**). These inhibitor concentrations are used to generate **Figures 3.2–3.5**. In addition, we performed calculations using two more inhibitor concentrations to evaluate the dose-dependent effect on complement dynamics under the disease state induced by FH impairment. Concentrations of compstatin and eculizumab were taken to be one-to-one and 5-fold lower than the concentrations of their respective targets. In total, in the dose-dependent study of compstatin we used concentrations: 1.4×10^{-4}M (20-fold higher than C3), 7.1×10^{-6}M (1-to-1 to C3) and 1.4×10^{-6}M (5-fold lower than C3). In the dose-dependent study of eculizumab we used concentrations: 7.4×10^{-6}M (20-fold higher than C5), 3.7×10^{-7}M (1-to-1 to C5) and 7.4×10^{-8}M (5-fold lower than C5).

3.5.9 Limitations of disease model

Concentrations of complement proteins in the normal state are based on standard ranges from individuals that are not influenced by complement-mediated disease states. Hence, our disease model also uses the same basal concentration levels. However, individuals with autoimmune disorders may have different initial concentrations of complement proteins, which is not taken into account in the model. Here, we investigate the effect of FH perturbations on the normal state and how the concentration dynamics of complement proteins are influenced by those perturbations. The applied perturbations correspond to genetic origins of disease, such as mutations/polymorphisms. Given that FH

is the most potent complement regulator, FH perturbations are present in many complement-mediated diseases, in addition to mutations in other complement proteins and regulators, e.g. C3, FI, FB, FH related proteins, etc. Diseases such as C3GN and DDD may also have acquired causes of alternative pathway dysregulation through antibody action, i.e. C3 nephritic factors that stabilize C3/C5 convertases [24]. Hence, if a heterogenous disease involves various genetic and acquired factors, our model may not account for the full magnitude of the disease.

3.6 References

1. Merle NS, Church SE, Fremeaux-Bacchi V, Roumenina LT. Complement System Part I - Molecular Mechanisms of Activation and Regulation. Front Immunol. 2015;6: 262. doi:10.3389/fimmu.2015.00262

2. Schmidt CQ, Lambris JD, Ricklin D. Protection of host cells by complement regulators. Immunol Rev. 2016;274: 152–171. doi:10.1111/imr.12475

3. Schatz-Jakobsen JA, Pedersen DV, Andersen GR. Structural insight into proteolytic activation and regulation of the complement system. Immunol Rev. 2016;274: 59–73. doi:10.1111/imr.12465

4. Ziccardi RJ. Spontaneous activation of the first component of human complement (C1) by an intramolecular autocatalytic mechanism. J Immunol Baltim Md 1950. 1982;128: 2500–2504.

5. Merle NS, Noe R, Halbwachs-Mecarelli L, Fremeaux-Bacchi V, Roumenina LT. Complement System Part II: Role in Immunity. Front Immunol. 2015;6. doi:10.3389/fimmu.2015.00257

6. Ricklin D, Reis ES, Mastellos DC, Gros P, Lambris JD. Complement component C3 - The “Swiss Army Knife” of innate immunity and host defense. Immunol Rev. 2016;274: 33–58. doi:10.1111/imr.12500

7. Morgan BP, Boyd C, Bubeck D. Molecular cell biology of complement membrane attack. Semin Cell Dev Biol. 2017; doi:10.1016/j.semcdb.2017.06.009

8. Lutz HU, Jelezarova E. Complement amplification revisited. Mol Immunol. 2006;43: 2–12. doi:10.1016/j.molimm.2005.06.020

9. Meri S, Pangburn MK. A mechanism of activation of the alternative complement pathway by the classical pathway: protection of C3b from inactivation by covalent attachment to C4b. Eur J Immunol. 1990;20: 2555–2561. doi:10.1002/eji.1830201205

10. Rawal N, Pangburn M. Formation of high-affinity C5 convertases of the alternative pathway of complement. J Immunol Baltim Md 1950. 2001;166: 2635–2642.

11. Rawal N, Pangburn MK. Formation of High Affinity C5 Convertase of the Classical Pathway of Complement. J Biol Chem. 2003;278: 38476–38483. doi:10.1074/jbc.M307017200

12. Sagar A, Dai W, Minot M, LeCover R, Varner JD. Reduced order modeling and analysis of the human complement system. PLoS ONE. 2017;12. doi:10.1371/journal.pone.0187373

13. Korotaevskiy AA, Hanin LG, Khanin MA. Non-linear dynamics of the complement system activation. Math Biosci. 2009;222: 127–143. doi:10.1016/j.mbs.2009.10.003

14. Hirayama H, Yoshii K, Ojima H, Kawai N, Gotoh S, Fukuyama Y. Linear systems analysis of activating processes of complement system as a defense mechanism. Biosystems. 1996;39: 173–185. doi:10.1016/0303-2647(96)01617-6

15. Liu B, Zhang J, Tan PY, Hsu D, Blom AM, Leong B, et al. A Computational and Experimental Study of the Regulatory Mechanisms of the Complement System. PLoS Comput Biol. 2011;7: e1001059. doi:10.1371/journal.pcbi.1001059

16. Lang SN, Germerodt S, Glock C, Skerka C, Zipfel PF, Schuster S. Molecular crypsis by pathogenic fungi using human factor H. A numerical model. PloS One. 2019;14: e0212187. doi:10.1371/journal.pone.0212187

17. Zewde N, Jr RDG, Dorado A, Morikis D. Quantitative Modeling of the Alternative Pathway of the Complement System. PLOS ONE. 2016;11: e0152337. doi:10.1371/journal.pone.0152337

18. Ricklin D, Reis ES, Lambris JD. Complement in disease: a defence system turning offensive. Nat Rev Nephrol. 2016;12: 383–401. doi:10.1038/nrneph.2016.70

19. Liszewski MK, Java A, Schramm EC, Atkinson JP. Complement Dysregulation and Disease: Insights from Contemporary Genetics. Annu Rev Pathol. 2017;12: 25–52. doi:10.1146/annurev-pathol-012615-044145

20. Vernon KA, Ruseva MM, Cook HT, Botto M, Malik TH, Pickering MC. Partial Complement Factor H Deficiency Associates with C3 Glomerulopathy and Thrombotic Microangiopathy. J Am Soc Nephrol JASN. 2016;27: 1334–1342. doi:10.1681/ASN.2015030295

21. De Vriese AS, Sethi S, Van Praet J, Nath KA, Fervenza FC. Kidney Disease Caused by Dysregulation of the Complement Alternative Pathway: An Etiologic Approach. J Am Soc Nephrol JASN. 2015;26: 2917–2929. doi:10.1681/ASN.2015020184

22. Józsi M, Tortajada A, Uzonyi B, Goicoechea de Jorge E, Rodríguez de Córdoba S. Factor H-related proteins determine complement-activating surfaces. Trends Immunol. 2015;36: 374–384. doi:10.1016/j.it.2015.04.008

23. Pickering MC, D'Agati VD, Nester CM, Smith RJ, Haas M, Appel GB, et al. C3 glomerulopathy: consensus report. Kidney Int. 2013;84: 1079–1089. doi:10.1038/ki.2013.377

24. Zhang Y, Nester CM, Martin B, Skjoedt M-O, Meyer NC, Shao D, et al. Defining the complement biomarker profile of C3 glomerulopathy. Clin J Am Soc Nephrol CJASN. 2014;9: 1876–1882. doi:10.2215/CJN.01820214

25. Angioi A, Fervenza FC, Sethi S, Zhang Y, Smith RJ, Murray D, et al. Diagnosis of complement alternative pathway disorders. Kidney Int. 2016;89: 278–288. doi:10.1016/j.kint.2015.12.003

26. Nester CM, Smith RJH. Complement inhibition in C3 glomerulopathy. Semin Immunol. 2016;28: 241–249. doi:10.1016/j.smim.2016.06.002

27. Servais A, Frémeaux-Bacchi V, Lequintrec M, Salomon R, Blouin J, Knebelmann B, et al. Primary glomerulonephritis with isolated C3 deposits: a new entity which shares common genetic risk factors with haemolytic uraemic syndrome. J Med Genet. 2007;44: 193–199. doi:10.1136/jmg.2006.045328

28. Servais A, Noël L-H, Roumenina LT, Le Quintrec M, Ngo S, Dragon-Durey M-A, et al. Acquired and genetic complement abnormalities play a critical role in dense deposit disease and other C3 glomerulopathies. Kidney Int. 2012;82: 454–464. doi:10.1038/ki.2012.63

29. Gorham RD, Forest DL, Khoury GA, Smadbeck J, Beecher CN, Healy ED, et al. New compstatin peptides containing N-terminal extensions and non-natural amino acids exhibit potent complement inhibition and improved solubility characteristics. J Med Chem. 2015;58: 814–826. doi:10.1021/jm501345y

30. Gorham RD, Forest DL, Tamamis P, López de Victoria A, Kraszni M, Kieslich CA, et al. Novel compstatin family peptides inhibit complement activation by drusen-like

deposits in human retinal pigmented epithelial cell cultures. Exp Eye Res. 2013;116: 96–108. doi:10.1016/j.exer.2013.07.023

31. Mohan RR, Cabrera AP, Harrison RES, Gorham RD, Johnson LV, Ghosh K, et al. Peptide redesign for inhibition of the complement system: Targeting age-related macular degeneration. Mol Vis. 2016;22: 1280–1290.

32. Mallik B, Katragadda M, Spruce LA, Carafides C, Tsokos CG, Morikis D, et al. Design and NMR characterization of active analogues of compstatin containing non-natural amino acids. J Med Chem. 2005;48: 274–286. doi:10.1021/jm0495531

33. López de Victoria A, Gorham RD, Bellows ML, Ling J, Lo DD, Floudas CA, et al. A New Generation of Potent Complement Inhibitors of the Compstatin Family. Chem Biol Drug Des. 2011;77: 431–440. doi:10.1111/j.1747-0285.2011.01111.x

34. Dmytrijuk A, Robie-Suh K, Cohen MH, Rieves D, Weiss K, Pazdur R. FDA Report: Eculizumab (Soliris®) for the Treatment of Patients with Paroxysmal Nocturnal Hemoglobinuria. The Oncologist. 2008;13: 993–1000. doi:10.1634/theoncologist.2008-0086

35. Rother RP, Rollins SA, Mojcik CF, Brodsky RA, Bell L. Discovery and development of the complement inhibitor eculizumab for the treatment of paroxysmal nocturnal hemoglobinuria. Nat Biotechnol. 2007;25: 1256–1264. doi:10.1038/nbt1344

36. Schatz-Jakobsen JA, Zhang Y, Johnson K, Neill A, Sheridan D, Andersen GR. Structural Basis for Eculizumab-Mediated Inhibition of the Complement Terminal Pathway. J Immunol Baltim Md 1950. 2016;197: 337–344. doi:10.4049/jimmunol.1600280

37. Coulthard LG, Woodruff TM. Is the complement activation product C3a a proinflammatory molecule? Re-evaluating the evidence and the myth. J Immunol Baltim Md 1950. 2015;194: 3542–3548. doi:10.4049/jimmunol.1403068

38. Pangburn MK, Schreiber RD, Müller-Eberhard HJ. Formation of the initial C3 convertase of the alternative complement pathway. Acquisition of C3b-like activities by spontaneous hydrolysis of the putative thioester in native C3. J Exp Med. 1981;154: 856–867.

39. Mastellos DC, Yancopoulou D, Kokkinos P, Huber-Lang M, Hajishengallis G, Biglarnia AR, et al. Compstatin: a C3-targeted complement inhibitor reaching its prime for bedside intervention. Eur J Clin Invest. 2015;45: 423–440. doi:10.1111/eci.12419

40. Risitano AM, Ricklin D, Huang Y, Reis ES, Chen H, Ricci P, et al. Peptide inhibitors of C3 activation as a novel strategy of complement inhibition for the treatment of

paroxysmal nocturnal hemoglobinuria. Blood. 2014;123: 2094–2101. doi:10.1182/blood-2013-11-536573

41. Morgan BP, Harris CL. Complement, a target for therapy in inflammatory and degenerative diseases. Nat Rev Drug Discov. 2015;14: 857–877. doi:10.1038/nrd4657

42. Pangburn MK, Müller-Eberhard HJ. The C3 convertase of the alternative pathway of human complement. Enzymic properties of the bimolecular proteinase. Biochem J. 1986;235: 723–730.

43. Law SK, Lichtenberg NA, Levine RP. Evidence for an ester linkage between the labile binding site of C3b and receptive surfaces. J Immunol Baltim Md 1950. 1979;123: 1388–1394.

44. Law SK, Levine RP. Interaction between the third complement protein and cell surface macromolecules. Proc Natl Acad Sci U S A. 1977;74: 2701–2705.

45. Sim RB, Twose TM, Paterson DS, Sim E. The covalent-binding reaction of complement component C3. Biochem J. 1981;193: 115–127.

46. Rawal N, Pangburn MK. C5 convertase of the alternative pathway of complement. Kinetic analysis of the free and surface-bound forms of the enzyme. J Biol Chem. 1998;273: 16828–16835.

47. Law SK, Dodds AW. The internal thioester and the covalent binding properties of the complement proteins C3 and C4. Protein Sci Publ Protein Soc. 1997;6: 263–274.

48. Harboe M, Johnson C, Nymo S, Ekholt K, Schjalm C, Lindstad JK, et al. Properdin binding to complement activating surfaces depends on initial C3b deposition. Proc Natl Acad Sci U S A. 2017;114: E534–E539. doi:10.1073/pnas.1612385114

49. Hourcade DE. The role of properdin in the assembly of the alternative pathway C3 convertases of complement. J Biol Chem. 2006;281: 2128–2132. doi:10.1074/jbc.M508928200

50. Diebolder CA, Beurskens FJ, de Jong RN, Koning RI, Strumane K, Lindorfer MA, et al. Complement is activated by IgG hexamers assembled at the cell surface. Science. 2014;343: 1260–1263. doi:10.1126/science.1248943

51. Wang G, de Jong RN, van den Bremer ETJ, Beurskens FJ, Labrijn AF, Ugurlar D, et al. Molecular Basis of Assembly and Activation of Complement Component C1 in Complex with Immunoglobulin G1 and Antigen. Mol Cell. 2016;63: 135–145. doi:10.1016/j.molcel.2016.05.016

52. Gaboriaud C, Ling WL, Thielens NM, Bally I, Rossi V. Deciphering the Fine Details of C1 Assembly and Activation Mechanisms: “Mission Impossible”? Front Immunol. 2014;5. doi:10.3389/fimmu.2014.00565

53. Müller-Eberhard HJ. The membrane attack complex of complement. Annu Rev Immunol. 1986;4: 503–528. doi:10.1146/annurev.iy.04.040186.002443

54. Serna M, Giles JL, Morgan BP, Bubeck D. Structural basis of complement membrane attack complex formation. Nat Commun. 2016;7: ncomms10587. doi:10.1038/ncomms10587

55. Meri S, Morgan BP, Davies A, Daniels RH, Olavesen MG, Waldmann H, et al. Human protectin (CD59), an 18,000-20,000 MW complement lysis restricting factor, inhibits C5b-8 catalysed insertion of C9 into lipid bilayers. Immunology. 1990;71: 1–9.

CHAPTER 4

Mathematical Model of the Complement System under Pathogenic Invasion

4.1 Introduction

The human respiratory tract is a complex organ system whose primary function is to exchange oxygen and carbon dioxide to meet the metabolic requirements of an organism. However, this physiological need also creates vulnerability in the respiratory tract through constant exposure to toxic particles and pathogens [1–3]. This vulnerability however is counteracted by the respiratory defense mechanisms that clear entrapped particles and the immune system that rapidly targets pathogens to prevent infections [4]. Part of the innate immunity, the complement system forms a defensive unit in the respiratory tract to identify and remove infectious agents [4–7]. The complement system is composed of three pathways known as alternative, classical, and lectin that coordinate an immune response to directly engage pathogens. In the fluid phase, AP is activated through the tick-over mechanism of complement protein C3, while CP is activated through a spontaneous intramolecular autoactivation of C1 [8–11]. In addition to solution phase activation, the classical and lectin pathways contain pattern recognition molecules that identify and subsequently activate complement on the surface of microbes [12–14]. After activation, propagation of complement ensues where all three pathways converge to cleave the protein C3 into C3a and C3b. While the soluble peptide C3a mediates inflammation (anaphylatoxins), C3b is an opsonins that attaches to the surface of pathogens to propagate complement on the solid phase [8,15]. Subsequently, continued propagation of the

complement system will initiate the terminal step that cleaves the protein C5 into C5a and C5b. Similar to C3a, C5a mediates inflammation whereas C5b binds to complement proteins C6, C7, C8, and multiple $C9_{n=1-18}$ to form a pore known as MAC [16,17]. This complex directly induces bacterial killing without the assistance of immune cells [18,19]. Altogether, complement achieves host defense against pathogens by generating anaphylatoxins, opsonins, and MACs.

To counteract the deadly effects of complement activation, microorganisms evolved several strategies to evade the immune system [20–24].These counterstrategies include recruitment of complement regulators to the pathogen's surface, secretion of proteins that inhibit complement activation, and proteases that cleave complement effector molecules. Utilizing these strategies, several microbes not only evade the complement system but may cause infections if left unchecked. For instance, human specific *N. meningitidis* is an important cause of meningitis and septicaemia; it is associated with average mortality rates ranging from 10% to 40% [25,26]. Of the many counterstrategies used by *N. meningitidis*, one method involves evading the complement system by expressing a surface lipoprotein known as factor H binding protein [27–30]. Presence of this lipoprotein promotes survival of *N. meningitidis* by recruiting the complement regulators FH and FHL-1 to its surface. In addition to recruiting AP regulators, *N. meningitidis* uses additional membrane proteins such as porin A (porA) and Meningococcal surface fibril (Msf) to recruit regulators C4BP and Vn, respectively [20]. Consequently, C4BP deactivates classical/lectin pathway components whereas Vn interferes with process of MAC assembly. By utilizing these strategies, *N. meninigitidis* inhibits all three pathways

of the complement system and effectively interferes with complement's bactericidal activity.

Deficiencies in the terminal cascade are also associated with an increased predisposition to invasive meningococcal disease and disseminated gonococcal infection [32]. Individuals with defective MAC components (C5-C9) have 7,000- to 10,000-fold higher risk of developing meningococcal disease [37]. Furthermore, 40-50% of MAC deficient individuals will suffer from recurrent infections at a rate approximately 100-150 times greater than the normal population. What's more, using complement inhibitors to interfere with MAC assembly might also increase the susceptibility of acquiring bacterial infections [38]. Patients with paroxysmal nocturnal hemoglobinuria PNH, eculizumab treatment inhibits MAC formation but also predisposes them to infections caused by *Neisseria, Pseudomonas aeruginosa*, *Escherichia coli*, and *Enterococcus faecium* [38–40].

Altogether, a competent complement system spanning all three pathways from activation to termination step plays a pivotal role in fight against invading pathogens. Knowing this importance, mathematical models have been assembled to shed light into the dynamics of complement activation and propagation [41–45]. However, to our knowledge, a comprehensive mathematical model that covers all three pathways of the complement system has not been developed. Here, we have implemented a systems biology approach by developing a comprehensive mathematical model of the complement system that contains all three pathways; alternative, classical, and lectin. Our new model is built on the frameworks of our previous two models [46,47], but below we list the updates. Our refined model contains the IgM, MBL trimers and tetramer, CL-L1, CL-K1, CL-LK, ficolin-1,

ficolin-2, and ficolin-3, MASPs-1, MASP-2, MASP-3, MAp19 and MAp44, FHR1-5, and CRP, SAP, and PTX3. In addition, our model contains three types of pathogens: (type 1) cannot evade complement system, (type 2) evades complement by recruiting FH, FHL-1, C4BP, Vn, and (type 3) pathogen specific model of *N. meningitidis* located in either nasopharynx or bloodstream. In all three pathogenic cases, we compare the different phases of complement activation by generating concentration profiles of the pathogen surface that is occupied due to complement-mediated opsonization/recruited regulators, and MAC production.

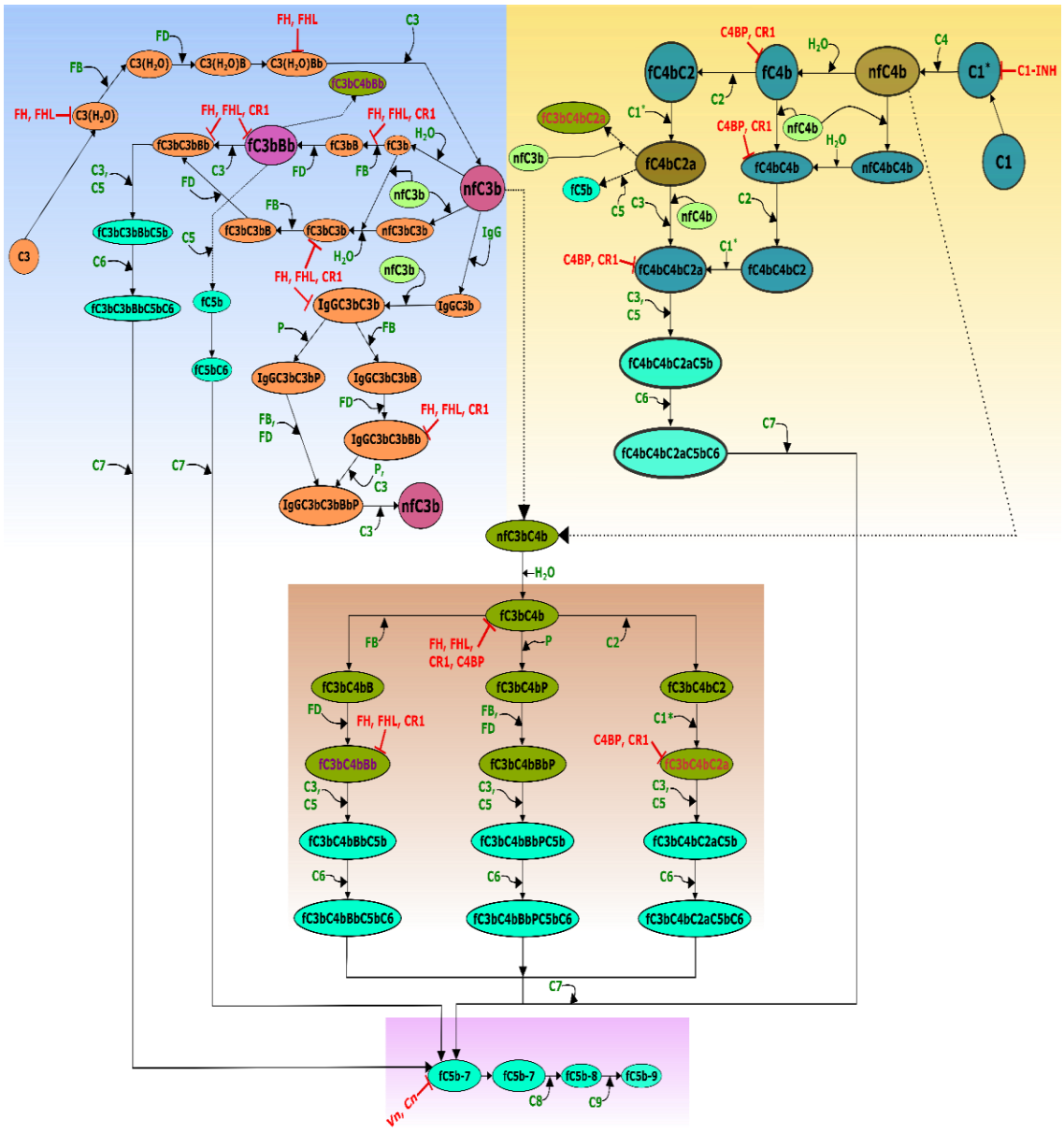

Figure 4.1. Biochemical network of the complement system. Activation of the alternative pathway is shown in orange circle and classical pathway is shown in blue circles. Crosstalk between the alternative and classical pathways are shown in green circles, and the terminal cascade is shown in cyan circles. Fluid phase complement regulators (FH, FHL-1, C4BP, and C1-INH) and membrane regulator CR1, coordinate immune regulation to protect host cell. All regulatory proteins are shown in red.

4.2 Results

In this study, we compare the different phases of complement activation and regulation as summarized in **Figure 4.1**. We start with complement targeting of type 1 pathogens by comparing the different modes of complement activations: fluid phase (FP) of alternative and classical pathways, classical pathway, lectin pathway, and factor H-related proteins 1-5 in generating complement components that occupy the pathogen surface and form MAC pores (**Figure 4.2**). In FP, activation of the alternative and classical pathways produces nascent C3b and C4b that covalently attach to the pathogen surface and active the complement system. In CP, IgG clusters (IgG_6) or IgM activate complement by first binding to the pathogen surface and recruiting/assembling C1. In LP, MBL, ficolins, and collectins bind to the pathogen surface and initiate complement. Similarly, FHR1-5 will also directly bind to the surface of pathogens and initiate complement. All four modes will then lead to the terminal cascade that forms MAC pores ($C5b9_{18}$).

Under FP, about 99% of the total pathogen surface remains unoccupied (**Figure 4.2A** blue), whereas under CP (green), LP (cyan), and FHR1-5 (brown) we observe a much higher level of surface occupation as shown in **Figure 4.2A**. CP-based surface occupation did however take longer (~12 minutes) compared to LP/FHR-based pathogen surface occupation (<1 minute). Soon after generating concentration profiles for surface occupation, we next generated concentration profiles for MAC production within 180 minutes. As shown in **Figure 4.2B**, FP produces the highest concentration of MAC (2.1×10^{-23}M, blue), followed in order by FHR1-5 (2.3×10^{-25}M, brown), LP (1.3×10^{-25}M, cyan), and CP (5.3×10^{-26}M, green). MAC production under FP is about two orders of magnitude higher compared to the other modes of complement activation (FHR1-5, LP,

and CP). Overall, these results show under CP, LP, and FHR1-5, complement-mediated opsonization is the primary immune response against type 1 pathogens. In contrast, under FP, MAC production is the main immune response. It should be noted however, MACs under FP only occupied <<1.0% of the total pathogen surface.

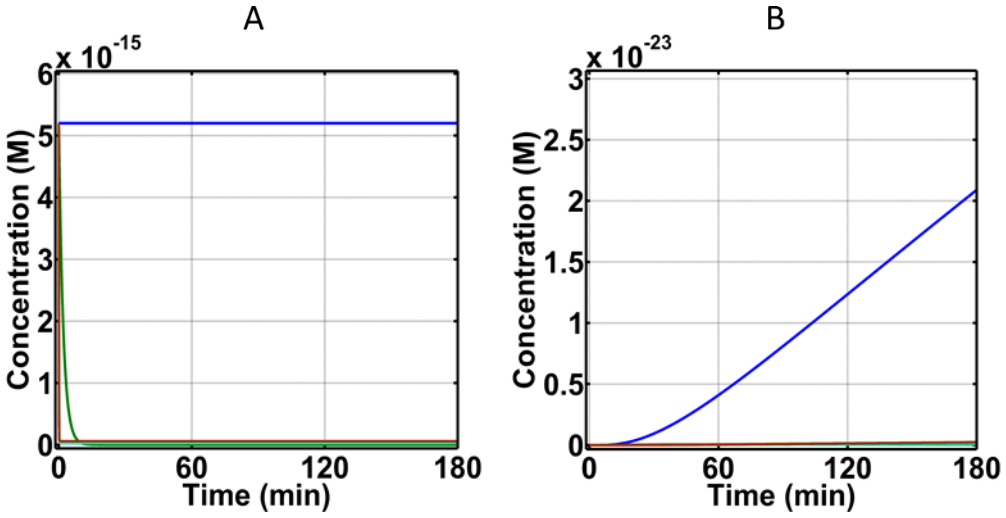

Figure 4.2. Time profiles for surface occupation and MAC production under FP (blue), CP (green), LP (cyan), and FHR1-5 (brown) on type 1 pathogen. (A) Substantial level of surface occupation under CP, LP, and FHR1-5, whereas more than 99% of pathogen surface remains unoccupied under FP. (B) Highest level of MAC produced under FP, whereas CP, LP, and FHR1-5 produced about two orders of magnitude lower.

We then compared the different modes of complement activation (FP, CP, LP, and FHR1-5) on a type 2 pathogen that evades the complement system by recruiting regulators FH, FHL-1, C4BP, and Vn to its surface (**Figure 4.3**). Under type 2 pathogens, the competition between complement activators and regulators will determine the dominant surface occupier. As shown in **Figure 4.3A**, the surface of a type 2 pathogen was rapidly (within five minutes) occupied by the different modes of complement activation. Next, we generated percent profiles to determine how much of the occupied surface (**Figure 4.3A**)

was due to recruited complement regulators. As shown in **Figure 4.3A** (inset), recruited regulators under FP accounted for nearly 100.0% of the occupied surface. This is followed by FHR1-5 activation where complement regulators (recruited) occupy 91.5% of the total pathogen surface. Under CP and LP activation, recruited regulators occupy ~89.0% of the total pathogen surface. After generating profiles for surface occupation, we continued our calculations to generate MAC profiles on type 2 pathogens. Compared to MAC levels on type 1 pathogens (**Figure 4.2B**), production of MAC is lower in type 2 pathogens under the different modes of complement activation (**Figure 4.3B**). For instance, MAC levels under FP (blue) and FHR1-5 (brown) are ~2.1×10^{-26}M for type 2 pathogens, whereas corresponding complement modes on type 1 pathogens produced MAC levels of 2.1×10^{-23}M (FP) and 2.3×10^{-25}M (FHR1-5) as shown in **Figure 4.2B**. Moreover, MAC production is even lower under CP (green) and LP (cyan) where MAC levels reached a concentration of ~1.9×10^{-26}M in 180 minutes (**Figure 4.3B**). However, comparing all four modes of complement activation, FP produced the largest difference where MAC is reduced by about three orders of magnitude compared to type 1 pathogens (**Figure 4.2B**). Altogether, the production of MAC is lower under pathogens that evade complement (type 2 pathogens) and recruitment of complement regulators (FH, FHL, C4BP, and Vn) occupied from 89.0%-99.5% of the pathogen surface under the conditions of FP, CP, LP, and FHR1-5.

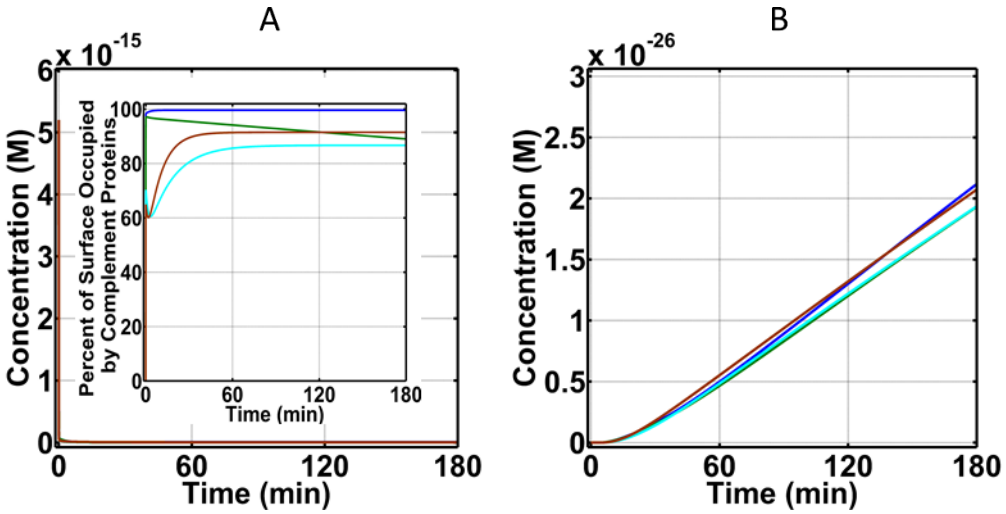

Figure 4.3. Time profiles for surface occupation and MAC production under FP (blue), CP (green), LP (cyan), and FHR1-5 (brown) on type 2 pathogen. (A) Recruited regulators account for at least 89% of the occupied pathogen surface under all four conditions (inset). (B) Production of MAC is similar under all four conditions, where their concentration levels reached ~2.0×10^{-26} M in 180 minutes.

As a final step in using types 1 and 2 pathogens**,** we combined the different modes of FP, CP, LP, and FHR1-5 into a single complement activation mode. We then incorporated pentraxins (PTX3, SAP, and CRP) to generate a combined system containing both complement and pentraxins (CSP). Similar to the calculations above, we compared the effects of CSP on surface occupation and MAC production. As shown in **Figure 4.4A**, type 1 (blue) and type 2 pathogens (green) are rapidly occupied by complement proteins in less than five minutes. However, recruited complement regulators in type 2 pathogens accounted for 69.4% of total occupied surface (in 180 minutes). Next, we continued our modeling efforts by generating profiles of MAC pores. As shown in **Figure 4.4B**, type 1 pathogens (blue) produced a higher MAC level with concentration 5.3×10^{-26}M in 180 minutes, whereas type 2 pathogens (green) produced a lower MAC level of 1.5×10^{-26}M in 180 minutes (**Figure 4.4B**). Overall, the combined complement system with pentraxin

rapidly occupied both pathogens types, however recruited complement regulators (FH, FHL-1, C4BP, and Vn) were the dominant surface occupiers on type 2 pathogens. And similar to the results mentioned above, MAC pores accounted for << 1.0% of the total pathogen surface.

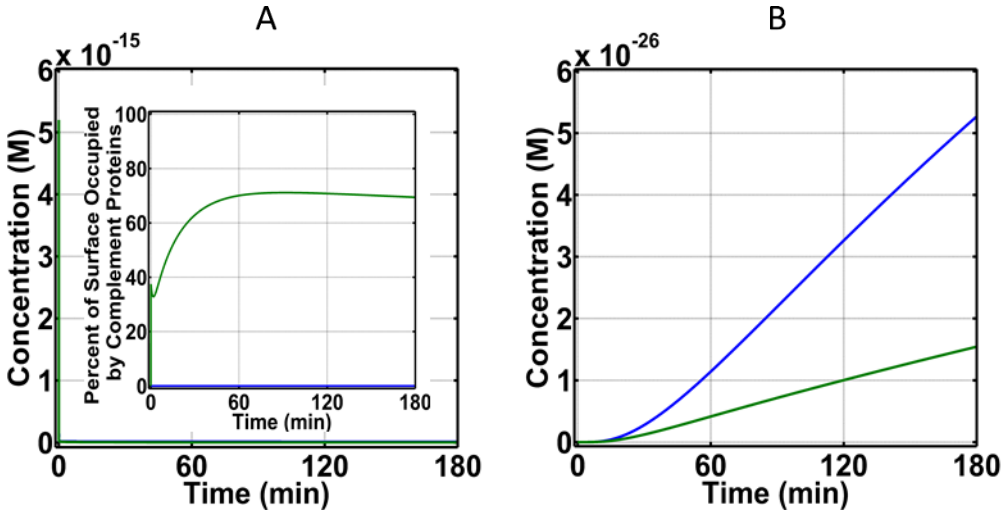

Figure 4.4. Time profiles for surface occupation and MAC production under combined complement modes with pentraxins on type 1 (blue) and 2 (green) pathogens. (A) Surface of pathogens were rapidly occupied but recruited regulators on type 2 pathogens accounted for 69.4% of total occupied surface. (B) In 180 minutes, type 1 pathogens produced the highest MAC (5.3×10^{-26}M), whereas type 2 pathogens produced a lower concentration of MAC pores (1.5×10^{-26}M).

After generating profiles on generic pathogens that enter the bloodstream, we continued our modeling efforts for a specific pathogen (*Neisseria meningitidis*). We used serum and nasal complement levels to account for complement activity against *N. meningitidis* in the bloodstream and nasopharynx, respectively. And unlike type 1 pathogens, *N. meningitidis* evades the complement system by recruiting regulators C4BP, Vn, FH, and FHL-1 to its surface. *N. meningitidis* recruits C4BP and Vn by using membrane proteins known as porA and Msf, respectively. Additionally, alternative

pathways regulators (FH and FHL-1) are also recruited to the surface using a membrane lipoprotein known as fHbp. However, fHbp also recruits a promotor of complement activation known as FHR-3. Hence survival of *N. meningitidis* will depend on the dynamics between complement regulators (C4BP, Vn, FH, and FHL-1) and promotor (FHR-3). To better understand this dynamic, we generated three conditions: (i) FP activation and recruitment of FHR-3 on *N. meningitidis* (ii) FP activation and recruitment of C4BP, Vn, FH, and FHL-1 on *N. meningitidis,* and (iii) FP activation and recruitment of C4BP, Vn, FH, FHL-1, and FHR-3 on *N. meningitidis.*

Starting with nasal complement levels under condition (i) shown in **Figure 4.5A** (blue), we observe a 40.4% occupation (3.1×10^{-15}M) of *N. meningitides* surface in about 15 minutes. And this is level of occupation is maintained until about the 90^{th} minute, whereafter there is another increase in the occupation level to reach a final concentration of 2.5×10^{-15}M (51.9% occupation). Under condition (ii) we observe a rapid occupation of *N. meningitidis* in less than five minutes (**Figure 4.5A**, green). However, this phase of rapid occupation is followed by a minor increase in the available pathogen surface and then a subsequent decrease in the available pathogen surface to reach a final concentration of 9.8×10^{-16}M (81.2% occupation). Lastly, under condition (iii) shown in **Figure 4.5A** (red) where we have competition between a complement promotor (FHR-3) and regulators (C4BP, Vn, FH, and FHL-1), we see a similar concentration profile as condition (ii) where there is a rapid occupation of the pathogen surface followed by a small period of an increase in the available surface right before the concentration settles to a final value of 8.7×10^{-16}M (83.3% occupation).

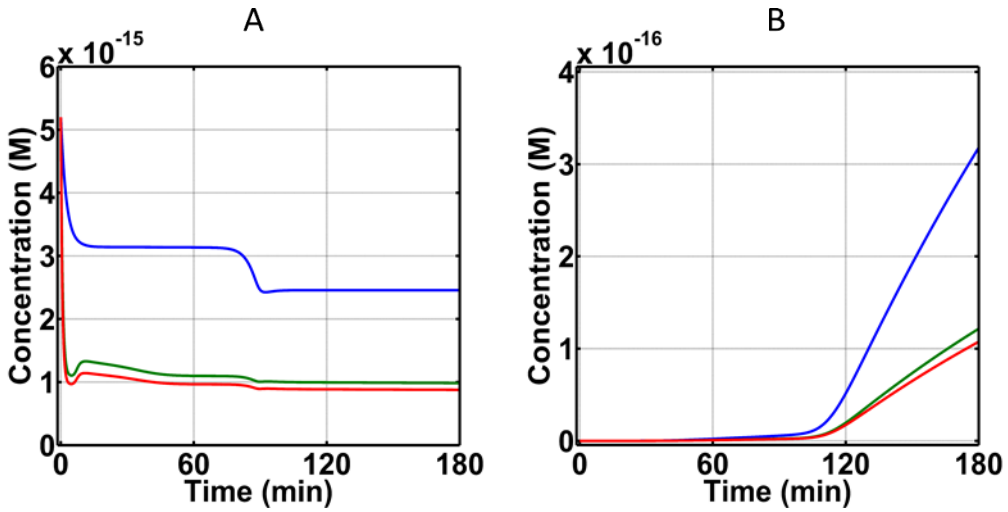

Figure 4.5. Time profiles for surface occupation and MAC production under three conditions using nasal concentrations: (i) complement activation with recruitment of FHR-3 to *N. meningitidis* (ii) complement activation with recruitment of C4BP, Vn, FH, and FHL-1 to *N. meningitidis*, and (iii) complement activation with recruitment of C4BP, Vn, FH, FHL-1, and FHR-3 to *N. meningitidis.* (A) 40.4% of *N. meningitidis* surface was occupied under condition (i), whereas a higher level of 51.9% occupation is seen under conditions (ii) and (iii). (B) MAC levels reached the highest level of 3.2×10^{-16}M under condition (i), followed by conditions (ii) and (iii) of 1.2×10^{-16} M and 1.1×10^{-16} M, respectively.

After generating complement occupation levels on *N. meningitidis*, we continued our calculations for MAC levels (**Figure 4.5B**). Condition (i) generates the highest level of MAC with concentration 3.2×10^{-16}M in 180 minutes (blue). This corresponds to 6.2% of the total pathogen surface being occupied by MAC pores. Condition (ii) generates the second highest MAC level with concentration of about 1.2×10^{-16}M in 180 minutes (green). This corresponds to 2.3% of the pathogen surface being occupied by MAC pores. And lastly, the lowest level of MAC pores is generated under condition (iii) where the concentration of MAC is 1.1×10^{-16}M in 180 minutes (red). This corresponds to 2.1% of the pathogen surface being occupied by MAC pores. Altogether, condition (i) produced the highest MAC, followed by conditions (ii) and then (iii).

We next implemented complement serum levels to assess how the concentration profiles for surface occupation and MAC production changes in the bloodstream under the three conditions mentioned above. As shown in **Figure 4.6A**, the surface of *N. meningitidis* is rapidly occupied under all three conditions. However, condition (i) shown in blue, does not fully occupy the pathogen surface as conditions (i) and (ii), shown in green and red, respectively. Moreover, recruited complement regulators (C4BP, Vn, FH, and FHL-1) under conditions (ii) and (iii) account for nearly 100% of the occupied surface (**Figure 4.6A** inset). This is followed by a lower surface occupation under condition (i), where complement FHR-3 occupies 84.5% of *N. meningitidis*, as shown in the inset of **Figure 4.6A**. Finally, we generated MAC production under the three conditions mentioned above. We observe the highest MAC concentration of 3.2×10^{-24}M under condition (i), followed by condition (iii) with MAC concentration of 8.4×10^{-27}M, and finally the lowest under condition (ii) with MAC concentration of 5.5×10^{-27}M as shown in **Figure 4.6B** (inset). Overall, these results show MAC levels on *N. meningitidis* are similar to generic pathogens (types 1 and 2) in the bloodstream, where MAC levels for all pathogen types occupy <<1.0% of the total available surface. However, MAC production under condition (i) in nasopharynx is about eight orders of magnitude higher to that generated under condition (i) in the bloodstream. Similarly, under conditions (ii) and (iii) in the nasopharynx, MAC levels are about ten orders of magnitude higher compared to those generated using serum complement levels under conditions (ii) and (iii).

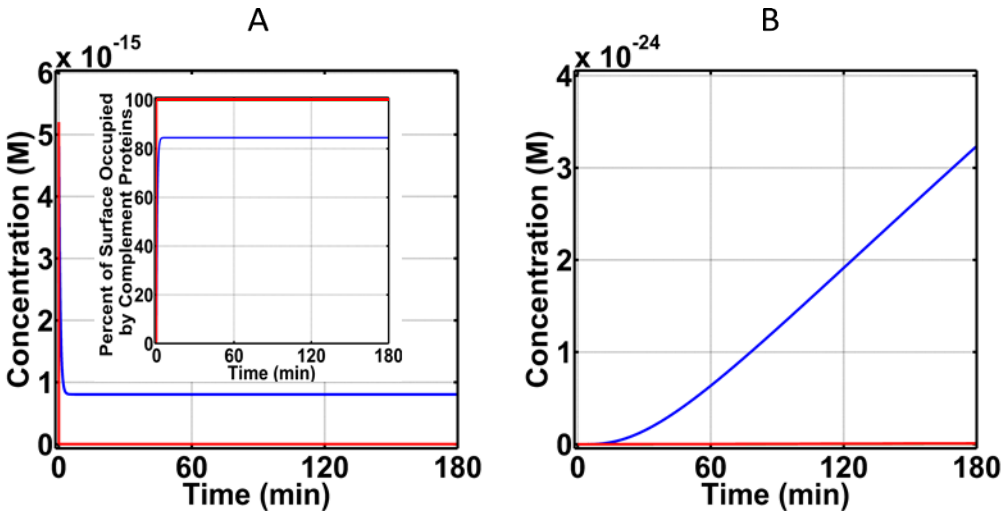

Figure 4.6. Time profiles for surface occupation and MAC production under three conditions using serum concentrations: (i) complement activation with recruitment of FHR-3 to *N. meningitidis* (ii) complement activation with recruitment of C4BP, Vn, FH, and FHL-1 to *N. meningitidis*, and (iii) complement activation with recruitment of C4BP, Vn, FH, FHL-1, and FHR-3 to *N. meningitidis.* (A) Surface of *N. meningitidis* was rapidly occupied but condition (i) does not fully occupy the pathogen surface. (B) Highest MAC level produced under condition (i) with concentration 3.2×10^{-24} M. Lower MAC levels produced under condition (iii) with concentration 8.4×10^{-27} M, followed by condition (ii) with concentration 5.5×10^{-27} M.

Since using serum complement levels nearly saturated the surface of *N. meningitidis* by complement regulators or promotor, we instead focused on nasal complement levels where MAC deposition was much more elevated. For this calculation, we asked in the absence of FHR-3, can enhancing complement activation (FP) offset the protective effects of recruiting C4BP, Vn, FH, and FHL-1. For this, we first divide our initial concentrations into three modules: AP module (C3, factor B (FB), factor D (FD), and properdin), CP module (C1, C1q, $(C1rC1s)_2$, C2, and C4), and terminal module (C5, C6, C7, C8, and C9). We then increased the concentration of each protein to 20% of their serum levels. This choice is based on the assumption that nasal complement proteins like that of nasal C3 and IgG, can be as high as 20% of their serum levels. In **Figure 4.7** we present our result for the terminal module, whereas AP and CP modules are shown in

Figures C.1 and **C.2**, respectively. Compared to MAC levels on *N. meningitidis* without terminal module enhancement, increasing the concentration of C9 had the largest effect in MAC production where MAC level reached a concentration of 2.1×10^{-16}M in 180 minutes (yellow). Furthermore, increasing the concentration of C5 or C6 also increased production of MACs. This is shown in **Figure 4.7** where increasing the level of C5 increased MAC production to 1.9×10^{-16}M (green), whereas increasing C6 lead to a MAC level of 1.7×10^{-16}M (blue) in 180 minutes. Conversely, increasing the concentrations of C7 (cyan) or C8 (magenta) had minor effects in the production of MAC. Lastly, increasing AP or CP modules also had minor effects in MAC production (**Figures C.1** and **C.2**). Overall, our results show increasing the terminal components C5, C6, and C9 to 20% of their serum levels, led to an increase in MAC levels despite the protective effects of recruiting C4BP, Vn, FH, and FHL-1.

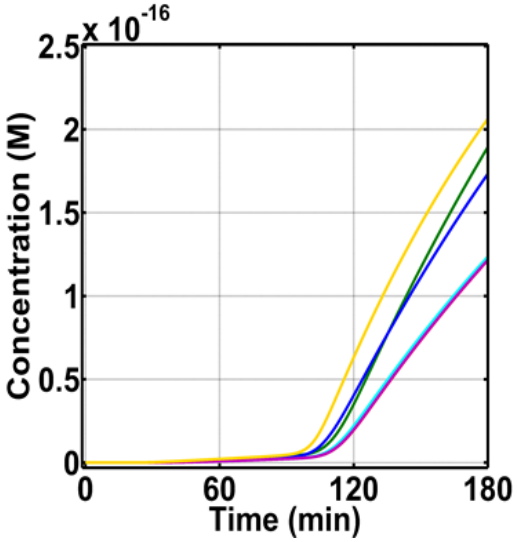

Figure 4.7. Time profiles for MAC production with 20% increase in under terminal modules C5 (green), C6 (blue), C7 (cyan), C8 (magenta), and C9 (yellow). Increasing C9 had the largest effect on MAC production, followed by C5 and C6. In contrast, C7 and C8 had minor effects on MAC production.

Since enhancing terminal components (C5, C6, and C9) led to an increased MAC deposition on *N. meningitidis*, we next examined which of the recruited complement regulators (C4BP, Vn, FH, and FHL-1) had a greater effect on MAC production. For this, we first carried our calculations by removing (making association rate constant zero) the ability of *N. meningitidis* to recruit C4BP, while still having the ability to recruit Vn, FH and FHL-1. Subsequently, we performed a similar calculation by removing the ability of *N. meningitidis* to recruit Vn (making association rate constant zero), while still having the ability to recruit C4BP, FH and FHL-1. We completed our calculations by removing the recruitment ability of FH and FHL-1. All permutations where compared to *N. meningitidis* that recruits all four regulators. As shown in **Figure 4.8**, removing the ability of *N. meningitidis* to recruit Vn led to the largest effect where MAC level on *N. meningitidis* increased from 1.2×10^{-16}M to 2.2×10^{-16}M in 180 minutes (green). This equates to about a 2-fold increase in MAC production. This is followed by the loss in the ability of FH and FHL-1 recruitment, where MAC level increased from 1.2×10^{-16}M to 1.6×10^{-16}M in 180 minutes (red). Lastly, removing the ability of *N. meningitidis* to recruit C4BP led to a minor increase in MAC production from 1.2×10^{-16}M to 1.3×10^{-16}M in 180 minutes (blue). Altogether, our model shows removing the ability to recruit Vn had the largest effect in MAC production, followed by FH and FHL-1, and then C4BP.

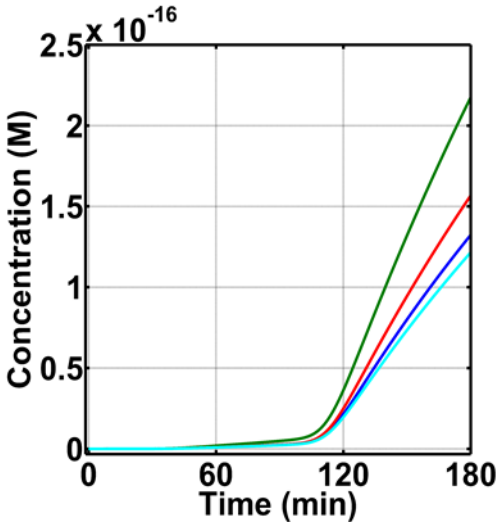

Figure 4.8. Time profiles for MAC production by removing the ability of *N. meningitidis* to recruit C4BP (blue), Vn (green), FH and FHL-1 (red), and condition (ii) (cyan). Removing Vn recruitment produced the highest effect on MAC concentration (2.2×10^{-16} M). This is followed by removal of FH and FHL-1 recruitment (1.6×10^{-16} M). C4BP had a minor effect on MAC production (1.3×10^{-16} M) compared to conditions (ii) of 1.2×10^{-16} M.

We concluded our studies by exploring how the board range in nasal regulatory levels (0.2% to 0.0002% of serum) may affect MAC production on *N. meningitidis.* For this, we reduced the concentrations of C1-INH, C4BP, Vn, Cn, FH, and FHL-1 between nasal ranges of 0.2% to 0.0002% of serum S1 Table. As shown in **Figure 4.9**, as we reduce the concentrations of complement regulators from 0.2% to 0.0002% of their serum levels, we see an increase in MAC deposition. MAC level increases from 6.8×10^{-17}M under 0.2% of serum (red) to a concentration of 3.4×10^{-16}M under 0.02% of serum (green), and to a final concentration of about 5.0×10^{-16}M under 0.002% (blue) or 0.0002% (magenta) of serum regulator levels. In contrast, if we increase the concentration of complement regulators to 2% of their serum levels, production of MAC decreases from 6.8×10^{-17}M (under 0.2% of serum) to 4.0×10^{-19}M (under 2% of serum), as shown in **Figure 4.9**, yellow. From this, our model predicts if complement activators are maintained around 12% of their

serum levels, and nasal C1-INH, C4BP, Vn, Cn, FH, and FHL-1 are maintained at 0.02% or below their serum levels, MAC pores can go from occupying 6.5% (0.02% of serum) to about 10% (under 0.002% or 0.0002% of serum) of the total available surface on *N. meningitidis.* This potentially makes *N. meningitidis* more susceptible to MAC-mediated attacks when the concentrations of complement activators are at least about three orders of magnitude higher than complement regulators. Conversely, as the concentration difference decreases below two orders of magnitude, MAC pores occupation is reduced to about 0.01% (2.0% of serum). Altogether, our model shows mounting higher levels of MAC may require a concentration barrier between complement activators and regulators of at least three orders of magnitude to reach elevated deposition on *N. meningitidis* (within 180 minutes). However, as this concentration barrier is reduced, MAC deposition is modulated on the surface of *N. meningitidis*.

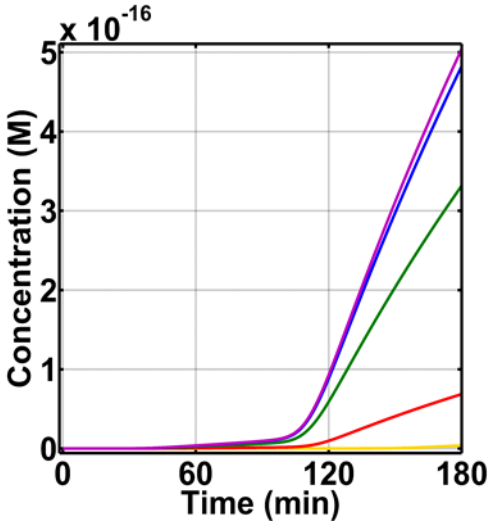

Figure 4.9. Time profiles for MAC production by reducing the concentrations of C1-INH, C4BP, Vn, Cn, FH, and FHL-1 between nasal ranges of 0.2% to 0.0002%: 2% (yellow), 0.2% (red), 0.02% (green), 0.002% (blue), and 0.0002% (magenta). As the concentration of regulators is reduced from 0.2% to 0.0002%, MAC pores go from occupying 1.3% (0.2% of serum) to about 10% of the pathogen surface. In contrast, increasing concentration to 2% decreased MAC level from 6.8×10^{-17}M (0.2% of serum regulator levels) to 4.0×10^{-19}M (2% of serum regulator levels).

4.3 Discussion

In this study, we developed a mathematical model of the complement system that includes all three pathways and their respective crosstalk with other parts of the immune system. Our comprehensive model includes the alternative, classical, and lectin pathways of the complement system and components of the humoral immunity such as IgG, IgM, CRP, SAP, and PTX3. The biomolecular details and kinetic parameters of the complement system are assembled from the available literature data, whereas unknown parameters are estimated/assumed based as mentioned in the Methods section. Subsequently, since complement activation leads to indirect killing through opsonophagocytosis and directed killing through MAC production, we used our computational model to determine the primary immune response in the presence of three types of pathogens: (type 1) cannot evade complement system, (type 2) evades complement by recruiting C4BP, Vn, FH, and FHL-1, and (type 3) pathogen specific model of *N. meningitidis* that recruits complement regulators (C4BP, Vn, FH, and FHL-1) and also an activator (FHR-3).

Our computational model shows by using serum complement levels, type 1 pathogens are rapidly opsonized whereas recruitment of complement regulators shields types 2 and 3 (*N. meningitidis*) from opsonization. However, consistent across all pathogen types, our model shows MACs may not play a major role as they occupied <<1.0% of the total pathogen surface. Thus, our model predicts if a pathogen enters the bloodstream, the complement system will use opsonization as the main immune response as oppose to MAC. And that phagocytosis, following opsonization, may serve as the primary mechanism of eliminating pathogens that have entered the bloodstream. This applies also to evasive

pathogens of type 2 or 3 (*N. meningitidis*), assuming recruitment of complement regulators are counteracted. To highlight this point, in the absence of MAC, specific antibodies in conjunction with complement activation can elicit bacterial killing *of N. meningitidis* through opsonophagocytosis [48–50]. Furthermore, in patients with MAC deficiency, opsonophagocytosis may also play a compensatory role where absence of the membrane attack complex is limited to a predominant increase risk in only *Neisseria* and disseminated gonococcal infections [51]. What's more, these patients are not at a greater risk of contracting other gram-negative infections [51]. Altogether, indirect pathogen elimination through opsonization followed by phagocytosis, may form a competent immune response in the absence of MAC-based directed response.

Unlike serum complement levels, using nasal concentrations produced much higher levels of MAC. Production of MAC under condition (i) occupied 6.2% of the total pathogen surface (*N. meningitidis*), followed by condition (ii) with 2.3% surface occupation, and then by condition (iii) with 2.1% surface occupation. This corresponds to concentrations of 3.2×10^{-16}M, 1.2×10^{-16}M, and 1.1×10^{-16}M for conditions (i), (ii), and (iii), respectively, as shown in **Figure 4.5B**. If we compare the lowest nasal MAC level to that generated under the highest MAC level in serum by FP activation in **Figure 4.2B** (2.1×10^{-23}M), nasal level are about seven orders of magnitude higher. And this elevated MAC production in nasopharynx stems from the differences between levels of complement activators and regulators. For instance, nasopharyngeal secretions of C3 are estimated to be between 4.2 to 20.2% of serum C3 levels, whereas levels of mucosal FH are below 0.2% (in range between 0.2% to 0.0002%) of serum FH levels. Using a mean concentration of

7.1μM for serum C3, the nasopharyngeal secretions of C3 are between 0.3μM to 1.4μM. However, nasal range for FH are below 6nM. This difference equates to nasal C3 levels being 50- to 233-fold greater than nasal FH. Conversely, serum C3 (7.1μM) is about 2-fold higher than serum FH (3.2μM). With this difference, nasopharynx will favor under-regulation of the complement system, whereas bloodstream favors proper regulation. It should be noted, unlike other regulators of the alternative pathway, FH is the main regulator of AP that targets complement proteins such as C3(H_2O) and C3b or complement complexes such as C3/C5 convertases C3bBb. Altogether, *N. meningitidis* may be susceptible to MAC mediated attacks due to a combination of over-activation and under-regulation of the complement system in the nasopharynx environment.

Our model shows recruitment of FHR-3 by fHbp enhances MAC production whereas recruitment of C4BP, Vn, FH, and FHL-1 decreases MAC deposition (**Figure 4.5B**). When however, we combine C4BP, Vn, FH, FHL-1, and FHR-3 we observe an even lower MAC production. This shows the amount of surface (*N. meningitidis*) MACs occupy depends on how much of it was initially occupied by a complement activator FHR-3 and regulators C4BP, Vn, FH, and FHL-1. Moreover, although our model shows recruitment of just FHR-3 enhances MAC deposition, our model predicts even in the absence of FHR-3, if complement activators are about three orders of magnitude higher than regulators, complement can still mount higher levels of MAC and counteract the immune invasiveness caused by recruitment of C4BP, Vn, FH, and FHL-1 (**Figure 4.9**). Furthermore, removing the ability of *N. meningitidis* to recruit complement regulators C4BP, Vn, FH, and FHL-1 also led to an increase in MAC deposition (**Figure 4.8**). Thus, complement regulators

modulated MAC deposition on *N. meningitidis.* In part, support for this is shown in a recent genome-wide association studies where variants on the factor H gene are associated with susceptibility of meningococcal disease, caused by *N. meningitidis* [52,53]. It should be noted FHL-1 is an alternative splice variant of FH and that the earlier study [53] did also show genetic variation within FHR-3. Although these studies did not find an association in genes of other complement regulators with susceptibility to meningococcal disease, our model predicts recruitment of Vn as a major factor used to evade the complement system. And this may explain why majority of the sequenced meningococcal isolates contain Msf [54].

Increasing the concentration of complement proteins to 20% of their serum values showed the terminal module (C5, C6, and C9) enhanced MAC production and subsequently counteracted the effects of porA and Msf, and fHbp. In contrast, increasing the concentrations AP and CP modules had minor effects on MAC production as shown in **Figures C.1 and C.2**, respectively. To our surprise, increasing the concentration of properdin in the AP module did not enhance MAC deposition. This was unexpected because properdin is considered a positive regulator of the complement system that plays a major role in the amplification loop of the alternative pathway. In our current model, properdin is taken as a stabilizer of the convertases and not as a recognition molecule. This choice in properdin function comes from recent studies showing properdin binding to zymosan, *Escherichia coli*, human umbilical vein endothelial cells, and *N. meningitidis* is solely dependent on the initial C3b deposition [55,56]. Although studies have shown the properdin as a recognition molecule that initiates AP [57–61], caution needs to be taken

when interpreting these results depending on the serum conditions of intact C3 and molecular structure of properdin [55,62]. If however, we chose properdin as recognition molecule, we have shown in our previous model it can significantly increase MAC deposition on pathogens [46]. And this form of properdin may potential counteract the effects of recruiting C4BP, Vn, FH, and FHL-1 by *N. meningitidis*. To highlight this point, a recent study showed generating highly polymerized artificial form of properdin by recombinant techniques was able to directly bind to *N. meningitidis* and elicit an enhanced complement activation [63]. Furthermore, this low-dose of recombinant properdin also had beneficial effects in mouse infection models with pathogens *N. meningitidis* and *S. pneumonia* [63]. Hence, high-order oligomers of properdin have additional functions that includes direct binding to pathogens and serving as a platform for complement activation. And this function may potentially be manipulated for therapeutic interventions to target invasive pathogens such as *N. meningitidis.*

4.4 Methods

4.4.1 Mathematical model

Our mathematical model is based on construction of biochemical reactions of the complement system. **Figure 4.1** summarizes the biochemical reactions of the three pathways (alternative, classical and lectin) that form a network of complement proteins, fragments, and complexes that either activate or regulate the complement system. This network of interactions was also coupled with other segments of the humoral immunity that includes IgM, CRP, SAP, and PTX3 that either enhance complement

activation/opsonization or regulation via recruitment of regulators. This biochemical network will entail the different phases of complement activation, propagation, and regulation in both fluid and cellular surface. Human erythrocytes were used as a host cell model, whereas *Escherichia coli* was used as a pathogen cell model [46]. Lastly, we included three types of pathogens: (type 1) cannot evade complement system, (type 2) evades complement by recruiting C4BP, Vn, FH, and FHL-1, and (type 3) pathogen specific model of *N. meningitidis* that also recruits complement regulators (C4BP, Vn, FH, and FHL-1) and an activator (FHR-3).

Using this biochemical network of interactions, we assembled a system of 670 ordinary differential equations (ODEs) with 328 kinetic parameters, as shown in **Supplemental Equations C.1**. The equations describe the reaction rates of complement proteins, fragments, complexes, in conjunctions with immunoglobulins and pentraxins. Enzymatic reactions are based on Michaelis–Menten kinetics with substrate competitions taken into account for complement complexes such C3/C5 convertases [68]. Model parameters of concentration and kinetic parameters, when available, are acquired from published literature data or experimental measurements. We used the ode15s solver of Matlab (Mathworks, Natick, MA), to solve our ODEs.

For unknown kinetic rate constants in our model, we assumed those parameters to be the same for proteins that are structurally or functionally homologous with experimentally determined parameter values. For instance, decay rate of C3bBb by FH is known [69], whereas for the decay of $C3(H_2O)Bb$ by the regulatory function of FH is not. However, we assumed these to two rates to be same for the following reasons. First,

$C3(H_2O)$ is known as a C3b-like molecules that has a homologous function as C3b by forming a proconvertase with FB. Second, proconvertase $C3(H_2O)B$, just like C3bB, is activated by the serine protease factor D to form convertases ($C3(H_2O)Bb$ and C3bBb). Lastly, without FH involvement, both convertases of $C3(H_2O)Bb$ and C3bBb have very similar decay rates of 9.0×10^{-3} s^{-1} and 7.7×10^{-3} s^{-1}, respectively [70]. Similarly, we assumed complement regulators complement receptor 1 (CR1), decay-accelerating factor (DAF), and C4BP accelerate the decay of C3/C5 convertases with the same kinetic rate constant as FH. We made this assumption because all three regulators are functional homologous to FH by either inhibiting or deactivating C3/C5 convertases.

Biochemical model

4.4.2 Alternative pathway

The alternative pathway auto-activates in the fluid phase by the spontaneous hydrolysis of the complement protein C3. Once activated, C3 will generate a C3b-like molecule known as $C3(H_2O)$ [71]. This activated molecule is targeted by the complement protease FB to form a proconvertase known as $C3(H_2O)B$ [72]. Subsequently, this complex is targeted by the serine protease FD, that cleaves the bound FB complex into Ba and Bb. While Ba is released into the fluid, Bb remains attached to $C3(H_2O)$ to form the initial C3 convertase of the alternative pathway, $C3(H_2O)Bb$ [70,71]. This short-lived enzyme catalyzes the cleavage of C3 into a smaller fragment C3a and a larger molecule called nascent C3b (nC3b) [70,71]. The first product, C3a plays a major role in mediating inflammation by inducing histamine production by mast and basophils cells, resulting in

vasodilatation [13,73,74]. Whereas, in other cases C3a plays an anti-inflammatory role by preventing neutrophil migration and degranulation [13,75]. Nascent fluid C3b (nfC3b) is highly reactive due to its exposed internal thioester bond and is capable of indiscriminately attaching to cell surfaces via covalently [76–78]. However, the newly formed nfC3b has a short half-life of 60 μsec before it loses the ability to covalently attach to nearby cell surfaces and remain solely in the fluid phase to form fluid C3b (fC3b) [79]. Similar to cascade of reactions initiated by C3(H_2O), fC3b or surface bound nC3b can associate with FB, followed by FD cleavage to form the C3/C5 convertase C3bBb [70,80]. This reaction scheme is also followed by nC3b if it interacts with immunoglobulin G (IgG) already in complex with nC3b, to form IgGC3bC3b, and subsequently interacts with FB and FD to form the C3 convertase IgGC3bC3bBb [81].

Formation of surface bound convertases will then recruit the complement protein properdin to form the C3/C5 convertase such as C3bBbP [82,83]. The recruitment of properdin stabilizes C3/C5 convertases by extending their half-lives by 10-fold and hence initiating the amplification loop. Presence of stabilized convertases will cleave more C3 (into C3a and nC3b) and C5 (into C5a and C5b) than convertases without properdin. The smaller fragments C3a and C5a are mediators of inflammation but C5a is more potent [13]. Whereas the larger fragments, nC3b will initiate the same cascade of reaction by interacting with FB and FD to form C3bBb, while C5b initiates the terminal step by first interacting with C6 to form C5b6. This step in complex formation between C5b and C6, is affected by C5b's short half-life of 2.3 minutes before irreversibly losing its binding ability to C6 [84]. However, if C5b6 complex is formed, C7 and C8 will sequentially interact C5b6 to form

C5b-8. This complex (C5b-8) forms a small pore that later expands by the insertion of multiple C9s to form the membrane attack complex [16,85,86].

4.4.3 Classical pathway

Similar to the spontaneous activation of C3 in the alternative pathway, the classical pathway is also spontaneously activated in the fluid phase through its first component of complement, C1 [9–11]. C1 is composed of two complexes of C1q and the heterotetramer $(C1rC1s)_2$ containing two copies of C1r and C1s serine proteases. Activation of C1 proceeds by the autocatalytic cleavage of C1r which subsequently activates/cleaves C1s subunits (C1s*). Activated C1 (C1*) will use C1s* to cleave C4 into C4a and nascent C4b (nC4b). Similar to nC3b, nC4b can covalently attach to nearby cell surface and initiate complement. However, nC4b has a short half-life for its exposed thioester and hence becomes rapidly hydrolyzed in solution to generate the fluid C4b (fC4b) [87]. This molecule cannot covalently attach to cell surfaces but can associate with complement C2 to form the classical pathway proconvertase C4bC2. Soon after, C1* will cleave C2 to the C3/C5 convertase of the classical pathway, C4b2a. The same cascade of reactions is followed by surface bound C4b to form C4b2a. The formation of C4b2a leads to cleavage of C3 into C3a and nC3b to propagate the alternative pathway. On the other hand, nC3b or nC4b molecules can also form covalent linkage with each other to form homo- or heterodimes such as C3bC3b/C4bC4b and C3bC4b that can interact with FB or C2 to form C3/C5 convertases (C3bC3bBb/C4bC4bC2a, C3bC4bBb/C3bC4bC2a) [88–90].

In addition to fluid phase activation, the classical pathway can directly activate on cells through the presence or absence of antigen-antibody complexes [91]. In the presence of antigen–antibody immune complexes, C1q (as part of C1) will bind to fragment crystallizable (Fc) portion region of IgG/IgG clusters and IgM [91–95]. However, in the absence of antigen–antibody immune complexes, C1q recognizes different targets such as the short pentraxin CRP and the long pentraxin PTX3. Once C1 binds to its different targets, it the follows the same cascade of reaction as in the fluid phase by the autoactivation of C1r, which subsequently activates C1s (C1*). This will lead to cleavage of C4 and C2 to form the convertase C4b2a. Overall, the classical pathway has the ability to recognize various targets through the recognition molecule C1q. But once bound, C1 goes through the same cascade of reactions to generate C1*.

4.4.4 Lectin pathway

Unlike the alternative and classical pathways, the lectin pathway contains numerous pattern recognition molecules (PRM) in complex with either three types of serine proteases or with two types of nonenzymatic protein molecules. The pattern recognition molecules of the lectin pathway include MBL, CL-L1, CL-K1, CL-LK, M-ficolin, L-ficolin, and H-ficolin [96,97]. These molecules have a common feature where they can associate with serine proteases known as MASP-1, MASP-2, and MASP-3. In addition to associating with MASPs, the pattern recognition molecules can also interact with two types of MAp19 and MAp44 that do not contain a serine protease domain [98,99]. The serine proteases (MASP-1, -2, and -3) are in their zymogen forms and follow subsequent

mechanisms to become activated with various cross-activation steps. For instance, MASP-1 in complex with PRM autoactivates and cleaves zymogen MASP-2 and MASP-3 [100,101]. Furthermore, activated MASP-1 cleaves zymogen MASP-1, whereas activated MASP-2 cross-activates zymogen MASP-1 [100,102]. However, once PRM-MASP-1 or PRM-MASP-2 are activated, they both can propagate the lectin pathway by cleaving complement proteins C2 and C4 to generate the C3/C5 convertase C4b2a [103,104]. Once this convertase is formed, it can generate C3a and nC3b or C5a and C5b. And through this mechanism, the lectin pathway can initiate either the alternative pathway or the terminal step to forms MACs.

4.4.5 Factor H-related proteins

Factor H is the main regulator of alternative pathway that deactivates C3b and accelerates the decay of C3/C5 convertases. However, factor H belongs to a family proteins that includes factor H-like protein 1 and five factor H-related proteins (FHR-1, FHR-2, FHR-3, FHR-4, and FHR-5) [105–107]. The genes of FHRs are located downstream of the *FH* gene and each gene codes for complement control proteins (CCP) that are homologous to CCP domains 6-9 and 18-20 of FH [105–107]. However, FHRs lack the regulatory domains of CCP1-4 of FH/FHL-1, and hence implies FHRs may not inhibit complement. Recent evidence suggest factor H-related proteins may function as positive regulators of the complement system that compete against FH and further enhance complement activation and propagation. For instance, FHR-1 was shown to enhance complement in several ways such as binding to C3b and allowing convertase formation, not accelerating

the decay of convertases, and not inhibiting convertase decay activity of FH [108]. Furthermore, FHR-4 in complex with CRP, was able to activate complement and result in C3 and C4 deposition [109]. Lastly, FHR-5 was shown to generate the C3/C5 convertase when incubated with C3b, FB, FD, and properdin [110].

4.4.6 Regulation

Due to the potency of complement activation and propagation, multiple regulatory checkpoints are present to ensure host cell protection. In the alternative pathway, FH, followed by FHL-1, are the two main the regulators present in both fluid and cellular surfaces. Both FH and FHL-1 bind to C3b and act as cofactors for Factor I (FI) cleavage of C3b into inactivated C3b (iC3b) [111–113]. Additionally, FH and FHL-1 also target convertases such as C3bBb and accelerate the rate of decay into its respective components of C3b and Bb [111–113]. Similarly, the classical and lectin pathways also contain two main regulatory proteins known as C1-INH and C4BP, that act in both fluid and surface phases. Activated C1, MASP-1, and MASP-2 in complex with PRMs are all regulated by C1-INH [114,115]. Whereas C4b is targeted by C4BP and subsequently deactivated into C4d with the help of the serum protease FI [116]. Furthermore, C4BP targets convertases such as C4b2a and accelerates their decay into their respective components [116].

As a second checkpoint, host cells also contain membrane bound regulators such as CR1 that regulate activation of the complement system. CR1 regulates in a similar manner as FH/C4BP by binding to either C3b/C4b and using the serum protease FI to deactivate the active opsins into iC3b/C4d [117]. Furthermore, iC3b is further cleaved into

C3dg by the action of CR1 in collaboration with FI. CR1 also possess the ability to induce decay acceleration of C3/C5 convertases into their respective parts [118]. In addition, another membrane bound regulator, DAF, also targets C3/C5 convertases and rapidly dissociates the components [119,120]. While DAF only targets convertases, another cell-bound regulator, membrane cofactor protein (MCP), deactivates C3b or C4b with the aid of FI. Since our system uses erythrocytes as a cellular model [46], MCP is not included because it is not expressed on erythrocytes. Lastly, the terminal cascade is regulated through the action of vitronectin or clusterin that inhibit surface binding of C5b-7, while CD59 (protectin) inhibits C9 polymerization to regulate MAC pore formation [113,121].

4.5 References

1. Bosch AATM, Biesbroek G, Trzcinski K, Sanders EAM, Bogaert D. Viral and Bacterial Interactions in the Upper Respiratory Tract. PLoS Pathog. 2013;9. doi:10.1371/journal.ppat.1003057

2. Gorguner M, Akgun M. Acute Inhalation Injury. Eurasian J Med. 2010;42: 28–35. doi:10.5152/eajm.2010.09

3. Dickson RP, Erb-Downward JR, Martinez FJ, Huffnagle GB. The Microbiome and the Respiratory Tract. Annu Rev Physiol. 2016;78: 481–504. doi:10.1146/annurev-physiol-021115-105238

4. Iwasaki A, Foxman EF, Molony RD. Early local immune defenses in the respiratory tract. Nat Rev Immunol. 2017;17: 7–20. doi:10.1038/nri.2016.117

5. Nicod LP. Lung defences: an overview. Eur Respir Rev. 2005;14: 45–50. doi:10.1183/09059180.05.00009501

6. Kulkarni HS, Liszewski MK, Brody SL, Atkinson JP. The complement system in the airway epithelium: An overlooked host defense mechanism and therapeutic target? J Allergy Clin Immunol. 2018;141: 1582–1586.e1. doi:10.1016/j.jaci.2017.11.046

7. Pandya PH, Wilkes DS. Complement System in Lung Disease. Am J Respir Cell Mol Biol. 2014;51: 467–473. doi:10.1165/rcmb.2013-0485TR

8. Ricklin D, Reis ES, Mastellos DC, Gros P, Lambris JD. Complement component C3 - The “Swiss Army Knife” of innate immunity and host defense. Immunol Rev. 2016;274: 33–58. doi:10.1111/imr.12500

9. Ziccardi RJ. Spontaneous activation of the first component of human complement (C1) by an intramolecular autocatalytic mechanism. J Immunol Baltim Md 1950. 1982;128: 2500–2504.

10. Tseng Y, Poon PH, Zavodszky P, Schumaker VN. Spontaneous activation of serum C1 in vitro. Role of C1 inhibitor. J Immunol. 1991;147: 1884–1890.

11. Bianchino AC, Poon PH, Schumaker VN. A mechanism for the spontaneous activation of the first component of complement, C1, and its regulation by C1-inhibitor. J Immunol. 1988;141: 3930–3936.

12. Schatz-Jakobsen JA, Pedersen DV, Andersen GR. Structural insight into proteolytic activation and regulation of the complement system. Immunol Rev. 2016;274: 59–73. doi:10.1111/imr.12465

13. Merle NS, Noe R, Halbwachs-Mecarelli L, Fremeaux-Bacchi V, Roumenina LT. Complement System Part II: Role in Immunity. Front Immunol. 2015;6. doi:10.3389/fimmu.2015.00257

14. Reis ES, Mastellos DC, Hajishengallis G, Lambris JD. New insights into the immune functions of complement. Nat Rev Immunol. 2019; doi:10.1038/s41577-019-0168-x

15. Hajishengallis G, Reis ES, Mastellos DC, Ricklin D, Lambris JD. Novel Mechanisms and Functions of Complement. Nat Immunol. 2017;18: 1288–1298. doi:10.1038/ni.3858

16. Sharp TH, Koster AJ, Gros P. Heterogeneous MAC Initiator and Pore Structures in a Lipid Bilayer by Phase-Plate Cryo-electron Tomography. Cell Rep. 2016;15: 1–8. doi:10.1016/j.celrep.2016.03.002

17. Serna M, Giles JL, Morgan BP, Bubeck D. Structural basis of complement membrane attack complex formation. Nat Commun. 2016;7: ncomms10587. doi:10.1038/ncomms10587

18. Menny A, Serna M, Boyd CM, Gardner S, Joseph AP, Morgan BP, et al. CryoEM reveals how the complement membrane attack complex ruptures lipid bilayers. Nat Commun. 2018;9: 5316. doi:10.1038/s41467-018-07653-5

19. Berends ETM, Mohan S, Miellet WR, Ruyken M, Rooijakkers SHM. Contribution of the complement Membrane Attack Complex to the bactericidal activity of human serum. Mol Immunol. 2015;65: 328–335. doi:10.1016/j.molimm.2015.01.020

20. Hovingh ES, van den Broek B, Jongerius I. Hijacking Complement Regulatory Proteins for Bacterial Immune Evasion. Front Microbiol. 2016;7. doi:10.3389/fmicb.2016.02004

21. Bennett KM, Rooijakkers SHM, Gorham RD. Let's Tie the Knot: Marriage of Complement and Adaptive Immunity in Pathogen Evasion, for Better or Worse. Front Microbiol. 2017;8: 89. doi:10.3389/fmicb.2017.00089

22. Zipfel PF, Hallström T, Riesbeck K. Human complement control and complement evasion by pathogenic microbes--tipping the balance. Mol Immunol. 2013;56: 152–160. doi:10.1016/j.molimm.2013.05.222

23. Lambris JD, Ricklin D, Geisbrecht BV. Complement evasion by human pathogens. Nat Rev Microbiol. 2008;6: 132–142. doi:10.1038/nrmicro1824

24. Garcia BL, Zwarthoff SA, Rooijakkers SHM, Geisbrecht BV. Novel Evasion Mechanisms of the Classical Complement Pathway. J Immunol Baltim Md 1950. 2016;197: 2051–2060. doi:10.4049/jimmunol.1600863

25. Stephens DS, Greenwood B, Brandtzaeg P. Epidemic meningitis, meningococcaemia, and Neisseria meningitidis. Lancet Lond Engl. 2007;369: 2196–2210. doi:10.1016/S0140-6736(07)61016-2

26. Martinón-Torres F. Deciphering the Burden of Meningococcal Disease: Conventional and Under-recognized Elements. J Adolesc Health Off Publ Soc Adolesc Med. 2016;59: S12-20. doi:10.1016/j.jadohealth.2016.03.041

27. Schneider MC, Prosser BE, Caesar JJE, Kugelberg E, Li S, Zhang Q, et al. Neisseria meningitidis recruits factor H using protein mimicry of host carbohydrates. Nature. 2009;458: 890–893. doi:10.1038/nature07769

28. Caesar JJE, Lavender H, Ward PN, Exley RM, Eaton J, Chittock E, et al. Competition between antagonistic complement factors for a single protein on N. meningitidis rules disease susceptibility. eLife. 2014;3. doi:10.7554/eLife.04008

29. Schneider MC, Exley RM, Chan H, Feavers I, Kang Y-H, Sim RB, et al. Functional significance of factor H binding to Neisseria meningitidis. J Immunol Baltim Md 1950. 2006;176: 7566–7575.

30. Granoff DM, Welsch JA, Ram S. Binding of Complement Factor H (fH) to Neisseria meningitidis Is Specific for Human fH and Inhibits Complement Activation by Rat and Rabbit Sera. Infect Immun. 2009;77: 764–769. doi:10.1128/IAI.01191-08

31. Skattum L, van Deuren M, van der Poll T, Truedsson L. Complement deficiency states and associated infections. Mol Immunol. 2011;48: 1643–1655. doi:10.1016/j.molimm.2011.05.001

32. Ram S, Lewis LA, Rice PA. Infections of People with Complement Deficiencies and Patients Who Have Undergone Splenectomy. Clin Microbiol Rev. 2010;23: 740–780. doi:10.1128/CMR.00048-09

33. Jönsson G, Truedsson L, Sturfelt G, Oxelius V-A, Braconier JH, Sjöholm AG. Hereditary C2 deficiency in Sweden: frequent occurrence of invasive infection, atherosclerosis, and rheumatic disease. Medicine (Baltimore). 2005;84: 23–34.

34. Munthe-Fog L, Hummelshøj T, Honoré C, Madsen HO, Permin H, Garred P. Immunodeficiency associated with FCN3 mutation and ficolin-3 deficiency. N Engl J Med. 2009;360: 2637–2644. doi:10.1056/NEJMoa0900381

35. Wright V, Hibberd M, Levin M. Genetic polymorphisms in host response to meningococcal infection: the role of susceptibility and severity genes. Vaccine. 2009;27 Suppl 2: B90-102. doi:10.1016/j.vaccine.2009.05.002

36. S Reis E, Falcão DA, Isaac L. Clinical aspects and molecular basis of primary deficiencies of complement component C3 and its regulatory proteins factor I and factor H. Scand J Immunol. 2006;63: 155–168. doi:10.1111/j.1365-3083.2006.01729.x

37. Figueroa JE, Densen P. Infectious diseases associated with complement deficiencies. Clin Microbiol Rev. 1991;4: 359–395.

38. Heesterbeek DAC, Angelier ML, Harrison RA, Rooijakkers SHM. Complement and Bacterial Infections: From Molecular Mechanisms to Therapeutic Applications. J Innate Immun. 2018;10: 455–464. doi:10.1159/000491439

39. Kawakami T, Nakazawa H, Kurasawa Y, Sakai H, Nishina S, Senoo N, et al. Severe Infection of Pseudomonas aeruginosa during Eculizumab Therapy for Paroxysmal Nocturnal Hemoglobinuria. Intern Med Tokyo Jpn. 2018;57: 127–130. doi:10.2169/internalmedicine.9151-17

40. Vellanki VS, Bargman JM. Aspergillus Niger peritonitis in a peritoneal dialysis patient treated with eculizumab. Ren Fail. 2014;36: 631–633. doi:10.3109/0886022X.2014.882712

41. Sagar A, Dai W, Minot M, LeCover R, Varner JD. Reduced order modeling and analysis of the human complement system. PLoS ONE. 2017;12. doi:10.1371/journal.pone.0187373

42. Lang SN, Germerodt S, Glock C, Skerka C, Zipfel PF, Schuster S. Molecular crypsis by pathogenic fungi using human factor H. A numerical model. PloS One. 2019;14: e0212187. doi:10.1371/journal.pone.0212187

43. Liu B, Zhang J, Tan PY, Hsu D, Blom AM, Leong B, et al. A Computational and Experimental Study of the Regulatory Mechanisms of the Complement System. PLoS Comput Biol. 2011;7: e1001059. doi:10.1371/journal.pcbi.1001059

44. Hirayama H, Yoshii K, Ojima H, Kawai N, Gotoh S, Fukuyama Y. Linear systems analysis of activating processes of complement system as a defense mechanism. Biosystems. 1996;39: 173–185. doi:10.1016/0303-2647(96)01617-6

45. Korotaevskiy AA, Hanin LG, Khanin MA. Non-linear dynamics of the complement system activation. Math Biosci. 2009;222: 127–143. doi:10.1016/j.mbs.2009.10.003

46. Zewde N, Jr RDG, Dorado A, Morikis D. Quantitative Modeling of the Alternative Pathway of the Complement System. PLOS ONE. 2016;11: e0152337. doi:10.1371/journal.pone.0152337

47. Zewde N, Morikis D. A computational model for the evaluation of complement system regulation under homeostasis, disease, and drug intervention. PLOS ONE. 2018;13: e0198644. doi:10.1371/journal.pone.0198644

48. Granoff DM. Relative importance of complement-mediated bactericidal and opsonic activity for protection against meningococcal disease. Vaccine. 2009;27: B117–B125. doi:10.1016/j.vaccine.2009.04.066

49. Forthal DN. Functions of Antibodies. Microbiol Spectr. 2014;2: 1–17.

50. Fijen CA, Bredius RG, Kuijper EJ, Out TA, De Haas M, De Wit AP, et al. The role of Fcgamma receptor polymorphisms and C3 in the immune defence against Neisseria meningitidis in complement-deficient individuals. Clin Exp Immunol. 2000;120: 338–345.

51. Lewis LA, Ram S. Meningococcal disease and the complement system. Virulence. 2014;5: 98–126. doi:10.4161/viru.26515

52. Martinón-Torres F, Png E, Khor CC, Davila S, Wright VJ, Sim KS, et al. Natural resistance to Meningococcal Disease related to CFH loci: Meta-analysis of genome-wide association studies. Sci Rep. 2016;6: 35842. doi:10.1038/srep35842

53. Davila S, Wright VJ, Khor CC, Sim KS, Binder A, Breunis WB, et al. Genome-wide association study identifies variants in the CFH region associated with host susceptibility to meningococcal disease. Nat Genet. 2010;42: 772–776. doi:10.1038/ng.640

54. Andreae CA, Sessions RB, Virji M, Hill DJ. Bioinformatic analysis of meningococcal Msf and Opc to inform vaccine antigen design. PloS One. 2018;13: e0193940. doi:10.1371/journal.pone.0193940

55. Harboe M, Johnson C, Nymo S, Ekholt K, Schjalm C, Lindstad JK, et al. Properdin binding to complement activating surfaces depends on initial C3b deposition. Proc Natl Acad Sci U S A. 2017;114: E534–E539. doi:10.1073/pnas.1612385114

56. Harboe M, Garred P, Lindstad JK, Pharo A, Müller F, Stahl GL, et al. The role of properdin in zymosan- and Escherichia coli-induced complement activation. J Immunol Baltim Md 1950. 2012;189: 2606–2613. doi:10.4049/jimmunol.1200269

57. Pillemer L, Blum L, Lepow IH, Ross OA, Todd EW, Wardlaw AC. The properdin system and immunity. I. Demonstration and isolation of a new serum protein, properdin, and its role in immune phenomena. Science. 1954;120: 279–285.

58. Cortes C, Ferreira VP, Pangburn MK. Native Properdin Binds to Chlamydia pneumoniae and Promotes Complement Activation. Infect Immun. 2011;79: 724–731. doi:10.1128/IAI.00980-10

59. Spitzer D, Mitchell LM, Atkinson JP, Hourcade DE. Properdin can initiate complement activation by binding specific target surfaces and providing a platform for de novo convertase assembly. J Immunol Baltim Md 1950. 2007;179: 2600–2608.

60. Saggu G, Cortes C, Emch HN, Ramirez G, Worth RG, Ferreira VP. Identification of a novel mode of complement activation on stimulated platelets mediated by properdin and C3(H2O). J Immunol Baltim Md 1950. 2013;190: 6457–6467. doi:10.4049/jimmunol.1300610

61. Kemper C, Mitchell LM, Zhang L, Hourcade DE. The complement protein properdin binds apoptotic T cells and promotes complement activation and phagocytosis. Proc Natl Acad Sci U S A. 2008;105: 9023–9028. doi:10.1073/pnas.0801015105

62. Chen JY, Cortes C, Ferreira VP. Properdin: A multifaceted molecule involved in inflammation and diseases. Mol Immunol. 2018;102: 58–72. doi:10.1016/j.molimm.2018.05.018

63. Ali YM, Hayat A, Saeed BM, Haleem KS, Alshamrani S, Kenawy HI, et al. Low-dose recombinant properdin provides substantial protection against Streptococcus pneumoniae and Neisseria meningitidis infection. Proc Natl Acad Sci U S A. 2014;111: 5301–5306. doi:10.1073/pnas.1401011111

64. Caswell JL. Failure of respiratory defenses in the pathogenesis of bacterial pneumonia of cattle. Vet Pathol. 2014;51: 393–409. doi:10.1177/0300985813502821

65. Rawlings BA, Higgins TS, Han JK. Bacterial pathogens in the nasopharynx, nasal cavity, and osteomeatal complex during wellness and viral infection. Am J Rhinol Allergy. 2013;27: 39–42. doi:10.2500/ajra.2013.27.3835

66. Man WH, de Steenhuijsen Piters WAA, Bogaert D. The microbiota of the respiratory tract: gatekeeper to respiratory health. Nat Rev Microbiol. 2017;15: 259–270. doi:10.1038/nrmicro.2017.14

67. Esparza-Gordillo J, Soria JM, Buil A, Almasy L, Blangero J, Fontcuberta J, et al. Genetic and environmental factors influencing the human factor H plasma levels. Immunogenetics. 2004;56: 77–82. doi:10.1007/s00251-004-0660-7

68. Schäuble S, Stavrum AK, Puntervoll P, Schuster S, Heiland I. Effect of substrate competition in kinetic models of metabolic networks. FEBS Lett. 2013;587: 2818–2824. doi:10.1016/j.febslet.2013.06.025

69. Wu J, Wu Y-Q, Ricklin D, Janssen BJC, Lambris JD, Gros P. Structure of complement fragment C3b-factor H and implications for host protection by complement regulators. Nat Immunol. 2009;10: 728–733. doi:10.1038/ni.1755

70. Pangburn MK, Müller-Eberhard HJ. The C3 convertase of the alternative pathway of human complement. Enzymic properties of the bimolecular proteinase. Biochem J. 1986;235: 723–730.

71. Pangburn MK, Schreiber RD, Müller-Eberhard HJ. Formation of the initial C3 convertase of the alternative complement pathway. Acquisition of C3b-like activities by spontaneous hydrolysis of the putative thioester in native C3. J Exp Med. 1981;154: 856–867.

72. Laich A, Sim RB. Complement C4bC2 complex formation: an investigation by surface plasmon resonance. Biochim Biophys Acta. 2001;1544: 96–112.

73. Kretzschmar T, Jeromin A, Gietz C, Bautsch W, Klos A, Köhl J, et al. Chronic myelogenous leukemia-derived basophilic granulocytes express a functional active receptor for the anaphylatoxin C3a. Eur J Immunol. 1993;23: 558–561. doi:10.1002/eji.1830230239

74. el-Lati SG, Dahinden CA, Church MK. Complement peptides C3a- and C5a-induced mediator release from dissociated human skin mast cells. J Invest Dermatol. 1994;102: 803–806.

75. Coulthard LG, Woodruff TM. Is the complement activation product C3a a proinflammatory molecule? Re-evaluating the evidence and the myth. J Immunol Baltim Md 1950. 2015;194: 3542–3548. doi:10.4049/jimmunol.1403068

76. Law SK, Lichtenberg NA, Levine RP. Evidence for an ester linkage between the labile binding site of C3b and receptive surfaces. J Immunol Baltim Md 1950. 1979;123: 1388–1394.

77. Tack BF, Harrison RA, Janatova J, Thomas ML, Prahl JW. Evidence for presence of an internal thiolester bond in third component of human complement. Proc Natl Acad Sci U S A. 1980;77: 5764–5768.

78. Law SK, Levine RP. Interaction between the third complement protein and cell surface macromolecules. Proc Natl Acad Sci U S A. 1977;74: 2701–2705.

79. Sim RB, Twose TM, Paterson DS, Sim E. The covalent-binding reaction of complement component C3. Biochem J. 1981;193: 115–127.

80. Rawal N, Pangburn MK. C5 convertase of the alternative pathway of complement. Kinetic analysis of the free and surface-bound forms of the enzyme. J Biol Chem. 1998;273: 16828–16835.

81. Lutz HU, Jelezarova E. Complement amplification revisited. Mol Immunol. 2006;43: 2–12. doi:10.1016/j.molimm.2005.06.020

82. Pedersen DV, Roumenina L, Jensen RK, Gadeberg TA, Marinozzi C, Picard C, et al. Functional and structural insight into properdin control of complement alternative pathway amplification. EMBO J. 2017;36: 1084–1099. doi:10.15252/embj.201696173

83. Hourcade DE. The role of properdin in the assembly of the alternative pathway C3 convertases of complement. J Biol Chem. 2006;281: 2128–2132. doi:10.1074/jbc.M508928200

84. Cooper NR, Müller-Eberhard HJ. THE REACTION MECHANISM OF HUMAN C5 IN IMMUNE HEMOLYSIS. J Exp Med. 1970;132: 775–793.

85. Bayly-Jones C, Bubeck D, Dunstone MA. The mystery behind membrane insertion: a review of the complement membrane attack complex. Philos Trans R Soc Lond B Biol Sci. 2017;372. doi:10.1098/rstb.2016.0221

86. Zalman LS, Müller-Eberhard HJ. Comparison of channels formed by poly C9, C5b-8 and the membrane attack complex of complement. Mol Immunol. 1990;27: 533–537.

87. Sepp A, Dodds AW, Anderson MJ, Campbell RD, Willis AC, Law SK. Covalent binding properties of the human complement protein C4 and hydrolysis rate of the internal thioester upon activation. Protein Sci Publ Protein Soc. 1993;2: 706–716. doi:10.1002/pro.5560020502

88. Meri S, Pangburn MK. A mechanism of activation of the alternative complement pathway by the classical pathway: protection of C3b from inactivation by covalent attachment to C4b. Eur J Immunol. 1990;20: 2555–2561. doi:10.1002/eji.1830201205

89. Rawal N, Pangburn M. Formation of high-affinity C5 convertases of the alternative pathway of complement. J Immunol Baltim Md 1950. 2001;166: 2635–2642.

90. Rawal N, Pangburn MK. Formation of High Affinity C5 Convertase of the Classical Pathway of Complement. J Biol Chem. 2003;278: 38476–38483. doi:10.1074/jbc.M307017200

91. Kishore U, Ghai R, Greenhough TJ, Shrive AK, Bonifati DM, Gadjeva MG, et al. Structural and functional anatomy of the globular domain of complement protein C1q. Immunol Lett. 2004;95: 113–128. doi:10.1016/j.imlet.2004.06.015

92. Diebolder CA, Beurskens FJ, de Jong RN, Koning RI, Strumane K, Lindorfer MA, et al. Complement is activated by IgG hexamers assembled at the cell surface. Science. 2014;343: 1260–1263. doi:10.1126/science.1248943

93. Bally I, Inforzato A, Dalonneau F, Stravalaci M, Bottazzi B, Gaboriaud C, et al. Interaction of C1q With Pentraxin 3 and IgM Revisited: Mutational Studies With Recombinant C1q Variants. Front Immunol. 2019;10: 461. doi:10.3389/fimmu.2019.00461

94. Wang G, de Jong RN, van den Bremer ETJ, Beurskens FJ, Labrijn AF, Ugurlar D, et al. Molecular Basis of Assembly and Activation of Complement Component C1 in Complex with Immunoglobulin G1 and Antigen. Mol Cell. 2016;63: 135–145. doi:10.1016/j.molcel.2016.05.016

95. Ugurlar D, Howes SC, de Kreuk B-J, Koning RI, de Jong RN, Beurskens FJ, et al. Structures of C1-IgG1 provide insights into how danger pattern recognition activates complement. Science. 2018;359: 794–797. doi:10.1126/science.aao4988

96. Garred P, Genster N, Pilely K, Bayarri-Olmos R, Rosbjerg A, Ma YJ, et al. A journey through the lectin pathway of complement-MBL and beyond. Immunol Rev. 2016;274: 74–97. doi:10.1111/imr.12468

97. Degn SE, Thiel S. Humoral pattern recognition and the complement system. Scand J Immunol. 2013;78: 181–193. doi:10.1111/sji.12070

98. Degn SE, Thiel S, Nielsen O, Hansen AG, Steffensen R, Jensenius JC. MAp19, the alternative splice product of the MASP2 gene. J Immunol Methods. 2011;373: 89–101. doi:10.1016/j.jim.2011.08.006

99. Degn SE, Hansen AG, Steffensen R, Jacobsen C, Jensenius JC, Thiel S. MAp44, a human protein associated with pattern recognition molecules of the complement system and regulating the lectin pathway of complement activation. J Immunol Baltim Md 1950. 2009;183: 7371–7378. doi:10.4049/jimmunol.0902388

100. Megyeri M, Harmat V, Major B, Végh Á, Balczer J, Héja D, et al. Quantitative characterization of the activation steps of mannan-binding lectin (MBL)-associated serine proteases (MASPs) points to the central role of MASP-1 in the initiation of the complement lectin pathway. J Biol Chem. 2013;288: 8922–8934. doi:10.1074/jbc.M112.446500

101. Degn SE, Kjaer TR, Kidmose RT, Jensen L, Hansen AG, Tekin M, et al. Complement activation by ligand-driven juxtaposition of discrete pattern recognition complexes. Proc Natl Acad Sci U S A. 2014;111: 13445–13450. doi:10.1073/pnas.1406849111

102. Héja D, Kocsis A, Dobó J, Szilágyi K, Szász R, Závodszky P, et al. Revised mechanism of complement lectin-pathway activation revealing the role of serine protease MASP-1 as the exclusive activator of MASP-2. Proc Natl Acad Sci U S A. 2012;109: 10498–10503. doi:10.1073/pnas.1202588109

103. Ambrus G, Gál P, Kojima M, Szilágyi K, Balczer J, Antal J, et al. Natural Substrates and Inhibitors of Mannan-Binding Lectin-Associated Serine Protease-1 and -2: A Study on Recombinant Catalytic Fragments. J Immunol. 2003;170: 1374–1382. doi:10.4049/jimmunol.170.3.1374

104. Rossi V, Teillet F, Thielens NM, Bally I, Arlaud GJ. Functional Characterization of Complement Proteases C1s/Mannan-binding Lectin-associated Serine Protease-2 (MASP-2) Chimeras Reveals the Higher C4 Recognition Efficacy of the MASP-2 Complement Control Protein Modules. J Biol Chem. 2005;280: 41811–41818. doi:10.1074/jbc.M503813200

105. Józsi M, Tortajada A, Uzonyi B, Goicoechea de Jorge E, Rodríguez de Córdoba S. Factor H-related proteins determine complement-activating surfaces. Trends Immunol. 2015;36: 374–384. doi:10.1016/j.it.2015.04.008

106. Skerka C, Chen Q, Fremeaux-Bacchi V, Roumenina LT. Complement factor H related proteins (CFHRs). Mol Immunol. 2013;56: 170–180. doi:10.1016/j.molimm.2013.06.001

107. Medjeral-Thomas N, Pickering MC. The complement factor H-related proteins. Immunol Rev. 2016;274: 191–201. doi:10.1111/imr.12477

108. Csincsi ÁI, Szabó Z, Bánlaki Z, Uzonyi B, Cserhalmi M, Kárpáti É, et al. FHR-1 Binds to C-Reactive Protein and Enhances Rather than Inhibits Complement

Activation. J Immunol Baltim Md 1950. 2017;199: 292–303. doi:10.4049/jimmunol.1600483

109. Hebecker M, Okemefuna AI, Perkins SJ, Mihlan M, Huber-Lang M, Józsi M. Molecular basis of C-reactive protein binding and modulation of complement activation by factor H-related protein 4. Mol Immunol. 2010;47: 1347–1355. doi:10.1016/j.molimm.2009.12.005

110. Csincsi ÁI, Kopp A, Zöldi M, Bánlaki Z, Uzonyi B, Hebecker M, et al. Factor H-related protein 5 interacts with pentraxin 3 and the extracellular matrix and modulates complement activation. J Immunol Baltim Md 1950. 2015;194: 4963–4973. doi:10.4049/jimmunol.1403121

111. Dopler A, Guntau L, Harder MJ, Palmer A, Höchsmann B, Schrezenmeier H, et al. Self versus Nonself Discrimination by the Soluble Complement Regulators Factor H and FHL-1. J Immunol Baltim Md 1950. 2019;202: 2082–2094. doi:10.4049/jimmunol.1801545

112. Zipfel PF, Skerka C. FHL-1/reconectin: a human complement and immune regulator with cell-adhesive function. Immunol Today. 1999;20: 135–140.

113. Schmidt CQ, Lambris JD, Ricklin D. Protection of host cells by complement regulators. Immunol Rev. 2016;274: 152–171. doi:10.1111/imr.12475

114. Rossi V, Bally I, Ancelet S, Xu Y, Frémeaux-Bacchi V, Vivès RR, et al. Functional characterization of the recombinant human C1 inhibitor serpin domain: insights into heparin binding. J Immunol Baltim Md 1950. 2010;184: 4982–4989. doi:10.4049/jimmunol.0902016

115. Kerr FK, Thomas AR, Wijeyewickrema LC, Whisstock JC, Boyd SE, Kaiserman D, et al. Elucidation of the substrate specificity of the MASP-2 protease of the lectin complement pathway and identification of the enzyme as a major physiological target of the serpin, C1-inhibitor. Mol Immunol. 2008;45: 670–677. doi:10.1016/j.molimm.2007.07.008

116. Ermert D, Blom AM. C4b-binding protein: The good, the bad and the deadly. Novel functions of an old friend. Immunol Lett. 2016;169: 82–92. doi:10.1016/j.imlet.2015.11.014

117. Krych-Goldberg M, Atkinson JP. Structure-function relationships of complement receptor type 1. Immunol Rev. 2001;180: 112–122.

118. Krych-Goldberg M, Hauhart RE, Subramanian VB, Yurcisin BM, Crimmins DL, Hourcade DE, et al. Decay accelerating activity of complement receptor type 1

(CD35). Two active sites are required for dissociating C5 convertases. J Biol Chem. 1999;274: 31160–31168.

119. Harris CL, Abbott RJM, Smith RA, Morgan BP, Lea SM. Molecular Dissection of Interactions between Components of the Alternative Pathway of Complement and Decay Accelerating Factor (CD55). J Biol Chem. 2005;280: 2569–2578. doi:10.1074/jbc.M410179200

120. Claire L Harris DMP. Decay-accelerating factor must bind both components of the complement alternative pathway C3 convertase to mediate efficient decay. J Immunol Baltim Md 1950. 2007;178: 352–9. doi:10.4049/jimmunol.178.1.352

121. Morgan BP, Boyd C, Bubeck D. Molecular cell biology of complement membrane attack. Semin Cell Dev Biol. 2017; doi:10.1016/j.semcdb.2017.06.009

CHAPTER 5

Immunophysical Evaluation of the Initiating step in the Formation of the Membrane Attack Complex

5.1 Introduction

As part of the innate immunity, the complement system orchestrates a cascade of biochemical reactions that result in pathogen elimination and in activation of the adaptive immune response [1, 2]. The versatile response of the complement system emerges from its three pathways known as alternative, classical, and lectin, that are either constitutively active in the fluid phase (alternative and classical pathway [3–5]) or initiate upon sensing danger-associated molecular patterns on pathogens (classical and lectin pathways). Activation of all three pathways converges on the cleavage of complement protein C3 into C3b and C3a [6]. Subsequently, continued propagation leads to the terminal cascade by cleavage of complement C5 to form C5b and C5a. Complement C6 then binds to C5b to form the complex C5b6 [7]. This soluble complex then associates with C7 to form C5b67, which later anchors to a nearby surface. Subsequently, the surface bound C5b67 binds to C8 to form C5b678 [8]. This complex, unlike the anchored C5b67, forms a pore of 0.9-nm diameter, which expands later in time to a 3-nm pore [9–11]. Finally, surface bound C5b678 recruits multiple C9s, to a maximum of 18, to form the membrane attack complex (MAC or $C5b6789_n$ where n = 1–18) [9, 12]. Although the proteins that make up the MAC pores are the same (C5b, C6, C7, C8, and C9), there is oligomeric heterogeneity in the assembly process of MACs. For instance, oligomerization of two to four C5b678

complexes can bind to a variable number of C9s to form a joined MAC pore [9]. In any case, structures of a single MAC pore, comprised of C5b678 in complex with a polymerized C9, are cylindrical in shape, contain a single stalk protrusion, and have an inner lumen diameter of 10- to 11.5-nm [9, 12]. MACs evolved as the only direct killing mechanism deployed by the complement system to fight against pathogens; indeed MAC deficiency has been associated with an increased risk of recurrent meningitis [1]. In addition to eliminating pathogens, MAC instigates numerous signaling pathways that directly affect cell cycles. For instance, sublytic MACs affect cell proliferation and apoptosis by enhancing or inhibiting the processes [13]. In addition, MACs can directly mediate cytokine production and platelet activation [13].

The instigation of an immune response via C5b6 is also detrimental to host-cells unless complement is properly regulated at the terminal stage [14]. To ensure tissue homeostasis, multiple checkpoints are present in fluid and surface phases that target complement propagators such as C3/C5 convertases. Furthermore, membrane-bound complement regulator, CD59, is present on host-cells to directly inhibit the assembly of the MAC and mitigate its deadly effects. However, despite the regulatory checkpoints, disease-related mutations over-activate the complement system and disrupt tissue homeostasis by generating elevated levels of MAC. This level of impairment propels complement in becoming one of the key drivers for diseases like aHUS, AMD, and PNH [15–20].

The formation of C5b6 complex sets the stage for a cascade of reactions that go beyond just the elimination of pathogens. C5b6 provides the junction at which the early-

and late-stage complement pathway propagation converge to instigate signaling cues that are vital for cell survival [13]. Thus, understanding the governing mechanism behind C5b6 formation provides the basis for the first step in the assembly of terminal MAC complex that initiates a range of events, from immune defense to development of autoimmune diseases.

Complement proteins C3, C4, and C5 are structurally homologous [21–23] but only C3 and C4 have an internal thioester bond moiety that is capable of undergoing hydrolysis, followed by covalent attachment to cell surfaces [24, 25]. After cleavage of C3 and C4 by convertases to form fragments C3a/C3b and C4a/C4b, the C3b and C4b fragments are opsonins that attach to cells surfaces through their thioester domains (TED), also known as C3d and C4d when they become stand-alone proteins after additional cleavage steps. The cell-bound C3b is recognizable by phagocytes for elimination of the C3b-tagged cells, and also C3b and C4b become part of the convertase complexes that are responsible for C3 and C5 cleavage. On the other hand, C5b is missing an internal thioester bond, but it contains a TED-like domain that is structurally homologous to the TEDs of C3 and C4. For simplicity we will call hereafter C3d, C4d, and C5d the TED domains of C3 and C4, and the TED-like domain of C5, respectively.

Crystal structures of C3b in complex with structurally homologous modular regulators, factor H, complement receptor 1, membrane cofactor protein, decay-accelerating factor, and smallpox inhibitor of complement enzymes (SPICE), are available [26, 27]. These regulators are composed of repeated complement control protein (CCP) modules and have shown a shared binding mode along the structure of C3b, comprising

modules CCP1-4 (FH, MCP, SPICE), CCP2-4 (DAF), and CCP15-17 (CR1). All regulators show contact of one module at the C3d domain of C3b. The viral vaccinia control protein (VCP), that is structurally and functionally homologous to SPICE, is also expected to have a similar binding mode to C3b. In addition, the stand-alone C3d domain, is known to interact with modules CCP1-2 of complement receptor 2 (CR2) [28], modules CCP19-20 of FH [29], in addition to modules CCP1-4 (mentioned above as interacting along C3b), and *S. aureus* proteins Efb-C, Ecb, and Sbi [30, 31]. These structural observations make the C3d domain multifunctional in interacting with complement natural and viral regulators, when C3d is part of C3b, and in attracting CR2, FH (CCP19-20), and bacterial regulators when C3d is stand-alone. On the other hand, C5b is not known to possess similar properties as C3b, and C5d is not known to exist in a stand-alone form. Instead, C5b acts as the first block of a scaffold that initiates the membrane attack complex, interacting first with C6, and subsequently with C7, C8, and several C9s, mentioned above. The crystal structures of C5b6 [32, 33] reveal that an elongated C6 surrounds half of the C5d domain and has three sites of contacts with C5b (**Figures 5.1A and 5.1B**). In addition, the crystal structure reveals the presence of charged patches on the surfaces of C5b and C6, and at the binding interface, which are expected to contribute to structural stability of the complex through the formation of ionic and hydrogen bonding contacts (**Figures 5.1C and 5.1D**).

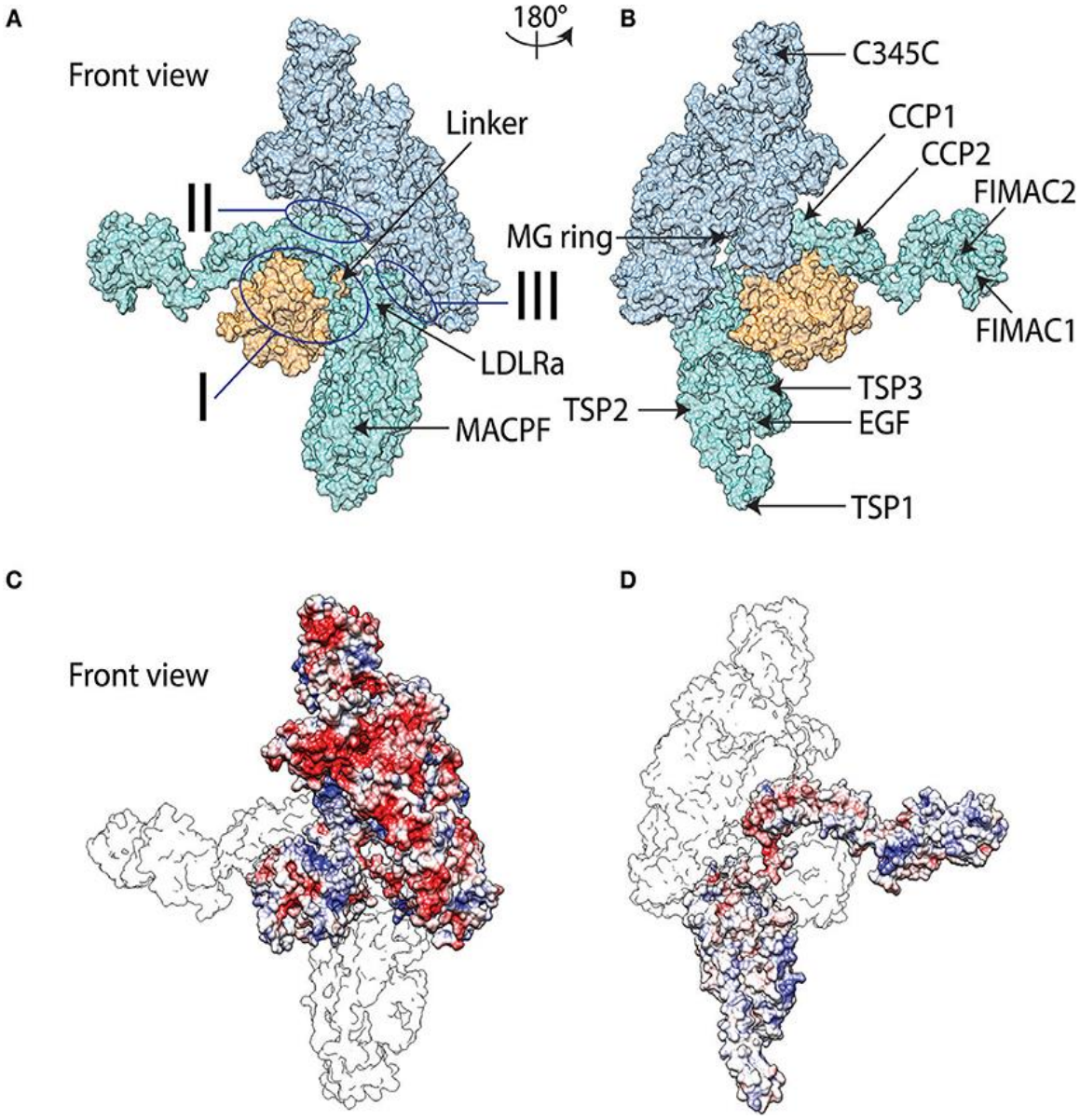

Figure 5.1. Surface representation molecular graphics of C5b6 complex in front view **(A)** and back view **(B)**. C5b is indicated in blue with the thioester-like domain colored orange while C6 represented in teal. The three sites of interaction between C5b and C6 are marked. Domains of C5b and C6 discussed in text are marked. Electrostatic potentials mapped onto molecular graphics of C5b6 in front view with C6b represented as transparent outline and on top of C5b **(C)**, and back view with C5b represented as transparent outline and on top of C6 **(D)**. The color transitions from red to white to blue represent electrostatic potential values of −5 to 0 to 5 k_BT/e. Abbreviations utilized are as follows: LDLRa, low-density lipoprotein receptor class A; MACPF, membrane attack complex perforin; MG, macroglobulin; C345C, netrin domain; CCP, complement control protein; FIMAC, Factor I/membrane attack complex; EGF, epidermal growth factor; and TSP, thrombospondin. Molecular graphics are generated using the final frame of the MD trajectory.

In this study, first we examine the physicochemical mechanism of the interaction between C5b and C6. Given that the C5d domain contributes to the interaction of C5b and C6, and the multifunctionality of C3d with several sites of interaction with native regulators and receptors and bacterial and viral regulators, we present a comparative sequence, structural, and physicochemical analysis between C5d and C3d. For completion, we also include C4d in the comparative analysis. Our goal is to contribute toward understanding mechanisms of function of C3d, C4d, and C5d at the structural and physicochemical property level. Finally, we present a systems-biology approach to understand the pathway dynamics of the terminal complement cascade that starts at C5b6 complex and ends at MAC [25]. We performed molecular dynamics (MD) simulations to relax the crystallographic structure from crystal packing effects, and to obtain insight on the dynamic character of the structure and the persistence of the intermolecular contacts at the amino acid side chain level. Guided by the findings of our MD analysis, and by our previous work that has shown that electrostatics plays a fundamental role on the regulation and function of C3b [34–40] and C3d [28–31, 41, 42], we performed electrostatic calculations using conformational states extracted from the MD data.

5.2 Results

5.2.1 Molecular dynamics analysis

Our goal is to identify the stabilizing interactions that lead to formation of the C5b6 complex, the initial scaffold for the assembly of MAC. The crystal structure [32] shows three major sites of interaction between C5b and C6, named I, II, III (**Figures 5.1A** and

5.1B). Interactions between C6 and the thioester domain of C5b fall under Site I, while interactions of C6 with the macroglobulin (MG) ring of C5b fall under Sites II and III. The crystal structure also shows the presence of charged patches on the surfaces of the two proteins, C5b and C6 (**Figures 5.1C** and **5.1D**), suggesting that charges may be contributing factors to binding. We performed an explicit solvent MD simulation, using a crystal structure as initial conformation, to optimize local geometries and chemistry and to delineate distinct conformational states visited throughout the simulation. Analysis of the MD trajectory, using the molecular mechanics-Poisson-Boltzmann surface area (MM-PBSA) method, showed an overall favorable binding energy for the solvated complex, dominated by van der Waals interactions (**Table 5.1**). Given the observation of many charged patches on the surfaces of C5b and C6 (**Figures 5.1C** and **5.1D**), but overall unfavorable polar contribution to binding (**Table 5.1**), we analyzed the frequency of occurrence of intermolecular pairwise polar interactions to obtain a closer look into the nature of polar contributions. Specific intermolecular salt bridges often stabilize protein complexes, an effect that has been termed ionic tethering, and so do intermolecular hydrogen bonds, even if the overall energetic contribution is dominated by van der Waals interactions of hydrophobic chemical groups [43].

Table 5.1. Calculated MM-PBSA energies from the MD trajectory.

Energy component	Mean ± SD (kJ/mol)
MM van der Waals (vdW)	−983.7 ± 107.5
MM electrostatic	795.4 ± 390.8
Poisson-Boltzmann (PB) solvation	−450.2 ± 386.6
Nonpolar solvation	−140.2 ± 11.7
ΔG(total)	−778.6 ± 94.1

We characterized the significance of intermolecular polar interactions by evaluating the number of salt bridges and hydrogen bonds that occur across the C5b6 binding interface at a frequency of at least 20% during the MD trajectory. **Figures 5.2A** and **5.2B** shows occupancy (frequency of occurrence during the MD trajectory) maps for intermolecular salt bridges and hydrogen bonds, respectively. The C5b6 complex has 13 intermolecular salt bridges with distance cutoff of 5 Å, and 11 intermolecular hydrogen bonds, demonstrating varying levels of persistence throughout the trajectory.

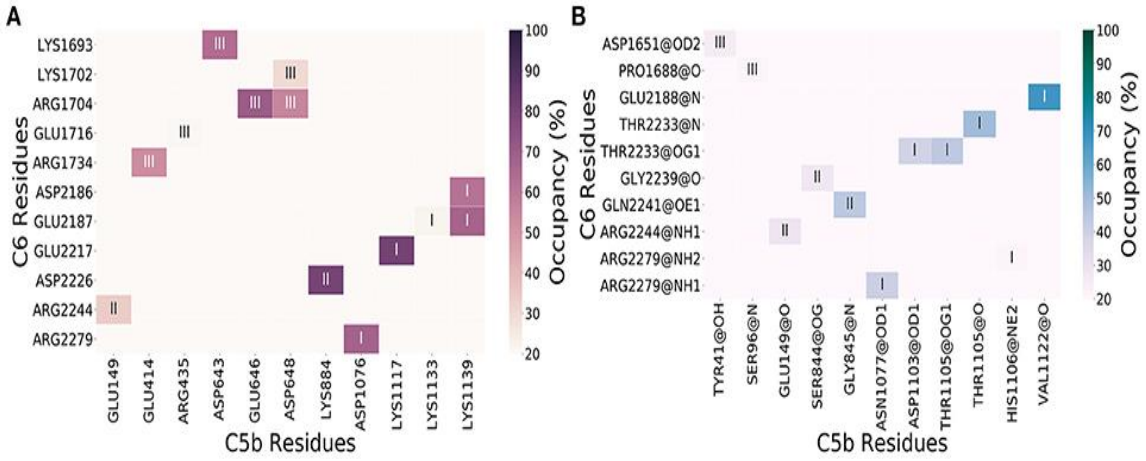

Figure 5.2. Intermolecular interaction occupancy maps for interactions persistent through at least 20% of the trajectory for salt bridges **(A)** and hydrogen bonds **(B)**. The C5b6 interactions sites I, II, and III (**Figure 5.1**) are marked. Heavy atoms of hydrogen bond donor and acceptor chemical groups are marked in panel **(B)**.

The 13 intermolecular salt bridges (and protein/domain) in decreasing order of persistence (81–20%) are: Lys1117(C5b/C5d)-Glu2217(C6/CCP1), Lys884(C5b/CUB)-Asp2226(C6/CCP1), Glu646(C5b/MG Ring)-Arg1704(C6/LDLRa), Asp1076(C5b/C5d)-Arg2279(C6/CCP2), Lys1139(C5b/C5d)-Glu2187(C6/CCP1), Asp643(C5b/MG Ring)-Lys1693(C6/TSP2), Lys1139(C5b/C5d)-Asp2186(C6/CCP1), Asp648(C5b/MG Ring)-Arg1704(C6/LDLRa), Glu414(C5b/MG Ring)-Arg1734(C6/LDLRa), Glu149(C5b/MG Ring)-Arg2244(C6/CCP1), Asp648(C5b/MG Ring)-Lys1702(C6/LDLRa), Arg435(C5b/MG Ring)-Glu1716(C6/LDLRa), and Lys1133(C5b/C5d)-Glu2187(C6/CCP1) (**Figure 5.2A**).

Unlike the persistence of intermolecular salt bridges, most of the intermolecular hydrogen bonds formed between C5b and C6 appear less than half of the time in the trajectory. The 11 intermolecular hydrogen bonds (and protein/domain) in decreasing order of persistence (68–20%) are: Val1122(C5b/C5d)-Glu2188(C6/CCP1), Thr1105(C5b/C5d)-Thr2233(C6/CCP1) (backbone-backbone), Gly845(C5b/CUB)-Gln2241(C6/CCP1), Thr1105(C5b/C5d)-Thr2233(C6/CCP1) (side chain-side chain), Asn1077(C5b/C5d)-Arg2279(C6/CCP2), Asp1103(C5b/C5d)-Thr2233(C6/CCP1), Glu149(C5b/MG Ring)-Arg2244(C6/CCP1), Ser844(C5b/CUB)-Gly2239(C6/CCP1), Tyr41(C5b/MG Ring)-Asp1651(C6/TSP2), Ser96(C5b/MG Ring)-Pro1688(C6/TSP2), and His1106(C5b/C5d)-Arg2279(C6/CCP2) (**Figure 5.2B**).

Six salt bridges occur in Site III, followed by five in Site I, and two in Site II (**Figures 5.1A** and **5.2A**). On the other hand, six hydrogen bonds occur in Site I, followed by three hydrogen bonds occurring in Site II and two hydrogen bonds occurring in site III

(**Figures 5.1A** and **5.2B**). Three bifurcated salt bridges are observed. These are Site I salt bridge Lys1139(C5b) with Asp2186(C6) and Glu2187(C6), Site III salt bridge Arg1704(C6) with Glu646(C5b) and Asp648(C5b), and Site III salt bridge Asp648(C5b) with Lys1702(C6) and Arg1704(C6) (**Figures 5.1A** and **5.2A**). Two residues of C6 are hydrogen bonded with more than one partner, both in Site I. These are Thr2233(C6) side chain with Asp1103(C5b) side chain and Thr1105(C5b) side chain, and Arg2279(C6) side chain with Asn1077(C5b) backbone and His1106(C5b) side chain (**Figures 5.1A** and **5.2A**). Finally, two residues of C5b and three of C6 participate in both salt bridge side chain-side chain interactions and hydrogen bonding side chain-backbone interactions. These are Glu149 and Asp648 of C5b, and Arg1704, Arg2244, and Arg2279 of C6. Among them are Arg1704(C6)-Asp648(C5b) salt bridge and hydrogen bond, involving Arg1704(C6) which is also part of a bifurcated salt bridge with Glu646(C5b) (Site III), Arg2244(C6)-Glu149(C5b) salt bridge and hydrogen bond (Site II), and Arg2279(C6) salt bridge with Asp1070(C6b), and hydrogen bond Asn1077(C5b) (Site I) (**Figures 5.1A** and **5.2**).

Unfavorable charge-charge interactions within 5 Å of each other were not observed at occupancies greater than 10% (Supplementary Data Sheet 4). Thirteen unfavorable charge-charge interactions were observed within 8 Å of each other using the 20% occupancy threshold, as follows: four at Site I, three at Site II, and six at Site III. At Site I, the unfavorable charge-charge interactions are between Lys1139(C5b) and Lys1889(C6), Asp1140(C5b) and Glu2187(C6), Asp1167(C5b) and Glu2217(C6) and, Glu1181(C5b) and Asp2185(C6). At Site II, the unfavorable charge-charge interactions are between

Arg177(C5b) and Arg2244(C6), Arg840(C5b) and Arg2252(C6) and, Lys884(C5b) and Arg2244(C6). At Site III, the unfavorable charge-charge interactions are between Asp43(C5b) and Asp1651(C6), Arg98(C5b) and Lys1690(C6), Arg435(C5b) and Arg1734(C6), Asp643(C5b) and Asp1706(C6), Glu646(C5b) and Glu1695(C6) and, Lys652(C5b) and Lys1702(C6). Of these, the only interactions with frequency above 50% are between Asp1167(C5b) and Glu2217(C6) at Site I, and Lys884(C5b) and Arg2244(C6) at Site II. All unfavorable Coulombic interactions with cutoff distances 5 Å and 8 Å at all occupancy levels are listed in Supplementary Data Sheets 4, 5, respectively. Overall, unfavorable charge-charge interactions are weak.

We further analyzed the MD trajectory to capture the dynamic changes in electrostatic contributions, by evaluating distinct conformational states. We identified six representative structures from the MD trajectory through principal component analysis (PCA) decomposition on phi and psi angles, followed by k-means clustering of the PCA components. The cluster centers (**Figure 5.3**) were extracted as representative structures. Structural representation of clustering conformational states is shown in **Figure D.1**.

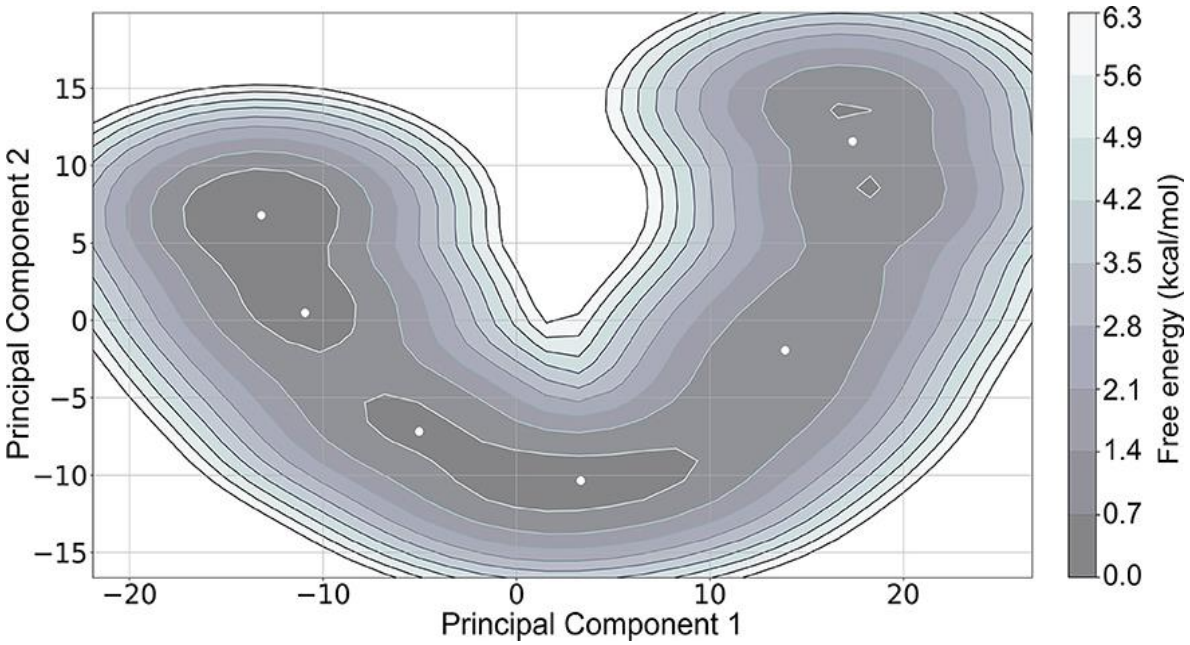

Figure 5.3. Free energy landscape of the first two principal components, Principal Component 1 and Principal Component 2, with cluster centers represented as white dots. The lowest energy regions (colored in dark gray as indicated in the color bar) represent energy minima.

We performed MM-PBSA calculations for the 20 most representative structures of each cluster to evaluate possible differences in the binding free energies among the six clusters. Although we observe differences among the clusters, the overall trends in their free energies are similar (**Table 5.2**).

Table 5.2. Calculated MM-PBSA energies of six conformational states, extracted from the MD trajectory.

Energy	Mean ± SD (kJ/mol)					
	Cluster 1	Cluster 2	Cluster 3	Cluster 4	Cluster 5	Cluster 6
MM vdW	−869.9 ± 36.4	−1115.9 ± 34.3	−876.5 ± 46.9	−901.2 ± 31.0	−985.3 ± 47.7	−887.4 ± 35.6
MM electrostatic	786.2 ± 171.1	511.7 ± 119.2	931.4 ± 100.0	1190.8 ± 349.8	555.2 ± 172.8	−1290.3 ± 184.1
PB solvation	−523.0 ± 151.9	−125.5 ± 109.2	−664.0 ± 106.7	−819.2 ± 332.2	−224.7 ± 173.2	−954.4 ± 168.6
Non-polar solvation	−133.1 ± 3.8	−154.4 ± 3.3	−130.5 ± 2.9	−124.3 ± 4.6	−137.7 ± 2.9	−131.0 ± 3.8
ΔG(total)	−736.4 ± 35.6	−884.1 ± 40.6	−739.7 ± 33.5	−654.0 ± 47.7	−791.6 ± 32.2	−682.8 ± 37.2

5.2.2 Electrostatic Analysis

We used the alanine scan method of our AESOP computational framework [44] to explore in detail the significance of the many pairwise charge-charge interactions in contributing to the stability of the C5b6 complex. We performed computational alanine scan by mutating every ionizable amino acid residue to alanine, one at a time, to generate families of single mutants for C5b and C6, and their C5b6 complex. Subsequently, we performed Poisson-Boltzmann electrostatic calculations to obtain electrostatic contributions to the free energies of binding for the binding reaction of each mutant. We present the results in reference to the parent structure, as differences between the calculated electrostatic free energies of binding of mutant structures minus the electrostatic free energy of the parent structure (see Methods). We performed the calculations for the representative structures of all six conformational clusters, and the results for those residues that participate in salt bridges (shown in **Figure 5.2A**) are presented in **Figure 5.4**. Loss of binding upon mutation is denoted by an electrostatic free energy of binding with a positive value, whereas gain of binding is denoted by a negative value. Loss of binding for the mutant indicates that the mutated residue is a contributor to binding of the parent protein by forming favorable charge-charge interactions. Likewise, gain of binding for the mutant indicates that the mutated residue opposes binding of the parent protein by contributing to unfavorable charge-charge interactions.

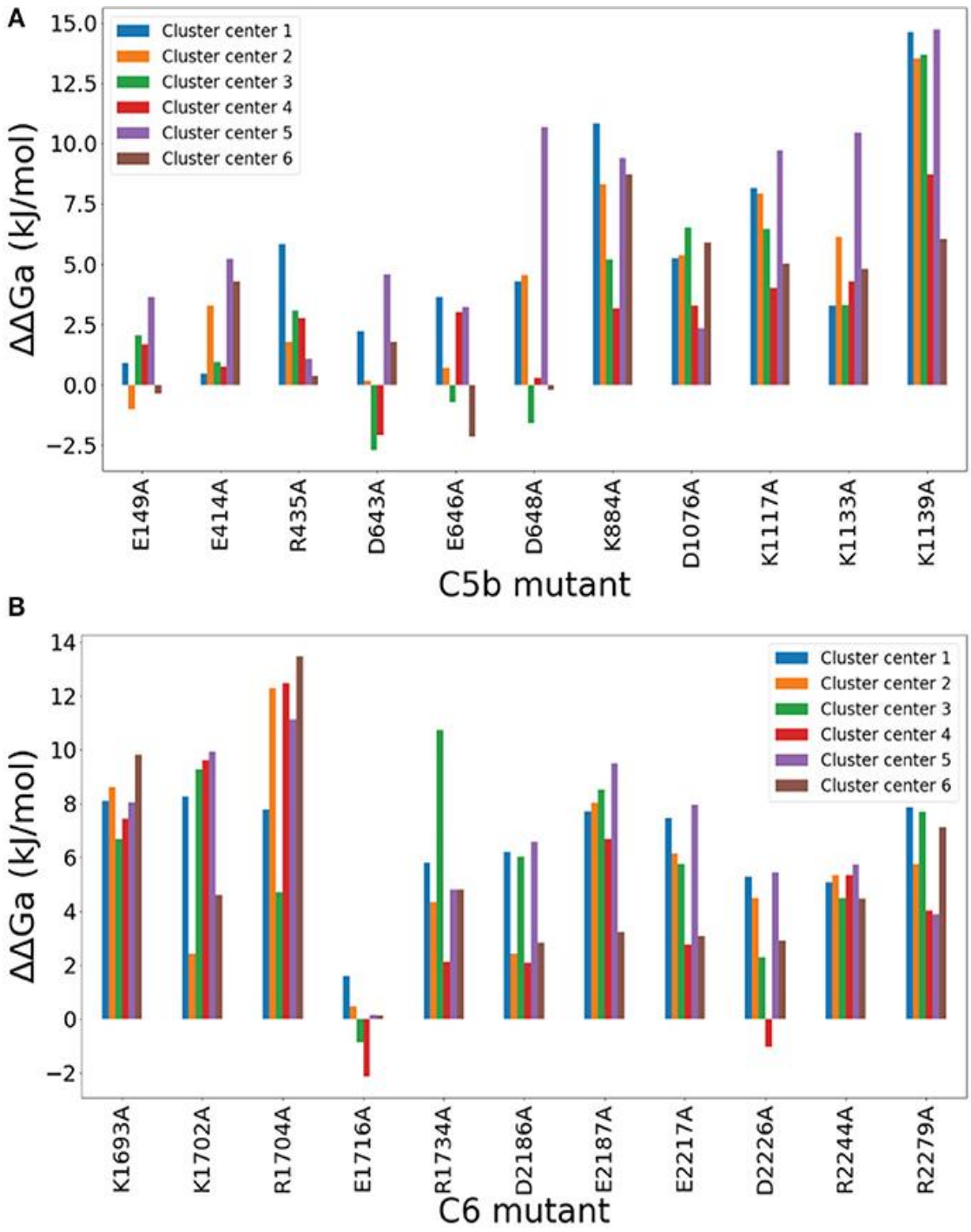
A
Cluster center 1
Cluster center 2
Cluster center 3
Cluster center 4
Cluster center 5
Cluster center 6
ΔΔGa (kJ/mol)
15.0
12.5
10.0
7.5
5.0
2.5
0.0
−2.5
E149A
E414A
R435A
D643A
E646A
D648A
K884A
D1076A
K1117A
K1133A
K1139A
C5b mutant
B
Cluster center 1
Cluster center 2
Cluster center 3
Cluster center 4
Cluster center 5
Cluster center 6
ΔΔGa (kJ/mol)
14
12
10
8
6
4
2
0
−2
K1693A
K1702A
R1704A
E1716A
R1734A
D2186A
E2187A
E2217A
D2226A
R2244A
R2279A
C6 mutant

Figure 5.4. Computational Alanine Scan results of C5b **(A)** and C6 **(B)** mutants that participate in salt bridges. The vertical axis represents differences in the calculated electrostatic free energies of binding between the mutant and the parent structure for the mutants shown in the horizontal axis. Each mutant is represented by six free energy values, corresponding to the six representative (cluster center) structures of the conformational clusters of the MD simulation. The mutant notation denotes the residue number surrounded by the type of replaced residue on the left and the replacing residue (alanine, A) on the right. A positive value denotes that the mutation causes loss of binding, indicating that the mutated residue favors binding in the parent structure. A negative value denotes that the mutation causes gain of binding, indicating that the mutated residue disfavors binding in the parent structure. The one-letter amino acid code is used, instead if the three-letter code used in text, to simplify the figure.

A few mutants show perturbations greater than thermal energy of $2k_BT$ at room temperature, most notably Lys1139A of C5b, followed by Lys884A, Asp1076A, Lys1117A, and Lys1133A (**Figure 5.4A**), and nearly every mutant of C6, most notably Arg1704, with the exception of Glu1716A (**Figure 5.4B**). These significant charge interactions depicted by the mutations of **Figure 5.4** have been identified in the salt bridge occupancy maps of **Figure 5.2A**. AESOP data for all ionizable amino acid replacements within 8 Å of the C5b6 complex interface are listed in Supplementary Data Sheet 6. The most notable charge interactions, involving Lys1139(C5b) and Arg1704(C6) as depicted by the data of **Figure 5.4**, form strong bifurcated salt bridges in Sites I and II, respectively (see above). Another charge interaction, but of lower strength, involving Asp648(C5b) also forms a bifurcated salt bridge in Site III (see above).

5.2.3 Sequence and Electrostatic Potential Comparison of Thioester Domains of C3d, C4d, and C5d

The complement system contains thioester domains, referred herein as C3d and C4d, that can covalently attach to different surfaces and tag the cellular species with complement complexes and fragments. However, the C5d thioester-like domain of C5 is distinct from C3d and C4d because it does not have the ability to covalently tag a surface, or to exist as a standalone domain, but has gained the molecular capability to instigate MAC formation [32, 33]. Despite all three thioester/thioester-like domains, C3d, C4d, and C5d, having similar structures, C3d is a molecular hub for reactions that mediate inflammatory processes such as opsonophagocytosis and B-cell activation, whereas C5d

participates in the binding of C6 and acts as the cornerstone for the MAC assembly. Thus, to elucidate on how C3d and C5d achieve their versatile functions, we performed a comparative analysis of the physicochemical properties of C3d and C5d, also including a comparative analysis of C3d and C4d for completion. Earlier studies have identified the residues of C3d that interact with FH [29] and CR2 [28]. FH is a potent regulator of C3b, and C3b's convertase complexes, that inhibits opsonophagocytosis on host cells. The CR2-C3d complex is formed as part of the B cell receptor-coreceptor complex and is a link between innate and adaptive immunity.

First, we performed a sequence alignment of all three domains, C3d, C4d, and C5d, to compare the conservation of their structurally and functionally important residues (**Figure 5.5**). The percent identity between C3d and C5d is 29.2%, between C3d and C4d is 35.7%, and between C4d and C5d is 28.8%. The contact sites with FH and CR2 are spread across the sequence of C3d. Of the total 310 C3d residues, 87 residues are involved in contacts with FH and CR2 combined (union of red and blue horizontal boxes in **Figure 5.5**). On the other hand, only nine C5d residues are involved in contacts with C6 (green horizontal boxes in **Figure 5.5**), and from those nine only one is a common site with C3d, that of Asp1104(C5d) and Gly1179(C3b). From the 87 residues that are involved in C3d-CR2/FH interactions, only 19 are homologous to C5d residues (intersection of red/blue horizontal boxes and identical C5d and C3d residues, denoted by vertical blue blocks, in **Figure 5.5**).

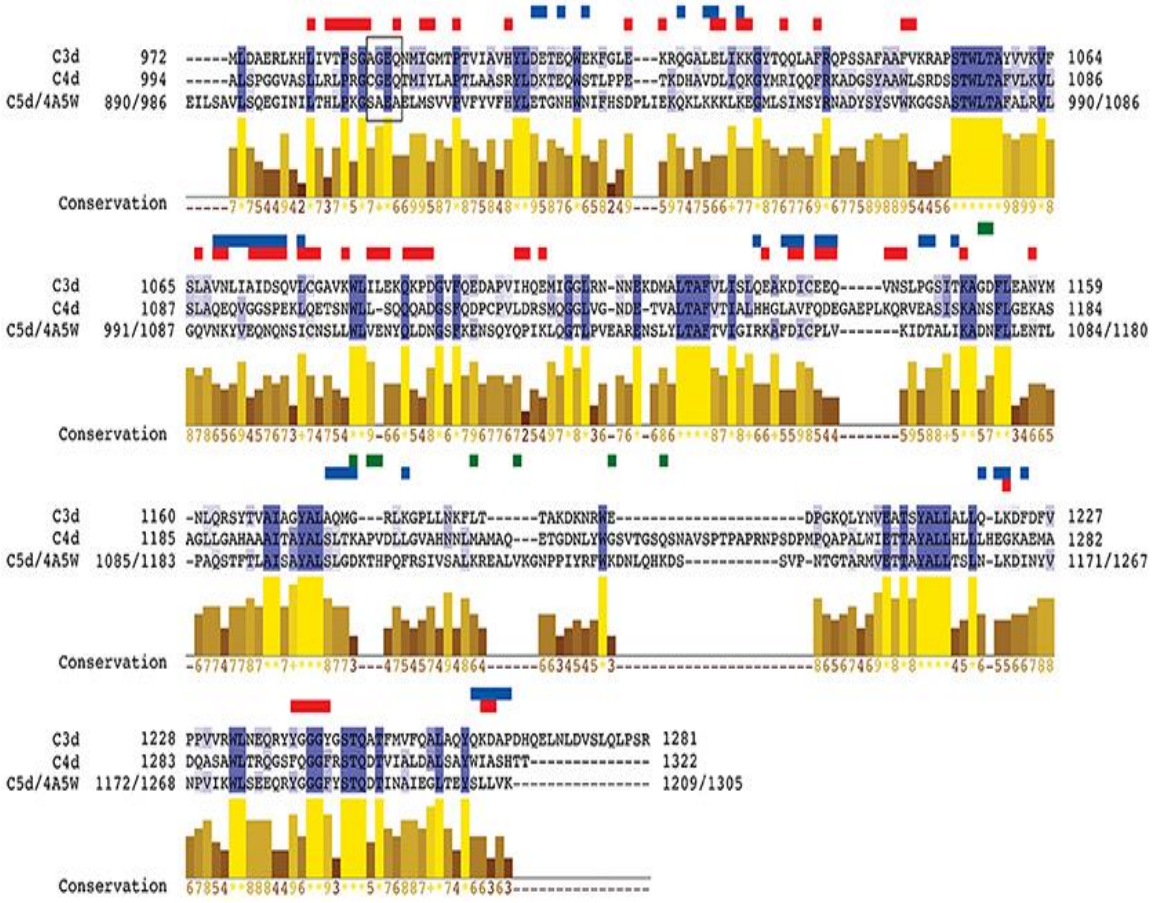

Figure 5.5. Sequence alignment of C3d, C4d, and C5d. Regions of intermolecular polar contacts between C3d and FH, C3d and CR2, and C5d and C6 are designated with horizontal rectangles above the sequences, colored in red, blue, and green respectively. Polar contacts: ionic interactions (salt bridges and long-range Coulombic) and hydrogen bonds (including side chain and backbone donor/acceptor groups). The vertical blocks in dark blue color denote identity in all three sequences, and those in light blue color denote identity in two out of three sequences. The bar plots denote similarity in conservation across all three sequences with numbers in yellow indicating the level of conservation where a larger number corresponds to higher conservation ("*" and "+" correspond to scores of 11 and 10 respectively). Residue numbering corresponds to the numbering of the crystal structures used for C3d and C4d. For C5d the residue numbering used in our study is shown, followed by the numbering of the crystal structure (PDB code 4A5W, see Methods). The thioester moiety for all three sequences is represented within a black box. Note that the cysteine that participates in the thioester bond is mutated to alanine, as was the case in the crystal structure used (PDB code 3OED).

Lastly, of the nine residues of C5d that are involved in binding to C6, four are charged residues (Asp1076, Lys1117, Lys1133, and Lys1139) that interact by forming salt bridges with residues in the CCP1 and CCP2 domains of C6 (Site I, **Figures 5.1** and **5.2A**). Contact map analysis showed that Lys1137 forms strong bifurcated salt bridges (**Figure 5.2A**). Also, the AESOP analysis showed that out of these four charged residues, alanine perturbation of Lys1139, produces the highest loss of binding mutation, hence making it one of the most important contact sites (**Figure 5.4**). In addition, Val1122 of C5d also makes a strong a hydrogen bond with Glu2188 in the CCP1 domain of C6, with a 68% frequency of contact from the total trajectory (**Figure 5.2**). Thus, from the nine residues of C5d that are involved in contacts with C6, Lys1139, and Val1122 play the most important role by participating in salt bridges and a hydrogen bond.

We also performed comparative binding/conservation analysis for C3d and C4d. There are 19 conserved C4d residues with C3d that are also found in the binding interfaces of C3d with FH and CR2 (union of red and blue horizontal boxes in **Figure 5.5**). The majority of the conserved C4d residues (17 out of 19) overlap with the FH contact sites of C3d (red-only horizontal boxes in **Figure 5.5**), with one of them overlapping with FH and CR2 contact site and two additional ones overlapping with CR2 only (blue-only horizontal boxes in **Figure 5.5**). The side chains of the two C4d/C3d conserved residues that overlap with CR2 contact sites are negatively charged. On the other hand, 11 of the 17 C4d/C3d conserved residues that overlap with FH contact sites have hydrophobic side chains, including the residue that overlaps with both FH and CR2 contact sites.

We also performed a comparative analysis of the electrostatic properties of C3d, C4d, and C5d. Earlier works have studied the properties of a highly negatively charged concave surface on C3d that is involved in recognition and binding of complement regulators [29] and receptors [28, 41] as well as bacterial inhibitors [30, 31]. **Figure 5.6A** shows the C3d concave surface with the negatively charged patch, surrounded by a neutral rim. C4d also has a negatively charged patch but spans mostly the cavity's periphery (**Figure 5.6C**). C5d on the other hand, contains a slightly shallower but more extended cavity, with a sparsely negatively charged patch on its center and distinct positively charged patches at the edges of the surface (**Figure 5.6E**). The size and charge density of the concave cavity in C3d may be the determining factor for binding to CR2, a property that is not shared by C4d and C5d. We also examined the electrostatic properties of the internal thioester bond face (**Figures 5.6B, 5.6D,** and **5.6F**), focusing on the small region that is responsible for covalently tagging pathogen surfaces after hydrolysis of the thioester bond. Both, C3d and C4d, contain positively charged patches, but the patch on C3d is more extended (**Figures 5.6B** and **5.6D**). Unlike C3d and C4d, the positively charge patch of the thioester bond moiety is lost in C5d, which has slightly negatively charged character. In addition, this region forms a crevice, which is absent in C3d and C4d, to assist packing of three hydrophobic residues of Phe2172, Ile2174, and Met2175 (part of C6's FSIM sequence motif), as stated in [33]. C6 contacts C5d through an elongated linker that contains the predominantly hydrophobic FSIM sequence motif at one end, and a polar/negatively charged DDEE sequence motif, proposed here, toward the other end, before it loops out and returns to form additional contacts with C5d. The occupancy of

intermolecular contacts of FSIM residues throughout the MD trajectory is as follows (>20% for 5 Å between heavy atoms): Phe2172-Gln898, 85.7%; Phe2172-Glu899, 62.6%; Phe2172-Asn902, 40.9%; Phe2172-Phe938, 39.2%; Ser2173-Gln898, 36.3%; Ile2174-Ala894, 25.0%; Ile2174-Gln898, 77.6%. The DDEE sequence motif comprises residues Asp2185, Asp2186, Glu2187, and Glu2188. Asp2186 and Glu2187 participate in the high-occupancy bifurcated salt bridge with C5b's Lys1139; Glu2187 also participates in bifurcated salt bridge with C5b's Lys1133 and Lys 1139; and Glu2188 participates in hydrogen bonding with C5b's Val1122, which is the highest occupancy hydrogen bond of the complex (**Figure 5.2**). Both, FSIM and DDEE side chains interact with part of Site I that is depicted by the ellipse of **Figure 5.6F**.

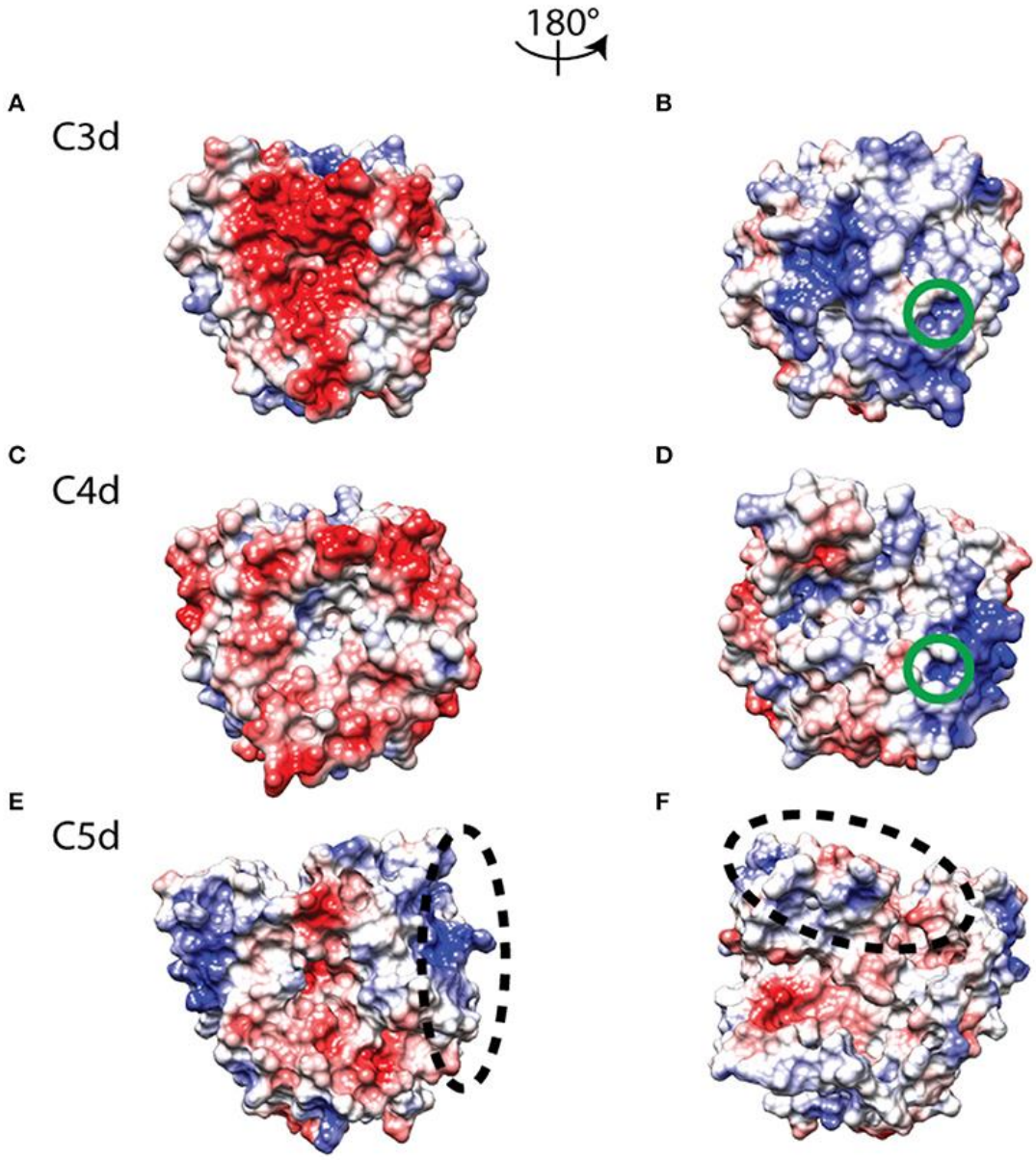

Figure 5.6. Electrostatic potentials mapped onto molecular surface representations of C3d **(A,B)**, C4d **(C,D)**, and C5d **(E,F)**, showing the CR2/FH binding face on left and the thioester face on right. The color transitions from red to white to blue represent electrostatic potential values of −3 to 0 to +3 kBT/e. The green circles mark the internal thioester bond region of C3d **(B)** and C4d **(D)**, and the two black dashed ellipses indicate distinct C6 binding regions in Site I of C5d **(E,F)**.

5.2.4 Pathway Modeling of Complement System Terminal Cascade

Formation of the MAC pore is propagated through the cleavage of complement C5 that forms C5b and C5a. The smaller fragment, C5a, is an anaphylatoxin that mediates inflammation through activation of immune cells. The larger fragment, C5b, interacts with C6 to form C5b6. The C5b6 complex interacts with C7 and C8 to form the C5b78 complex. Subsequently, multiple C9 molecules combine with C5b78 to form the transmembrane pore $C5b6789_{18}$ (MAC). We have recently developed quantitative models to study the dynamics of the alternative [24] and the combined alternative and classical pathways [25] of the complement system. These models are based on describing the biochemical reactions of the complement pathways using ordinary differential equations and are parameterized using experimental kinetic data. We used our latest model that encompasses the alternative and classical pathways to gain a systems level understanding of the terminal cascade of the complement system, starting at fluid phase C5 and ending in MAC pore formation on cell membranes [25]. **Figure 5.7** shows the concentration-time profiles of C5, C5b, C6, C5b6, and MAC pores. As C5 is consumed (**Figure 5.7A**), MAC is produced (**Figure 5.7B**). C5 is minorly consumed to form C5b (**Figure 5.7C**), and so does C6 (**Figure 5.7D**) when it combines with C5b to form the C5b6 complex (**Figure 5.7E**). C5b and C5b6 show similar time responses, but with different concentration magnitudes. The time response of MAC pore formation shows a short lag phase, followed by an accelerated production phase. Unlike complement products C5b and C5b6 that are mostly consumed in ~40 min, the profile of MAC pores shows a continuous production after the 90th min mark.

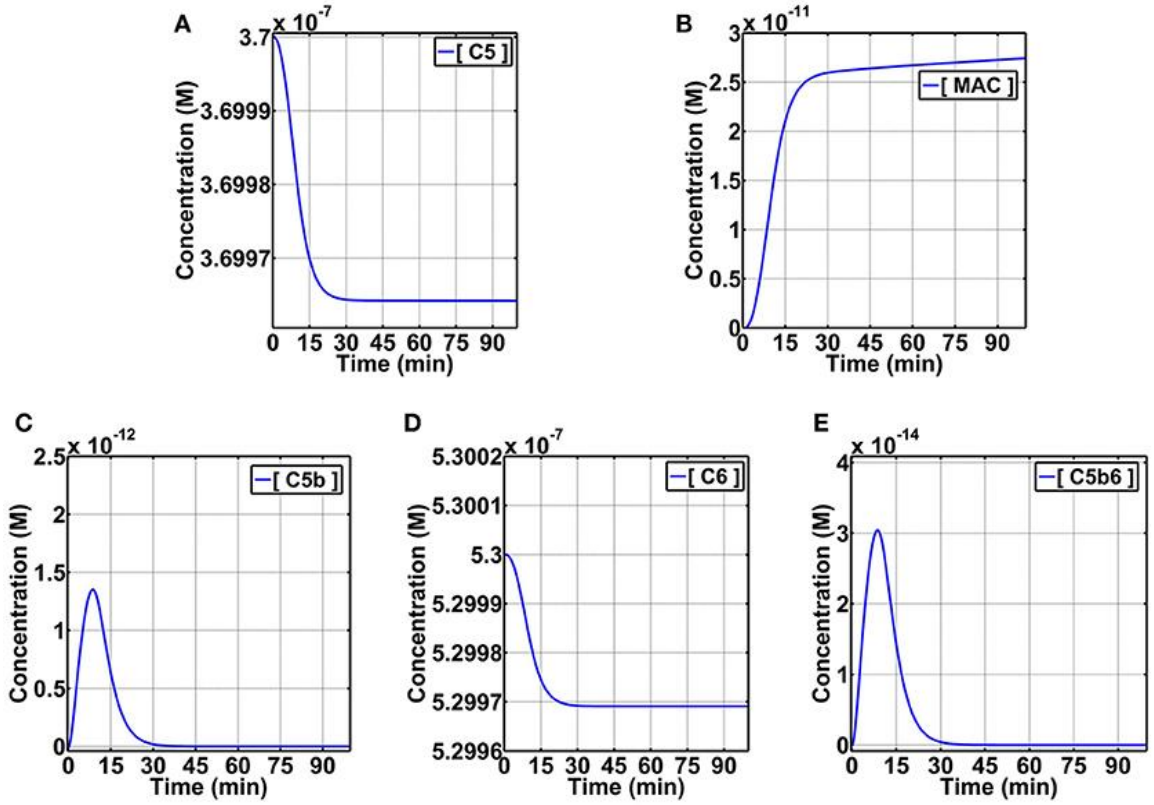

Figure 5.7. Dynamic pathway modeling of the complement terminal cascade. Rates of consumption of C5 **(A)** and production of MAC **(B)** are shown. Intermediate steps of production and consumption of C5b **(C)**, consumption of C6 **(D)**, and production and consumption of C5b6 **(E)** are also shown. C5, C5b, C6, and C5b6 are in fluid phase, whereas MAC is cell membrane bound.

Our results present the prompt activation and propagation kinetics of the complement system. In spite of the terminal pathway taking root later in the complement cascade (after the cleavage of C3), our results show MACs can be generated in less than 10 min. Furthermore, our results show despite the presence of complement regulators acting on the terminal cascade and numerous biochemical steps from C5 to C5b, C5b6, C5b67, C5b678, C5b6789, and the polymerization of C9 to form MACs ($C5b6789_{1-18}$), the rates of C5 or C6 consumption may be good predictors for the rate of MAC formation (**Figure 5.7**). This is highlighted where an accelerated rate of consumption for C5/C6 are

present within the first 30 min, and this rate subsequently is reduced after the 30th min. Similarly, but inversely related to the concentration-time profiles of C5/C6, the MAC production exhibits an accelerated phase within the first 30 min that also subsequently diminishes after 30 min. However, it should be pointed out that the rate of production in MACs is still higher compared to the rate of C5/C6 consumption after the 30th min. In summary, kinetics of C5 or C6 consumption may be sufficient to study the kinetics of MAC formation despite the presence of numerous biochemical steps from C5/C6 to MACs.

5.3 Discussion

Activation and propagation of the complement system through the alternative, classical, and lectin pathways leads to the cleavage of C5 to form C5b and C5a. Presence of C5b sets the stage for recruitment of complement protein C6 through C9 to form the MAC pore. Pathogens such as *Neisseria* species (causing meningitis) are susceptible to MAC-induced killing, and deficiency in the terminal proteins leads to recurrent meningitis [45]. On the other hand, dysregulation of the complement system leads to excessive propagation of the terminal step that plays a critical role in diseases such as AMD, aHUS, and PNH [15–20]. In addition to diseases, sublytic MAC of the terminal cascade can induce multiple signaling pathways associated with proliferation, apoptosis, and protein synthesis [13, 46]. Overall, formation of C5b6 initiates a cascade of reactions that affects numerous events from pathogen killing, to complement-mediated diseases, and signaling pathways. Here, we performed biophysical analysis on C5b6 complex to identify the key components that are involved in the mechanism of C5b and C6 binding.

We initiated our study to quantify the physicochemical origins of C5b6 binding, with focus on electrostatic interactions, guided by the large number of charged patches on the surfaces of C5b and C6 and in their binding interface. Our analysis is based on the crystal structure and MD trajectory of the C5b6 complex. MM-PBSA calculations throughout the MD trajectory showed an overall unfavorable electrostatic energy component in the free energy of binding, which is dominated by favorable van der Waals interactions. However, analysis of the binding interface throughout the MD trajectory revealed the presence of 13 intermolecular salt bridges and 11 intermolecular hydrogen bonds, which is a large number of electrostatic interactions for a complex of approximately 3200 $Å^2$ buried solvent accessible surface area (**Figure D.2**). Additionally, AESOP analysis using six representative structures from MD conformational clusters, identified several charged residues with strong contributions to the electrostatic free energy of binding. Therefore, we conclude that the stability of the C5b6 complex is dominated by van der Waals interactions and by the presence of several distinct pairwise electrostatic interactions in the form of hydrogen bonds and salt bridges. Disrupting the electrostatic interactions of residues identified herein as being important for structural stability of the C5b6 complex, may be a good strategy for future drug discovery aiming to inhibit MAC assembly.

The complement system contains two thioester domains, C3d and C4d, and one thioester-like domain, C5d, which function as initiators and propagators of the cascade of reactions that leads to the elimination of pathogens or apoptotic/damaged cells [1]. C3d and C4d function as parts of C3b and C4b, respectively, and unlike C5d both C3b and C4b

can covalently attach to host/pathogen cell surfaces and tag the cellular species for inflammatory response and opsonophagocytosis. C3d and C4d also exist as standalone proteins, after degradation cleavage of C3b by complement regulators, and remain covalently linked to the surface of cells long after complement activation. On the other hand, the thioester-like domain of C5d cannot covalently attach to surfaces of pathogens/apoptotic cells; however, C5d makes extensive contacts with C6 to form the complex C5b6 [32, 33]. The assembly of C5b6 presents the junction between the different phases of complement activation that initiates the formation of MAC. But unlike C5d (and also C4d), complement fragment C3d has numerous binding partners ranging from complement components to pathogenic proteins [41, 47–49]. For instance, C3d can mediate adhesion by interacting with complement receptors, bind the domain of *Staphylococcus aureus* protein Sbi, and also form the link between innate and adaptive immunity by interacting with CR2 on B-cells [50–54]. Although all three thioester domains are structurally similar, they have distinct electrostatic potential projections on their surfaces (**Figure 5.6**). We identified C3d has 87 of its 310 residues that are involved in binding to complement proteins FH and CR2. Furthermore, 19 of the 87 C3d residues are conserved on both C4d and C5d (**Figure 5.5**). These differences indicate that C3d has evolved to have multiple binding partners by having more binding residues present its thioester domain.

A major contributing factor to the multifaceted functionality of C3d, has been associated with its dual electrostatic nature, through two distinct faces [41]. The thioester face is positively charged and functions by tagging cells. The concave negatively charged

face functions for recruiting (or as an aid to) adaptive immunity and inducing immune response. These charged regions contain functional sites that serve to accelerate protein association and stabilize protein complexes [55, 56]. Furthermore, our results also show complement C4d contains a negatively charged ring surrounding the concave face, rather than entirely covering it, and differences in the distribution of positive charge in its thioester face (**Figure 5.6**). C5d also shows electrostatic differences on both the concave face and the thioester-like face compared to C3d and C4d (**Figure 5.6**). Another difference in C5d is the presence of a positive region that accommodates the C6 domain for the formation of C5b6 complex (**Figure 5.6**). This C6-binding site of C5d contains a deep groove, which facilitates the binding of conserved C6 linker residues of the ^{2172}FSIM^{2175} sequence motif. In addition, the linker contains the ^{2185}DDEE^{2188} sequence motif of acidic charged residues Asp2186 and Glu2187, which form salt bridges with basic residues of Lys1139 (Asp2186 and Glu2187) and Lys1133 (Glu2187) of C5d, respectively (**Figure 5.2A**). The perturbation Lys1139Ala most notably showed the strongest destabilizing effect on the interaction of C5b6 in AESOP analysis (**Figure 5.4**). Similar to C6, complement protein C7 also contains an analogous linker. However, as stated in [33], C5b may discriminate toward C6 because C7 lacks the FSIM motif and has a shorter linker that makes less extensive contacts with C5d. Overall, these results show complement proteins C3d and C4d that perform similar functions by covalently attaching to different surfaces for propagation of complement cascades, also have similar electrostatic profiles. However, C5d shows distinct charge properties, with lower densities of negative and positive charges in its concave and thioester-like surfaces.

Instead, C5d has a positive groove that facilitates C6 binding and instigates the terminal step of complement propagation.

A distinct structural feature of C3 activation product, C3b, is that its C3d domain packs at the bottom of macroglobulin domain MG1. In contrast, the C5d domain of C5b is located 50 Å from the base of MG1 when in complex with C6 [32, 33]. Although C3 and C5 are structurally similar, the distinct locations of their C3d/C5d domains in their active products C3b/C5b highlight not only how their active products are topologically different, but also on how each of them propagates its distinct function on a surface of pathogen/host cells. For instance, C3b uses its C3d domain to covalently attach to nearby pathogens and interact with FB to form C3bB. This complex subsequently is activated by FD to form the C3/C5 convertase, C3bBb [57, 58]. C3bBb then propagates a cascade of reactions on the surface by cleaving C3 to form more C3b and C3a, and to promote pathogen elimination through enhanced opsonophagocytosis. The placement of C3d close to base of MG1, in conjunction with the active thioester moiety and the positively charged thioester face, makes the covalent attachment of C3b possible. On other hand, C5b does not covalently attach to surface using its C5d domain but promotes a complementary mechanism of pathogen elimination through the formation of the pore-forming MAC. Recent cryo-electron microscopy and tomography studies of MACs proposed that the role of C5b is to assist priming C6 to initiate the pore formation [9, 12]. Close examination of MAC showed the cholesterol-dependent cytolysin/MAC perforin (CDC/MACPF) domain in C6, C7, C8, and C9 are responsible for pore formation, and this domain is absent in C5b. Furthermore, these studies showed that the structural arrangement of C5b6 is also maintained in the

MAC pore assembly. The conformation of C5b6, where C5d remains half-way elevated from the base of the MG1 domain, ensures the absence of steric clashes with complement C9, which is situated below the thioester-like domain of C5b in the MAC assembly. Subsequently, the maximum number of C9s (18 polymerization copies) can fit to form the MAC's cylindrical shape. Furthermore, downstream reactions of C5b6 to form C5b678 also affects the arc-like structure formed by C9 polymerization. Recent cryo-electron microscopy studies show polymerized C9 (poly-C9) in the absence of C5b678, assembles into a closed symmetric ring with 22 C9 components [59, 60]. This contrasts the recent MAC structures where MACs are shown to be asymmetric with a maximum number of 18 C9s [9, 12]. Superposition of poly-C9 ring with that of a physiological MAC pore shows dimensional differences in height and spacing of C9 molecules [61]. These data highlight the presence of C5b678 as one of the key factors in affecting the molecular assembly of C9s to form an asymmetric pore. All in all, formation of the C5b6 complex results in priming C6 for MAC assembly and aiding in the polymerization of C9. These functions are brought together by the stabilization of C5d's position by C6 (in the complex C5b6), and the downstream reactions that form C5b678 complex.

Through the course of our analysis of the structural and physicochemical properties underlying the mechanism of formation and stability of the C5b6 complex, we identified druggable C5d regions with the potential to disrupt C5b6 interface. In **Figure 5.8**, the C5d intermolecular polar contacts contributing to the stability of the C5b6 complex are emphasized, with surrounding residues that are in close proximity to C6 highlighted as well. The number of polar intermolecular interactions at Site I are restricted to a few narrow

regions due to the shape and size of C6. Deriving short peptides from C6 and applying modifications to improve the interfacial SASA and specific intermolecular interactions could result in stronger binders to C5d in search of inhibitory ligands against C6 binding. We also observe that several of the polar intermolecular contacts are adjacent to pockets that could be leveraged in the development of drug-like or peptidic inhibitors (**Figures 5.8C** and **5.8D**).

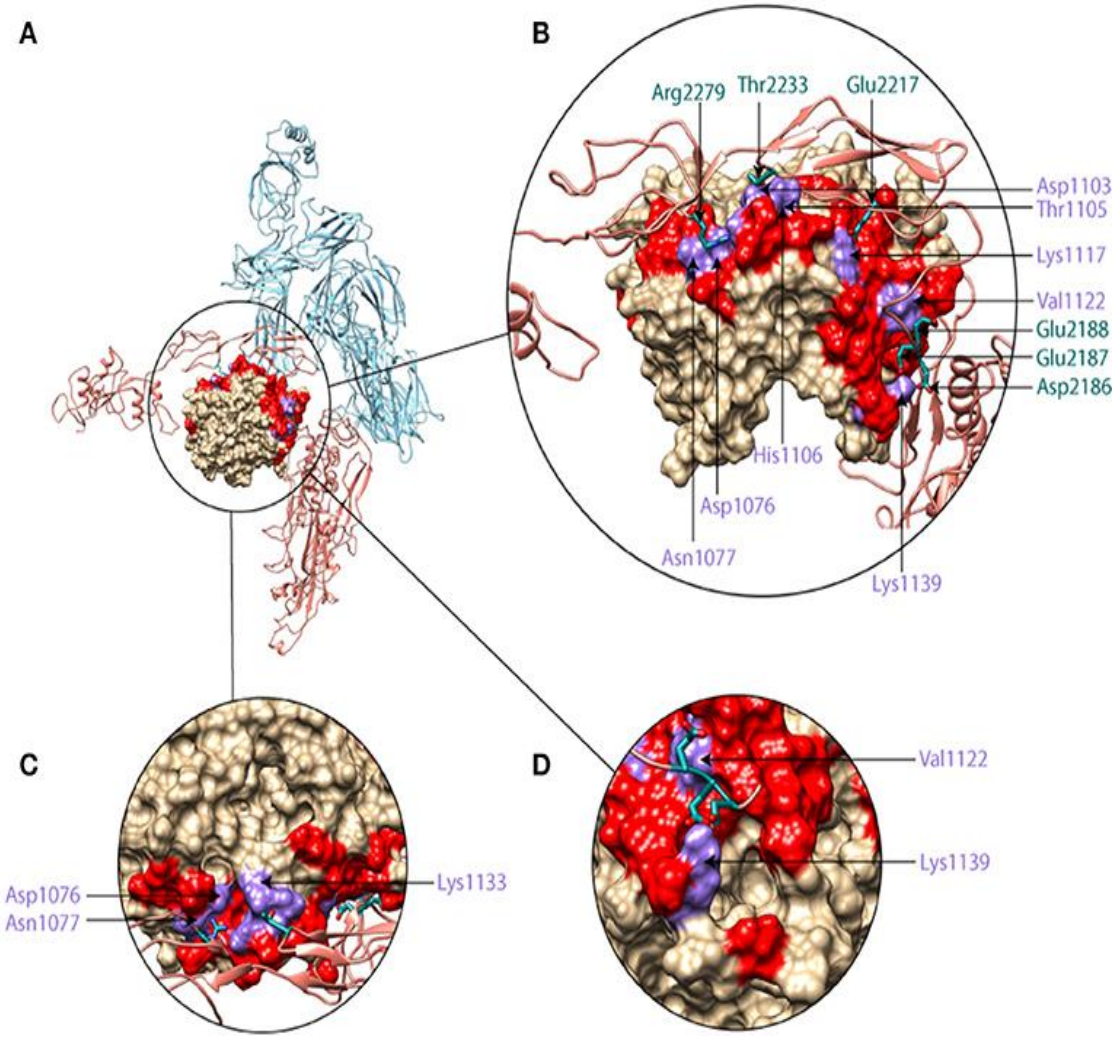

Figure 5.8. Molecular graphics representation of C5b6 with insets showing zoomed in and rotated views of Site I, highlighting the druggability of C5d. **(A)** C5b6 in ribbon form with C5d shown in surface representation (brown), and the rest of C5b (light blue) and C6 (brick) shown in ribbon representation. **(B)** Zoomed-in view of the region circled in panel A and rotated toward the viewer by 40°. **(C)** Zoomed-in view of the region circled in panel A and rotated towards the viewer by 100°. **(D)** Zoomed-in view of the region circled in A and rotated around the vertical axis by −60°. In the C5d surface, red coloring indicates regions within 5 Å of C6 and purple coloring indicates regions where polar intermolecular interactions with C6 (salt bridges and hydrogen bonds in site I, **Figure 5.2**), observed in the MD simulation trajectory. Side-chains of C6 residues taking part in polar intermolecular interactions are shown and labeled in dark green while their C5d pairing partner residues are labeled in purple.

In contrast to the potential therapeutic sites on C5d, C5 inhibitors eculizumab and SKY59 interact with domains MG7 and MG1, respectively [62, 63]. Unlike C5d, MG7 and MG1 do not contain deep pockets but have charged residues that are critical for interactions with eculizumab or SKY59. For instance, MG1 domain has three charged residues, Glu48, Asp51, and Lys109 (within 3.5 Å from SKY59 antigen-binding fragment, Fab) that mediate binding by forming critical salt bridges and numerous hydrogen bonds [62]. Mutating any of these charged residues on C5 to alanine had severe effects on the binding affinity of SKY59 [62]. And hence, the binding interface between C5 and SKY59 is highly mediated by the charged residues positioned in MG1. Similarly, the MG7 domain of C5 (targeted by eculizumab) does not contain deep pockets as observed for the thioester domains of C3d/C4d or that of C5d (TED-like). Similarly the eculizumab epitope on MG7 is also highly charged, containing six charged residues comprised of one glutamic acid (Glu915) and five positively charged residues of four lysine (Lys858, Lys882, Lys887, Lys920) and one arginine (Arg885) [63]. Furthermore, Schatz-Jakobsen et al. showed out of the 66 single-point mutants on Fab residues that interact with C5, three residues in the heavy chain (Trp107, Phe101, Trp33) and one residue in light chain (Ala32) severely impaired hemolysis inhibition when mutated to histidine [63]. Using PDBsum [64] on the binding interface between C5 and the Fab fragment, we observed half of these key mutants (Phe101 and Trp33) make extensive contacts with the positively charged residue Arg885 on the MG7 domain of C5. Interestingly, a small number of PNH patients that are resistant to eculizumab carry a common single nucleotide polymorphism where Arg885 is replaced by histidine [65]. These results show mutations on C5 that affect charged residues in drug

sites have severe consequences on the functionality of the complement inhibitors. And hence, accounting for the electrostatic nature of the C5 epitopes may significantly improve binding affinities and subsequently enhance complement inhibition.

Although most of our study is structure/dynamics-based at molecular level, we expanded our efforts to understand the role of C5b and C6 at pathway dynamics level. There is small consumption of C5 and C6 from their initial blood plasma concentrations, and this is reflected in the production of C5b and C5b6, and eventually in MAC production. C5b and C6 show an initial accelerated production phase, followed by a consumption phase as they are converted to MAC. The production of MAC shows a lag phase, corresponding to the production phases of C5b and C5b6, followed by an accelerated production phase, corresponding to the consumption phases of C5b and C6. Despite this level of production, the concentration of MAC pores in 90 min is 27 pM, about four orders of magnitude lower than the initial concentrations of C5 and C6. Given that the calculation has performed with full complement regulation in place, representing homeostasis, such MAC pore concentration is not expected to have any significant effects on host cells. However, in pathogen cells, where negative complement regulation is absent, a larger amount of MAC deposition is observed [24]. Substantial increase in MAC pore formation is also expected in host diseases such as AMD, where there is severe complement dysregulation.

Overall, our molecular dynamics and electrostatics study revealed that the large and multi-site C5b6 interface is stabilized predominantly by van der Waals interactions, but also contains an unusually large number of stabilizing salt bridges and hydrogen bonds. We identified critical salt bridges and hydrogen bonds for the stability of the C5b6

complex. Furthermore, the C5d domain of C5b contains a sparsely negatively charged patch enclosed with positively charged patches. C5d does not contain a C3d-like cavity which in C3d is an electrostatic hotspot primed for interaction with CR2 for the formation of a link between innate and adaptive immunity. This suggests mono-functionality for C5b for the formation of the MAC assembly. We propose that C5d is a target for drug discovery, by designing inhibitors capable of disrupting the critical salt bridge and hydrogen bonding interactions at the C5d-C6 interface. We also showed the presence of small cavities neighboring the critical electrostatic contacts that can be leveraged in the development of drug-like or peptidic inhibitors. Lastly, we extended our study from molecular level dynamics to pathway dynamics to demonstrate the specifics in consumption-production rates of C5, C5b, C6, C5b6, toward MAC formation. Inhibition of the C5b6 interaction may be an efficient way to block MAC formation for diseases such as PNH, where MAC is responsible for hemolytic activity of red blood cells.

5.4 Methods

5.4.1 Structure preparations

The three-dimensional cocrystal structure of C5b6 with code 4A5W [32] was obtained from the Protein Data Bank (PDB). C5b is represented as chain A, whereas C6 is represented as chain B. All missing residues of C5b and C6 were added with MODELLER [66]. The crystal structure of C3d with code 3OED [35] was obtained from the PDB. The structures of C4d and C5d were extracted from the crystal structures of C4b and C5b6, with PDB codes 5JTW [36] and 4A5W, respectively. Missing residues for C4d were

modeled using SWISS-MODEL [67]. Structural visualization and comparisons were performed using Chimera [68]. Molecular graphics were generated using Chimera. Protonation states of histidine were assigned using PDB2PQR [69]. The following transformations are needed to convert residue numbering used in 4A5W [32] to residue numbering used in our study: for C5b residues 19-765, subtract 18 from the 4A5W residue numbers; for C5b residues 766-1676, subtract 96 from the 4A5W residue numbers; for C6 residues 22-934, add 1559 to the 4A5W residue numbers.

5.4.2 Sequence alignment and analysis

Sequences of C3d, C4d, and C5d were extracted from the PDB entries 3OED [70], 5JTW [71], and 4A5W [32], respectively. Sequence alignments of C3d, C4d, and C5d were performed using Clustal Omega [72] and visualized with Jalview [73]. Identification of C3d residues involved in binding with FH and CR2 were acquired from MD simulation analysis performed in previous studies [28, 29]. Identification of C5b6 intermolecular interactions was performed as outlined in the MD trajectory analysis section, below.

5.4.3 Molecular dynamics

Initial minimization of structure in the absence of water was performed using NAMD and the CHARMM36 force field [74, 75]. Subsequently, the structure was solvated in a cubic TIP3P water box leaving a minimum margin of 12 Å between any protein atom and the cube boundary. Sodium and chloride counterions were added to the system to achieve 150 mM ionic strength and neutralize protein charges. Adding water and

counterions increased the total system size to 747,620 atoms. The solvated structure was energy minimized by undergoing 50,000 steps of conjugate gradient energy minimization before heating from 0 to 310 K with all protein atoms harmonically constrained to their positions after minimization. Next, five equilibration steps were performed in which the first five steps for a total time of 7 ns. During the four stages of equilibration, all protein atoms were constrained at a force constant of 10, 5, 2, and 1 kcal/mol/Å, respectively. The final equilibration step was concluded by only constraining backbone atoms with a force constant of 1 kcal/mol/Å. Following equilibration, AMBER16 [76, 77] was used for the production run for 100 ns with the following conditions: periodic boundary conditions, Langevin temperature control, a non-bonded interaction cutoff of 12 Å, with SHAKE algorithm used for constraining hydrogen bonds, and an integration time step of 2 fs.

5.4.4 Molecular dynamics trajectory analysis

Characterization and visualization of intermolecular interactions was performed using CPPTRAJ, pandas, and seaborn [78–80]. Analysis of buried solvent accessible surface area upon binding and visualization were performed with MDTraj [81] and matplotlib [82], respectively over all 2,000 frames in the trajectory. MSMBuilder [83] and MSMExplorer [84] were used for clustering, visualization and extracting representative structures from the trajectory for electrostatic analysis. Salt bridges between C5b and C6 residues was calculated with custom R scripts in conjunction with Bio3D package [85]. A distance cutoff of 5 Å was used. CPPTRAJ was used to analyze hydrogen bonds formed between C5b and C6 over the course of the trajectory. For hydrogen bonds, the default

distance cutoff of 3 Å was used between acceptor to donor heavy atom, and an angle cutoff of 135°. To extract representative structures, PCA decomposition was performed on the phi and psi angles observed throughout the trajectory to reduce to four principal components using MSMBuilder. The MiniBatchKMeans method in MSMBuilder was utilized to cluster the four principal components to six distinct clusters and cluster centers were extracted as representative structures.

MM-PBSA calculations were performed using a thermodynamic cycle that decomposes the calculation of the free energy of binding into molecular mechanics (MM) force field calculations in a state of low dielectric coefficient (ε = 2) and solvation calculations by transferring the proteins from the low dielectric coefficient environment to a high dielectric environment (ε = 80). A frame interval of 4 was chosen for the MM-PBSA calculations, and hence a total of 500 frames from a total of 2,000 were processed. In our case, the MM calculations include van der Waals and electrostatic free energies, but not covalent geometry energy (bonds, angles, torsions) or entropic effects. We use the one-trajectory approximation, according to which we separate the structures of the components of the complex from the structure of the complex without additional minimization and without performing separate MD simulations of the complex components. Given that we used the one-trajectory approximation, covalent geometry energies and entropic effects are expected to cancel out in the binding scheme

$$C5 + C6 \xrightarrow{\Delta G^0_{bind}} C5b6.$$

The solvation free energy calculations include electrostatic contribution according to Poisson-Boltzmann electrostatic calculations, and nonpolar contribution (cavity

solvation) described by an empirical term based on loss of solvent accessible surface area upon binding [86]. The following equations describe the MM-PBSA calculations.

$$\Delta G^0_{bind} = G^0_{C5b6} - (G^0_{C5b} + G^0_{C6}) \quad (1)$$

where the binding free energy according to MM force field calculations is given by

$$\Delta \mathrm{E}^0_{bind,MM} = \Delta \mathrm{E}^0_{MM,vdW} + \Delta \mathrm{E}^0_{MM,electro} \quad (2),$$

and electrostatic contributions of individual components, C5b and C6, and complex, C5b6, to solvation free energy are given by Poisson-Boltzmann (PB) free energy differences

$$\Delta G^0_{solv,polar} = \mathrm{G}^0_{PB,\varepsilon=80} - \mathrm{G}^0_{PB,\varepsilon=2} \quad (3).$$

The overall solvation contributions to binding, including polar and nonpolar effects, and are given by

$$\Delta\Delta G^0_{solv} = \Delta \mathrm{G}^0_{solv,C5b6} - \left(\Delta \mathrm{G}^0_{solv,C5b} + \Delta \mathrm{G}^0_{solv,C6}\right) + \Delta \mathrm{G}^0_{nonpolar} \quad (4),$$

and the MM-PBSA free energy of binding is given by

$$\Delta G^0_{bind,solv} = \Delta E^0_{MM,vdW} + \Delta E^0_{MM,electro} + \Delta\Delta G^0_{solv} \quad (5).$$

5.4.5 Electrostatic analysis

The Alanine scan method in the AESOP (Analysis of Electrostatic Structures Of Proteins) python package [44] was utilized to perform a computational alanine scan on ionizable residues at the C5b6 interface, and to evaluate their electrostatic contributions to binding. Alanine scans were performed for each of the six representative structures of the MD-derived conformational states.

AESOP utilizes the Adaptive Poisson-Boltzmann Solver (APBS) [87] to calculate grid-based electrostatic potentials, which are converted to electrostatic free energies. The

program PDB2PQR is used to pre-assign charges and atomic radii for each atom according to the PARSE force field [88, 89], as well as to convert the PDB format to PQR format used by APBS. The selection of parameters for AESOP calculations has been described before [90].

Electrostatic free energies of binding were calculated according to a thermodynamic cycle that is similar to the one used for the MM-PBSA calculations, described above, except that binding at the reference state is evaluated using Coulomb's equation instead of the molecular mechanics method. The following equations are used, as described previously [44] and in recent applications of AESOP on C3d and its ligands [28–30]:

$$\Delta G^0_{bind,solv} = \Delta E^0_{bind,Coulomb} - \Delta G^0_{solv,C5b6} - \left(\Delta G^0_{solv,C5b} + \Delta G^0_{solv,C6}\right) \qquad (6)$$

where,

$$\Delta G^0_{solv} = \Delta G^0_{electro,\varepsilon=80} - \Delta G^0_{electro,\varepsilon=20} \qquad (7)$$

Electrostatic free energies of binding for the family of alanine scan mutants are generated as deviations from the electrostatic free energy of binding of the parent protein, according to:

$$\Delta G^0_{bind} = \Delta G^0_{bind,solv,mutant} - \Delta G^0_{bind,solv,parent} \qquad (8).$$

APBS is used to calculate electrostatic potentials for the solvation steps, and the program COULOMB (part the APBS suite) is used to calculate binding at the reference state. For the solvated state, dielectric coefficients of 78.54 and 20 were used for solvent and protein interior, respectively, while for the reference state a dielectric coefficient of 20

was used to resemble that of the protein interior [90]. The ionic strength of the solvated state corresponded to monovalent counterions of 150 mM concentration (physiological ionic strength), whereas the reference state had zero ionic strength. For the electrostatic analysis of the representative structures of C5b6 the number of grid points and mesh dimensions were set to 321 × 257 × 257 and 282 Å × 245 Å × 239 Å, respectively. For the electrostatic analysis of C3d, C4d, and C5d, the number of grid points and mesh dimensions were set to 84 × 98 × 96 and 129 Å × 129 Å × 97 Å, respectively.

5.4.6 Pathway dynamics of the terminal cascade

The dynamics of the terminal cascade of complement system activation were modeled using a previously developed mathematical model that describes the biochemical reactions of the alternative and classical pathways [25]. The output of the model is reaction rates in the form of concentration-time profiles for all complement system proteins, enzymatic cleavage fragments, and association complexes. The model consists of a system of 290 ordinary differential equations (ODEs) and 142 kinetic parameters. Equations, initial concentrations, and kinetic parameters can be found in the Supplementary Information of [25]. The system of ODEs was solved using the ode23tb solver of MATLAB (Mathworks, Natick, MA).

5.5 References

1. Merle NS, Church SE, Fremeaux-Bacchi V, Roumenina LT. Complement System Part I - Molecular Mechanisms of Activation and Regulation. Front Immunol. 2015;6: 262. doi:10.3389/fimmu.2015.00262

2. Schatz-Jakobsen JA, Pedersen DV, Andersen GR. Structural insight into proteolytic activation and regulation of the complement system. Immunol Rev. 2016;274: 59–73. doi:10.1111/imr.12465

3. Tseng Y, Poon PH, Zavodszky P, Schumaker VN. Spontaneous activation of serum C1 in vitro. Role of C1 inhibitor. J Immunol. 1991;147: 1884–1890.

4. Bianchino AC, Poon PH, Schumaker VN. A mechanism for the spontaneous activation of the first component of complement, C1, and its regulation by C1-inhibitor. J Immunol. 1988;141: 3930–3936.

5. Ziccardi RJ. Spontaneous activation of the first component of human complement (C1) by an intramolecular autocatalytic mechanism. J Immunol Baltim Md 1950. 1982;128: 2500–2504.

6. Ricklin D, Reis ES, Mastellos DC, Gros P, Lambris JD. Complement component C3 - The "Swiss Army Knife" of innate immunity and host defense. Immunol Rev. 2016;274: 33–58. doi:10.1111/imr.12500

7. Bayly-Jones C, Bubeck D, Dunstone MA. The mystery behind membrane insertion: a review of the complement membrane attack complex. Philos Trans R Soc Lond B Biol Sci. 2017;372. doi:10.1098/rstb.2016.0221

8. Morgan BP, Boyd C, Bubeck D. Molecular cell biology of complement membrane attack. Semin Cell Dev Biol. 2017; doi:10.1016/j.semcdb.2017.06.009

9. Sharp TH, Koster AJ, Gros P. Heterogeneous MAC Initiator and Pore Structures in a Lipid Bilayer by Phase-Plate Cryo-electron Tomography. Cell Rep. 2016;15: 1–8. doi:10.1016/j.celrep.2016.03.002

10. Ramm LE, Whitlow MB, Mayer MM. Size of the transmembrane channels produced by complement proteins C5b-8. J Immunol. 1982;129: 1143–1146.

11. Zalman LS, Müller-Eberhard HJ. Comparison of channels formed by poly C9, C5b-8 and the membrane attack complex of complement. Mol Immunol. 1990;27: 533–537.

12. Serna M, Giles JL, Morgan BP, Bubeck D. Structural basis of complement membrane attack complex formation. Nat Commun. 2016;7: ncomms10587. doi:10.1038/ncomms10587

13. Morgan BP. The membrane attack complex as an inflammatory trigger. Immunobiology. 2016;221: 747–751. doi:10.1016/j.imbio.2015.04.006

14. Schmidt CQ, Lambris JD, Ricklin D. Protection of host cells by complement regulators. Immunol Rev. 2016;274: 152–171. doi:10.1111/imr.12475

15. Liszewski MK, Java A, Schramm EC, Atkinson JP. Complement Dysregulation and Disease: Insights from Contemporary Genetics. Annu Rev Pathol. 2017;12: 25–52. doi:10.1146/annurev-pathol-012615-044145

16. De Vriese AS, Sethi S, Van Praet J, Nath KA, Fervenza FC. Kidney Disease Caused by Dysregulation of the Complement Alternative Pathway: An Etiologic Approach. J Am Soc Nephrol JASN. 2015;26: 2917–2929. doi:10.1681/ASN.2015020184

17. Angioi A, Fervenza FC, Sethi S, Zhang Y, Smith RJ, Murray D, et al. Diagnosis of complement alternative pathway disorders. Kidney Int. 2016;89: 278–288. doi:10.1016/j.kint.2015.12.003

18. Clark SJ, Bishop PN. The eye as a complement dysregulation hotspot. Semin Immunopathol. 2018;40: 65–74. doi:10.1007/s00281-017-0649-6

19. Ricklin D, Reis ES, Lambris JD. Complement in disease: a defence system turning offensive. Nat Rev Nephrol. 2016;12: 383–401. doi:10.1038/nrneph.2016.70

20. Merle NS, Noe R, Halbwachs-Mecarelli L, Fremeaux-Bacchi V, Roumenina LT. Complement System Part II: Role in Immunity. Front Immunol. 2015;6. doi:10.3389/fimmu.2015.00257

21. Janssen BJC, Huizinga EG, Raaijmakers HCA, Roos A, Daha MR, Nilsson-Ekdahl K, et al. Structures of complement component C3 provide insights into the function and evolution of immunity. Nature. 2005;437: 505–511. doi:10.1038/nature04005

22. Kidmose RT, Laursen NS, Dobó J, Kjaer TR, Sirotkina S, Yatime L, et al. Structural basis for activation of the complement system by component C4 cleavage. Proc Natl Acad Sci U S A. 2012;109: 15425–15430. doi:10.1073/pnas.1208031109

23. Laursen NS, Andersen KR, Braren I, Spillner E, Sottrup-Jensen L, Andersen GR. Substrate recognition by complement convertases revealed in the C5-cobra venom factor complex. EMBO J. 2011;30: 606–616. doi:10.1038/emboj.2010.341

24. Zewde N, Jr RDG, Dorado A, Morikis D. Quantitative Modeling of the Alternative Pathway of the Complement System. PLOS ONE. 2016;11: e0152337. doi:10.1371/journal.pone.0152337

25. Zewde N, Morikis D. A computational model for the evaluation of complement system regulation under homeostasis, disease, and drug intervention. PLOS ONE. 2018;13: e0198644. doi:10.1371/journal.pone.0198644

26. Wu J, Wu Y-Q, Ricklin D, Janssen BJC, Lambris JD, Gros P. Structure of complement fragment C3b-factor H and implications for host protection by complement regulators. Nat Immunol. 2009;10: 728–733. doi:10.1038/ni.1755

27. Forneris F, Wu J, Xue X, Ricklin D, Lin Z, Sfyroera G, et al. Regulators of complement activity mediate inhibitory mechanisms through a common C3b-binding mode. EMBO J. 2016;35: 1133–1149. doi:10.15252/embj.201593673

28. Mohan RR, Gorham RD, Morikis D. A theoretical view of the C3d:CR2 binding controversy. Mol Immunol. 2015;64: 112–122. doi:10.1016/j.molimm.2014.11.006

29. E S Harrison R, Gorham RD, Morikis D. Energetic evaluation of binding modes in the C3d and Factor H (CCP 19-20) complex. Protein Sci Publ Protein Soc. 2015;24: 789–802. doi:10.1002/pro.2650

30. Gorham RD, Rodriguez W, Morikis D. Molecular Analysis of the Interaction between Staphylococcal Virulence Factor Sbi-IV and Complement C3d. Biophys J. 2014;106: 1164–1173. doi:10.1016/j.bpj.2014.01.033

31. Gorham RD, Kieslich CA, Morikis D. Complement Inhibition by Staphylococcus aureus: Electrostatics of C3d-EfbC and C3d-Ehp Association. Cell Mol Bioeng Dordr. 2012;5: 32–43. doi:http://dx.doi.org/10.1007/s12195-011-0195-6

32. Hadders MA, Bubeck D, Roversi P, Hakobyan S, Forneris F, Morgan BP, et al. Assembly and regulation of the membrane attack complex based on structures of C5b6 and sC5b9. Cell Rep. 2012;1: 200–207. doi:10.1016/j.celrep.2012.02.003

33. Aleshin AE, DiScipio RG, Stec B, Liddington RC. Crystal structure of C5b-6 suggests structural basis for priming assembly of the membrane attack complex. J Biol Chem. 2012;287: 19642–19652. doi:10.1074/jbc.M112.361121

34. Ojha H, Panwar HS, Gorham RD, Morikis D, Sahu A. Viral regulators of complement activation: structure, function and evolution. Mol Immunol. 2014;61: 89–99. doi:10.1016/j.molimm.2014.06.004

35. Kieslich CA, Tamamis P, Jr RDG, Victoria AL de, Sausman NU, Morikis GA and D. Exploring Protein-Protein and Protein-Ligand Interactions in the Immune System using Molecular Dynamics and Continuum Electrostatics. In: Current Physical Chemistry [Internet]. 30 Nov 2012 [cited 6 Jul 2018]. Available: http://www.eurekaselect.com/102786/article

36. Gorham RD, Kieslich CA, Morikis D. Electrostatic clustering and free energy calculations provide a foundation for protein design and optimization. Ann Biomed Eng. 2011;39: 1252–1263. doi:10.1007/s10439-010-0226-9

37. Kieslich CA, Vazquez H, Goodman GN, López de Victoria A, Morikis D. The effect of electrostatics on factor H function and related pathologies. J Mol Graph Model. 2011;29: 1047–1055. doi:10.1016/j.jmgm.2011.04.010

38. Pyaram K, Kieslich CA, Yadav VN, Morikis D, Sahu A. Influence of electrostatics on the complement regulatory functions of Kaposica, the complement inhibitor of Kaposi's sarcoma-associated herpesvirus. J Immunol Baltim Md 1950. 2010;184: 1956–1967. doi:10.4049/jimmunol.0903261

39. Zhang L, Morikis D. Immunophysical Properties and Prediction of Activities for Vaccinia Virus Complement Control Protein and Smallpox Inhibitor of Complement Enzymes Using Molecular Dynamics and Electrostatics. Biophys J. 2006;90: 3106–3119. doi:10.1529/biophysj.105.068130

40. Sfyroera G, Katragadda M, Morikis D, Isaacs SN, Lambris JD. Electrostatic Modeling Predicts the Activities of Orthopoxvirus Complement Control Proteins. J Immunol Baltim Md 1950. 2005;174: 2143–2151.

41. Kieslich CA, Morikis D. The Two Sides of Complement C3d: Evolution of Electrostatics in a Link between Innate and Adaptive Immunity. PLOS Comput Biol. 2012;8: e1002840. doi:10.1371/journal.pcbi.1002840

42. Mohan RR, Huber GA, Morikis D. Electrostatic Steering Accelerates C3d:CR2 Association. J Phys Chem B. 2016;120: 8416–8423. doi:10.1021/acs.jpcb.6b02095

43. Wade RC, Gabdoulline RR, Lüdemann SK, Lounnas V. Electrostatic steering and ionic tethering in enzyme-ligand binding: insights from simulations. Proc Natl Acad Sci U S A. 1998;95: 5942–5949.

44. Harrison RES, Mohan RR, Gorham RD, Kieslich CA, Morikis D. AESOP: A Python Library for Investigating Electrostatics in Protein Interactions. Biophys J. 2017;112: 1761–1766. doi:10.1016/j.bpj.2017.04.005

45. Lewis LA, Ram S. Meningococcal disease and the complement system. Virulence. 2014;5: 98–126. doi:10.4161/viru.26515

46. Morgan BP, Dankert JR, Esser AF. Recovery of human neutrophils from complement attack: removal of the membrane attack complex by endocytosis and exocytosis. J Immunol Baltim Md 1950. 1987;138: 246–253.

47. Lambris JD, Ricklin D, Geisbrecht BV. Complement evasion by human pathogens. Nat Rev Microbiol. 2008;6: 132–142. doi:10.1038/nrmicro1824

48. Serruto D, Rappuoli R, Scarselli M, Gros P, Strijp JAG van. Molecular mechanisms of complement evasion: learning from staphylococci and meningococci. Nat Rev Microbiol. 2010;8: 393–399. doi:10.1038/nrmicro2366

49. Clark EA, Crennell S, Upadhyay A, Zozulya AV, Mackay JD, Svergun DI, et al. A structural basis for Staphylococcal complement subversion: X-ray structure of the complement-binding domain of Staphylococcus aureus protein Sbi in complex with ligand C3d. Mol Immunol. 2011;48: 452–462. doi:10.1016/j.molimm.2010.09.017

50. Shaw CD, Storek MJ, Young KA, Kovacs JM, Thurman JM, Holers VM, et al. Delineation of the Complement Receptor Type 2–C3d Complex by Site-Directed Mutagenesis and Molecular Docking. J Mol Biol. 2010;404: 697–710. doi:10.1016/j.jmb.2010.10.005

51. Kovacs JM, Hannan JP, Eisenmesser EZ, Holers VM. Mapping of the C3d Ligand Binding Site on Complement Receptor 2 (CR2/CD21) Using Nuclear Magnetic Resonance and Chemical Shift Analysis. J Biol Chem. 2009;284: 9513–9520. doi:10.1074/jbc.M808404200

52. Li K, Okemefuna AI, Gor J, Hannan JP, Asokan R, Holers VM, et al. Solution Structure of the Complex Formed between Human Complement C3d and Full-length Complement Receptor Type 2. J Mol Biol. 2008;384: 137–150. doi:10.1016/j.jmb.2008.08.084

53. Clemenza L, Isenman DE. Structure-Guided Identification of C3d Residues Essential for Its Binding to Complement Receptor 2 (CD21). J Immunol. 2000;165: 3839–3848. doi:10.4049/jimmunol.165.7.3839

54. Nagar B, Jones RG, Diefenbach RJ, Isenman DE, Rini JM. X-ray crystal structure of C3d: a C3 fragment and ligand for complement receptor 2. Science. 1998;280: 1277–1281.

55. Honig B, Nicholls A. Classical electrostatics in biology and chemistry. Science. 1995;268: 1144–1149.

56. Sheinerman FB, Norel R, Honig B. Electrostatic aspects of protein–protein interactions. Curr Opin Struct Biol. 2000;10: 153–159. doi:10.1016/S0959-440X(00)00065-8

57. Pangburn MK, Müller-Eberhard HJ. The C3 convertase of the alternative pathway of human complement. Enzymic properties of the bimolecular proteinase. Biochem J. 1986;235: 723–730.

58. Rawal N, Pangburn MK. C5 convertase of the alternative pathway of complement. Kinetic analysis of the free and surface-bound forms of the enzyme. J Biol Chem. 1998;273: 16828–16835.

59. Spicer BA, Law RHP, Caradoc-Davies TT, Ekkel SM, Bayly-Jones C, Pang S-S, et al. The first transmembrane region of complement component-9 acts as a brake on its self-assembly. Nat Commun. 2018;9: 3266. doi:10.1038/s41467-018-05717-0

60. Dudkina NV, Spicer BA, Reboul CF, Conroy PJ, Lukoyanova N, Elmlund H, et al. Structure of the poly-C9 component of the complement membrane attack complex. Nat Commun. 2016;7: 10588. doi:10.1038/ncomms10588

61. Morgan BP, Walters D, Serna M, Bubeck D. Terminal complexes of the complement system: new structural insights and their relevance to function. Immunol Rev. 2016;274: 141–151. doi:10.1111/imr.12461

62. Fukuzawa T, Sampei Z, Haraya K, Ruike Y, Shida-Kawazoe M, Shimizu Y, et al. Long lasting neutralization of C5 by SKY59, a novel recycling antibody, is a potential therapy for complement-mediated diseases. Sci Rep. 2017;7: 1080. doi:10.1038/s41598-017-01087-7

63. Schatz-Jakobsen JA, Zhang Y, Johnson K, Neill A, Sheridan D, Andersen GR. Structural Basis for Eculizumab-Mediated Inhibition of the Complement Terminal Pathway. J Immunol Baltim Md 1950. 2016;197: 337–344. doi:10.4049/jimmunol.1600280

64. Laskowski RA. PDBsum new things. Nucleic Acids Res. 2009;37: D355–D359. doi:10.1093/nar/gkn860

65. Nishimura J, Yamamoto M, Hayashi S, Ohyashiki K, Ando K, Brodsky AL, et al. Genetic Variants in C5 and Poor Response to Eculizumab. N Engl J Med. 2014;370: 632–639. doi:10.1056/NEJMoa1311084

66. Webb B, Sali A. Comparative Protein Structure Modeling Using MODELLER. Curr Protoc Bioinforma. 2016;54: 5.6.1-5.6.37. doi:10.1002/cpbi.3

67. Waterhouse A, Bertoni M, Bienert S, Studer G, Tauriello G, Gumienny R, et al. SWISS-MODEL: homology modelling of protein structures and complexes. Nucleic Acids Res. 2018; doi:10.1093/nar/gky427

68. Pettersen EF, Goddard TD, Huang CC, Couch GS, Greenblatt DM, Meng EC, et al. UCSF Chimera--a visualization system for exploratory research and analysis. J Comput Chem. 2004;25: 1605–1612. doi:10.1002/jcc.20084

69. Dolinsky TJ, Nielsen JE, McCammon JA, Baker NA. PDB2PQR: an automated pipeline for the setup of Poisson-Boltzmann electrostatics calculations. Nucleic Acids Res. 2004;32: W665-667. doi:10.1093/nar/gkh381

70. van den Elsen JMH, Isenman DE. A crystal structure of the complex between human complement receptor 2 and its ligand C3d. Science. 2011;332: 608–611. doi:10.1126/science.1201954

71. Croll TI, Andersen GR. Re-evaluation of low-resolution crystal structures via interactive molecular-dynamics flexible fitting (iMDFF): a case study in complement C4. Acta Crystallogr Sect Struct Biol. 2016;72: 1006–1016. doi:10.1107/S2059798316012201

72. Sievers F, Higgins DG. Clustal Omega, accurate alignment of very large numbers of sequences. Methods Mol Biol Clifton NJ. 2014;1079: 105–116. doi:10.1007/978-1-62703-646-7_6

73. Waterhouse AM, Procter JB, Martin DMA, Clamp M, Barton GJ. Jalview Version 2—a multiple sequence alignment editor and analysis workbench. Bioinformatics. 2009;25: 1189–1191. doi:10.1093/bioinformatics/btp033

74. Phillips JC, Braun R, Wang W, Gumbart J, Tajkhorshid E, Villa E, et al. Scalable molecular dynamics with NAMD. J Comput Chem. 2005;26: 1781–1802. doi:10.1002/jcc.20289

75. MacKerell AD, Bashford D, Bellott M, Dunbrack RL, Evanseck JD, Field MJ, et al. All-atom empirical potential for molecular modeling and dynamics studies of proteins. J Phys Chem B. 1998;102: 3586–3616. doi:10.1021/jp973084f

76. Case DA, Cheatham TE, Darden T, Gohlke H, Luo R, Merz KM, et al. The Amber biomolecular simulation programs. J Comput Chem. 2005;26: 1668–1688. doi:10.1002/jcc.20290

77. Pearlman DA, Case DA, Caldwell JW, Ross WS, Cheatham TE, DeBolt S, et al. AMBER, a package of computer programs for applying molecular mechanics, normal mode analysis, molecular dynamics and free energy calculations to simulate the structural and energetic properties of molecules. Comput Phys Commun. 1995;91: 1–41. doi:10.1016/0010-4655(95)00041-D

78. Roe DR, Cheatham TE. PTRAJ and CPPTRAJ: Software for Processing and Analysis of Molecular Dynamics Trajectory Data. J Chem Theory Comput. 2013;9: 3084–3095. doi:10.1021/ct400341p

79. McKinney W. Data Structures for Statistical Computing in Python. In: Walt S van der, Millman J, editors. Proceedings of the 9th Python in Science Conference. 2010. pp. 51–56.

80. Waskom M, Botvinnik O, drewokane, Hobson P, David, Halchenko Y, et al. seaborn: v0.7.1 (June 2016) [Internet]. 2016. doi:10.5281/zenodo.54844

81. McGibbon RT, Beauchamp KA, Harrigan MP, Klein C, Swails JM, Hernández CX, et al. MDTraj: A Modern Open Library for the Analysis of Molecular Dynamics Trajectories. Biophys J. 2015;109: 1528–1532. doi:10.1016/j.bpj.2015.08.015

82. Hunter JD. Matplotlib: A 2D Graphics Environment. Comput Sci Eng. 2007;9: 90–95. doi:10.1109/MCSE.2007.55

83. Beauchamp KA, Bowman GR, Lane TJ, Maibaum L, Haque IS, Pande VS. MSMBuilder2: Modeling Conformational Dynamics at the Picosecond to Millisecond Scale. J Chem Theory Comput. 2011;7: 3412–3419. doi:10.1021/ct200463m

84. Hernández CX, Harrigan MP, Sultan MM, Pande VS. MSMExplorer: Data Visualizations for Biomolecular Dynamics. J Open Source Softw. 2017;2. doi:10.21105/joss.00188

85. Grant BJ, Rodrigues APC, ElSawy KM, McCammon JA, Caves LSD. Bio3d: an R package for the comparative analysis of protein structures. Bioinforma Oxf Engl. 2006;22: 2695–2696. doi:10.1093/bioinformatics/btl461

86. Kollman PA, Massova I, Reyes C, Kuhn B, Huo S, Chong L, et al. Calculating structures and free energies of complex molecules: combining molecular mechanics and continuum models. Acc Chem Res. 2000;33: 889–897.

87. Baker NA, Sept D, Joseph S, Holst MJ, McCammon JA. Electrostatics of nanosystems: application to microtubules and the ribosome. Proc Natl Acad Sci U S A. 2001;98: 10037–10041. doi:10.1073/pnas.181342398

88. Tang CL, Alexov E, Pyle AM, Honig B. Calculation of pKas in RNA: on the structural origins and functional roles of protonated nucleotides. J Mol Biol. 2007;366: 1475–1496. doi:10.1016/j.jmb.2006.12.001

89. Sitkoff D, Sharp KA, Honig B. Accurate Calculation of Hydration Free Energies Using Macroscopic Solvent Models. J Phys Chem. 1994;98: 1978–1988. doi:10.1021/j100058a043

90. Gorham RD, Kieslich CA, Nichols A, Sausman NU, Foronda M, Morikis D. An evaluation of Poisson-Boltzmann electrostatic free energy calculations through

comparison with experimental mutagenesis data. Biopolymers. 2011;95: 746–754. doi:10.1002/bip.21644

CHAPTER 6

CONCLUSION

6.1 Summary

The complement system is an ancient form of innate immunity that targets invading pathogens. It is a potent defense system that is constantly on the "look out" and once activated unleashes an immune response capable of rapidly removing the stimulus. However, due to the potency of the complement system, regulators present in fluid phase and bound to cell membranes are also on the "look out" for an improper complement activation. Once the delicate balance between activation and regulation is compromised, it leads to a viscous cycle of host cell damage.

In this thesis, our quantitative models have shown tight regulation of the complement system starts in fluid phase through the dismantlement of fluid phase convertases. Moreover, we have shown FH-mediated disorder induces a substantial level of complement activation compared to homeostasis by generating reduced levels of C3 and FB, and to a lesser extent C5, and elevated levels of C3a-desArg, Ba, Bb, C5a-desArg, and fC5b-9. These trends are consistent with clinically observed biomarkers associated with complement-mediated diseases. Furthermore, we introduced therapy states by modeling known inhibitors of the complement system, a compstatin variant (C3 inhibitor) and eculizumab (C5 inhibitor). Compstatin demonstrated strong restorative effects for early-stage biomarkers, whereas eculizumab has strong restorative effects on late-stage biomarkers. These results highlight the need for patient-tailored therapies that target early

complement activation at the C3 level, or late-stage propagation of the terminal cascade at the C5 level, depending on the specific FH-mediated disease and the manifestations of a patient's genetic profile in complement regulatory function.

The complex between C5b and C6 is the cornerstone for the assembly of the membrane attack complex. MAC is the terminal product of three converging pathways of the complement system and functions as a pore forming complex. In our study, we performed a molecular dynamics simulations and electrostatics study to elucidate the mechanism of interaction between C5b and C6 and the formation of the C5b6 complex. The C5b6 interface consists of three binding sites stabilized predominantly by van der Waals interactions, and several critical salt bridges and hydrogen bonds. Furthermore, we show C3d, C4d, and C5d are structural homologous, however C5d's mono-functionality for MAC formation comes from its electrostatic properties.

The importance of complement in the fight against pathogen is shown where deficiency in the MAC leads to a 7,000- to 10,000-fold higher risk in developing meningococcal disease. Our studies show a balanced complement activation and regulation is essential to avoid inflammatory disorders, however an imbalanced complement system (favoring over-activation) may signify complement homeostasis in regions such as nasopharynx that experiences constant insults from toxins and pathogens. To counteract the effects of porA, Msf, and fHbp on *N. meningitidis*, our computational model predicts in a concentration barrier where nasal levels of complement activators should be at least three orders of magnitude higher than C1-INH, C4BP, Vn, Cn, FH, and FHL-1. However, if this concentration barrier is compromised such that the difference is less than three orders

of magnitude, MAC production will be reduced. Altogether, if complement homeostasis is reached by increasing the concentration of complement regulators to that of activators in a region that is physiologically under homeostatic imbalance, this new state may promote increased survival of pathogens. And this subsequently makes elevated nasal levels of C1-INH, C4BP, Vn, Cn, FH, and FHL-1 as early biomarkers for an individual potentially developing meningococcal disease.